AERODYNAMIC AND HYDRODYNAMIC INVESTIGATIONS ON UPSCALING EFFECTS AND OPTIMIZATION OF OFFSHORE WIND TURBINES

A THESIS SUBMITTED TO
THE GRADUATE SCHOOL OF NATURAL AND APPLIED SCIENCES
OF
MIDDLE EAST TECHNICAL UNIVERSITY

BY

MUHAMMAD JUANDA PUTRA

IN PARTIAL FULFILLMENT OF THE REQUIREMENTS
FOR
THE DEGREE OF MASTER OF SCIENCE
IN
CIVIL ENGINEERING

SEPTEMBER 2022

Approval of the thesis:

AERODYNAMIC AND HYDRODYNAMIC INVESTIGATIONS ON UPSCALING EFFECTS AND OPTIMIZATION OF OFFSHORE WIND TURBINES

submitted by **MUHAMMAD JUANDA PUTRA** in partial fulfillment of the requirements for the degree of **Master of Science** i**n Civil Engineering, Middle East Technical University** by,

Prof. Dr. Halil Kalıpçılar
Dean, Graduate School of **Natural and Applied Sciences** _____

Prof. Dr. Erdem Canbay
Head of the Department, **Civil Engineering** _____

Assoc. Prof. Dr. Elif Oğuz
Supervisor, **Civil Engineering, METU** _____

Assoc. Prof. Dr. Nilay Sezer Uzol
Co-Supervisor, **Aerospace Engineering, METU** _____

Examining Committee Members:

Prof. Dr. Altan Kayran
Aerospace Engineering, METU _____

Assoc. Prof. Dr. Elif Oğuz
Civil Engineering, METU _____

Assoc. Prof. Dr. Nilay Sezer Uzol
Aerospace Engineering, METU _____

Assoc. Prof. Dr. Munir Elfarra
Aerospace Engineering, AYBU. _____

Assist. Prof. Dr. Mehmet Adil Akgül
Civil Engineering, Yeditepe University _____

Date: 02.09.2022

I hereby declare that all information in this document has been obtained and presented in accordance with academic rules and ethical conduct. I also declare that, as required by these rules and conduct, I have fully cited and referenced all material and results that are not original to this work.

Name, Surename : Muhammad Juanda Putra

Signature :

ABSTRACT

AERODYNAMIC AND HYDRODYNAMIC INVESTIGATIONS ON UPSCALING EFFECTS AND OPTIMIZATION OF OFFSHORE WIND TURBINES

Putra, Muhammad Juanda
Master of Science, Civil Engineering
Supervisor: Assoc. Prof. Dr. Elif Oğuz
Co-Supervisor: Assoc. Prof. Dr. Nilay Sezer Uzol

September 2022, 182 pages

Scarcity and emission issues of conventional fossil fuels have caused a fast shift to renewable energy over the last decades. Wind energy, as one of the cheapest and most advanced forms of renewable energy, is expected to lead the energy market. A recent trend is to develop bigger wind turbines since upscaled wind turbines' rotor size increases power production and reduces a significant amount of operational and maintenance costs of wind turbines. However, there are strict limitations to the design of onshore wind turbines due to transportation issues. Together with noise problems, land usage, and terrain roughness' effects on the vertical distribution of wind speed, offshore wind energy has become more popular. This study aims to investigate the aerodynamic and hydrodynamic effects of upscaling floating offshore wind turbines. For this purpose, upscaling process of NREL 5 MW, IEA 10 MW, and IEA 15 MW atop the OC4DeepCwind semi-submersible floating platform up to 20 MW is presented, and their performances are compared. To enhance the performance of the upscaled turbines, an aerodynamic optimization using the Blade Element Momentum theory coupled with a multi-objective Genetic Algorithm (GA) via HARP_Opt is carried out. Also, composite all glass layup of the optimized blade

is analyzed with Classic Lamination Theory (CLT) in Co-Blade. The open-source code, OpenFAST, is used to analyze both the aero-elastic effects on the rotor and tower, coupled with the hydrodynamic load on the floating platforms. The results show that upscaling is feasible and beneficial. Upscaling increases the natural period in all degrees of freedom (DoF) and reduces the dynamic responses of the FOWT, which results in less movement under the same wave excitation as the baselines. Upscaling also increases the generated power, and optimization of the upscaled blade conservatively improves the performance of the turbines. Further increasing of blade length more than linear scale is needed and recommended to reduce the conservative effects of the upscaled turbines.

Keywords: Wind Energy, Floating Offshore Wind Turbine, Semi-submersible Platform, Upscaling, Optimization

ÖZ

AÇIK DENİZ RÜZGAR TÜRBİNLERİNİN YUKARI ÖLÇEKLENDİRME ETKİLERİ VE OPTİMİZASYONU ÜZERİNE AERODİNAMİK VE HİDRODİNAMİK ARAŞTIRMALAR

Putra, Muhammad Juanda
Yüksek Lisans, İnşaat Mühendisliği
Tez Yöneticisi: Doç. Dr. Elif Oğuz
Ortak Tez Yöneticisi: Doç. Dr. Nilay Sezer Uzol

Eylül 2022, 182 sayfa

Geleneksel fosil yakıtların kıtlığı ve emisyon sorunları, son on yılda yenilenebilir enerjiye hızlı bir geçişe neden olmuştur. Yenilenebilir enerjinin en ucuz ve en gelişmiş biçimlerinden biri olan rüzgar enerjisinin enerji piyasasına öncülük etmesi beklenmektedir. Yukarı ölçeklendirilmiş rüzgar türbinlerinin rotor boyutu, güç üretimini arttırdığından ve rüzgar türbinlerinin işletim ve bakım maliyetlerini önemli miktarda azalttığından, son zamanlardaki eğilim daha büyük rüzgar türbinleri geliştirmektir. Ancak, ulaşım sorunları nedeniyle karadaki rüzgar türbinlerinin tasarımında katı sınırlamalar vardır. Gürültü sorunları, arazi kullanımı ve arazi pürüzlülüğünün rüzgar hızının dikey dağılımı üzerindeki etkileri ile birlikte açık deniz (deniz üstü) rüzgar enerjisi daha popüler hale gelmiştir. Bu çalışma, yüzer açık deniz (deniz üstü) rüzgar türbinlerinin yukarı ölçeklendirilmesinin aerodinamik ve hidrodinamik etkilerini araştırmayı amaçlamaktadır. Bu amaçla, OC4DeepCwind yarı-batık yüzer platform üzerinde 20 MW'a kadar NREL 5 MW, IEA 10 MW ve IEA 15 MW'ın ölçek büyütme süreci sunulmuş ve performansları karşılaştırılmıştır. Yukarı ölçeklendirilmiş türbinlerin performansını artırmak için, HARP_Opt aracılığıyla çok amaçlı bir Genetik Algoritma (GA) ile birleştirilmiş pala elemanı

momentum teorisini kullanan bir aerodinamik optimizasyon gerçekleştirilmiştir. Ayrıca, optimize edilmiş kanadın kompozit tüm cam yerleşimi, Co-Blade'de Klasik Laminasyon Teorisi (CLT) ile analiz edilmiştir. Açık kaynaklı kod OpenFAST, yüzer platformlardaki hidrodinamik yük ile birlikte rotor ve kule üzerindeki aero-elastik etkileri analiz etmek için kullanılmaktadır. Sonuçlar yukarı ölçeklendirmenin uygulanabilir ve faydalı olduğunu göstermektedir. Yukarı ölçeklendirme, tüm serbestlik derecelerinde (DoF) doğal periyodu artırır ve FOWT'nin dinamik davranışlarını azaltır, bu da referans türbinlerle aynı dalga uyarımı altında daha az hareketle sonuçlanır. Yukarı ölçeklendirme ile ayrıca üretilen gücü arttırdığında gösterildi ve yukarı ölçeklendirilmiş kanadın optimizasyonu, türbinlerin performansını ihtiyatlı tahminle iyileştirdi. Kanat uzunluğunun doğrusal ölçeklendirme kuralından daha fazla artırılması ile ölçeği yükseltilmiş türbinlerin etkilerini azaltmak mümkün olabilmektedir.

Anahtar Kelimeler: Rüzgar Enerjisi, Yüzer Açık Deniz Rüzgar Türbini, Yarı-batık Platform, Yukarı Ölçeklendirme, Optimizasyon

To my family

ACKNOWLEDGMENTS

The completion of this thesis could not have been possible without the expertise of both author's supervisors, Assoc. Prof. Dr. Elif Oğuz and Assoc. Prof. Dr. Nilay Sezer Uzol. The author wishes to express his sincere gratitude to both outstanding supervisors for their advice, criticism, encouragement, and insight throughout the research. Their never-ending patience in guiding and believing in the author, especially during the pandemic moment of Covid-19, has been the only reason the author can carry out all of the work in this study.

The author also owed a debt of gratitude to Prof. Dr. Oğuz Uzol for introducing the wind energy subject to the author, which widens the author's vision of room for contributing to a better world. Prof. Oğuz's statement, "Wind energy is not rocket science. It's more difficult", has been one of the main reasons the author chooses to pursue a master's study selecting wind energy study.

The author would also thank Prof. Dr. Altan Kayran, Assoc. Prof. Dr. Munir Elfarra, and Assist. Prof. Dr. Mehmet Adil Akgül for accepting the author's invitation to be the examining committee member and for their valuable feedback for improving the quality of this thesis.

Lastly, the author acknowledges his parents, Dr. Abdul Pattawe and Dra. Fahriah, for their moral support, extended with love. The author has always been a proud son of beautiful parents. Now, the author wishes that this work can also make them proud as parents.

TABLE OF CONTENTS

LIST OF TABLES

TABLES

LIST OF FIGURES

FIGURES

LIST OF ABBREVIATIONS

AEP	Annual Energy Production
BEM	Blade Element Momentum
CB	Center of Buoyancy
CFD	Computational Fluid Dynamics
CLT	Classic Lamination Theory
CM	Center of Mass
DLCs	Design Load Cases
DOWEC	Dutch Offshore Wind Energy Converter
DTU	Technical University of Denmark
DU	Delft University
FFT	Fast Fourier Transformation
FOWT	Floating Offshore Wind Turbine
GA	Genetic Algorithm
GDF	Geometric Data Files
GWEC	Global Wind Energy Council
HAMS	Hydrodynamic Analysis of Marine Structures
HARP_Opt	Horizontal Axis Rotor Performance Optimization
HAWC2	Horizontal Axis Wind turbine simulation Code 2nd generation
HAWTopt2	Horizontal Axis Wind Turbine Optimization 2nd generation
IEA	International Energy Agency

INNWIND	Innovation in Wind Energy
IRENA	International Renewable Energy Agency
LCOE	Levelized Cost of Energy
MSL	Mean Sea Level
NREL	National Renewable Energy Laboratory
OpenFAST	Open-source Fatigue, Aerodynamic, Servo, Turbulence
OC4	Offshore Code Comparison Collaboration Continuation
PSD	Power Spectrum Density
RAO	Response Amplitude Operator
RNA	Rotor Nacelle Assembly
ROSCO	Reference Open-Source Controller
RWTs	Reference Wind Turbines
SNL	Sandia National Laboratory
SWL	Still-Water Level
TSR	Tip Speed Ratio
WindPACT	Wind Partnership for Advanced Component Technology
WT-Perf	Wind Turbine Performance analysis code

LIST OF SYMBOLS

SYMBOLS

C_D	Drag coefficient
C_L	Lift coefficient
C_P	Power coefficient
C_T	Thrust coefficient
D_b	Baseline turbine's rotor diameter
D_u	Upscaled turbine's rotor diameter
E	Young's modulus of elasticity
FD_b	Baseline turbine's drag force
FD_u	Upscaled turbine's drag force
FL_b	Baseline turbine's lift force
FL_u	Upscaled turbine's lift force
I_r	Moment of inertia at any radial station along the blade
m_b	Baseline turbine's mass
m_u	Upscaled turbine's mass
M_r	Bending moment at any radial station along the blade
P_b	Baseline turbine's produced power
P_u	Upscaled turbine's produced power
s	Linear scaling factor
S_q	Response spectral density

S_η	Wave spectral density
T	Thrust force
v_b	Baseline turbine's volume
v_u	Upscaled turbine's volume
V_{elem}	Local velocity at blade element
V_{hub}	Mean wind speed at hub height
ε_r	Local strain at any radial station along the blade
ρ_{air}	Density of air
$\rho_{material}$	Density of material
ρ_{steel}	Density of steel
ρ_{water}	Density of water
φ_d	Diffracted wave potential
φ_i	Incident wave potential
φ_r	Radiated wave potential
ω	Rotor's rotational speed

CHAPTER 1

INTRODUCTION

World's population increases every year. It is indisputable that the need for energy is also rising. However, conventional energy sources such as fossil fuels are limited, and continuous exploration brings up scarcity issues. Moreover, the utilization of fossil fuels negatively impacts the earth's sustainability as it leaves a carbon footprint directly related to the global warming issue. The shocking fact is that only 43% of the carbon emitted from fossil fuel burning reaches the atmosphere, while the remaining 57% is absorbed and accumulated in the ocean, taking centuries to neutralize [1]. Thus, dependency on fossil fuels imposes a real threat to human life.

In contrast to fossil fuels, renewable energy offers promising potential as an energy source. Yet, it comes with another benefit as it is sustainable and less pollutant than fossil fuels. Thus, to help tackling the global warming issue, a fast shift towards renewable energy is mandatory. Renewable energy shall not be seen as an alternative energy source but rather as a priority energy source in the near future.

There are many forms of renewable energy. Wind energy is one of the forms with a long history of utilization. In the past, the wind has been used for centuries for sailing and driving windmills for many reasons. In the modern era, wind energy also plays an essential role as a bridge to ensure a smooth transition from fossil fuels to green energy. Oil and gas industries have mature technology, skill, and experience in the deployment of offshore platforms. These extensive backgrounds are instrumental when designing an offshore wind turbine, especially a Floating Offshore Wind Turbine (FOWT).

Among all forms of renewable energy, wind energy is one of the leading forms of renewable energy in terms of installed capacity. According to WindEurope’s 2017 annual report [2], as shown in Figure 1.1, wind energy is currently the second largest

form of electricity source in Europe, with the most significant rise in terms of power generation capacity. It is supported by the fact that wind energy has the most competitive Levelized Cost of Electricity (LCOE) compared to other means, as the International Energy Agency (IEA) mentioned in its 2018 market report series [3], as can be observed in Figure 1.2. In its 2021 report, the Global Wind Energy Council (GWEC) underlined that 2020 was the best year in history for the wind industry despite the effect of Covid-19 pandemic as there was 93 GW of newly installed wind power, a 53% rise compared to the previous year [4]. This achievement proves how the wind energy sector always grows and adapts to difficult situations such as pandemics.

Extracting energy from the wind itself comes with several challenges. By nature, the wind flow is intermittent, and its velocity varies depending on altitude and terrain roughness. It is due to the atmospheric boundary layer. Wind flow inside an atmospheric boundary layer tends to have an irregular velocity profile and it is highly turbulent [5].

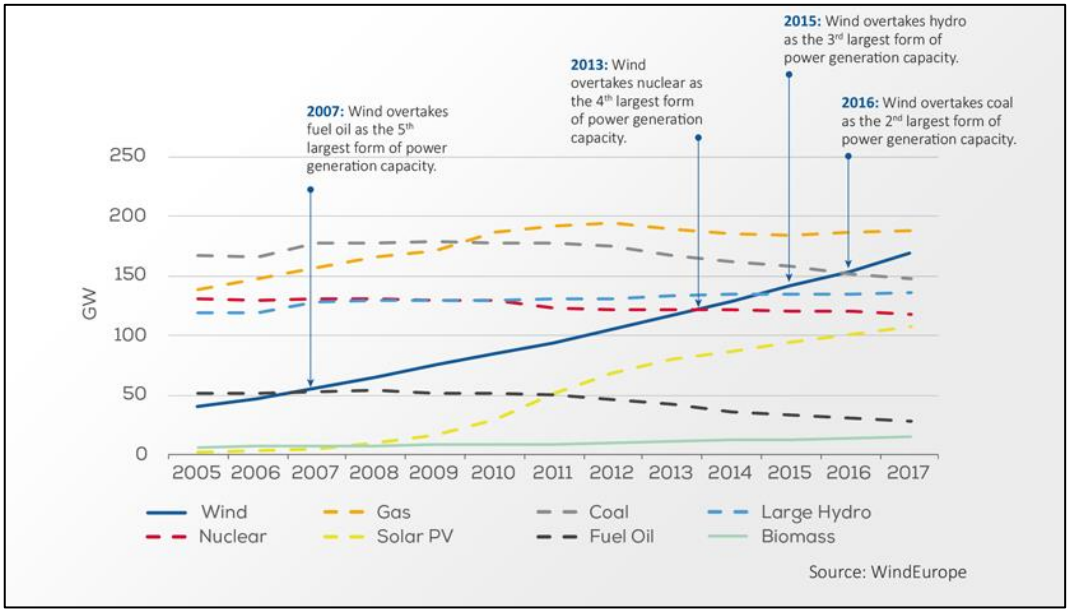

Figure 1.1. Total power generation capacity in the European Union 2005-2017 [2]

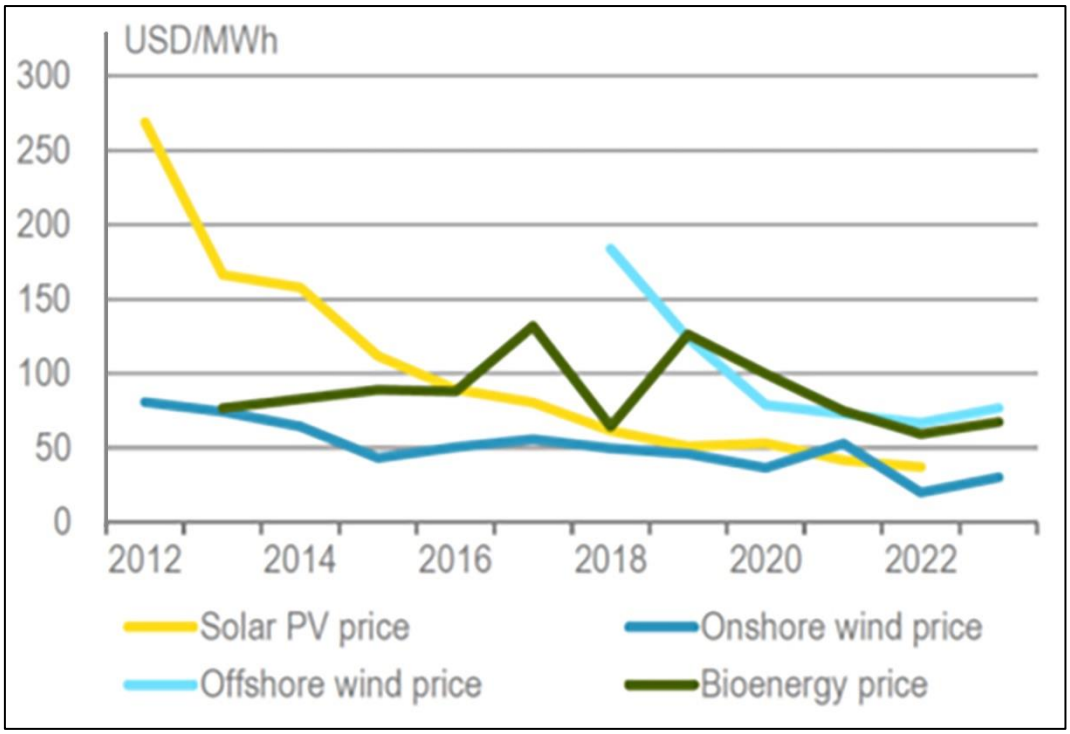

Figure 1.2. Average auction price by project commissioning date [3]

To make wind turbines more efficient, engineers have come up with a trend to optimize and upscale the rotor size of the turbines. Increasing the rotor size means a larger sweep area of the turbine, resulting in more power produced by a single turbine. It is beneficial because a single multi-megawatt turbine requires less land usage to produce a rated output power than several smaller turbines. The operation and maintenance (O&M) cost of a single higher-power wind turbine is also relatively cheaper compared to the operation and maintenance cost of several smaller turbines [6]. Larger turbines also allow for less maintenance time due to the utilization of less number of turbines operating in the wind farm. Thus, increasing rotor size can reduce the Levelized Cost of Electricity (LCOE).

International Renewable Energy Agency (IRENA), in its 2016 Technology Brief, showed the growth of wind turbine sizes from 1985 to 2016 and predicted the development of 250 meters blade diameter turbine in the near future [7]. The National Renewable Energy Laboratory (NREL) also predicted the utilization of 15

MW, 240-meter offshore wind turbines by 2030 in its 2020 Wind Energy Newsletter [8], as can be seen in Figure 1.3.

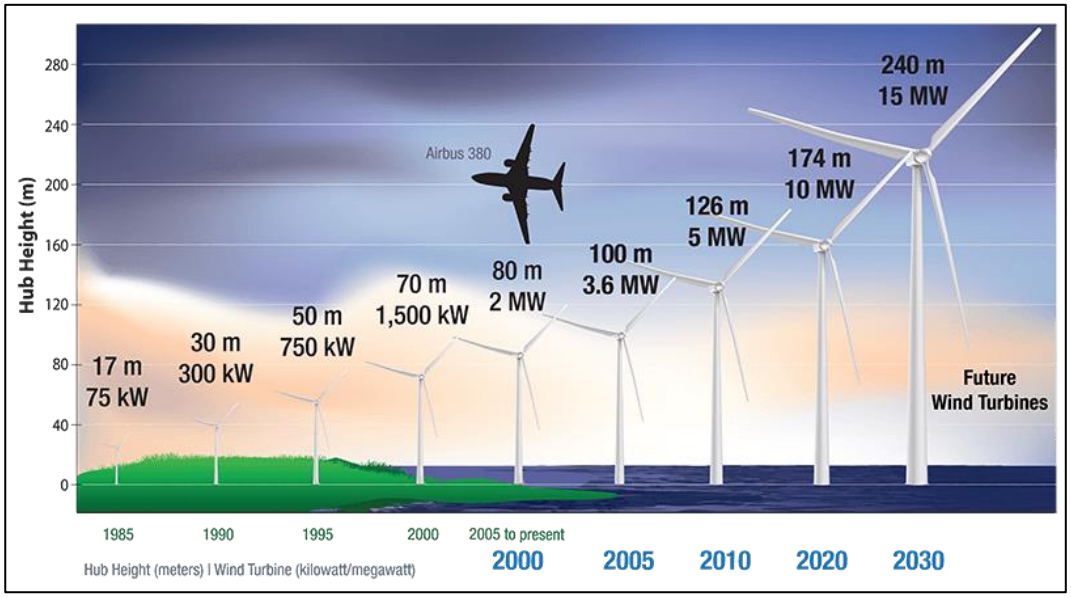

Figure 1.3. The growth of rotor diameter and rated power of wind turbines from 1985-2030 [8]

Increasing the size of the wind turbine rotor is not an easy process. A comprehensive analysis must be carried out during the upscaling of wind turbines. Several constraints need to be paid attention to when upscaling wind turbines. A larger rotor requires a higher hub altitude to maintain the clearance of the blade and the tower base. From the power production point of view, a higher hub altitude is beneficial since wind velocity is faster at higher altitudes. However, it will also result in a higher load on the tower. Correspondingly, a longer blade also results in more mass introduced to the rotor and higher structural bending in the blade component. Note that wind turbines are highly flexible rotating structures that perform under dynamic loading. Therefore, engineers must always maintain the clearance between the blade and the tower.

Apart from the structural consideration for onshore wind turbines, the most obvious limitation is the transportation of the turbines. There is a fixed ceiling dimension to carry the turbines across the road and bridges [9]. Thus, up to 5 MW turbines are

practically used in onshore wind farms. This limitation does not present in offshore turbines. Therefore, engineers have a larger envelope to design gigantic turbines and focus more on the structural part when upscaling the offshore wind turbines. Expanding onshore wind farms also requires more space which is sometimes problematic, especially for European countries.

Offshore wind energy also gains popularity among the wind energy community due to its advantages compared to onshore. Offshore wind velocity is generally faster than onshore. Recall that the atmospheric boundary layer can withstand up to several kilometers high from the mean sea level. Due to the flatter terrain of the sea, the roughness effect is less in offshore than in onshore. An example of a comparison between onshore and offshore mean wind speed in Turkey at 100 meters altitude is shown in Figure 1.4. As shown in the figure, offshore mean wind speed and intensity are higher than onshore.

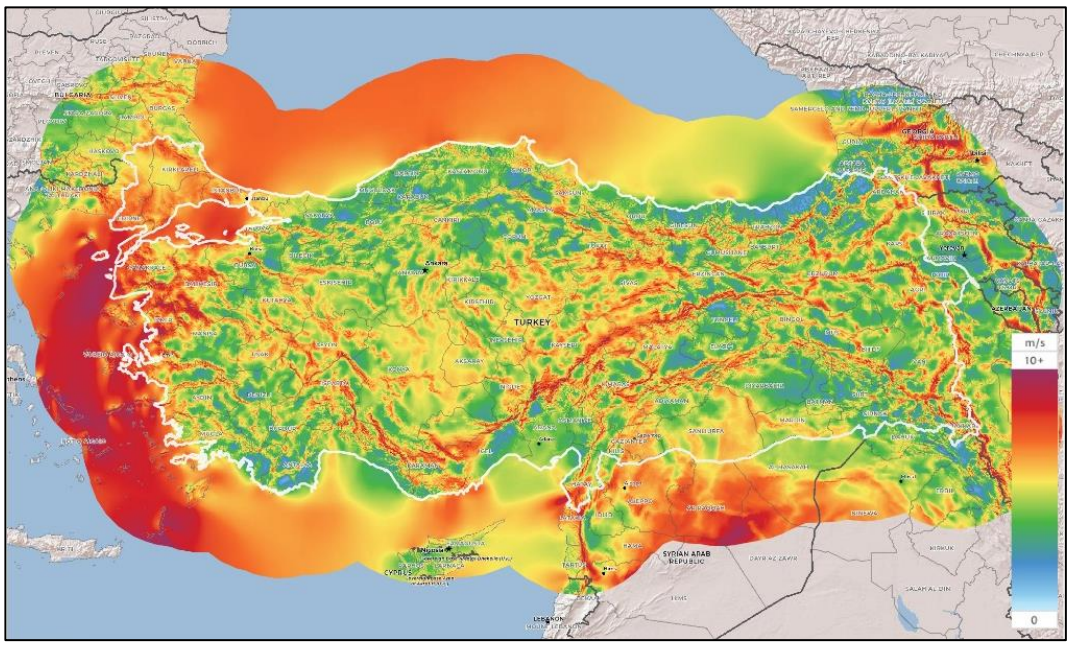

Figure 1.4. Mean wind speed distribution at 100 meters in Turkey from Global Wind Atlas [10]

One main difference that can be pointed out between onshore and offshore wind turbines is the support structures. There are a number of support structures used in offshore wind turbines, and each of them has its priorities and limitations [11]. However, based on their foundation type, the support structure can generally be categorized into two groups; fixed bottom and floating offshore wind turbines.

In fixed bottom offshore wind turbines, the foundation is built extensively rigid, starting from the seabed up to the mean sea water level. The majority of offshore wind farms installed nowadays are fixed bottom. However, fixed bottom structures are only efficient in shallow water and nearshore applications [9]. In the case of water depth greater than 30 meters, the capital expenses needed to construct a fixed bottom structure is high and make the energy price less competitive. Thus, for a significant water depth, generally above 50 meters, floating offshore structures are used.

A floating offshore wind turbine (FOWT) idea is to have enough buoyancy to erect the turbine above sea level. The design benefits from the principle of an offshore oil/gas platform to support an onshore wind turbine. Floating platforms are connected to the seabed through mooring lines. Based on the floatation principle, floating offshore platforms can be distinguished into four types: semi-submersibles, barges, SPARs, and tension leg platforms (TLPs) [12]. FOWT comes with benefits such that it can be deployed to the deep ocean, where the wind velocity profile is more consistent and faster.

Overall, floating offshore wind turbines are a relatively new and emerging technology. Currently, very few floating offshore wind farms are connected to the grid [13]. More research efforts are still ongoing to strengthen the knowledge of floating offshore wind turbines, including mounting multi-rotor turbines to a single tower, using a single floater for more than one turbine, etc. This study tries to assess the development of large-scale floating offshore wind turbines with the semi-submersible platform using linear scaling of the smaller existing floating offshore wind turbines.

1.1 The objective of the thesis

This study aims to develop the preliminary designs of multi-megawatt floating offshore wind turbines based on the linear scaling process and to analyze the aerodynamics coupled with the hydrodynamics effect resulting from the upscaling process on the performance of the FOWT.

The process started with the selection of baseline wind turbines. The NREL 5 MW [14] is used as one of the baseline turbines in this research, along with the latest IEA 10 MW [15] and IEA 15 MW [16] reference wind turbines (RWTs). The OC4DeepCwind semi-submersible floating platform [17] is used as the support structure. This floating platform is initially designed for NREL 5 MW.

The turbines are upscaled by using linear scaling rules, which determine the geometrical and structural properties of the turbines as a function of the rotor diameter. The same upscaling principle is applied to the floating platform. An optimization process is also performed to enhance the performance of the turbines and increase power production. The aero-elastic and hydrodynamic analysis of the baselines and upscaled turbines atop the semi-submersible platforms for specified design load cases are performed in OpenFAST [18]. The results are compared to understand the effect of upscaling on floating offshore wind turbines.

There are four indicators of aerodynamic performance analysis performed in this study. Those are the power coefficient (CP), thrust coefficient (CT), power curve and thrust curve. For the hydrodynamic performance, the system's natural period in the surge, heave, pitch and roll are analyzed. The analysis of the effect of the upscaling process on spectral density and Response Amplitude Operator (RAO) of the FOWTs in the surge, heave, and pitch motions are also carried out. Moreover, the study also discusses the increase in mooring tension, the bending moment in blade root and the tower's base as the size of FOWT increases.

1.2 Contribution and Novelty of the Thesis

The present study contributes to state of the art by strengthening the knowledge of the application of linear scaling on floating offshore wind turbines, especially for the latest IEA 10 MW and IEA 15 MW. These two RWTs are relatively new, there are still few upscaling studies performed to upscale IEA 10 MW and IEA 15 MW.

The present study's originality is presented in the application of coupled GA - BEM, followed by CLT with an Euler-Bernoulli and shear flow theory in the optimization process of the NREL 5 blade's aerodynamic and internal structure. The optimized blade is presented at 5, 10, 15, and 20 MW. Additionally, for 20 MW, another blade based on NREL 5 but matches the length of Upscaled IEA 15 at 20 MW is added and analyzed. Another originality is repositioning the anchor location of the three mooring lines, as previously suggested by [19]. The mooring is rearranged to maintain similar total tension as the baseline OC4 DeepCwind semisubmersible in still water conditions.

1.3 Organization of the Thesis

This thesis consists of 6 chapters. In Chapter 1, a brief introduction of floating offshore wind turbines, motivation for conducting the present study, research contribution, and the organization of the present study are stated. Literature reviews of existing upscaling and optimization studies are presented and discussed in Chapter 2. Chapter 3 focuses on the research methodology, explaining the upscaling theories, baseline wind turbines, baseline floating platforms, environmental conditions, and the numerical software used to carry out the present study. Following this, the numerical modeling of upscaled turbines and floating platforms and the process of optimizing turbine blades are presented in Chapter 4. Discussion of the turbines and platforms' free-decay simulation, together with the aerodynamic and hydrodynamic performance analysis, are presented in Chapter 5. Finally, Chapter 6 provides a summary of the present study and suggests recommendations for future studies.

CHAPTER 2

LITERATURE REVIEW

Upscaling and optimizing wind turbines has always become a challenge and shared interest of wind turbine engineers due to its well-known advantages. As a result, several projects have been carried out to upscale and optimize wind turbines. Most of the early upscaling and optimization studies are carried out for onshore wind turbines, assuming very large, multi-megawatt turbines can be installed onshore. However, as offshore wind energy trends rise, the application of upscaling on offshore platforms has also been explored.

This chapter presents the literature review of the existing upscaling studies of wind turbines and semi-submersible platforms, together with several existing studies on optimizing wind turbine rotors. The methodology and key findings of the existing studies are presented and discussed.

2.1 Previous Upscaling Studies

Wind Partnership for Advanced Component Technology (WindPACT) project focused on the effect of upscaling turbine size on turbine loads and costs of energy [20] [21]. Four different wind turbines rated 750 kW, 1.5 MW, 3.0 MW, and 5 MW were designed using an identical methodology. Different rotor configurations, upwind and downwind, were also investigated. The project developed an initial cost model for major components of wind turbines and proposed several initial turbines for research purposes.

The UPWIND project focused on the blade's aerodynamics, structure, and controller design [22]. It utilized the UPWIND 5 MW reference wind turbine atop a monopile offshore structure as its baseline and upscaled it to 20 MW. The scaling is performed

using the linear scaling rule. In addition, the airfoils' data are corrected for higher Reynold numbers, and a new optimized design of a 20 MW turbine was also developed. A new controller is implemented for both the upscaled and newly designed turbine. The performance of the newly designed turbine is compared to the scaled turbine. The project found that the newly developed 20 MW design needs about 20 tons more than the classically scaled 20 MW blade to meet the fatigue safety requirement. UPWIND suggests correcting the existing airfoils' data for a higher Reynolds number and validating the result with a wind tunnel test before designing large wind turbines.

Griffith and Ashwill from Sandia National Laboratories (SNL) developed the Sandia 100-meter all-glass baseline wind turbine blade, SNL100-00 [23]. The 61.5 meters blade of NREL 5 MW was linearly upscaled to a 100-meter blade, resulting in a 13.2 MW turbine. The study focused on the design and structural analysis of the blade. The aerodynamics of the blade was not optimized. SNL employed fiberglass-only composite material for the blade. The study succeeded in developing a 13.2 MW RWT that satisfied all strength, deflection, fatigue, and stability criteria applied in the study. However, the total mass of the SNL100-00 was found to be higher than the linear scaling trend due to the need for additional reinforcements to satisfy buckling and fatigue life requirements, the addition of a third shear web, and the use of all-glass materials.

Ashuri and Zaaijer studied the changes in two design drivers for large-scale wind turbine blades as the rotor size increases, namely the aerodynamic and inertial loads [24]. A linearly upscaled model and a finite element coupled with the blade element momentum model were used and compared. At 5 MW, aerodynamic force is the primary design driver. But, as the size of the blade increases, the significance of contributions of inertial load overcomes aerodynamic loads. Thus, the inboard sections need to be strengthened when designing large-scale turbines, and the utilization of lightweight materials when up-scaling wind turbines are necessary.

Capponi et al. investigated the non-linear upscaling approach for wind turbine blades based on stress levels [25]. A blade that maintained the same stress level as the reference blade was aimed. The reference 5 MW turbine blade was upscaled to 20 MW using the non-linear upscaling method by maintaining identical stresses in the blade throughout the entire upscaling process. The nonlinearly scaled blade were compared to linearly scaled blades. The study predicted an increase of 80% in the total stress may occur near the blade's root if the blade is linearly scaled. However, linearly scaled blades have a lighter mass than nonlinearly scaled blades. The blade's root section experiences an increase in stress mostly due to weight, while the tip section is affected mainly by aerodynamic forces.

Caduff et al. studied the environmental impact of upscaling wind turbines' size and power [26]. The study utilized hub height and rotor diameter as environmental key performance indicators to estimate the environmental impacts of a generic turbine. The result showed that upscaling wind turbines resulted in greener electricity mainly due to the utilization of larger turbines and due to the advancement of technology over time. In general, doubling the cumulative energy production reduces 14% of the global warming potential per kWh.

Sieros et al. examined the theoretical and practical aspects of upscaling wind turbines and their impact on energy costs [27]. The study underlined that, unfortunately, the weight of the blade increases during the upscaling process of wind turbines. Thus, the levelized component cost increases with turbine size without additional technology improvements.

Ashuri investigated how upscaling affects offshore wind turbines in terms of technical characteristics and economy [28]. The result showed that the design of more giant offshore wind turbines up to 20 MW is technically feasible, although economically not attractive. The blade's tip to tower clearance and the fatigues of the tower act as active design constraints which always need to be maintained in the upscaling process.

Kazacoks R. and Jamieson P. investigated how hub loads differ among the four horizontal axis wind turbines, rated 2 MW, 3 MW, 3.6 MW, and 5 MW [29]. The edgewise and the flap-wise bending moment of the blade root are investigated. The result on power spectral density graphs showed that the frequencies of the rotor and structural modes decrease with wind turbine size both on the edgewise and flap-wise bending moments.

Leimster R et al. investigated a rational approach to upscale the OC4DeepCwind semi-submersible floating platform to support Fraunhofer's 7.5 MW wind turbine (IWT-7.5-164) [19]. Water and concrete were used for ballasting the structure, and their performances were compared. The study showed that natural periods of the platform increase as the semi-submersible is upscaled. Water ballast is preferred due to its better pitch stability. An important consideration is to adjust the dimension of the main column according to the geometry of the intended turbine. The study also suggested adjusting the mooring system's total length and anchor locations for future studies.

Liu et al. proposed Froude scaling when upscaling the OC4DeepCwind semi-submersible to support the SNL 13.2-MW [30]. In this study, the mooring line properties are also upscaled. Thus, the diameter and mass of the mooring lines are also increased. The study finds that the natural frequencies of the upscaled platform are lower than the baseline semi-submersible.

2.2 Previous Optimization Studies

Sağol, E. performed site-specific design optimization of a three-bladed Horizontal Axis Wind Turbine (HAWT) to minimize the cost of energy [31]. The Genetic Algorithm (GA) was implemented to optimize the chord and twist angle of the blade at three locations (e.g., root, mid, and tip) with either S809 airfoil or NREL S-series airfoil families. The results showed that using specifically designed airfoils for wind

turbines reduced energy costs and improved turbine performance. Moreover, setting the turbine's rated power as a free variable resulted in a better energy cost reduction.

Yi and Sale optimized wind turbine blades using genetic algorithms and pattern search methods [32]. The Horizontal Axis Rotor Performance Optimization (HARP_Opt) was used to optimize the blade shape of a 1 MW turbine with FFA airfoil families. The objective of the study was to maximize the AEP. The result showed that the pattern search method performed better by achieving higher AEP and consistent optimal shapes. However, the genetic algorithm was better in reducing the calculation time.

Sale et al. performed structural optimization of composite blades for wind and hydrokinetic turbines [33]. In the study, a 550-kW hydrokinetic turbine was used as the baseline. The objective was to minimize the blade's mass subjected to constraints on maximum allowable stress, buckling, blade tip deflection, and avoid resonance between the blade's natural frequency and rotational frequencies. The study resulted in the development of Co-Blade, a structural optimization code based upon classical lamination theory combined with an Euler-Bernoulli and shear flow theory applied to composite beams.

Bekele and Ramayya performed a site-specific design optimization for Adama I wind farm to minimize the cost of energy [34]. In the study, the NREL S-series airfoil family was used to construct a turbine blade, and XFOIL was used to generate the polar data of the airfoils. Three design scenarios to construct three wind turbines were carried out with the HARP_Opt code. Results showed that an increase of 12 to 28.5% in net AEP was observed depending on the design scenarios. This increase corresponds to an 8.44 to 17.6% reduction in energy cost.

IEA developed two wind turbine models within the second work package (WP2) of Wind TCP Task 37, rated 3.4 MW for land-based and 10 MW for offshore-based wind turbines [15]. The overall characteristic of the 10 MW turbine was developed based on the DTU 10-MW. The Horizontal Axis Wind Turbine Optimization 2nd generation (HAWTOpt2), a multidisciplinary design tool developed by DTU for

predicting the structural properties and the aeroelastic response of wind turbines, was used to optimize the blade. The optimization aimed to maximize AEP with blade length as a free parameter and the load envelope of DTU 10 MW as the design constraint.

Within the Wind TCP Task 37, IEA also developed a 15 MW Offshore Reference Wind Turbine, the IEA 15 MW [16]. Again, the Horizontal Axis Wind Turbine Optimization 2nd generation (HAWTOpt2) was used in the optimization process. The blade chord, twist angle, airfoil location, tip speed ratio, and spar cap thickness were selected as free variables. The optimization process aimed to produce a 240 meters rotor diameter with a maximum of 65 tons of blade mass.

Kesikbaş, O. investigated of upscaling effects of the aerodynamic design of large wind turbine rotors using the Blade Element Momentum (BEM) theory [35]. In the study, land-based NREL 5 MW is upscaled up to 20 MW using the linear scaling law, and optimization of the blade's aerodynamic shape was performed with HARP_Opt. The study found that a higher power coefficient than the scaled blade can be achieved through the optimization process.

Oğuz, K. performed an aerodynamic optimization on wind turbines blade using the Class Shape Transformation (CST) method, Blade Element Momentum (BEM) theory, and Genetic Algorithm (GA) [36]. The study found that optimization with CST parameterization improves the turbine's power production. The study also underlined that BEM theory is sufficient in predicting the power performance of wind turbines' rotors.

Ram et al. designed small wind turbines, rated 20 kW, for rural areas' utilization [37]. The multi-objective genetic algorithm was used to design the USP07-45XX airfoil family to minimize the leading edge roughness and maximize the lift-to-drag ratio for an angle of attack range of 4^o to 10^o. To construct the wind turbine, HARP_Opt is used. The result succeeded in designing a 20 kW wind turbine with a cut-in velocity of 2 m/s and a rated velocity of 9 m/s. Due to the optimized airfoil profiles,

the soiling effect on the blade’s leading edge is reduced, and variation on the AEP due to corrosion issues is minimized.

Nour et al. optimized a small, 20 kW wind turbine for a rural area in Australia [38]. The NREL combined experiment rotor (NREL CER) was used as the baseline turbine and optimized. The HARP_Opt was used to optimize the rotor's aerodynamic shape subjected to the rural area's local wind condition. The investigation of the HAWT’s aerodynamic performance was carried out in ANSYS Fluent. This study showed due to the site-specific optimization, an improvement of 9.068% in AEP is achieved compared to the original NREL design.

CHAPTER 3

METHODOLOGY

This chapter presents the research methodology used in the present study. The workflow process performed in this study is summarized in a systematic flowchart, which can be found in Figure 3.1.

Initially, in Section 3.1, two upscaling models are discussed and the advantages and disadvantages of each model are discussed. Due to applicability reasons, the linear upscaling model is selected and used in the present study. Then, the design of three reference wind turbines (NREL 5 MW, IEA 10 MW, and IEA 15 MW) are presented in Section 3.2. The design characteristic of the three turbines are tabulated and the geometrical configurations of key design parameters are plotted and compared. Following that, in Section 3.3, the OC4 DeepCwind semi-submersible floating platform is presented. The platform and mooring lines' design characteristics are tabulated and their geometrical configurations are plotted.

In this study, three design load cases (DLCs) used to simulate and analyze the aerodynamic and hydrodynamic performance of all the turbines are taken directly from the Phase II of OC4 [39]. The selection of similar external loads with the benchmark OC4 is performed to understand the effect of upscaling on the turbines and platforms. Details of all the DLCs are shown in Section 3.4

Section 3.5 discusses the selection of numerical programs used to carry out analysis in this study. In general, four primary programs are needed to carry out the study. OpenFAST is used to perform the whole nonlinear simulation. The hydrodynamic analysis of the platform is carried out using HAMS. Optimization of the blade’s aerodynamic shape is performed in HARP_Opt, while the structural configuration of the blade is designed in Co-Blade. A brief review of all the software can be found in Section 3.5.

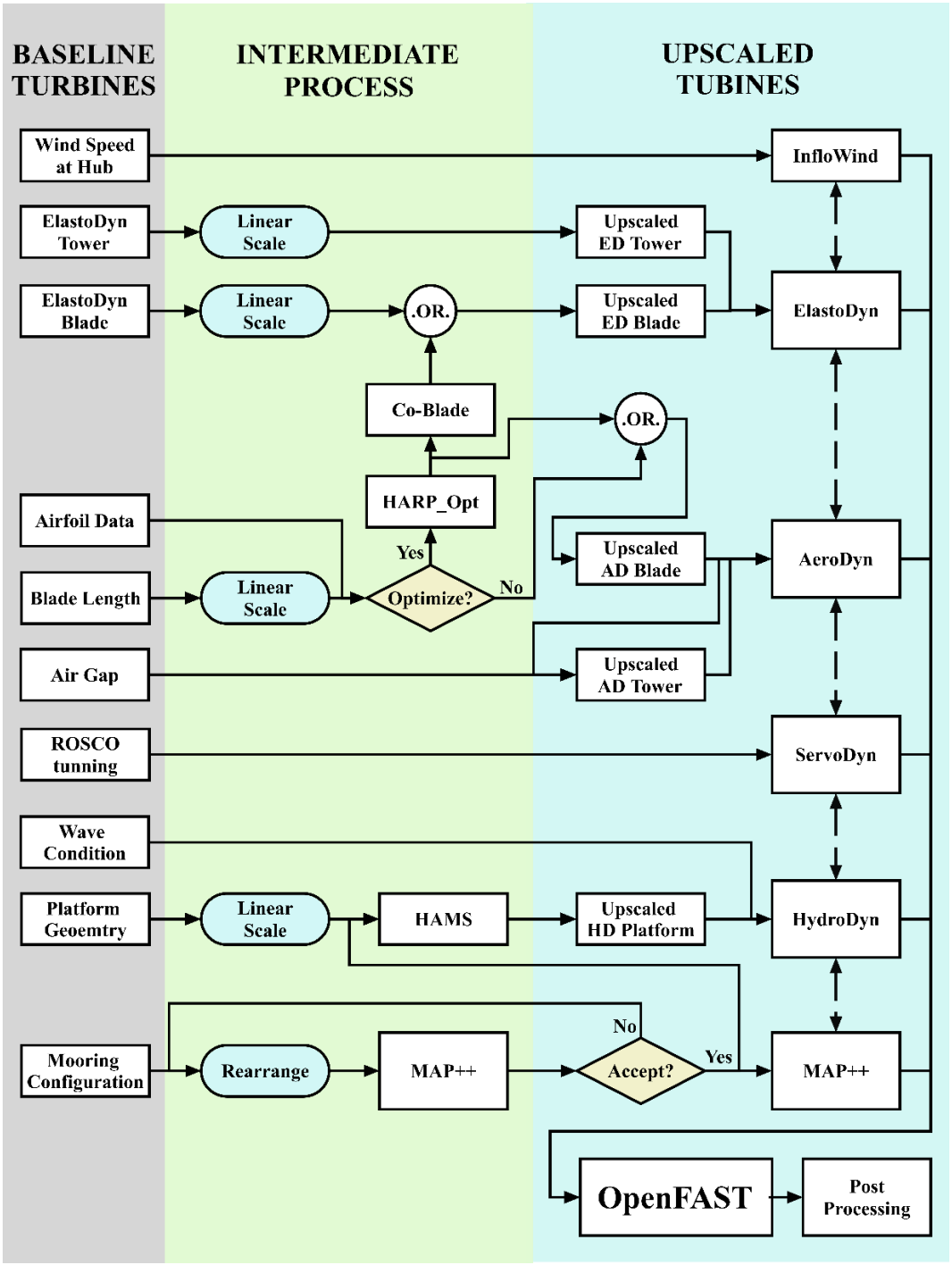

Figure 3.1. Flowchart of the study

3.1 Upscaling Methodology

Designing multi-megawatt offshore wind turbines can be performed in several ways. An engineer can develop a completely new design from scratch or utilize as much data from an already developed turbine and upscale and optimize it into a new, larger turbine. Designing an entirely new turbine requires an extensive theoretical background in many disciplines and experimental effort for validation purposes. For FOWT, the challenges are more complex since the turbine's sizes are much larger than onshore, and subjected to not only aerodynamic force on the tower and RNA but also hydrodynamic forces on the floating platform.

A relatively more straightforward approach is to upscale the existing turbines to a larger scale. The upscaling process of already existing turbines into a giant turbine is performed to estimate the new turbines' size, mass, structural characteristics, energy production, etc. The process is generally performed in 2 ways. Firstly, by extrapolating the data trends of many existing turbines into a giant turbine. Secondly, by choosing a baseline turbine and using an analytical model to upscale it. One of the most straightforward upscaling models is the linear (similarity) scaling model. Details of both upscaling approaches, including the advantages and disadvantages, will be discussed in this section.

3.1.1 Existing Data Trend

Upscaling the existing data trend can be performed by gathering as much data as possible on installed turbines. The data of the turbines are then tabulated, and curve fitting is used to establish the relationship between the intended design variables (e.g., rated power, turbine mass, blade stiffness, etc.) and the rotor size. This curve-fitted relation as a function of rotor size can be used to estimate data for a new turbine whose dimension is larger than the existing ones plotted in the curve. Examples of curve fitting for the mass of blades and towers can be found in the dissertation of Ashuri [28], as shown in Figure 3.2 and Figure 3.3, respectively.

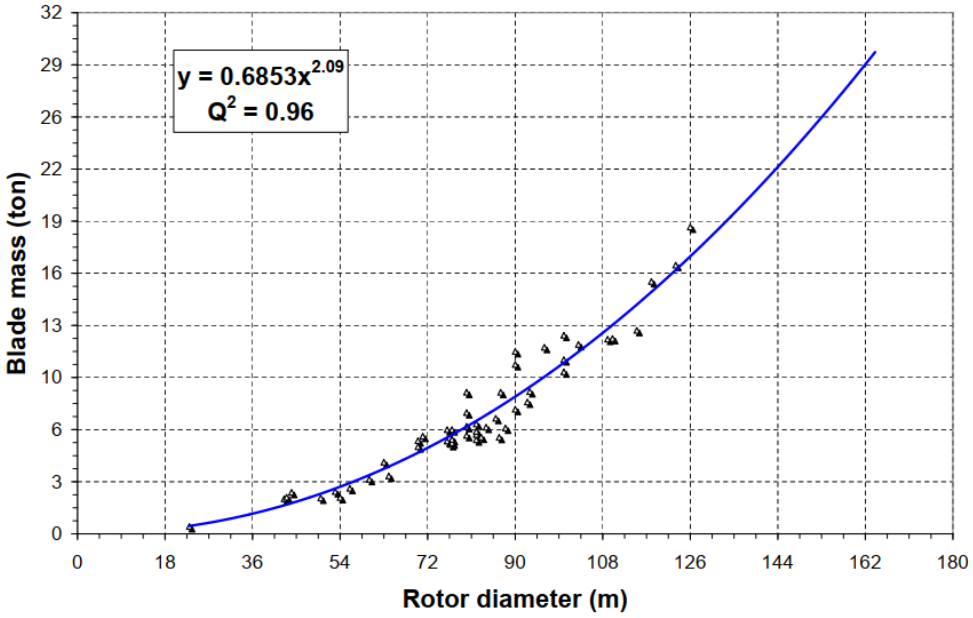

Figure 3.2. Increasing trend of blade mass with rotor diameter [28]

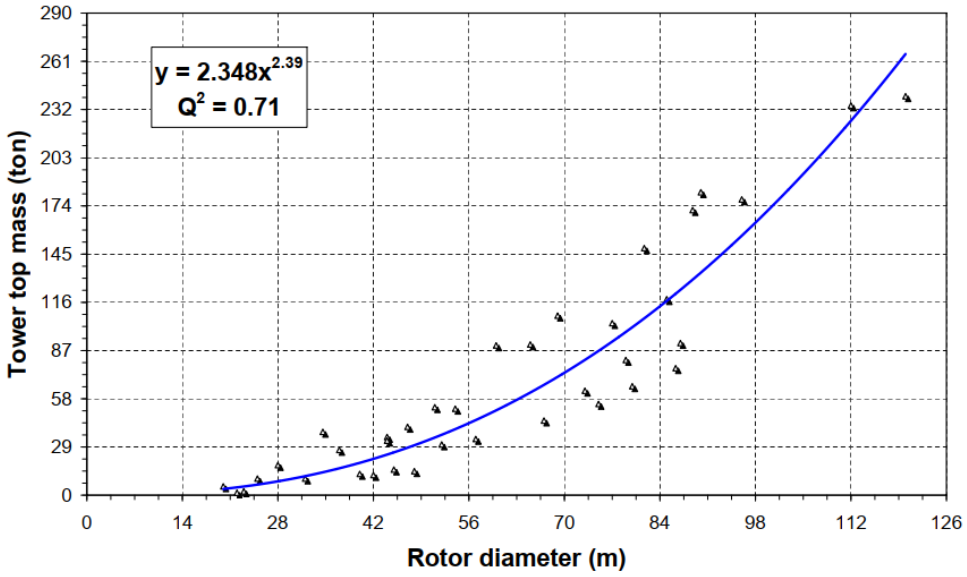

Figure 3.3. Increasing trend of tower top mass with rotor diameter [28]

As can be seen from Figure 3.2 and Figure 3.3, the blade mass has a relation of $x^{2.09}$, less than the tower mass of $x^{2.39}$. This is due to the introduction of composite material to the blade because steel blades are commonly used in previous technology. A holistic study of existing data trends in relation to mass and load on the rotor, nacelle,

and tower is shown in the Innovation in Wind Energy (INNWIND) project [40]. Examples of curve fitting for bending moments acting on the blade and tower are shown in Figure 3.4 to Figure 3.6.

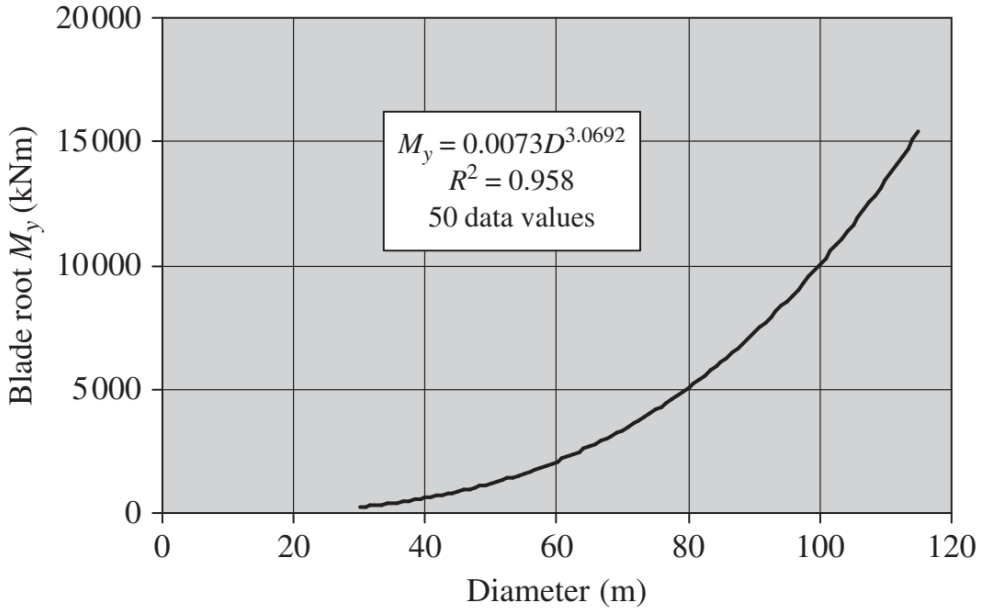

Figure 3.4. The trend of blade root out-of-plane bending moment [40]

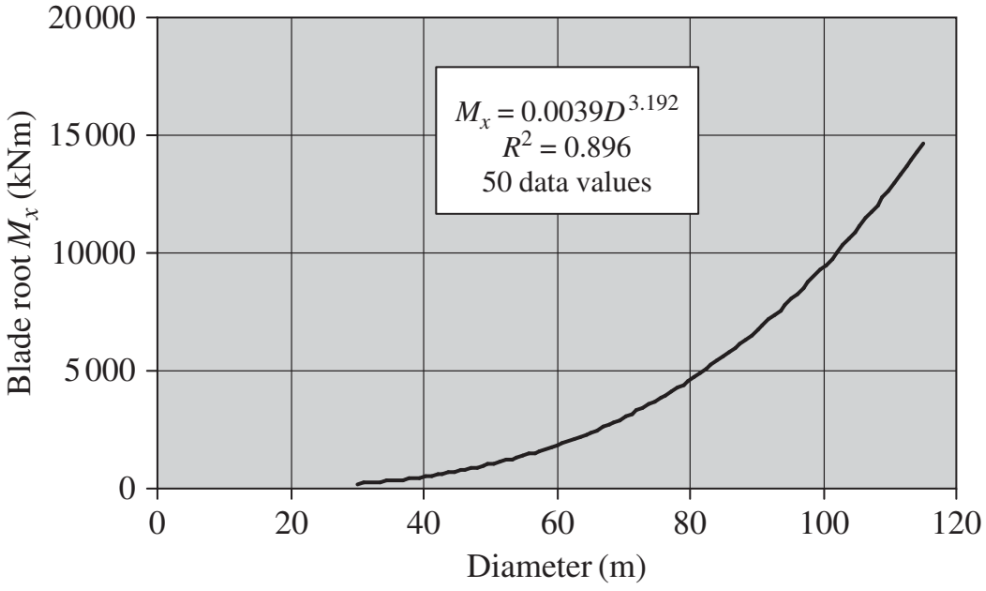

Figure 3.5. The trend of blade root in-plane bending moment [40]

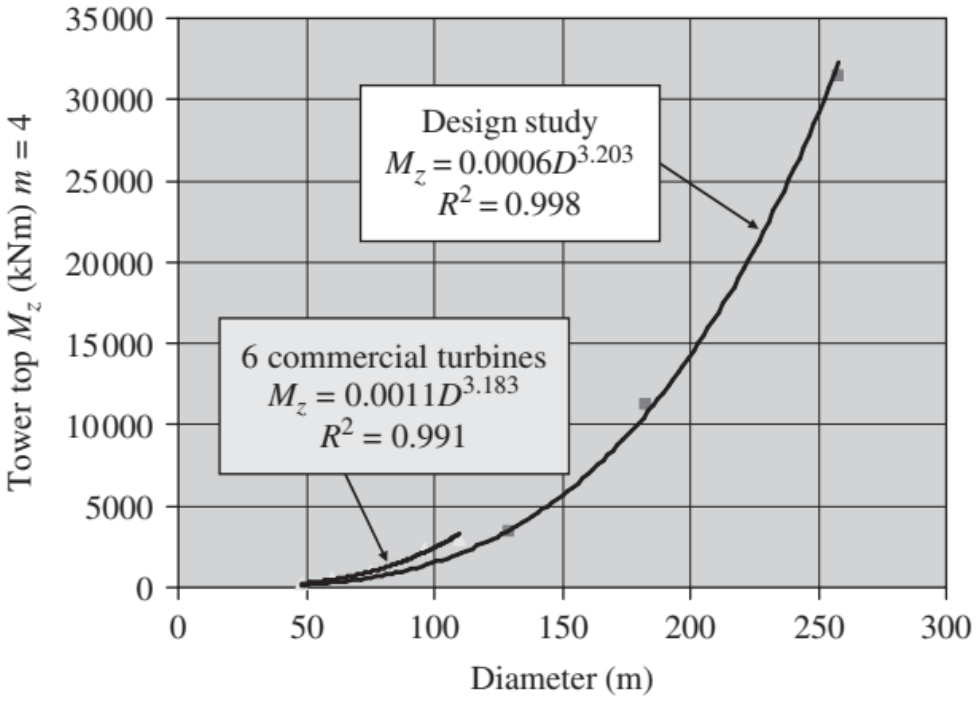

Figure 3.6. The trend of yaw torque on the tower [40]

As can be seen from Figure 3.4, the blade root out-of-plane bending moment follows $x^{3.069}$, a little less than the in-plane bending moment with $x^{3.192}$, shown in Figure 3.5. The tower torque follows $x^{3.203}$ relation with respect to the diameter of the rotor.

Upscaling the existing data trend has the advantage that it indirectly includes the improvement of technology due to the fact that as the turbine's size grows, the technology also gets more advanced. It is possible to utilize information from the turbines regardless of the state-of-the-art technology, starting from the early technology used in previous small wind turbines to the latest fully optimized direct-drive turbines. In fact, the more data of installed turbines gathered and used in the curve fitting process, the better the scaling relation between the intended design variables and rotor size will be.

The drawback of using existing data trends is that it is not recommended in designing very large turbines with rated power significantly higher than existing ones due to the uncertainties resulting from the extrapolation process [41]. Although it is a

straightforward procedure, it is not an easy process to do. An extensive amount of data is required to establish a fully functioning turbine. In many cases, detailed data on existing turbines are not publicly available since the competition in obtaining the most efficient turbine between companies is still going on. Obtaining publicly available data for floating offshore wind turbines is more challenging than for fixed bottom wind turbines. Because currently, a limited number of FOWT installations exist. Thus, establishing a curve-fitting relation for a floating platform is a challenge, and it is currently not practical.

3.1.2 Linear Scaling Rule

Upscaling process in this study is carried out using the linear scaling (similarity scaling) model. The linear scaling model is the most straightforward approach to designing large wind turbines. The process utilizes the analytical relation of some important variables in wind turbine design based on rotor size. The linear scaling rule benefits the research community by providing an initial approximation of large-scale wind turbines' structural, operational, and performance responses. It helps to identify the main design drivers when designing large wind turbines. However, considering that the scaling process does not contain any optimization, linear scaling will result in similar performance as the baseline turbine.

The linear scaling rule is based upon three main assumptions:

1. The number of blades and their material properties remains similar
2. The geometry of the turbines scaled linearly with the rotor size.
3. Constant tip speed ratio (TSR)

Having satisfied all the main assumptions, a scaling factor, s, is used to upscale the turbine. The scaling factor is defined as:

$$D_u = s\, D_b \quad \text{..... (3.1)}$$

where D denotes the rotor diameter, subscript *b* is for the baseline, and *u* is for the upscaled turbine.

The power of a wind turbine depends on the rotor's swept area. From the definition of power obtained from one-dimensional momentum theory and Equation 3.1, a relation between the scaling factor and power can be defined as:

$$\frac{P_u}{P_b} = \frac{\frac{1}{2}\rho_{air} V_{hub}^3 C_p \left(\frac{\pi}{4} s^2 D_b^2\right)}{\frac{1}{2}\rho_{air} V_{hub}^3 C_p \left(\frac{\pi}{4} D_b^2\right)} = s^2 \quad \text{..... (3.2)}$$

where P denotes power, ρ_{air} is the air density, V_{hub} is the mean wind speed at hub height, and C_p is the power coefficient. Thus, the scaling factor can be expressed as the square root of the turbine's rated power ratio.

To ensure the same material properties used in the baseline and upscaled turbines, the density of each component (the blade, tower, etc.) is kept constant. Considering Equation 3.1, the volume of the scaled blade will increase by the factor of s^3. Thus the relation between mass and scaling factor can be defined as:

$$\frac{m_u}{m_b} = \frac{\rho_{material}\, v_u}{\rho_{material}\, v_b} = \frac{\rho_{material}\,(v_b\, s^3)}{\rho_{material}\, v_b} = s^3 \quad \text{..... (3.3)}$$

where m denotes mass, $\rho_{material}$ is the material density, and v is the volume. Thus, the scaling factor can be expressed as the cubic root of the turbine's mass ratio. In other words, the mass has s^3 relation to rotor size. This is higher than the existing data trend due to the introduction of composite material for the giant blades.

Velocity for each blade element in a single blade is the same for the baseline and for the upscaled rotor due to the preservation of tip speed ratio (TSR). TSR is the ratio of the blade's tip velocity to the freestream velocity. When the length of the blade is increased by scaling factor s^1, the rotational speed (ω) is decreased by the factor of s^1 resulting in the product of the blade's rotational speed (ω) and the blade element's distance from the root (r) being independent of the power. It also causes the tip speed of the blade, and TSR in general, to be constant. The relation between the aerodynamic forces on the blade and the scaling factor can be defined as:

$$\frac{FL_u}{FL_b} = \frac{\int_{root_2^1}^{tip} \frac{1}{2}\rho_{air} V_{elem}^2 C_L \left(\frac{\pi}{4} s^2 D_b^2\right)}{\int_{root_2^1}^{tip} \frac{1}{2}\rho_{air} V_{elem}^2 C_L \left(\frac{\pi}{4} D_b^2\right)} = s^2 \quad \text{..... (3.4)}$$

$$\frac{FD_u}{FD_b} = \frac{\int_{root}^{tip} \frac{1}{2}\rho_{air} V_{elem}^2 C_D \left(\frac{\pi}{4} s^2 D_b^2\right)}{\int_{root}^{tip} \frac{1}{2}\rho_{air} V_{elem}^2 C_D \left(\frac{\pi}{4} D_b^2\right)} = s^2 \quad \text{..... (3.5)}$$

where FL denotes the lift force, FD is the drag force, C_L and C_D are the lift and drag coefficient, respectively. Thus, aerodynamic forces are increased by a factor of s^2 during the upscaling process.

Following the same procedure as aerodynamic forces, the aerodynamic moment shows a relation of s^3 during upscaling. This value agrees with the existing data trend shown in Figure 3.4 and 3.5. The blade element bending stiffness (EI) follows an s^4 rule, resulting in constant bending stress (My/EI) throughout the upscaling process.

Chaviaropoulos (2007), in the UPWIND project, carried out the analysis of most of the major components of the turbine, like rotor rotational speed, area inertia, mass inertia, etc. The similarity scaling is utilized to predict the turbine's loading and operational behavior as the turbine size increases. The scaling dependency used by Chaviaropoulos (2007) within the framework of the UPWIND project can be found in the UPWIND internal report, also cited in [28].

One main difference between the current study and Chaviaropoulos (2007) is in the tower length. In the present study, the tower length is upscaled such that the air gap between the tip of the blade and the base of the tower (top of the platform's main column) remains constant. The same approach of using a constant air gap in the upscaling process can be found in [22][42]. However, the diameter and shell thickness of the tower are scaled with the same scaling factor as the blade, s, to ensure the mass density distribution and the stiffness are consistent with the linear scaling law. The detailed scaling dependency of most of the components of the wind turbines used in this study (apart from the tower length) can be seen in Table 3.1, reproduced from the UPWIND internal report, as cited in [28].

Table 3.1 Size dependency of major design variables of a wind turbine (reproduced from [28])

Parameter	**Dependency**
Blade length	s
Blade mass	s^3
Rotor rotational speed	s^{-1}
Tip Speed	-
Chord length	s
Twist angle	-
Flapwise moment	s^3
Edgewise moment	s^3
Rotor power	s^2
Rotor torque	s^3
Rotor area moment of inertia	s^4
Rotor mass moment of inertia	s^5
Generator torque	s^3
Generator mass	s^3
Tower diameter and thickness	s
Tower fore-aft bending moment	s^3
Tower side-to-side bending moment	s^3
Torsional moment	s^3
Tower area moment of inertia	s^4
Tower mass moment of inertia	s^5

The OC4 semi-submersible floating platform is upscaled with the same scaling factor as the turbines, s. The geometry of the platform is assumed to vary linearly with rotor size. In the upscaling process, the diameter and shell thickness of main and outer columns, braces, and pontoons are upscaled with the s^1 relation. The elevation of the main and outer columns, offset distance of the outer columns, and the draft length of the semi-submersible is also upscaled to preserve the stabilization principle. The platform's steel and water ballast mass are scaled following the s^3 relation to maintaining the density of each material. The mass and inertia of the upscaled steel platform are input to the ElastoDyn, whereas the fluid ballast is used in the HydroDyn modules. The size dependency used in upscaling the platform is tabulated in Table 3.2.

Table 3.2 Size dependency of the semi-submersible platform

Parameter	Dependency
Length of the main and outer columns	s
Offset distance of outer columns	s
Elevation above mean seawater level	s
Draft length below mean seawater level	s
Shell thickness of all members	s
Mass of the platform	s^3
Mass of the ballast	s^3
The horizontal location of the fairing leads	s
Depth of the fairing lead	s

3.2 Baseline Wind Turbines

A faster improvement in wind energy technology can be achieved through a collective research contribution from many scientific backgrounds. However, detailed data on existing wind turbines are generally not publicly available, which creates a barrier to the collaborative development of the technology. In order to overcome this barrier, the National Renewable Energy Laboratory (NREL) and International Energy Agency (IEA) developed conceptual reference wind turbines (RWTs) to ensure that collaborative research can be carried out.

This study utilizes three reference wind turbines (RWTs). NREL 5 MW [14], together with the latest IEA 10 MW [15] and IEA 15 MW [16] reference wind turbines (RWTs), are used as the baseline turbines. All of the turbines are upwind, clockwise rotation turbines having variable speed and collective pitch control. The NREL Reference Open-Source Controller (ROSCO) [43] is used for all the reference turbines.

The blade of NREL 5 MW is based on DOWEC 6 MW blade [44][45][46], which utilizes the DU airfoil series. On the other hand, the blade of IEA 10 MW and IEA

15 MW are based on DTU 10 MW blade [47] having the FFA-W3 airfoil series. The key parameters of the three turbines are presented in Table 3.3.

Table 3.3 Characteristics of Reference Wind Turbines

Parameter	**NREL 5 MW** [14] [48]	**IEA 10 MW** [15]	**IEA 15 MW** [16][49]
Rated Electrical Power	5 MW	10 MW	15 MW
Number of Blades	3	3	3
Wind Regime	IEC class 2A	IEC class 1A	IEC Class 1B
Cut-in Wind Speed	3 m/s	4 m/s	3 m/s
Rated Wind Speed	11.40 m/s	11.00 m/s	10.59 m/s
Cut-out Wind Speed	25 m/s	25 m/s	25 m/s
Rotor Diameter	126.0 m	198.0 m	240.0 m
Airfoil Series	DU-Series	FFA-W3	FFA-W3
Hub Diameter	3.00 m	4.60 m	7.94 m
Hub Height	90 m	119 m	150 m
Drivetrain	Gearbox	Direct Drive	Direct Drive
Minimum Rotor Speed	6.9 rpm	6.0 rpm	5.0 rpm
Maximum Rotor Speed	12.10 rpm	8.68 rpm	7.56 rpm
Maximum Tip Speed	80 m/s	90 m/s	95 m/s
Hub Overhang	5.00 m	7.10 m	11.35 m
Shaft Tilt Angle	5.0 deg	6.0 deg	6.0 deg
Rotor Precone Angle	2.5 deg	4.0 deg	4.0 deg
Blade Prebend	-	6.2 m	4.0 m
Blade Mass	17,740 kg	47,700 kg	65,000 kg
Nacelle Mass	240,000 kg	542,600 kg	630,000 kg
Tower Mass	347,460 kg	628,442 kg	860,000 kg

A geometrical comparison of the three reference wind turbines is presented in Figure 3.7. All dimensions shown in the figure are in meters. The upper part of the figure

shows the top view of the three RWTs, where y-axis shows the rotor's overhang distance from the centerline of the tower. The precone angle of the three turbines can also be observed from the upper view of Figure 3.7. NREL 5 MW has a 2.5 degrees precone angle, whereas the other two RWTs have 4.0 degrees. The bottom part of Figure 3.7 shows the front view of the rotor, in which tower length and the rotor's size can be seen. Note that Figure 3.7 shows only the tower and Rotor-Nacelle-Assembly (RNA). Thus, the hub heights shown in Figure 3.7 are the hub height without the elevation of the semi-submersible included.

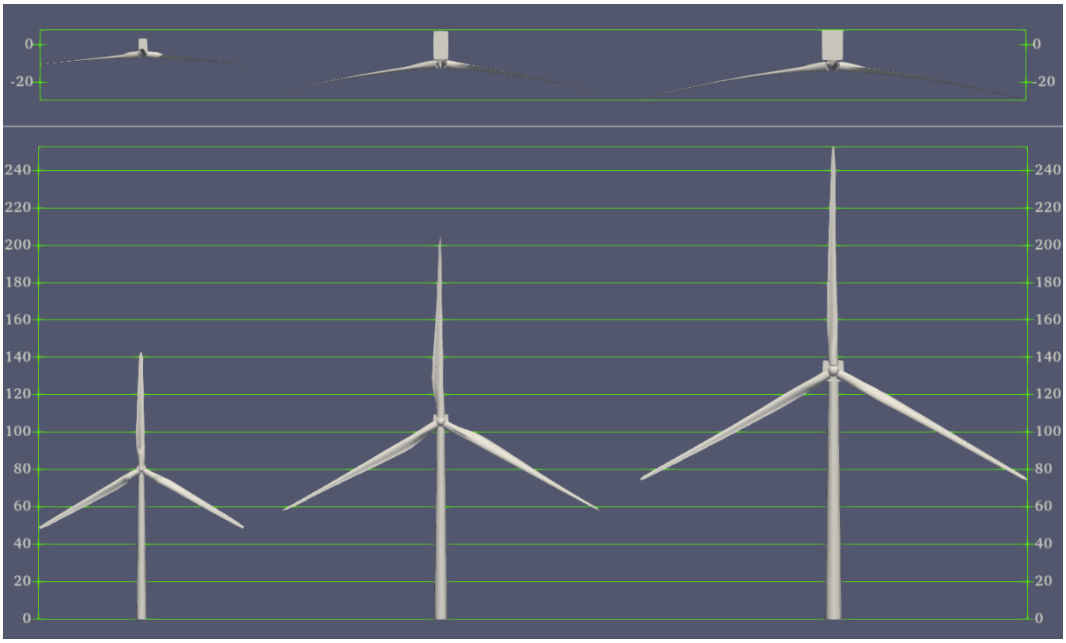

Figure 3.7. NREL 5 MW, IEA 10 MW, and IEA 15 MW Reference Wind Turbines

The normalized DU airfoil series' coordinates used in the DOWEC blade and FFA-W3 airfoil series' coordinates used in the DTU 10 MW are given in Figure 3.8. The airfoil coordinates are taken from the benchmark input files of NREL 5 MW and DTU 10 MW, available on the GitHub platform. The root of both blades is a cylinder, having a thickness to chord ratio of 100%. The last 2-digits of the DU-series represent the airfoil thickness to chord ratio, except for NACA64, whose airfoil thickness is 18%. For the FFA-W3 airfoil series, each airfoil's thickness to chord ratio is represented by the last 3-digits code.

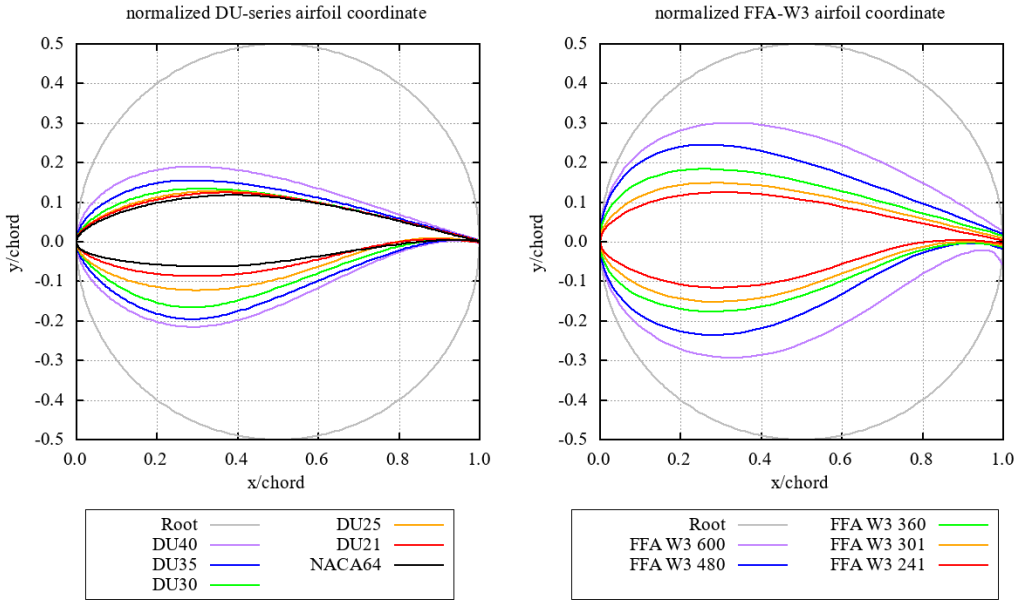

Figure 3.8. Normalized DU (left) and FFA-W3 (right) airfoil series coordinates

The distribution of chord length along the blade is shown in Figure 3.9. The data in the figure are taken from the AeroDyn module of the respective turbine. Despite being derived from the same blade of DTU 10 MW, the chord distribution of the IEA 10 MW and IEA 15 MW are relatively different, and the maximum chord of the IEA 10 MW is larger than the IEA 15 MW.

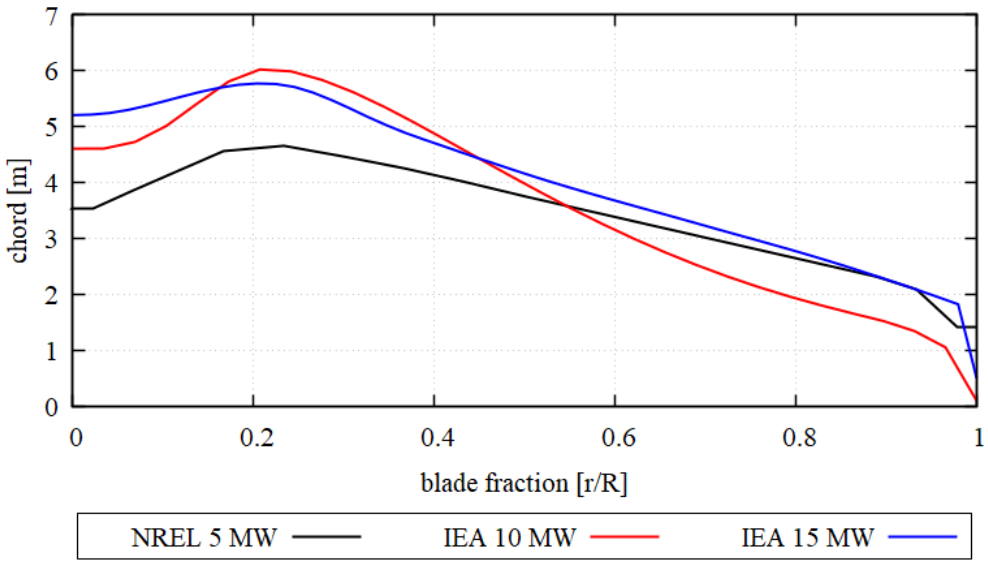

Figure 3.9. Chord length distribution of the reference wind turbines

The twist angle and blade mass density distribution are shown in Figure 3.10 and 3.11, taken from the AeroDyn and Elastodyn module of the respective turbine. The twist angle of IEA 10 MW and IEA 15 MW are alike due to the utilization of the same airfoil family. NREL 5 MW has a monotonic decrease in the twist angle that is different from the other two turbines. It can be seen in Figure 3.11 that only NREL 5 MW does not have a monotonic decrease in the mass density distribution.

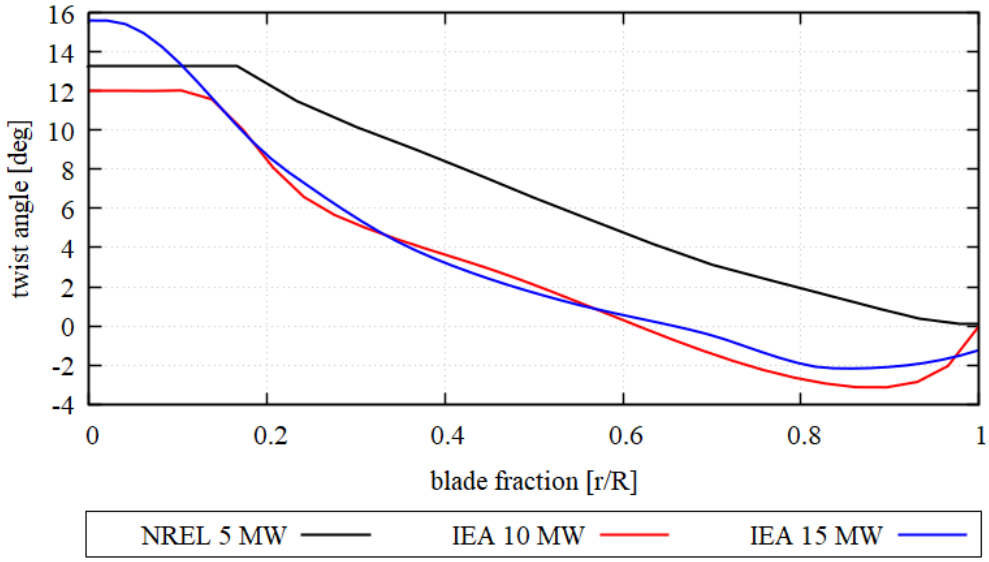

Figure 3.10. Twist angle distribution of the reference wind turbines

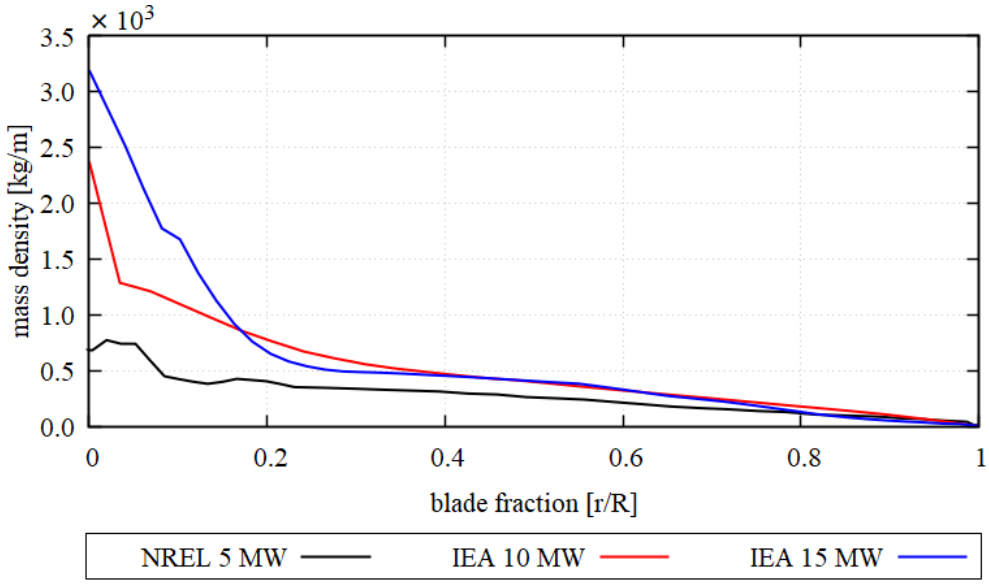

Figure 3.11. Blade's mass density distribution of the reference wind turbines

The edgewise and flapwise stiffness distribution along the blade is shown in Figure 3.12, taken from the ElastoDyn module of the respective turbine. Typically, the edgewise bending moment is present due to gravity, whereas the flapwise bending moment is due to aerodynamic loading. These stiffnesses are important design parameters since they help to determine the blade's structural behavior to resist bending in the in-plane and out-of-plane motion. The higher the blade's stiffness, the better the blade in resisting bending. However, higher stiffness is usually directly proportional to higher mass, which is counterproductive for upscaling.

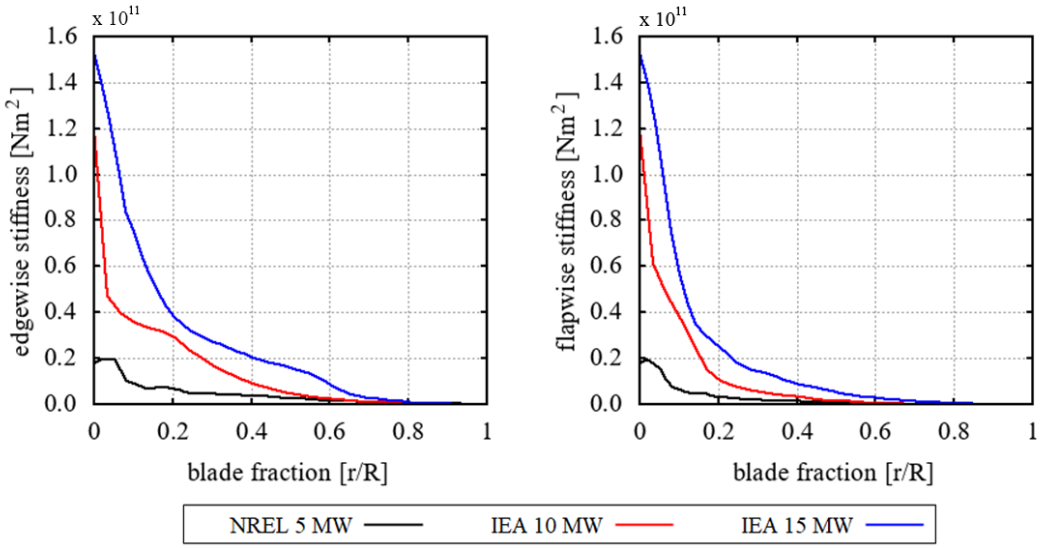

Figure 3.12. Blade's edgewise (left) and flapwise (right) stiffness distribution.

The tower of the three turbines has a hollow circular cross-section with varying diameters from base to top. Construction steel is used in the tower's design of the three turbines. Initially, the density of construction steel is 7850 kg/m^3. However, the density of the steel used for the tower structure of the three turbines is artificially increased to accommodate some secondary structures that are not accounted for in the model, such as ladders, elevators, etc. [15]. Due to having a circular cross-section, the forward-aft and side-side stiffness are identical to each other. The distribution of mass density, forward to aft, and side to side stiffness along the tower are given in Figure 3.13 and Figure 3.14, respectively. The properties distributions in both figures are taken from the ElastoDyn module of the respective turbine.

The base of all towers has the maximum mass density distribution due to having the largest cross-section (diameter and shell thickness) dimension. Then it gradually decreases, except for the topmost part of IEA 15 MW, where the shell thickness of the tower is reincreased, as described in [16].

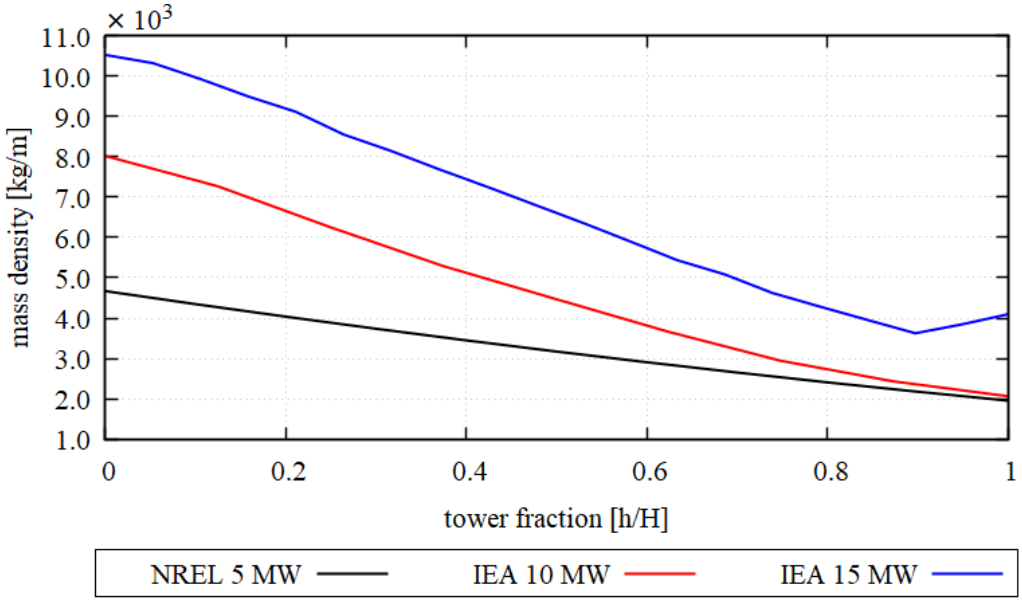

Figure 3.13. Tower's mass density distribution of the reference wind turbines

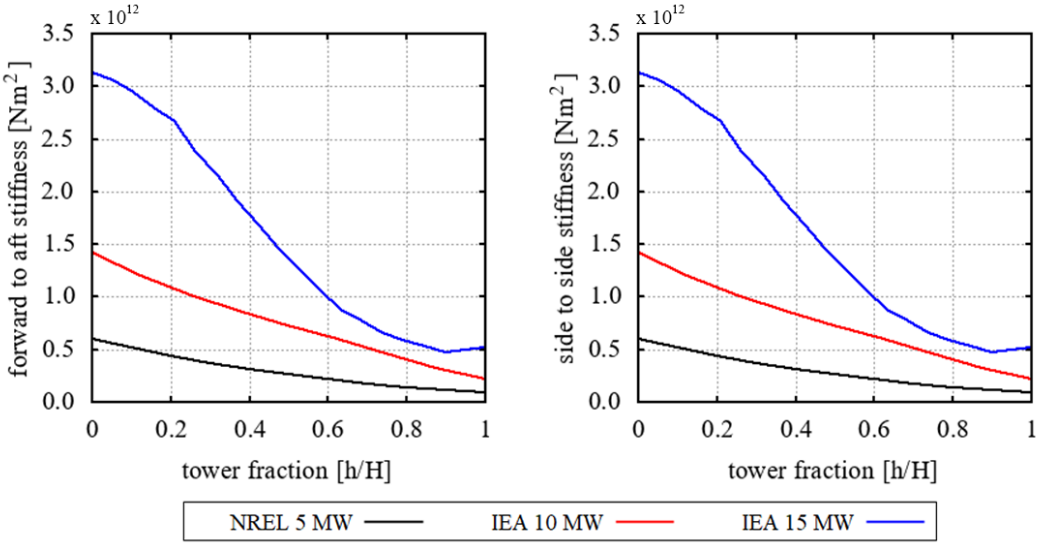

Figure 3.14. Forward-Aft (left) and Side-to-Side (right) stiffness distribution on the turbines' tower

3.3 Baseline Floating Platform

Phase II of the Offshore Code Comparison Collaboration Continuation (OC4) semi-submersible floating platform is used in this study [17]. This platform is made of steel (density = 7850 kg/m^3) and was initially designed to carry the NREL 5 MW in a 200-meter depth sea environment. The OC4-DeepCwind semi-submersible consists of 3 outer (offset) columns connected by braces to the central (main) column. Water ballast (density = 1025 kg/m^3) is used at the outer columns of the semi-submersible to lower the platform's center of gravity and increase pitch stability. The pontoons, cross braces and the main column is not ballasted.

Figure 3.15 shows the geometry of the OC4 semi-submersible and the mooring lines. The OC4-DeepCwind semi-submersible is anchored to the seabed using three catenary mooring lines and one of the mooring lines (green colored) is parallel to the global x-axis as can be seen from Figure 3.15. The fairleads are placed on top of the base column. The length of the mooring lines is designed such that some parts of the mooring lines lie on the seabed, causing only horizontal force on the anchor in still water conditions. In Figure 3.15, the thickness of the three mooring lines are exaggerated for visualization purposes.

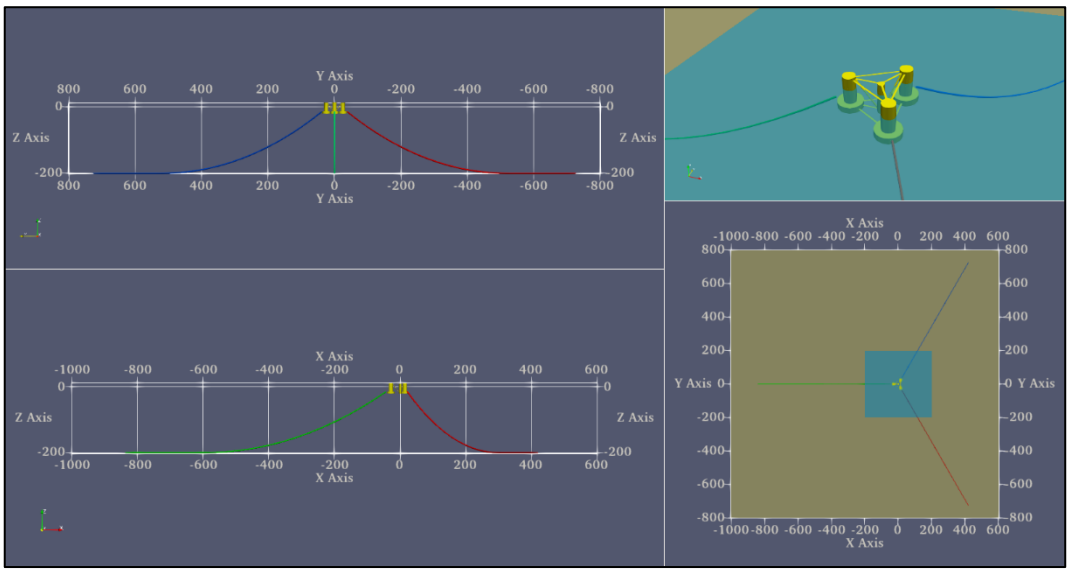

Figure 3.15. OC4-DeepCwind semi-submersible and the three mooring lines

As shown in Figure 3.15, not all the body of the OC4 semi-submersible platform is submerged in the water. The center column has a 10-meter elevation, whereas the three outer columns have a 12-meter elevation. Elevation of the main column of the platform, together with the tower length and RNA, as previously shown in Figure 3.7, extends the hub height of the NREL 5 MW to 90 meters above MSL.

The key parameters of the OC4-DeepCwind semi-submersible platform are shown in Table 3.4. and the properties of the mooring lines are presented in Table 3.5. Note that a perfectly flat seabed is assumed for the sea environment in this study. Thus, the properties of the mooring lines are identical to one another.

Table 3.4 Characteristics of OC4-DeepCwind semi-submersible [17]

Parameter	**Value**
Number of main (center) column	1
number of offset (outer) column	3
Elevation of the main column above SWL (tower base)	10.00 m
Elevation of offset column above SWL	12.00 m
Depth of platform base below SWL (total draft)	20.00 m
Distance of offset column from the main column	28.87 m
The angular displacement of the offset column	120 deg
Diameter of the main column	6.50 m
Length of the main column	30.00 m
Diameter of offset (upper) column	12.00 m
Length of offset (upper) column	26.00 m
Diameter of offset (lower) column	24.00 m
Length of offset (lower) column	6.00 m
Depth to top of offset (lower) column below SWL	14.00 m
Diameter of pontoon and cross braces	1.60 m
CM location below SWL	13.46 m
CB location below SWL	13.15 m

Table 3.5 Mooring lines of OC4-DeepCwind semi-submersible [17]

Parameter	Value
Number of Mooring Lines	3
Angle Between Adjacent Lines	120 deg
Depth to Anchors Below SWL	200.00 m
Depth to Fairleads Below SWL	14.00 m
Radius to Anchors from Main Column Centerline	837.60 m
Radius to Fairleads from Main Column Centerline	40.868 m
Unstretched Mooring Line Length	835.50 m
Mooring Line Diameter	0.0766 m
Equivalent Mooring Line Mass Density	113.35 kg/m
Equivalent Mooring Line Mass in Water	108.63 kg/m
Equivalent Mooring Line Extensional Stiffness	753.60 MN
Hydrodynamic Drag Coefficient for Mooring Lines	1.1

3.4 Design Load Cases (DLCs)

Design Load Cases (DLCs) are the environmental conditions, including wind and wave loads, applied to the turbines. Three of four DLCs are taken directly from phase II of Offshore Code Comparison Collaboration Continuation (OC4) in this study [39]. The details of the DLCs are presented in Table 3.6.

The key indicator for the hydrodynamic analysis performed in this study is the natural period, the Power Spectral Density (PSD), and the Response Amplitude Operator (RAO). RAO of the wind turbines is a nondimensional parameter based on a statistical method used to determine the likely behavior of wind turbines when operating under external load conditions. The RAO is used to determine the floating offshore wind turbine's response in one particular degree of freedom to one particular wave direction and period. If the RAO is equal to one, the FOWT moves together with the wave. If the RAO is larger than one, the FOWT moves more than

the wave and vice versa. The calculation of RAO of the FOWT is performed as mentioned in [19] using Equation 3.6:

$$S_q(\text{Hz}) = S_\eta(\text{Hz})\,|\text{RAO}\,(\text{Hz})|^2 \quad \text{..... (3.6)}$$

where S_q is the response spectral density, and S_n is the wave spectral density. The power spectral density (PSD) of the wave used in DLC 2.6 and 3.7 are shown in Figure 3.16.

The wave spectral density, $S_{n,}$ and the response spectral density, $S_{q,}$ are obtained using the Fast Fourier Transformation (FFT) method. The FFT method is used to decompose time series data into the frequency domain. The FFT results in complex numbers and a symmetric distribution, also known as mirroring. The absolute value and the first half of the mirror signals are used in constructing the PSD.

Table 3.6 Design Load Cases (DLCs) used in this study [39]

Load Case	**Description**	**Enabled DOFs**	**Wind Condition**	**Wave Condition**
1.3	Free Decay (surge, heave, pitch, yaw)	Platform, mooring	No wind	Still Water
2.6	RAO estimation without wind	Support structure	No wind	White noise PSD = $1m^2/Hz$ 0.05 - 0.25 Hz
3.7	RAO estimation with wind	All	Steady, uniform, V_{hub} = 8m/s	White noise PSD = $1m^2/Hz$ 0.05 - 0.25 Hz
-	Full speed range power Production	All	Steady, uniform, 3 to 25m/s	Irregular airy JONSWAP spectrum H_s = 6m, Tp = 10s

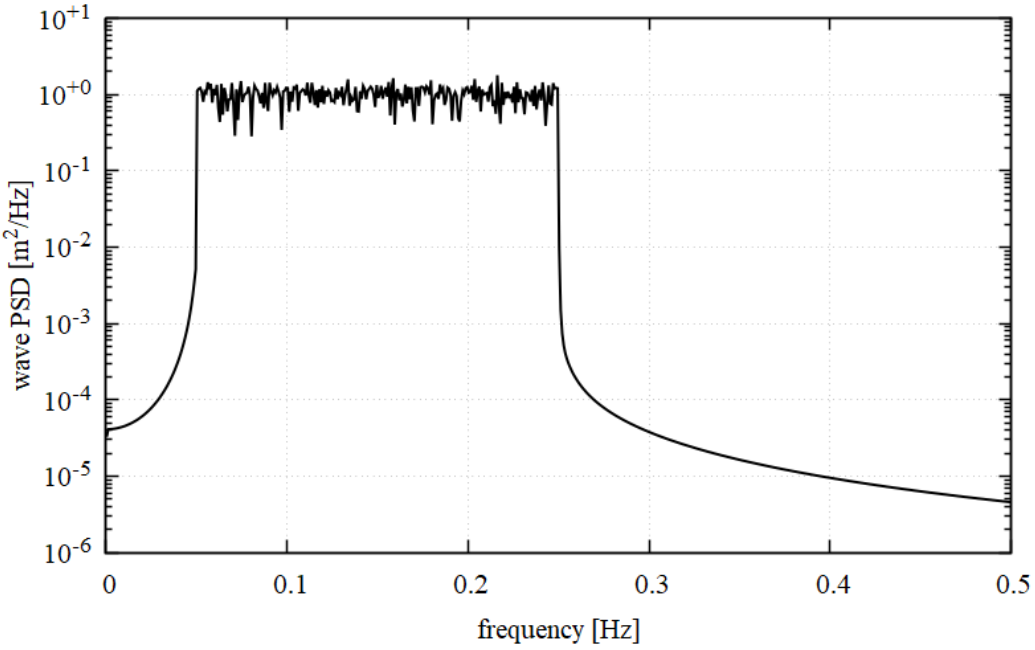

Figure 3.16. Power spectral density (PSD) of wave in DLC 2.6 and DLC 3.7

3.5 Numerical Programs

Numerical programs and methods are used in this study. Thus, the utilization of validated numerical programs to carry out the whole process in this study is crucial and mandatory. Apart from plotting and other post-processing software, there are at least four primary numerical programs needed to carry out the study. The hydrodynamic modeling of the platform is performed in HAMS. Optimization of the blade's aerodynamic shape is performed in HARP_Opt, while the structural configuration of the blade is designed in Co-Blade. Last but not least, OpenFAST is used to perform the nonlinear simulations of all the turbines. Brief reviews of each numerical program are summarized in the following subsections.

3.5.1 HAMS

Several options of numerical computation software like ANSYS AQWA, WAMIT, NEMOH, and HAMS are commonly used to analyze hydrodynamic structures.

Among the four codes, ANSYS AQWA and WAMIT are commercial software, whereas NEMOH and HAMS are open-source. In offshore wind industries, WAMIT is the most referred code, and its output can be directly used as an input for a time-domain solver like OpenFAST. However, the use of WAMIT is limited by its commercial license [50]. Summary of boundary element method solvers, generally used in analyzing hydrodynamic structures, are tabulated in Table 3.7.

Table 3.7 Boundary Element Method Solvers and their Characteristics from Combourieu et al., as cited in [50]

BEM Solver	Frequency domain	Time domain	Open-source	Usage (%)
WAMIT	+	-	-	80.5
NEMOH	+	-	+	19.5
AQWA	+	-	-	22.0
Aquaplus	+	-	-	9.8
ACHIL3D	-	+	-	4.9
WADAM	+	-	-	7.3
HAMS	+	-	+	NA

In the present study, Hydrodynamic Analysis of Marine Structures (HAMS) developed by Liu [51][52][53][54][55] is used. HAMS is software for computing wave diffraction and radiation of hydrodynamic structures. The selection of HAMS is due to its good agreement with WAMIT, despite being an open-source code. The comparison of the result of WAMIT, NEMOH, and HAMS can be found in [50]. HAMS' outputs are also available in WAMIT's format, which can be directly used in the HydroDyn module of OpenFAST.

The governing equations of HAMS are based on the potential flow theory. The flow is assumed to be inviscid, incompressible, and irrotational. In the entire fluid domain, potential flows automatically satisfy the Laplace equation due to the irrotational fluid assumption. The potential flow in HAMS is described as:

$$\varphi = \varphi_{\mathrm{i}} + \varphi_{\mathrm{d}} + \varphi_{\mathrm{r}} \quad \text{..... (3.7)}$$

whereas φ_i is the incident wave component, φ_d is the diffracted wave component, and φ_r represents the radiated wave component of the flow. A detailed and holistic explanation of the theory behind HAMS can be found in [51].

HAMS has a built-in mesh transformation code called WAMIT_MeshTran.exe to transform the geometric data files (.gdf) format of WAMIT into HAMS' meshing format. Only the platform's wetted (submerged) part is used in the calculation. The WAMIT_MeshTran.exe automatically distinguishes the hull from the waterplane area. The definition of the coordinate system used in HAMS is shown in Figure 3.17.

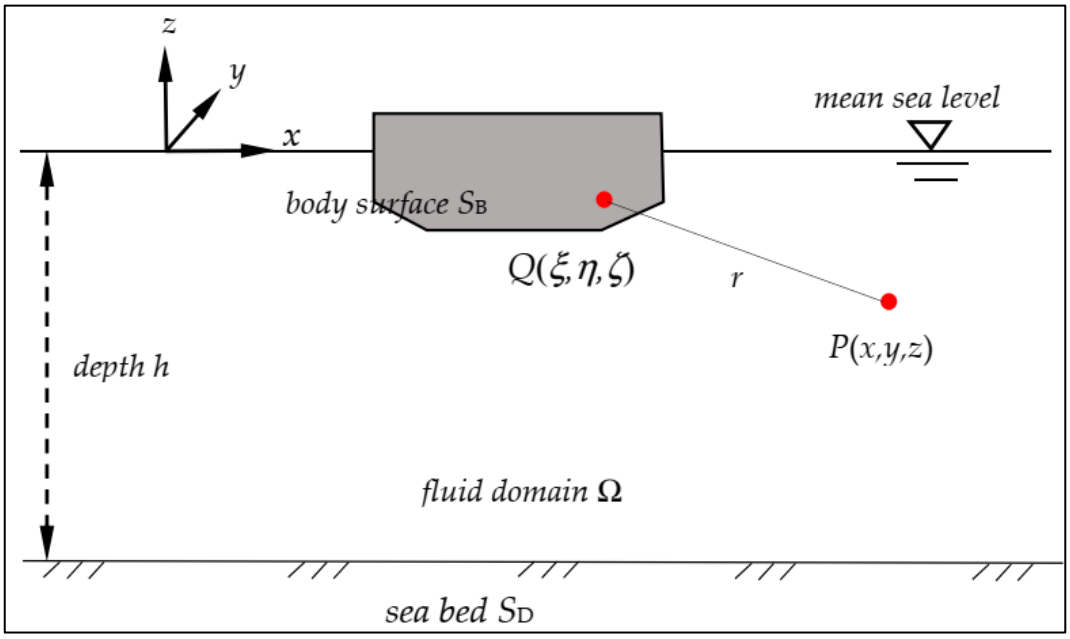

Figure 3.17. The coordinate system used in HAMS (reproduced from [51])

3.5.2 HARP_Opt

Optimization of the aerodynamic shape of turbines blade is important to improve the performance of wind turbines and increase power production. Several optimization codes are available to carry out the optimization process, like Horizontal Axis Wind Turbine Optimization 2nd generation (HAWT_Opt2) and Horizontal Axis Rotor Performance Optimization (HARP_Opt). HAWT_Opt2 has an interface to

Horizontal Axis Wind turbine simulation Code 2nd generation (HAWC2), a commercial aeroelastic simulation code developed by DTU. HARP_Opt, on the other hand, is an open-source code.

In the present study, the HARP_Opt code, written by Sale from NREL [56], is used to obtain the outer shell geometry to maximize the annual energy production (AEP). The HARP_Opt benefits from the genetic algorithm (GA) and from the NREL's WT-Perf, an open-source code to analyze wind turbine performance based on the blade element momentum (BEM) theory [57]. WT-Perf is developed by NREL before FAST's AeroDyn. Thus, most of the HARP_Opt's inputs are similar to the AeroDyn module. Recall that OpenFAST is in the present study. Thus, for practical reasons, HARP_Opt is used to perform the optimization in the present study. The workflow of HARP_Opt is shown in Figure 3.18.

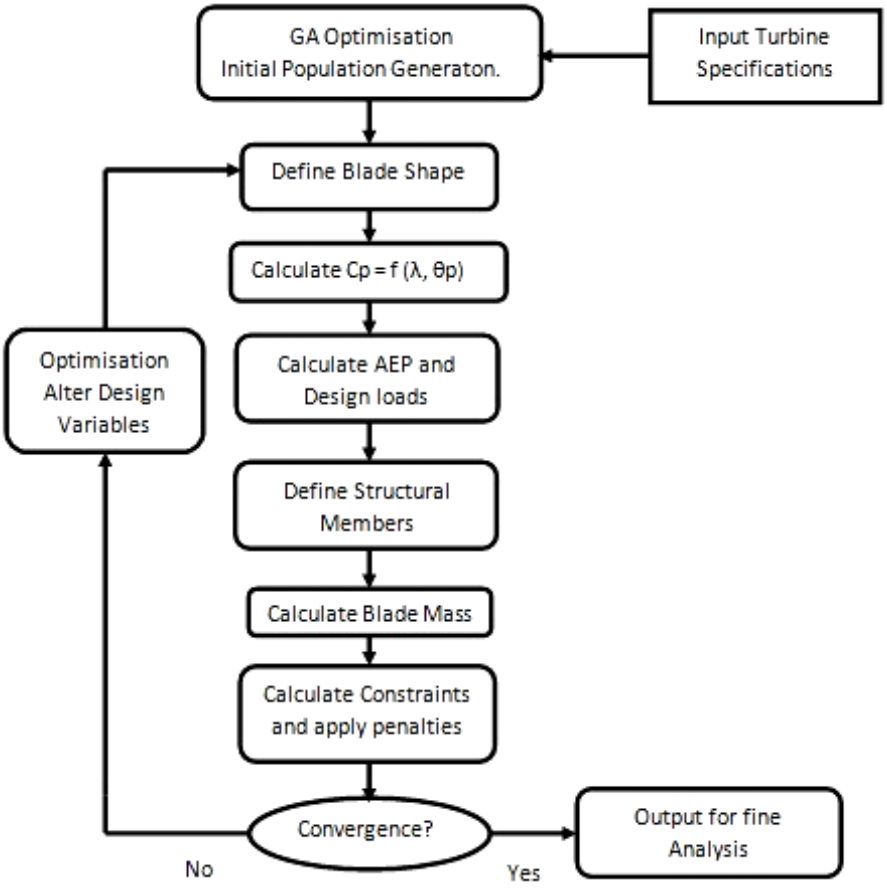

Figure 3.18. The working flowchart of HARP_Opt (reproduced from [35])

Genetic algorithm (GA) is an optimization technique based on the Darwinian evolution theory; survival of the fittest [58]. GA produces several sets of best individuals by mimicking the evolution theory on a set of random initial populations. That is by performing natural selection, mutation, inheritance, and crossover. The population dataset is modified one attribute at a time and run through numerous generations to assess the result and assign specific weights to each attribute. In this study, 100 individuals per generation are used, and 40% of it is created by cross-over. A maximum of 50 generations for GA iteration is used so that the computational cost of the optimization process can still be manageable.

The Blade Element Momentum (BEM) theory is one of the fundamental theories for wind energy. In the 1-dimensional momentum theory, the rotor is represented by a disk. The number of blades, actual of the rotor geometry, the twist and chord distribution, and the airfoils used is a blade is not considered. By coupling the 1-dimensional momentum theory with blade element theory, the local event occurring at any blade element can be better captured.

In the optimization process, to obtain high annual energy production (AEP), the location of airfoils, chord length, and twist angle are modified as free variables. The annual energy production of wind turbines is evaluated as given in Equation 3.8, as mentioned in [59].

$$AEP = \sum_{V_{cut-in}}^{V_{cut-out}} \frac{1}{2} (P(V_{i+1} + V_i)\, f(V_i < V < V_{i+1})) \,.\, 8760 \quad \text{..... (3.8)}$$

where P is the produced power as known in the turbine's power curve and f is the wind probability distribution function. 8760 denotes the number of hours within one year. A Weibull distribution with shape factor 2 and a scale factor of 6.8 is used in this study.

When HARP_Opt is used in the multi-objective genetic algorithm mode, a structural analysis is performed to minimize the blade mass. In HARP_Opt, the blade is modeled as a thin shell of bulk isotropic material without shear webs, and the mass of the blade is minimized such that the maximum allowable strain is never reached.

The strain at any local radial station along the blade is calculated using Equation 3.9 at four strain gages locations, as shown in Figure 3.19.

$$\varepsilon_r = \frac{S.F.\ M_r\ c_r}{E\ I_r} \quad \text{..... (3.9)}$$

where ε_r is the local strain, SF is the safety factor, M is the bending moment, c is the offset from the neutral axis, E is the young's modulus of elasticity of the material, and I is the area moment of inertia.

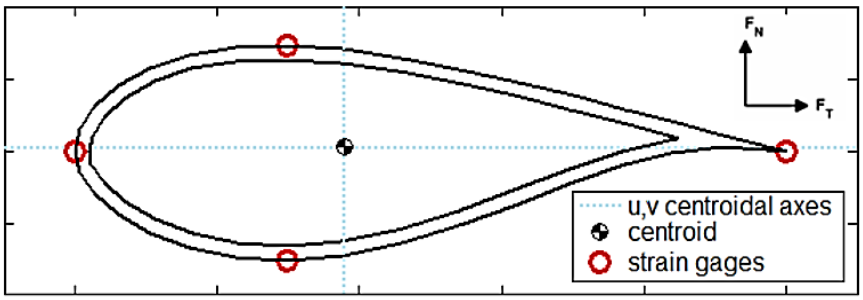

Figure 3.19. Location of four strain gauges at any radial station along the blade (reproduced from [56])

In the present study, the limit of the maximum chord and its location are set far above the unoptimized blade to make the optimization less constrained. But, the blade length and the root diameter are kept constant to use the same tower and hub. The same airfoil types as the original blade are used to minimize uncertainty in the optimization process. In doing so, the airfoil thickness distributions are modeled in a piecewise constant modeling. That is, by forcing an equal thickness percentage between the two control points.

A more detail explanation of the optimization process performed in this study will be discussed in Section 4.3. Prior to the present study, HARP_Opt has been widely used in the optimization process. For site-specific design optimization as carried out as in [34], for several small horizontal axis wind turbines as in [37][38], and for upscaling studies as performed in [35].

3.5.3 Co-Blade

Co-Blade is an open-source software capable of conducting structural analysis and design of composite blades [60]. Co-Blade was developed by the same author of HARP_Opt, Danny Sale. Thus, most of the inputs of Co-Blade are similar to HARP_Opt. In fact, Co-Blade was intended to be integrated with HARP_Opt to make a coupled aero-structural optimization program. The outputs of the Co-Blade are also tabulated in a similar fashion as ElastoDyn. For practical reasons, Co-Blade is selected to optimize the structural properties in this study.

Co-Blade is developed based on a combination of classical lamination theory (CLT) with an Euler-Bernoulli and shear flow theory applied on a composite beam. Classical lamination theory allows several layers of the lamina with different principle axis (commonly 0^o, $\pm 45^o$, 90^o) to be treated as a single material with superpositioned structural strength to a direction of interest. An illustration of the stacking of lamina and the effective multi-layer material resulting from classical lamination theory is presented in Figure 3.20

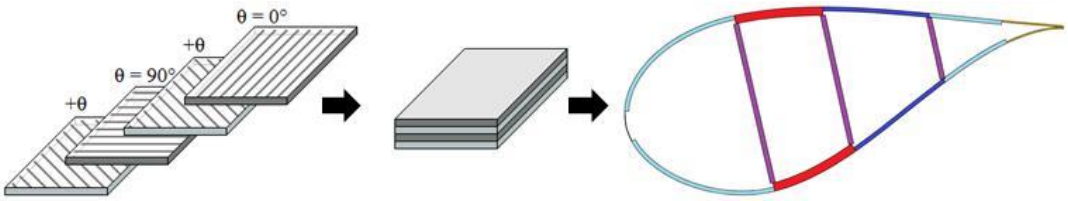

Figure 3.20. The illustration stacking of multiple lamina and the classical lamination theories' effective material used in Co-Blade (reproduced from [60])

Co-Blade models a turbine blade as an Euler-Bernoulli cantilever beam which undergoes flapwise and edgewise bending, elastic twist, and axial deflection [33]. In addition to the external load from wind, Co-Blade has the option to also include the body forces from self-weight and centrifugal forces to deflection of the beam to make the optimized blade more realistic.

The whole theory behind Co-Blade is beyond the scope of this thesis, and a more detailed explanation can be found in [60]. However, there are several assumptions used in Co-Blade:

1. Each blade section is a thin-walled, closed, single- or multi-cellular section.
2. The panels are modeled as thin plates with a pinned boundary condition on all edges of the plates.
3. The cross sections of the composite blade remain planar and consist of discrete areas of homogenous material.
4. The effective normal and shear stress acting on the beam are converted into equivalent thin plate loads.

If the optimization mode is enabled, Co-Blade determines the optimal location of the blade's pitching axis and the lightest composite layup that satisfies structural constraints such as maximum stress, buckling, etc. The illustration of the composite layup used in the Co-Blade is shown in Figure 3.21.

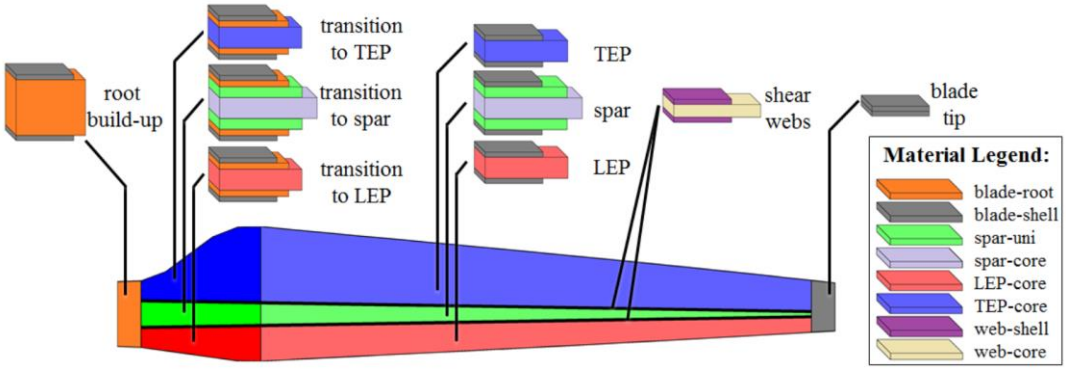

Figure 3.21. The illustration of the composite layup used in Co-Blade (reproduced from [60])

In the present study, the weight of the blade, centrifugal forces, and aerodynamic forces on the blade are enabled in the optimization process to produce a realistic optimized blade. The thickness of the blade shell, spar caps, shear web, and leading and trailing edge strengthener are free variables. A maximum tip deflection and a

minimum allowable difference between the blade rotation frequency and blade natural frequency are set as a constraint in the optimization process.

A more detail explanation of the optimization process performed in this study will be discussed in Section 4.3. Prior to the present study, Co-Blade was used in the optimization study of wind turbine's blade structure as in [61][62][63]. Sale, the author of Co-Blade, also optimize the structure of a 550 KW hydrokinetic turbines which had been previously designed in HARP_Opt [33].

3.5.4 OpenFAST v.2.5

Aero-elastic code is needed to simulate and analyze the performance of a wind turbine. In the present study, the OpenFAST v.2.5, developed by NREL [18], is used as the primary simulation tool, as well as the load and performance analysis tool for the floating offshore wind turbines. OpenFAST is an open-source code capable of simulating the dynamic response of two or three-blades, upwind or downwind horizontal axis wind turbines.

The selection of OpenFAST is due to its well-known reputation in the wind energy community for being user-friendly but accurate in simulating complex structures like floating offshore wind turbines. Another available aeroelastic code for simulating wind turbines is the Horizontal Axis Wind turbine simulation Code 2nd generation (HAWC2), developed by DTU. The HAWC2 code is an aero-elastic code intended for calculating wind turbine response in the time domain [65]. However, the use of HAWC2 is limited by its commercial license.

OpenFAST is developed upon the FAST v8.16 [64] open-source code as its starting point. Verification and validation of OpenFAST (or FAST) in simulating FOWT have been performed on many occasions and in several ways; against a real turbine, laboratory results, and other existing codes. Verification with real data of a 2.3 MW Siemens turbine mounted on a spar substructure showed a high agreement, as published in [66]. A validation case with a laboratory experiment focusing on the

mooring lines' dynamics had also been performed, as mentioned in [67]. Comparison with other existing codes focusing on semi-submersible platforms had been performed in the framework of Offshore Code Comparison Collaboration Continuation (OC4) wind task 30 [39].

OpenFAST couples a non-linear time-domain simulation for the wind turbine's structure, aerodynamics, hydrodynamics, control, and electrical system (servo). An example of modeling floating offshore wind turbines in OpenFAST is shown in the flowchart, shown in Figure 3.22. The flowchart is prepared by Jonkman from NREL, as can be found in [64] [68].

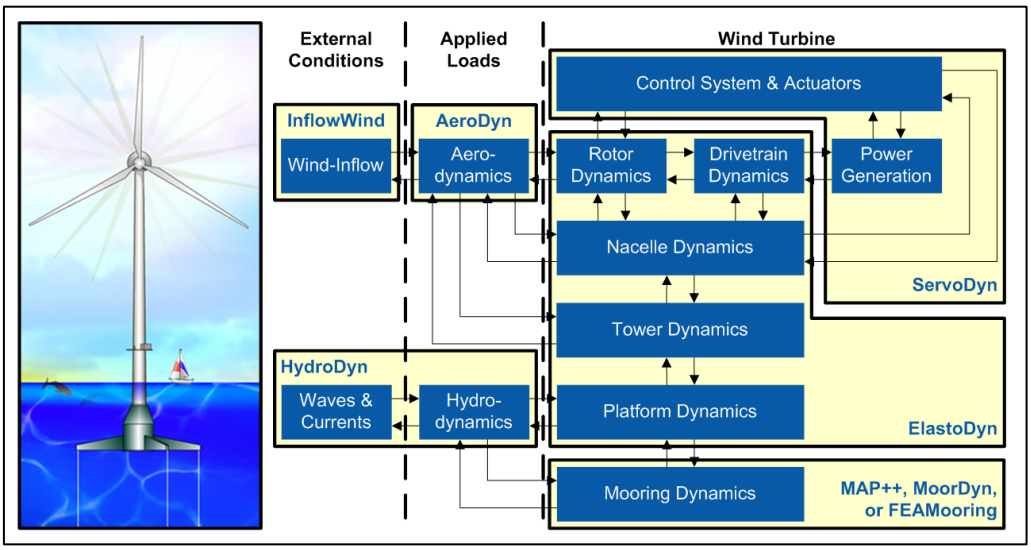

Figure 3.22. Flowchart of modeling in FAST (reproduced from [64])

As can be seen in Figure 3.22, OpenFAST is built upon several stand-alone open-source modules that can be coupled in the nonlinear simulation. The present study focuses on the aero-elastic and hydrodynamic parts of the simulation. In most simulations, the ElastoDyn, AeroDyn, InflowWind, ServoDyn, HydroDyn, and MAP++ modules are enabled, except in the design load case where no wind condition is applied.

The most updated wind turbine aerodynamics module of OpenFAST, AeroDyn15, calculates aerodynamic loads on both the blades and tower [69]. The AeroDyn15

requires the aerodynamic shape of the blade consisting of two-dimensional airfoil coordinates and aerodynamic force and moment coefficients, together with the span-wise distribution of airfoil location, chord length, and twist angle. The length-wise distribution of the tower's diameter and drag coefficients are needed for the tower. AeroDyn15 benefits from the blade element momentum (BEM) theory with dynamic stall and an optional dynamic inflow theory [70]. The wind loads are generated in the InflowWind module following the design load case mentioned in Section 3.4. The fluid properties used for the wind in the present study are ideal gas with a density of 1.225 kg/m^3 and kinematic viscosity of 1.478 x 10^5 m^2/s

In the HydroDyn module, the potential flow solution to substructures involving frequency to time domain transforms is applied. The utilization of a frequency domain panel code is necessary to obtain the linear hydrostatic restoring, the added mass and the damping coefficient. When coupled to OpenFAST, HydroDyn receives the substructure's real-time orientation, position, velocities, and accelerations. Hydrodyn then computes the hydrodynamic loads acting on the substructure and returns them to OpenFAST. During the calculation of loads in HydroDyn, the ElastoDyn module assumes the floating platform to be a rigid body. The wave loads are generated directly in the HydroDyn module following the design load case mentioned in Section 3.4. The fluid properties used in the present study are water with a density of 1025 kg/m^3, and water depth of 200-meters are applied to all floating offshore wind turbines in all ratings.

CHAPTER 4

NUMERICAL MODELING AND OPTIMIZATION

This chapter presents the numerical modeling of the baseline and the upscaled reference wind turbines and the OC4-DeepCwind semi-submersible platform. Additionally, in order to enhance the performance of NREL 5 MW, an aerodynamic optimization based on the blade element momentum and genetic algorithm theory, followed by structural optimization based on the classic lamination theory, is carried out and discussed.

4.1 Upscaling the Turbines

The upscaling of the wind turbines performed in this study follows the linear scaling approach explained in Section 3.1.2. All the turbines simulated in each power rating are summarized in Table 4.1.

Table 4.1 List of turbines compared in each power rating

Baseline RWTs	**Rated Power**			
	5 MW	**10 MW**	**15 MW**	**20 MW**
NREL 5	Baseline	Upscaled	Upscaled	Upscaled
NREL 5	Optimized	Upscaled + Optimized	Upscaled + Optimized	Upscaled + Optimized
IEA 10	-	Baseline	Upscaled	Upscaled
IEA 15	-	-	Baseline	Upscaled

Note that only NREL 5 is optimized in the present study, which will be discussed later in Section 4.3. At some plots from this section forward, the naming upscaled + optimized will be written as upscaled + opt to maintain the aesthetic of the figures. The geometries of all baseline and upscaled turbines are shown in Table 4.2.

Table 4.2 Result of linear upscaling of NREL 5 MW, IEA 10 MW and IEA 15 MW turbines

Parameter	Unit	5 MW	10 MW		15 MW			20 MW		
		NREL5	Upscaled NREL 5	IEA 10	Upscaled NREL 5	Upscaled IEA 10	IEA 15	Upscaled NREL 5	Upscaled IEA 10	Upscaled IEA 15
Scale Factor	-	1.00E+0	1.41E+0	1.00E+0	1.73E+0	1.22E+0	1.00E+0	2.00E+0	1.41E+0	1.15E+0
Rotor radius	m	6.30E+1	8.91E+1	9.92E+1	1.09E+2	1.21E+2	1.20E+2	1.26E+2	1.40E+2	1.39E+2
Hub radius	m	1.50E+0	2.12E+0	2.40E+0	2.60E+0	2.94E+0	3.00E+0	6.00E+0	3.39E+0	3.46E+0
Hub height	m	9.00E+1	1.20E+2	1.19E+2	1.43E+2	1.46E+2	1.50E+2	1.63E+2	1.66E+2	1.71E+2
Tower base diameter	m	6.50E+0	9.19E+0	7.85E+0	1.13E+1	9.61E+0	1.00E+1	1.30E+1	1.11E+1	1.16E+1
Tower top diameter	m	3.87E+0	5.47E+0	5.50E+0	6.70E+0	6.74E+0	6.50E+0	7.74E+0	7.78E+0	7.51E+0
Rotor Speed	rpm	1.21E+1	8.56E+0	8.68E+0	6.99E+0	7.09E+0	7.56E+0	6.05E+0	6.14E+0	6.55E+0

*the value of upscaled and upscaled + optimized version of NREL 5 for each power rating are identical

4.1.1 Linear Scaling of NREL 5 MW

The size comparison for NREL 5 MW and its upscaled versions at each power rating can be found in Figure 4.1. As can be observed from the figure, the rotor length is increased by a factor of s^1 so that the 20 MW's rotor radius is twice as big as the baseline's. However, hub height does not increase with the s^1 scaling factor since tower length is upscaled such that the air gap between the blade's tip and the base of the tower remains the same. Note that in Figure 4.1, the platforms' elevations have been reduced from the turbines' hub height at each power rating.

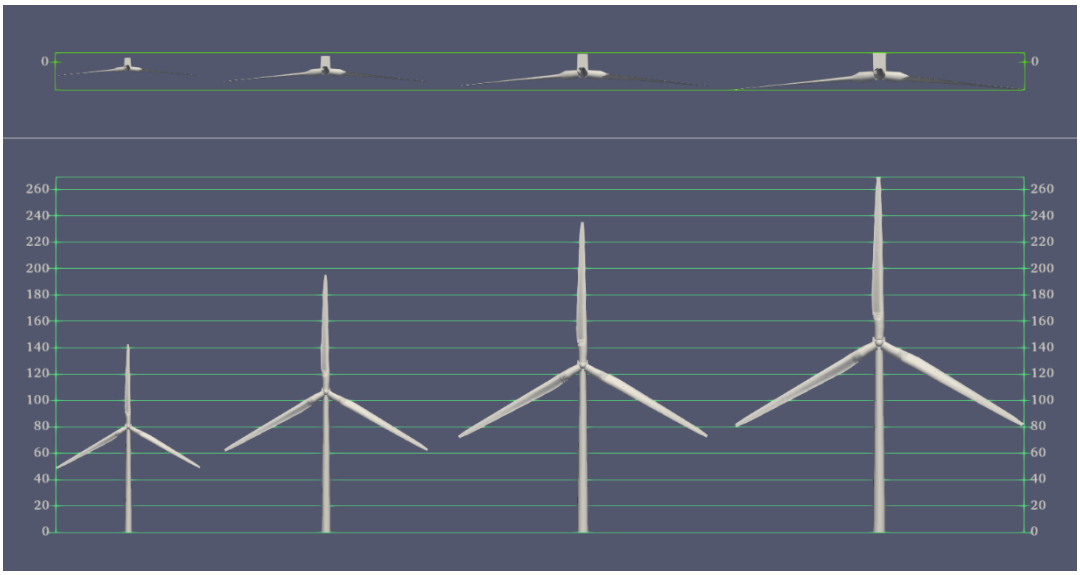

Figure 4.1. Size comparison of NREL 5 at 5 MW, 10 MW, 15 MW, and 20 MW

The distribution of chord length and twist angle along the blades are shown in Figure 4.2 to 4.3, respectively. From linear scaling, the chord length at each station follows the s^1 scaling factor so that the chord length of the 20 MW blade is twice as large as the original NREL 5 MW. However, the twist angle at each station is independent of rotor size. In other words, its distribution remains the same regardless of the size of the turbines. Thus, all the twist angles that are shown in Figure 4.3 lie on top of each other, and only one line can be seen in the figure. Notice that the twist angles are monotonically decreasing, which is typically true for the DU airfoil series.

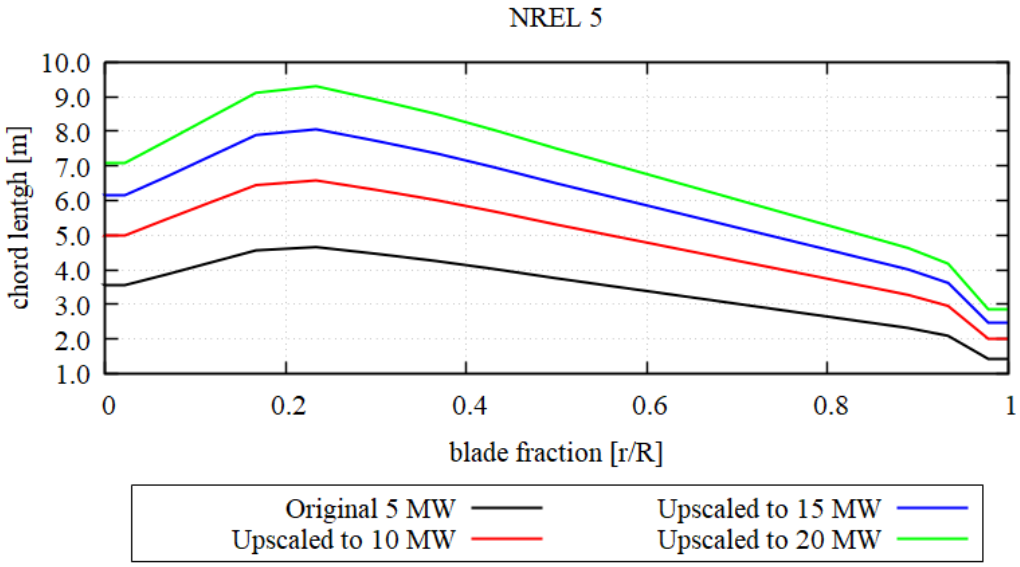

Figure 4.2. Chord distribution of NREL5 and its upscaled blade up to 20 MW

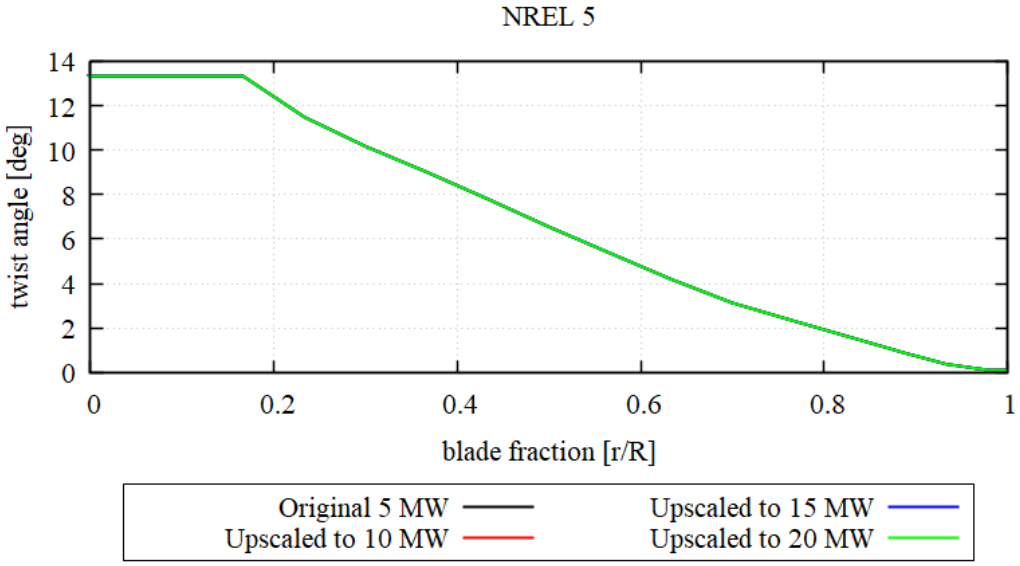

Figure 4.3. Twist angle distribution of NREL5 and its upscaled blade up to 20 MW

Following linear scaling, the mass of the blade has a scaling factor of s^3. However, in the ElastoDyn module, mass density (kg/m) distribution is used instead of mass (kg) distribution. Thus, a scaling factor of s^2 is used instead of s^3 in the upscaling process. The edgewise and flapwise stiffness, EI (in Nm^2), follows the s^4 scaling

factor. The distribution of mass density, edgewise stiffness, and flapwise stiffness along the blades are shown in Figure 4.4 – Figure 4.6.

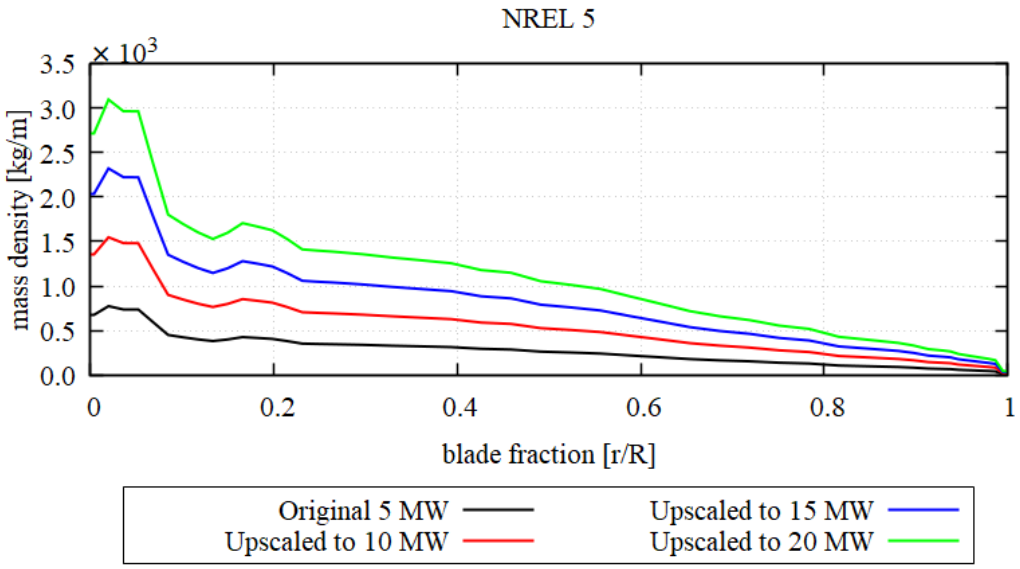

Figure 4.4. Blade mass density distribution of NREL5 and its upscaled blade up to 20 MW

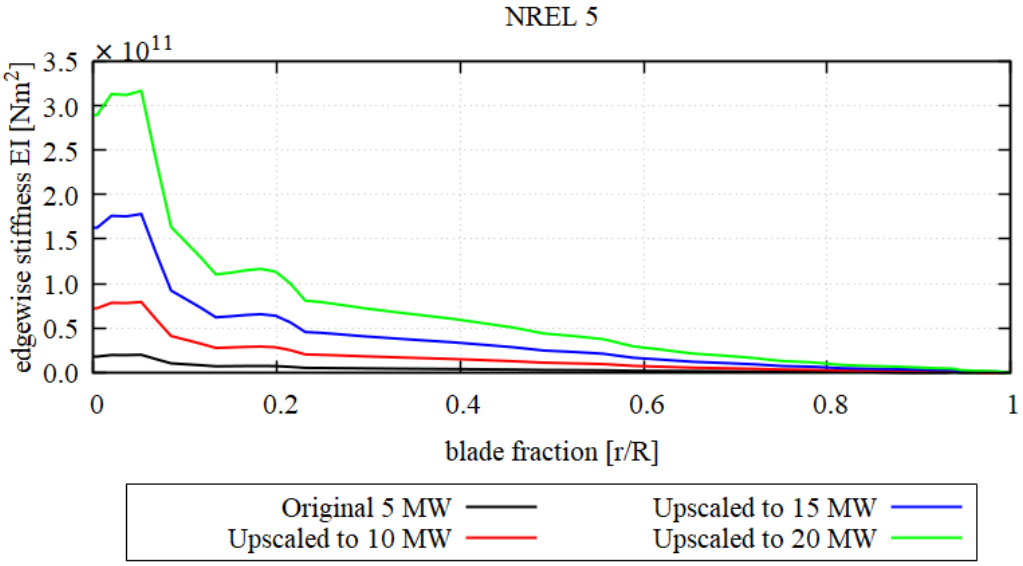

Figure 4.5. Blade edgewise stiffness distribution of NREL5 and its upscaled blade up to 20 MW

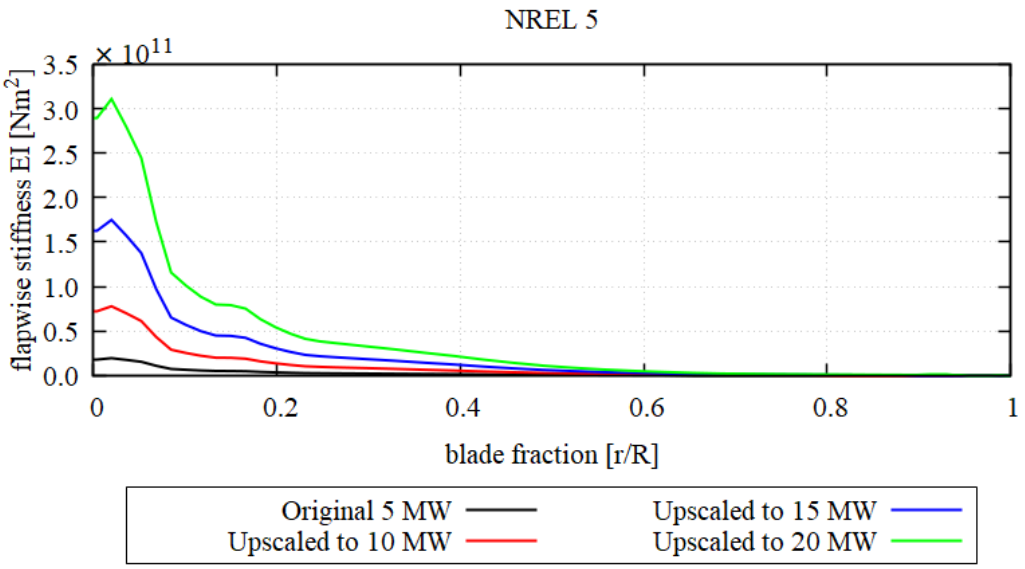

Figure 4.6. Blade flapwise stiffness distribution of NREL5 and its upscaled blade up to 20 MW

The mass density distribution along the towers is presented in Figure 4.7. The tower fraction indicates the normalized height of the tower element from the base to the top. As can be seen from Figure 4.7, the base of the tower has the maximum mass density distribution due to having the largest dimension. Then it gradually decreases to the top.

Following linear scaling, the tower's mass has a scaling factor of s^3. But again, in the ElastoDyn module, mass density (kg/m) distribution is used instead of mass (kg) distribution, and the properties are distributed for normalized tower length (i.e., 0 to 1). Thus, a scaling factor of s^2 is used instead of s^3 in the upscaling process. It is advantageous since the tower's length is not scaled with the s^1 scaling factor. However, the diameter and shell thickness of the tower follows the s^1 relation. Thus, using the scaling factor of s^2 guarantees that the material properties are conserved during the upscaling process.

The fore-aft and side-side stiffness of the tower, EI (in Nm^2), follows the s^4 scaling factor. Recall that the tower has a hollow circular cross-section. Thus, the fore-aft

and side-side stiffness in each section for each tower are identical. The distribution of the fore-aft and side-side stiffness along the tower can be seen in Figure 4.8.

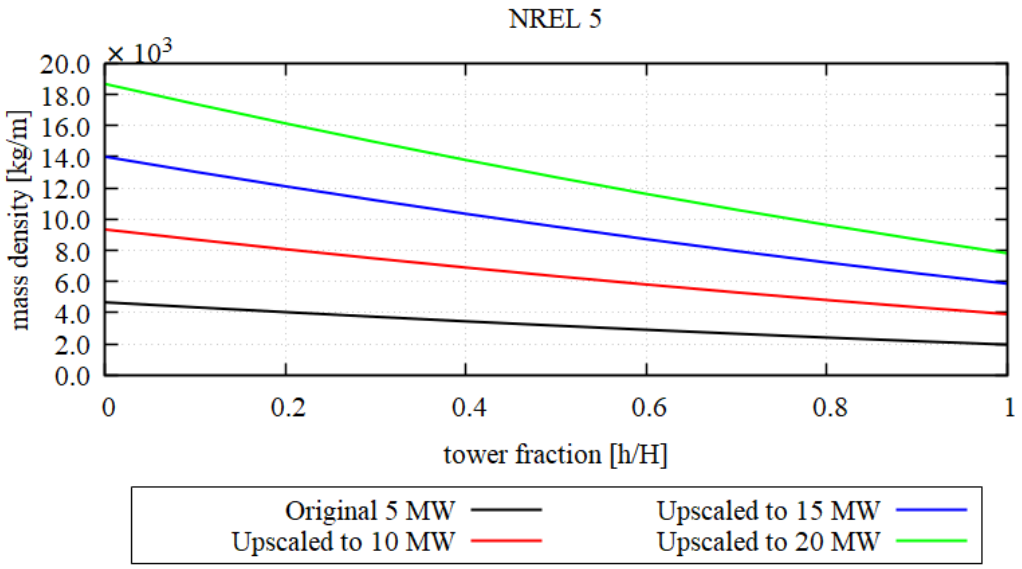

Figure 4.7. Tower mass density distribution of NREL 5 and its upscaled tower up to 20 MW

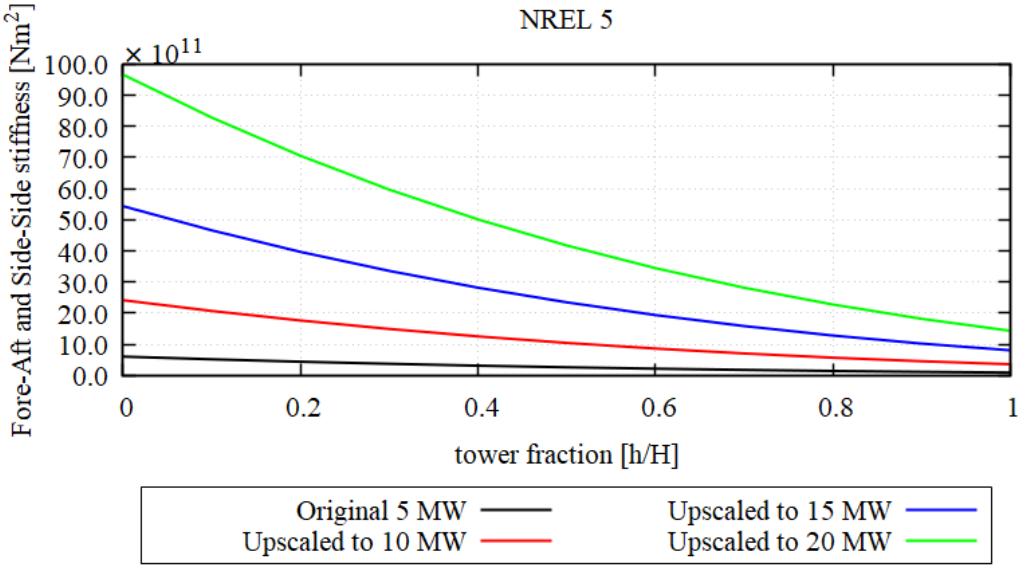

Figure 4.8. Tower fore-aft and side-side stiffness distribution of NREL 5 and its upscaled tower up to 20 MW

4.1.2 Linear Scaling of IEA 10 MW

Linear scaling of IEA 10 MW resulted in 2 larger turbines, rating 15 MW and 20 MW. The size comparison for IEA 10 MW and its upscaled versions up to 20 MW can be seen in Figure 4.9. Again, the platforms' elevations have been reduced from the turbines' hub height at each power rating. Rotor length is increased by a factor of s^1 so that the 20 MW's rotor radius is around 1.4 the size of the baseline, as shown in Figure 4.9. However, hub height does not increase with the s^1 scaling factor since tower length is upscaled such that the air gap between the blade's tip and the base of the tower remains constant during the upscaling process.

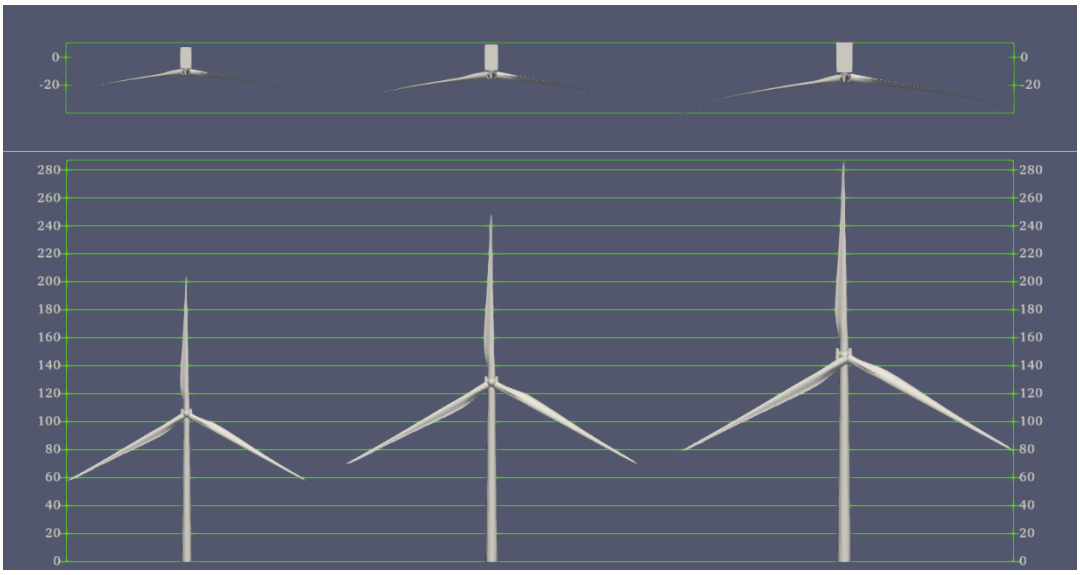

Figure 4.9. Size comparison of IEA 10 at 10 MW, 15 MW, and 20 MW

The distributions of chord length and twist angle along the blades are shown in Figure 4.10 and Figure 4.11, respectively. Following linear scaling, the chord length at each station follows has a s^1 scaling factor so that the chord length of the 20 MW blade is 1.4 times larger than the original IEA 10 MW. However, the twist angle at each station is independent of rotor size. In other words, its distribution remains the same regardless of the size of the turbines. Thus, all the twist angles that are shown in Figure 4.11 lie on top of each other and only one line can be seen in the figure.

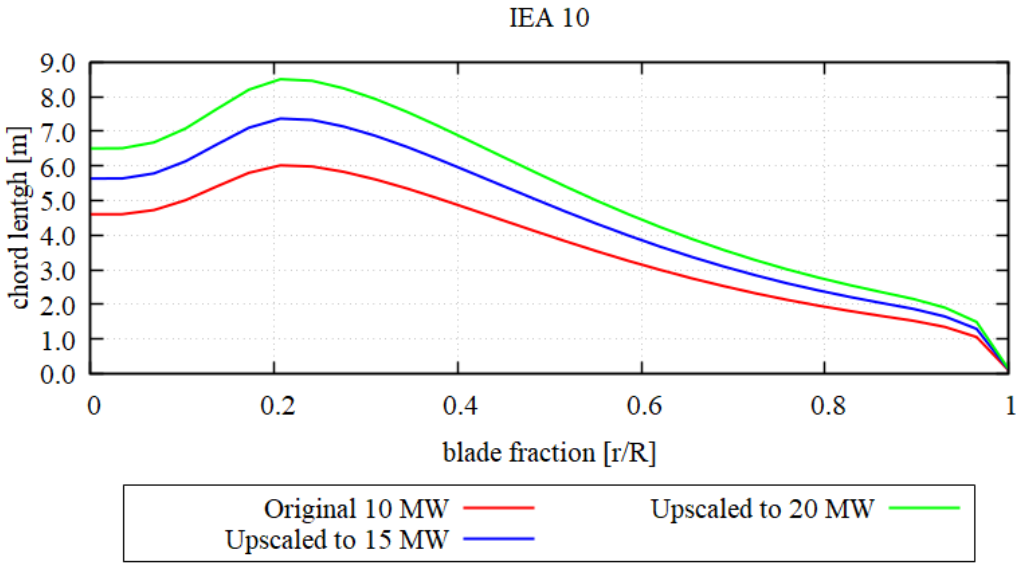

Figure 4.10. Chord distribution of IEA 10 and its upscaled blade up to 20 MW

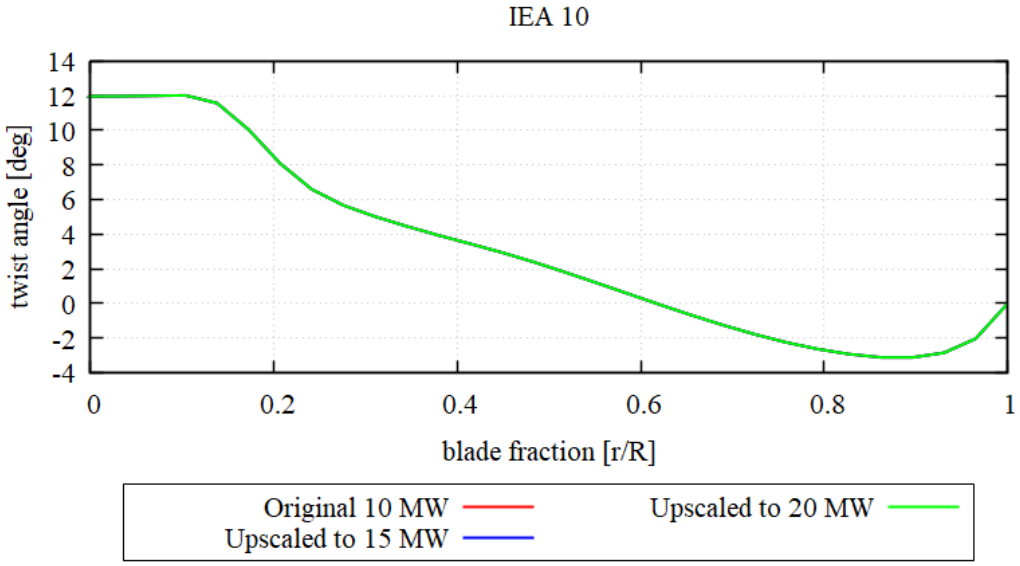

Figure 4.11. Twist angle of IEA 10 and its upscaled blade up to 20 MW

Following linear scaling, the mass of the blade has a scaling factor of s^3. However, the ElastoDyn module uses mass density (kg/m) distribution instead of mass (kg) distribution. Thus, a scaling factor of s^2 is used instead of s^3 in the upscaling process. The edgewise and flapwise stiffness, EI (in Nm^2), follows the s^4 scaling factor. The

distributions of mass density, edgewise stiffness, and flapwise stiffness along the normalized blade length are shown in Figure 4.12 – Figure 4.14.

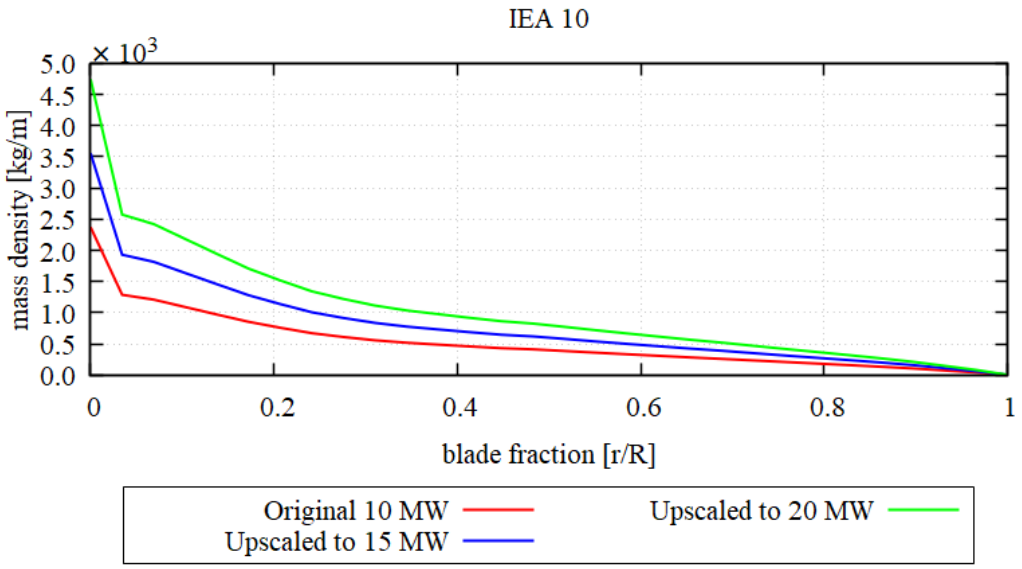

Figure 4.12. Blade mass density distribution of IEA 10 and its upscaled blade up to 20 MW

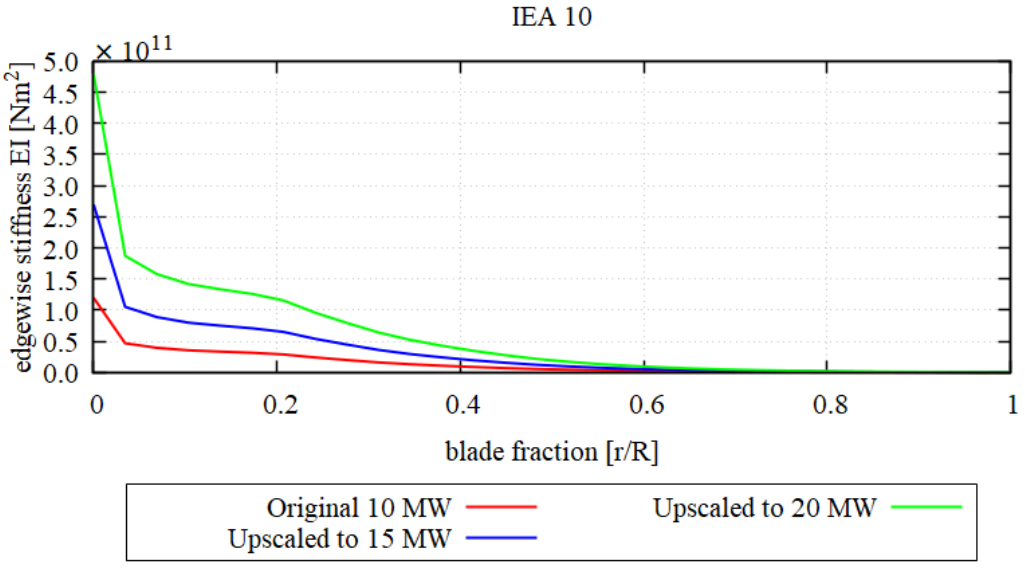

Figure 4.13. Blade edgewise stiffness distribution of IEA 10 and its upscaled blade up to 20 MW

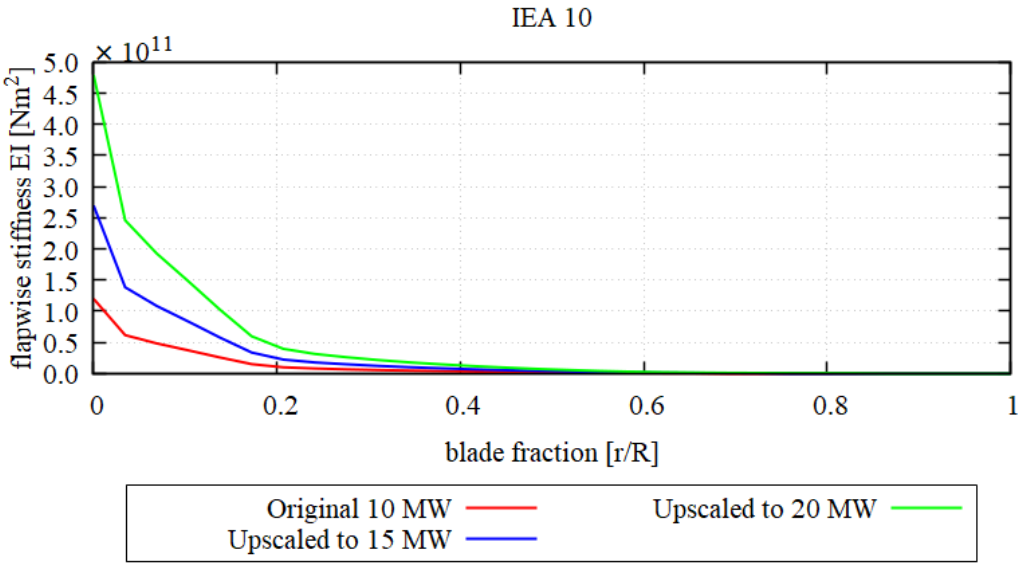

Figure 4.14. Blade flapwise stiffness distribution of IEA 10 and its upscaled blade up to 20 MW

The mass density distributions along the towers are presented in Figure 4.15. The tower fraction indicates the normalized height of the tower element from the base to the top. As can be seen from Figure 4.15, the base of the tower has the maximum mass density distribution due to having the largest dimension. Then it gradually decreases to the top.

Following linear scaling, the tower's mass has a scaling factor of s^3. But again, in the ElastoDyn module, mass density (kg/m) distribution is used instead of mass (kg) distribution, and the properties are distributed for normalized tower length (i.e., 0 to 1). Thus, a scaling factor of s^2 is used instead of s^3 in the upscaling process. It is advantageous since the tower's length is not scaled with the s^1 scaling factor. However, the diameter and shell thickness of the tower follows the s^1 relation. Thus, using the scaling factor of s^2 guarantees that the tower's material properties of the IEA 10 MW are conserved during the upscaling process.

The fore-aft and side-side stiffness of the tower, EI (in Nm^2), follows the s^4 scaling factor. Recall that the tower has a hollow circular cross-section. Thus, the fore-aft

and side-side stiffness in each section for each tower are identical. The distribution of the fore-aft and side-side stiffness along the tower can be seen in Figure 4.16.

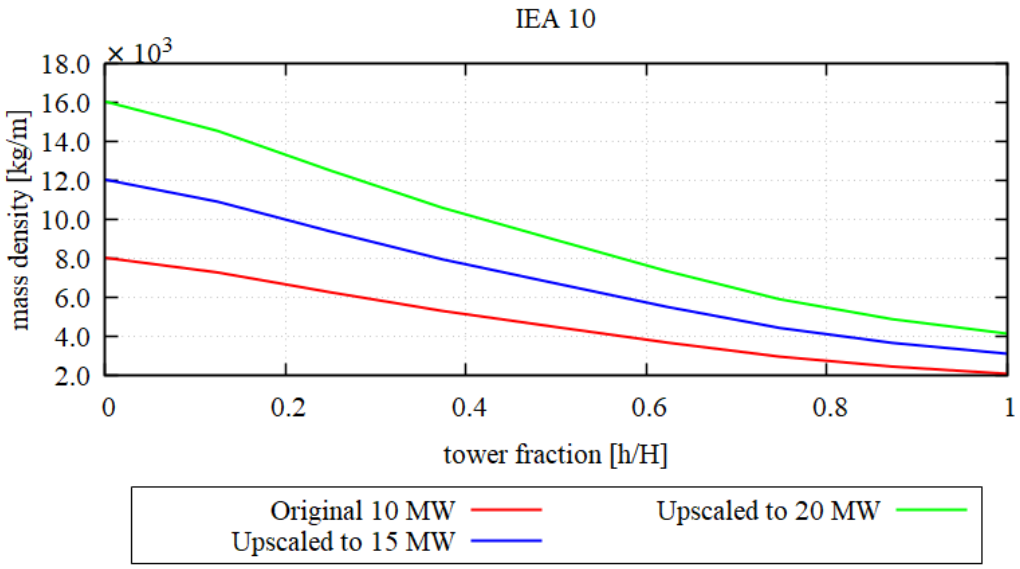

Figure 4.15. Tower mass density distribution of IEA 10 and its upscaled tower up to 20 MW

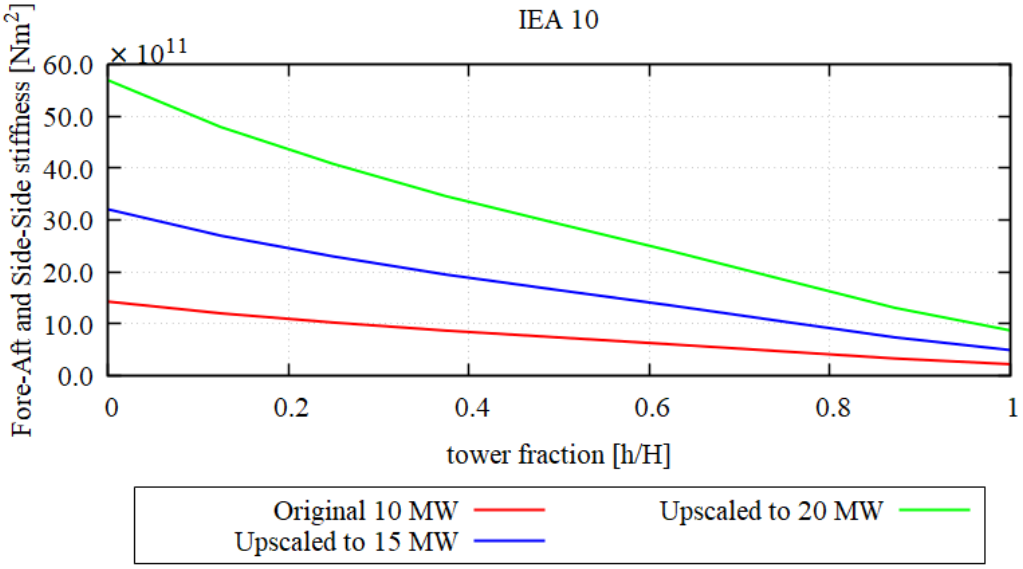

Figure 4.16. Tower fore-aft and side-side stiffness distribution of IEA 10 and its upscaled tower up to 20 MW

4.1.3 Linear Scaling of IEA 15 MW

Linear scaling of IEA 15 MW resulted in 1 larger turbine, rating 20 MW. Figure 4.17 shows the size comparison of IEA 15 MW and its upscaled version at 20 MW. Once again, the platforms' elevations have been reduced from the turbines' hub height at each power rating. The rotor length follows a scaling factor of s^1 so that the 20 MW's rotor radius is around 1.15 times the size of the baseline IEA 15 MW, as shown in Figure 4.17. However, hub height does not increase with the s^1 scaling factor since tower length is upscaled such that the air gap between the blade's tip and the base of the tower remains the same throughout the upscaling process.

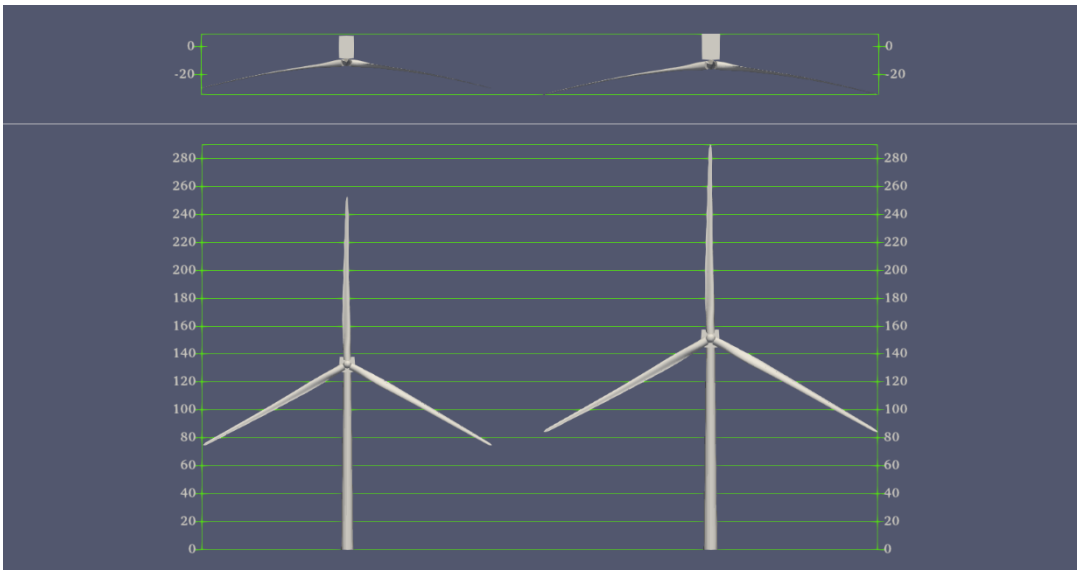

Figure 4.17. Size comparison of IEA 15 at 15 MW and 20 MW

The distributions of chord length and twist angle along the blades are shown in Figure 4.18 to Figure 4.19, respectively. Following linear scaling, the chord length at each station has an s^1 scaling factor so that the chord length of the 20 MW blade is 1.5 times larger than the original IEA 15 MW. However, the twist angle at each station is independent of rotor size. In other words, its distribution remains the same regardless of the size of the turbines. Thus, all the twist angles that are shown in Figure 4.19 lie on top of each other, and only one line can be seen in the figure.

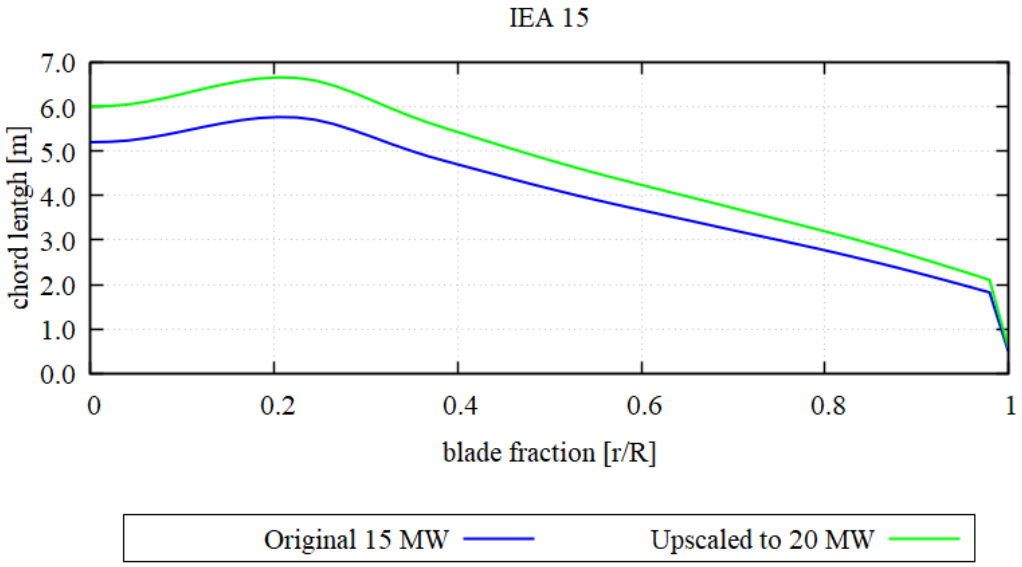

Figure 4.18. Chord length distribution of IEA 15 and its upscaled blade to 20 MW

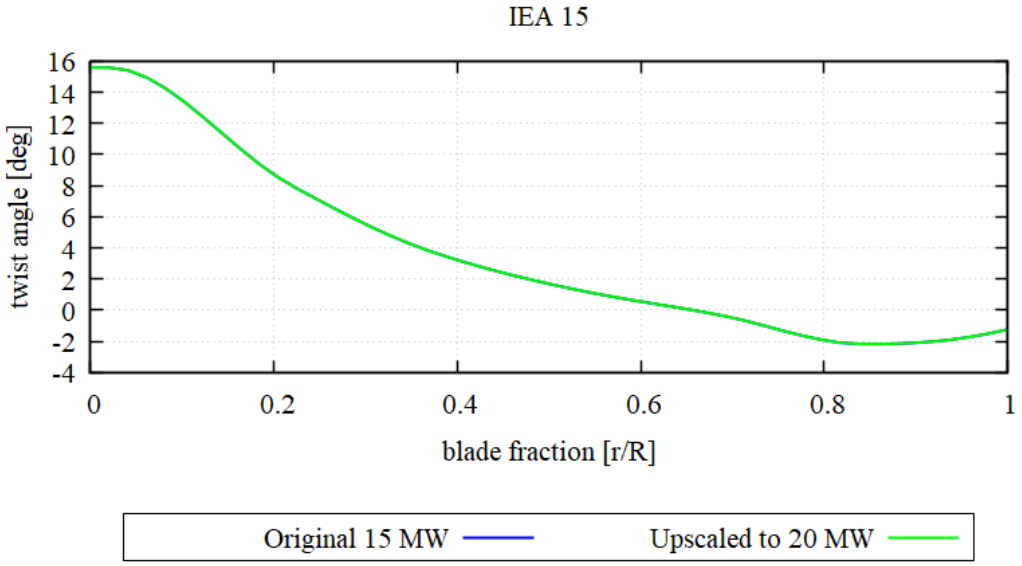

Figure 4.19. Twist angle distribution of IEA 15 and its upscaled blade to 20 MW

Following linear scaling, the mass of the blade has a scaling factor of s^3. However, the ElastoDyn module uses mass density (kg/m) distribution instead of mass (kg) distribution. Thus, a scaling factor of s^2 is used instead of s^3 in the upscaling process. The edgewise and flapwise stiffness, EI (in Nm^2), follows the s^4 scaling factor. The

distributions of mass density, edgewise stiffness, and flapwise stiffness along the normalized blade length are shown in Figure 4.20 – Figure 4.22.

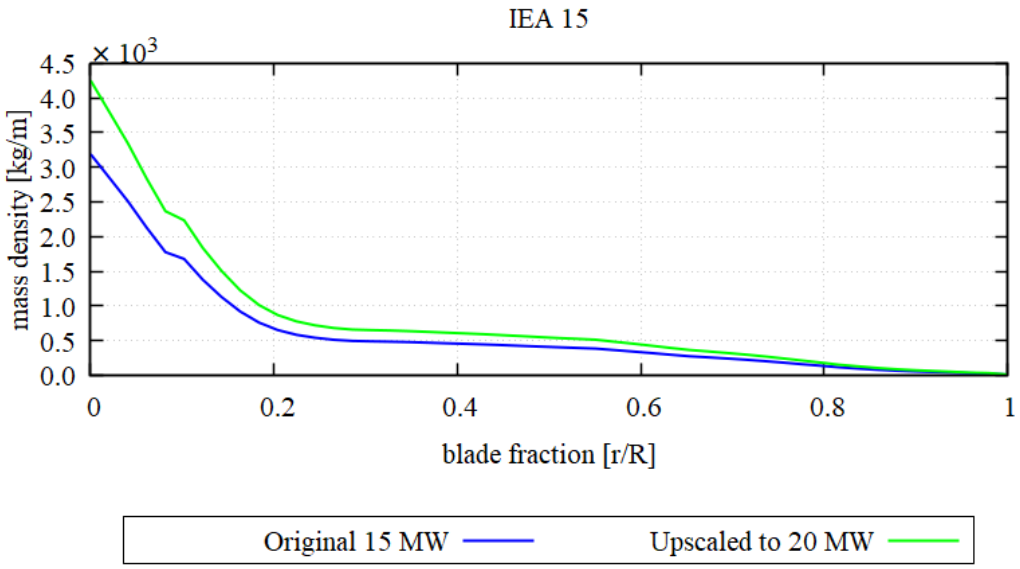

Figure 4.20. Blade mass density distribution of IEA 15 and its upscaled blade up to 20 MW

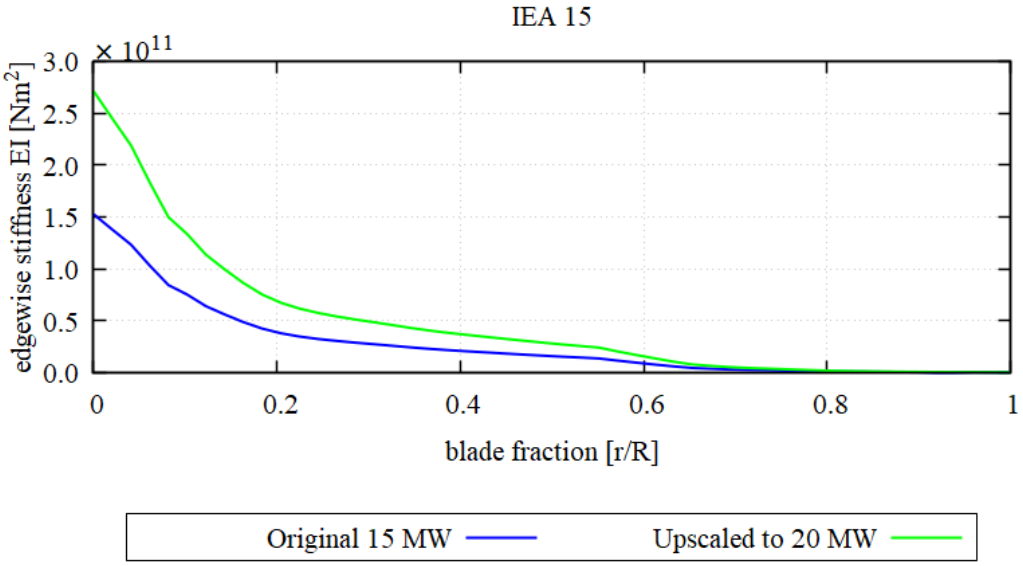

Figure 4.21. Blade edgewise stiffness distribution of IEA 15 and its upscaled blade up to 20 MW

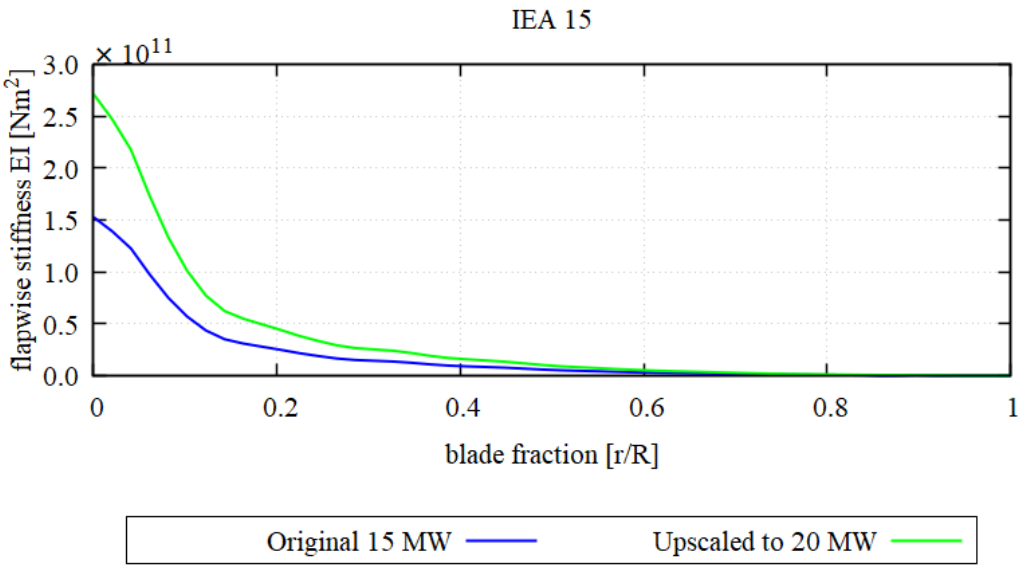

Figure 4.22. Blade flapwise stiffness distribution of IEA 15 and its upscaled blade up to 20 MW

The mass density distributions along the towers are presented in Figure 4.23. The tower fraction indicates the normalized height of the tower element from the base to the top. The base of the tower has the maximum mass density distribution due to having the largest dimension. Then it gradually decreases, except for the topmost part, where the shell thickness of the tower is re-increased, as can be found in [16].

Following linear scaling, the tower's mass has a scaling factor of s^3. But again, in the ElastoDyn module, mass density (kg/m) distribution is used instead of mass (kg) distribution, and the properties are distributed for normalized tower length (i.e., 0 to 1). Thus, a scaling factor of s^2 is used instead of s^3 in the upscaling process. It is advantageous since the tower's length is not scaled with the s^1 scaling factor. However, the diameter and shell thickness of the tower follows the s^1 relation. Thus, using the scaling factor of s^2 guarantees that the tower's material properties of the IEA 15 MW are conserved during the upscaling process.

The fore-aft and side-side stiffness of the tower, EI (in Nm^2), follows the s^4 scaling factor. Recall that the tower has a hollow circular cross-section. Thus, the fore-aft

and side-side stiffness in each section for each tower are identical. The distribution of the fore-aft and side-side stiffness along the tower can be seen in Figure 4.24.

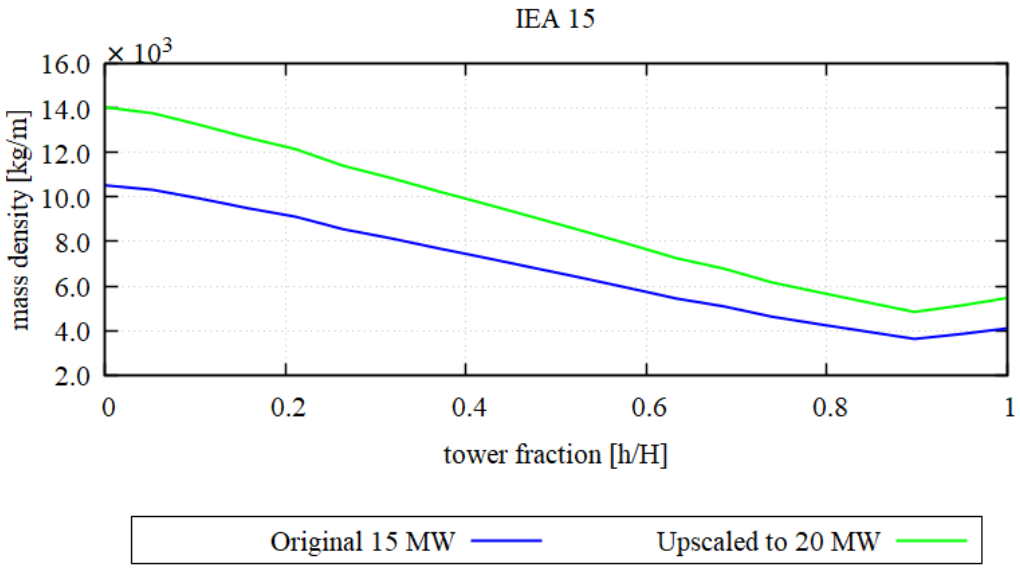

Figure 4.23. Tower mass density distribution of IEA 15 and its upscaled tower up to 20 MW

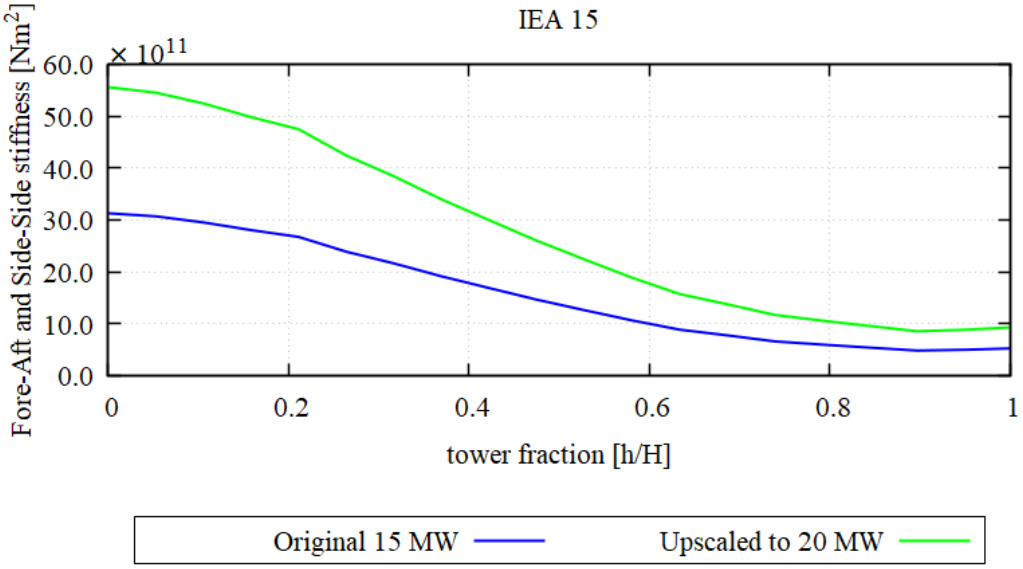

Figure 4.24. Tower fore-aft and side-side stiffness distribution of IEA 15 and its upscaled tower up to 20 MW

4.2 Linear Scaling of OC4 DeepCwind Semi-Submersible

The upscaling of the floating platform performed in this study follows the linear scaling approach explained in Section 3.1.2 with the same scaling factor as the turbines, s. The diameter and shell thickness of main and outer columns, braces, and pontoons are upscaled with the s^1 relation. The elevation of the main and outer columns, offset distance of the outer columns, and the draft length of the semi-submersible is also upscaled to preserve the stabilization principle. A visualization of the size growth of the OC4 semi-submersible platform with s^1 relation to 10, 15, and 20 MW turbines are shown in Figure 4.25.

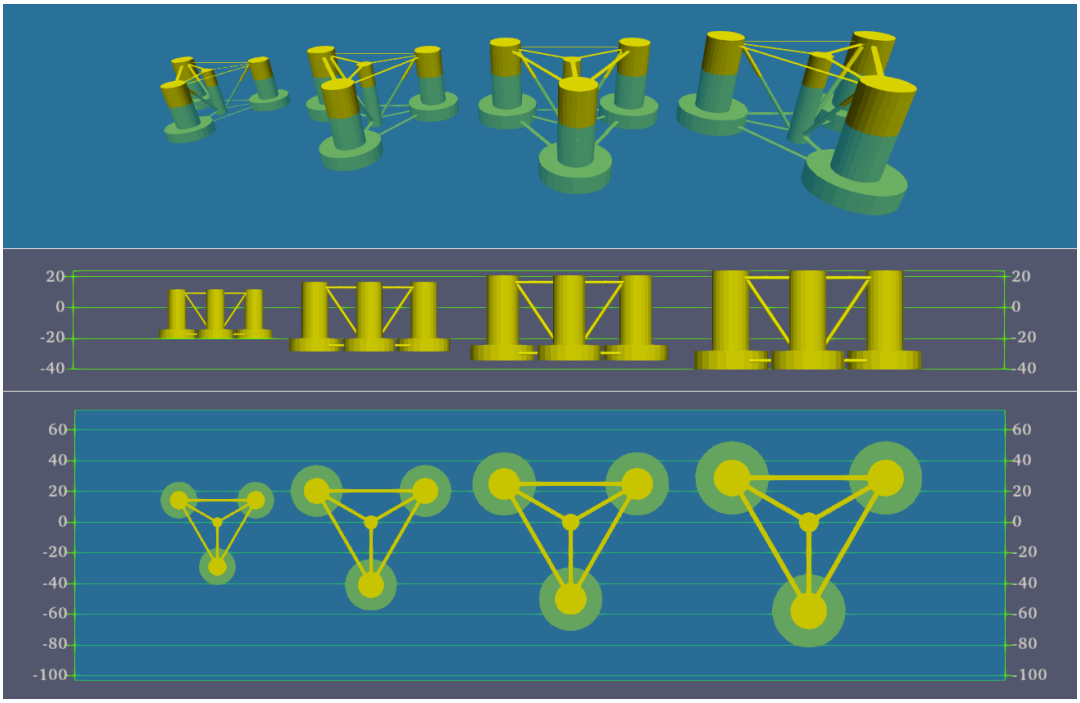

Figure 4.25. OC4 DeepCwind Semi-Submersible at 5, 10, 15, and 20 MW

As can be seen in Figure 4.25, the elevation of the 20 MW platform is twice as high as the baseline platforms' elevation, which is expected from the linear scaling. The same applies to the outer column's total draft length and offset distance. The geometrical results of the upscaling process of the OC4 DeepCwind semi-submersible are tabulated in Table 4.3.

Table 4.3 Result of linear scaling to the OC4 DeepCwind semi-submersible platform to 10, 15, and 20 MW turbine

Parameter	Unit	Intended turbine power			
		5 MW	**10 MW**	**15 MW**	**20 MW**
Scaling factor	-	1.00E+0	1.41E+0	1.73E+0	2.00E+0
Displaced volume	m^3	1.39E+4	3.94E+4	7.23E+4	1.11E+5
Main column elev.	m	1.00E+1	1.41E+1	1.73E+1	2.00E+1
Outer column offset	m	5.00E+1	7.07E+1	5.06E+1	1.00E+2
Draft length	m	2.00E+1	2.83E+1	3.46E+1	4.00E+1
Center of buoyancy	m	-1.32E+1	-1.86E+1	-2.29E+1	-2.63E+1
Center of gravity	m	-1.35E+1	-1.90E+1	-2.33E+1	-2.69E+1

Hydrodynamic Analysis of Marine Structures (HAMS) is used to calculate body mass matrices and generate the potential-flow model data used as the input in the HydroDyn module. The external hydrostatic restoring matrix of the mooring lines is generated by MAP++ and inputted to HAMS.

Only the wetted (submerged) part of the platform is used in the calculation. Recall from Section 3.5.2, HAMS has a built-in mesh transformation code called WAMIT_MeshTran.exe to transform the geometric data files (.gdf) format of WAMIT into HAMS' meshing format. There are two symmetrical planes available in HAMS. However, entire wetted bodies are used in this study, and the symmetry option is omitted.

An example of geometrical data file (gdf) meshing of OC4 semi-submersible's wetted area is shown in Figure 4.26. Correspondingly, an example of meshing resulting from WAMIT_MeshTran.exe of the same submerged body is shown in Figure 4.27. The WAMIT_MeshTran.exe automatically distinguishes the hull from the waterplane area. The blue part is the hull body, and the green part is the waterplane area.

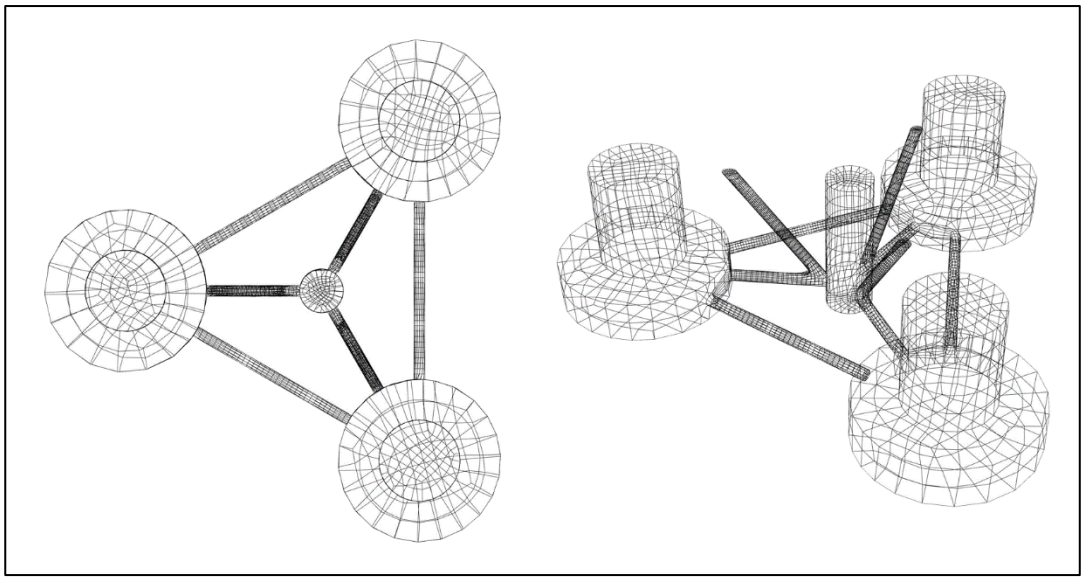

Figure 4.26. Example of .gdf meshing before transformed in HAMS'

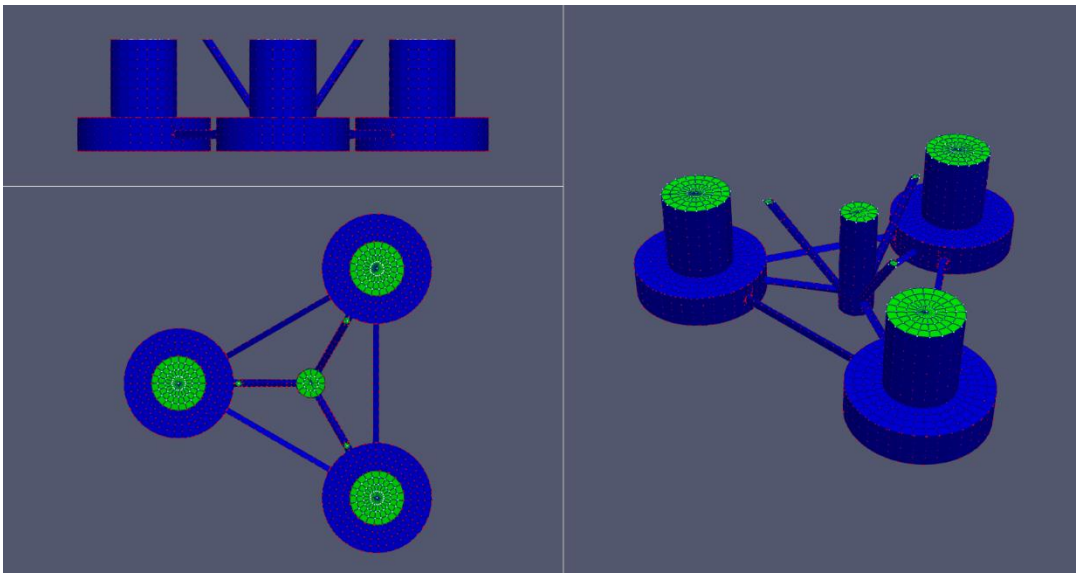

Figure 4.27. Example of mesh transformation result for HAMS

For each geometrical data file (.gdf) provided, HAMS' WAMIT_MeshTran.exe calculates several geometrical variables of the submerged body, like the size of the water plane area, the center of buoyancy, etc. The increasing trend of the water plane and immersed body area calculated by HAMS as the platform size upscaled are given

in Figure 4.28 to Figure 4.29, respectively. The blade radius of NREL 5 is used for deriving the relation since the platform was initially designed for NREL 5 MW.

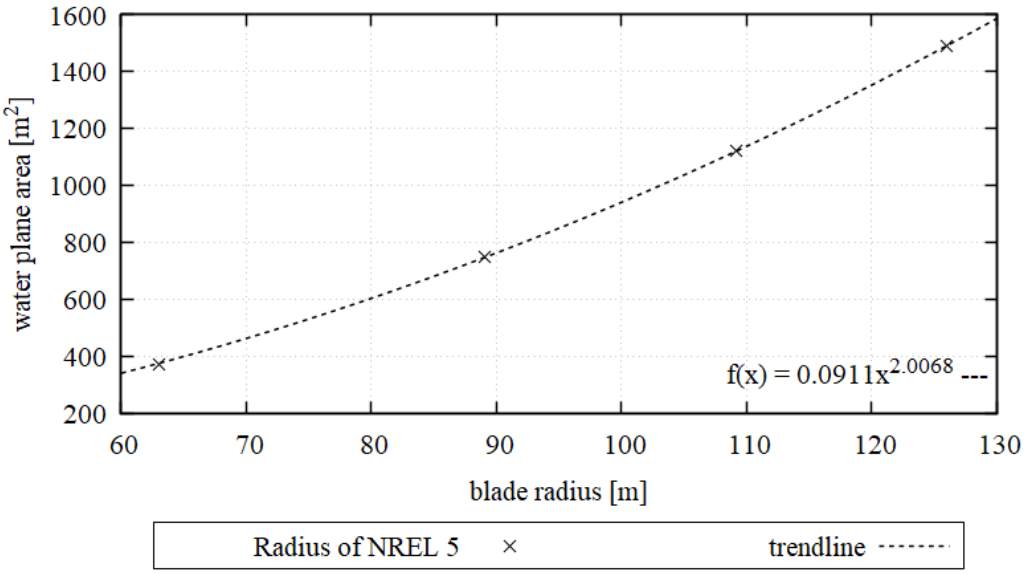

Figure 4.28. Increase in water plane area

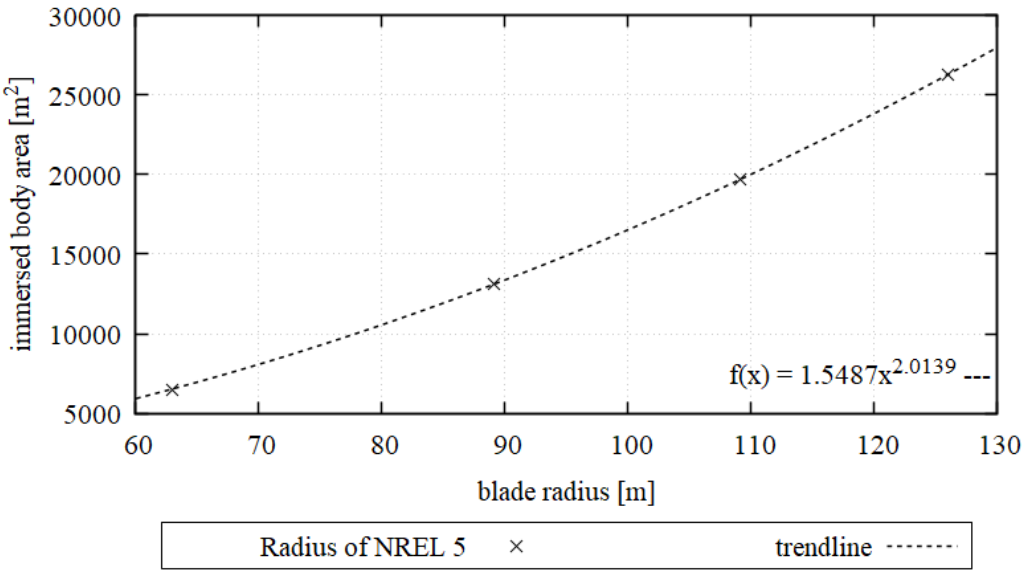

Figure 4.29. Increase in the immersed body area

From the trendline in Figure 4.28 and Figure 4.29, the water plane and immersed body area calculated by HAMS follow the s^2 relation, which is expected from linear

scaling. The increasing trend of the immersed body volume and lowering of the center of buoyancy calculated by HAMS as the platform upscaled are given in Figure 4.30 and Figure 4.31, respectively. Again, the blade radius of NREL 5 is used for deriving the relation since the platform was initially designed for NREL 5 MW.

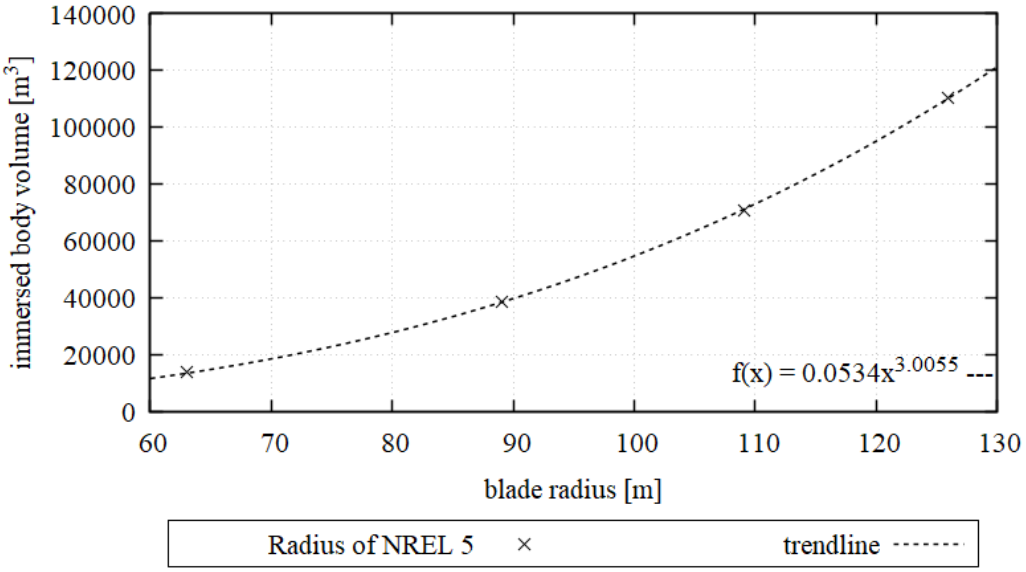

Figure 4.30. Increase in the immersed body volume

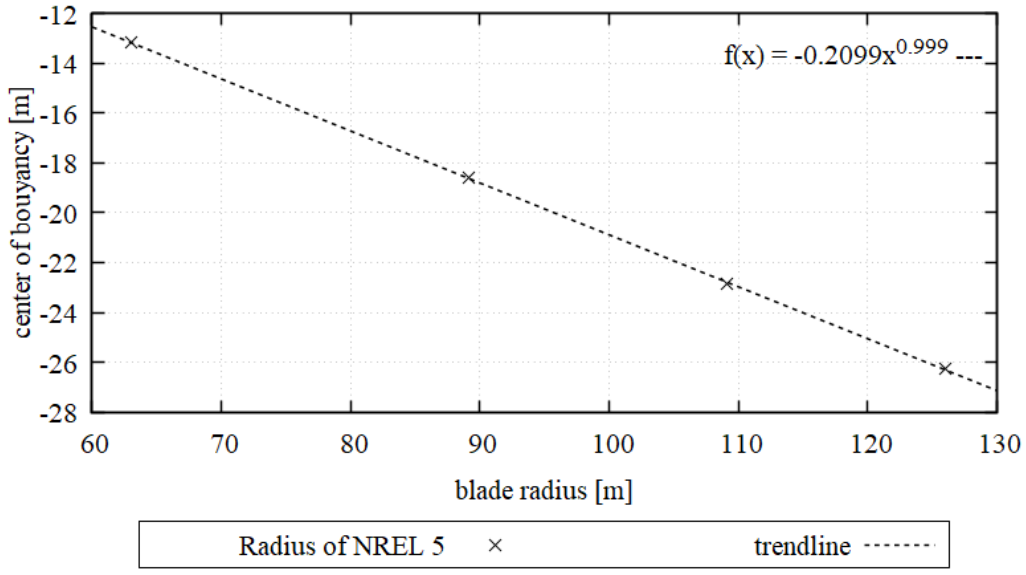

Figure 4.31. The lowering of the center of buoyancy

As can be seen in Figure 4.30 and Figure 4.31, the immersed body volume increases with s^3, while the center of buoyancy lowers linearly as the blade radius of NREL 5 increases. This is again expected from linear scaling.

The mooring line's unstretched length, diameter, and material properties are not scaled, and the placement of the mooring lines remains on the top of the outer base column. However, due to the upscaled platform size, the locations of the fairing leads are shifted. As a consequence, the locations of the anchors are readjusted. This approach is suggested in the future recommendation of [19].

This study's anchors' rearrangement is performed as the procedure explained in the definition of OC4 semi-submersible by iteratively shifting it 0.5 meters [17]. The rearrangement process aims to maintain similar total tension at the fairing leads with the baseline in still water conditions. MAP++ is used to calculate the fairing lead and anchor tension, suspended line length, the horizontal distance of the anchor, etc. The total forces acting on the anchors and fairing leads are shown in Table 4.4.

Table 4.4 Summary forces acting on the mooring lines at still water condition

Parameter	**Unit**	**Intended turbine power**			
		5 MW	**10 MW**	**15 MW**	**20 MW**
Unstretched Length	m	8.354E+02	8.354E+02	8.354E+02	8.354E+02
Line rest on seabed	m	2.423E+02	2.509E+02	2.575E+02	2.631E+02
H-Fairlead	N	9.094E+05	9.152E+05	9.199E+05	9.240E+05
V-Fairlead	N	6.317E+05	6.226E+05	6.156E+05	6.096E+05
T-Fairlead	N	1.107E+06	1.107E+06	1.107E+06	1.107E+06
α-Fairlead	deg	3.479E+01	3.423E+01	3.379E+01	3.342E+01
H-Anchor	N	6.512E+05	6.480E+05	6.456E+05	6.438E+05
V-Anchor	N	0.000E+00	0.000E+00	0.000E+00	0.000E+00
T-Anchor	N	6.512E+05	6.480E+05	6.456E+05	6.438E+05
α-Anchor	deg	0.000E+00	0.000E+00	0.000E+00	0.000E+00

H is the horizontal component of the tension, V is the vertical component of the tension, and T is the total tension force. The main aim of the rearrangement process

is to have an approximately similar total tension force acting on the fairing leads of all platforms. Figure 4.32 shows the configurations of the mooring line number 2 of the baseline and upscaled platforms. In the figure, the thickness of the mooring lines is exaggerated for visualization purposes.

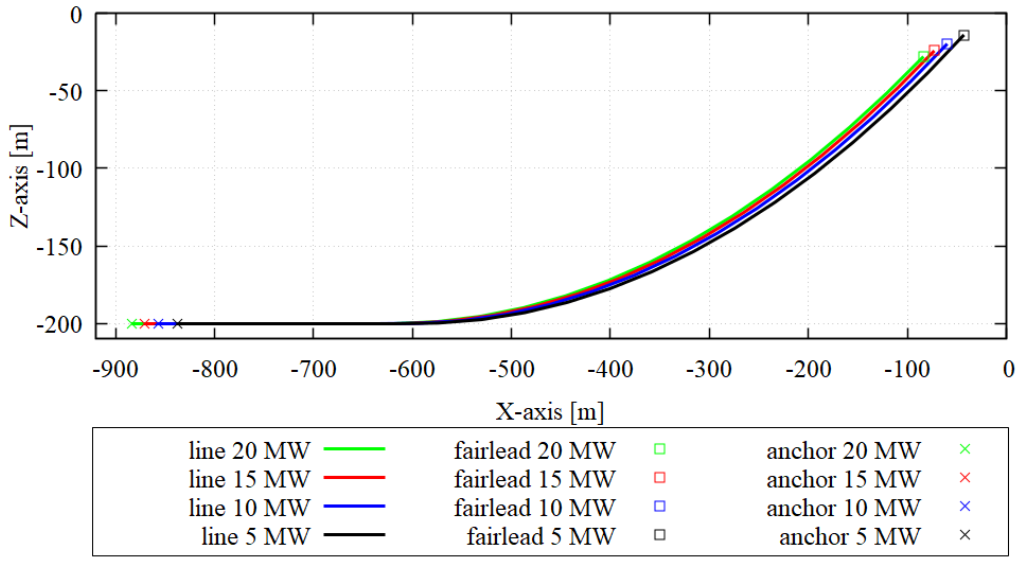

Figure 4.32. Mooring line number 2 at 5 MW, 10 MW, 15 MW, and 20 MW

As shown in Figure 4.32, the positions of the fairing leads are different due to the upscaled platform size. Locations of the anchors are readjusted, and some parts of the mooring lines rest on the seabed under still water conditions. It causes the anchors to experience only a horizontal force at the instance shown in Figure 4.32.

4.3 Optimization

Linear scaling resulted in a similar optimum performance of the turbine due to aerodynamic similarity introduced during upscaling by maintaining the tip speed ratio. Better performance and higher annual energy production (AEP) can be achieved by aerodynamic optimization. The blade shape (chord, twist angle, and airfoil distribution) must be optimized. However, upscaling the rotor also introduces a higher mass, which is counter-productive to the objective of upscaling. Thus,

optimization that results in a high AEP with a minimum blade mass that still satisfies structural constraints is intended.

Only NREL 5 MW is optimized in this study, as NREL 5 is the oldest among all the three RWTs, and the other IEA 10 MW and IEA 15 MW have been optimized during their design process. The rotor size of IEA 10 MW was optimized to maximize the annual energy production (AEP). In the optimization process of IEA 10 MW, the blade length act as a free parameter, and the load envelope of DTU 10 MW act as the structural constraint [15]. For IEA 15 MW, the distribution of airfoil positions, blade chord, twist angle, tip speed ratio, and spar cap thickness are the free variable [16]. 240-meter rotor diameter is specifically chosen for IEA 15 MW, and blade mass is forced not to exceed 65 tons.

The optimization process of all NREL 5's blades performed in this study started with optimizing the baseline NREL 5 MW to understand the effect of only optimization without upscaling. The blade length, root diameter, and airfoil type of the optimized blade are similar to the baseline so that the same hub and tower can be used.

For the 10, 15, and 20 MW blades, the baseline NREL 5 MW is linearly upscaled to each power rating before being optimized. The lengths of the optimized blades are taken from linear scaling. In addition, for the 20 MW blade, a new blade having the same length as the upscaled IEA15 to 20 MW (around 135.1 meters) are developed to understand better the effect of the different blade length on the overall performance. For all the optimized blades, chord length's upper and lower boundaries for each optimized blade are selected as ±25% of the maximum chord length, except for the root chord, whose dimensions are the same as the upscaled blade.

In this study, 100 individuals per generation are used, and 40% of it is created by cross-over. A maximum of 50 generations for GA iteration is used to anticipate the expensive computational cost of the optimization process. Multi-objective genetic algorithm is used in the optimization to minimize the blade mass while maximizing the AEP. It is done so that the blades produced are realistic. Disabling the multi-objective general algorithm, or in other words, only maximizing AEP, can lead

HARP_Opt to utilize many thinner airfoils with a higher lift-to-drag ratio than what is feasible to produce for a very long turbine's blade. The distribution of the optimized blade's chord length, relative thickness, and twist angle is given in Figure 4.33 to Figure 4.35. The twist angles of all turbines are alike due to the utilization of the same airfoil families.

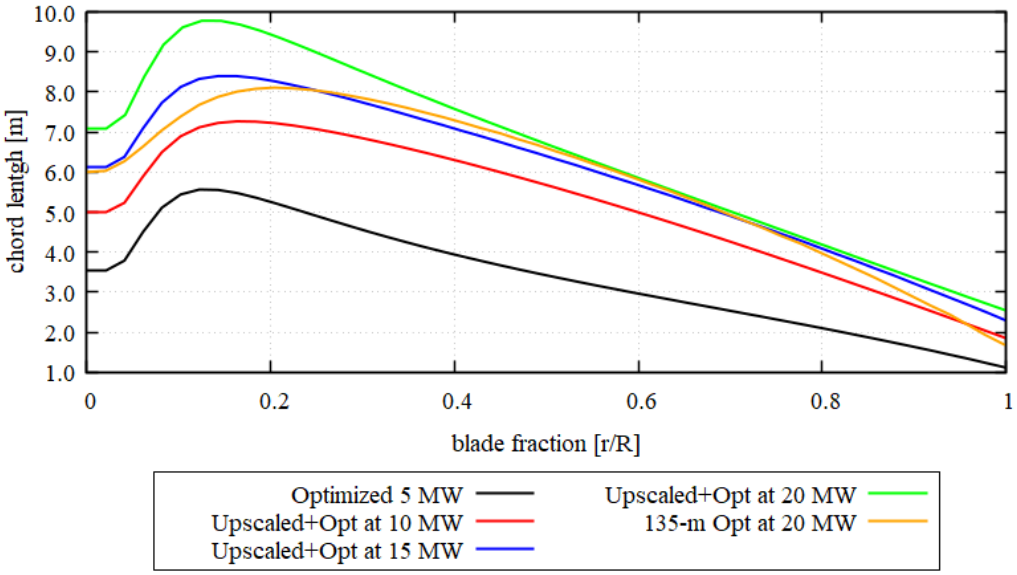

Figure 4.33. Chord distribution of all optimized NREL5 blades up to 20 MW

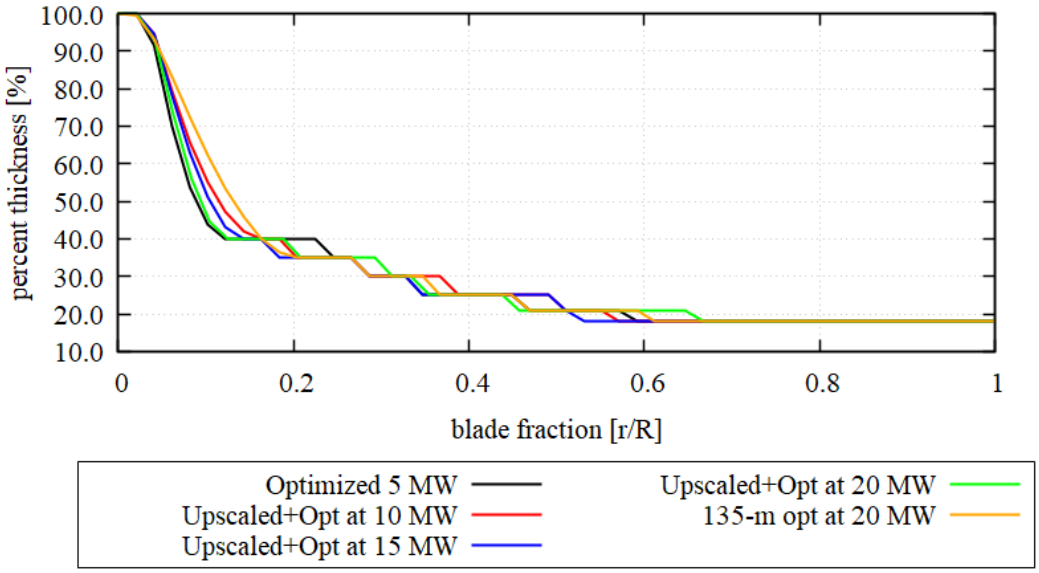

Figure 4.34. Relative thickness of all optimized NREL5 blades up to 20 MW

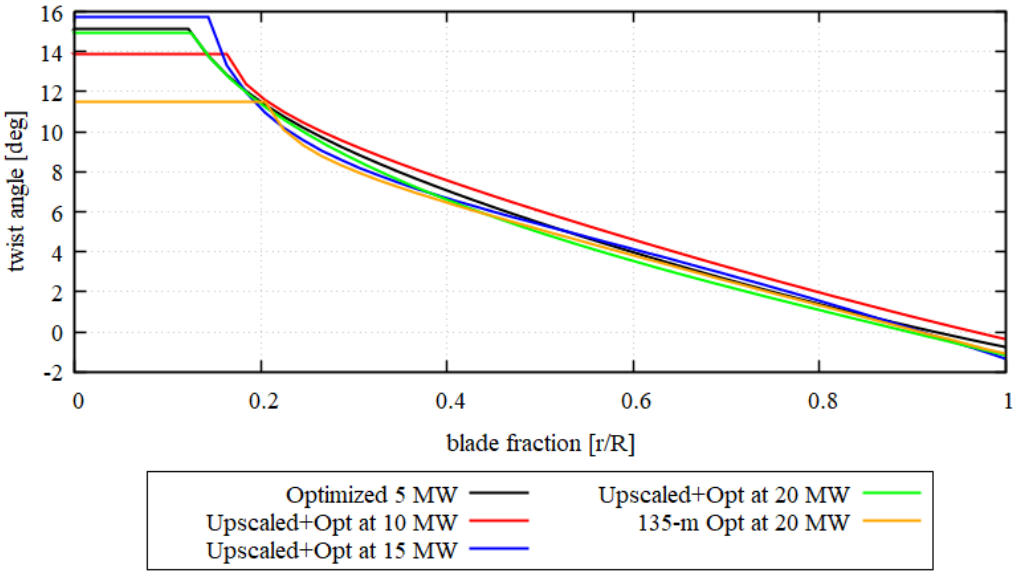

Figure 4.35. Twist angle distribution of all optimized NREL 5 blades up to 20 MW

Since HARP_Opt only models the blade as a thin shell without any internal structure, the composite material layups of the blades with the best aerodynamic geometries are further optimized in Co-Blade. Three shear web designs are selected to model all the optimized NREL 5 blades as suggested in [22] and are also used in [23]. Table 4.5 present the material used in constructing the blade, which is fiberglass material, taken from the Sandia 100 m all-glass blade, as cited in [63].

Table 4.5 Composite material properties of Sandia 100 m all-glass blade [23] (reproduced from [63])

E_{11} (Pa)	E_{22} (Pa)	G_{12} (Pa)	ν_{12}	ρ (kg/m^3)	Description
2.80E+10	1.40E+10	7.00E+09	4.00E-01	1.85E+03	blade-root
2.80E+10	1.40E+10	7.00E+09	4.00E-01	1.85E+03	blade-shell
4.20E+10	1.40E+10	3.00E+09	2.80E-01	1.92E+03	spar-uni
2.60E+08	2.60E+08	2.00E+07	3.00E-01	2.00E+02	spar-core
2.60E+08	2.60E+08	2.00E+07	3.00E-01	2.00E+02	LEP-core
2.60E+08	2.60E+08	2.00E+07	3.00E-01	2.00E+02	TEP-core
1.40E+10	1.40E+10	1.20E+10	5.00E-01	1.78E+03	web-shell
2.60E+08	2.60E+08	2.00E+07	3.00E-01	2.00E+02	web-core

In the present study, the weight of the blade, centrifugal forces, and aerodynamic forces on the blade are enabled in the optimization process to make the produced blade more realistic. The thickness of the lamina for the blade shell, spar caps, shear web, and leading and trailing edge strengthener are free variables. A maximum of 10 meters out-of-plane tip deflection and a minimum 1 Hz allowable difference between the blade rotation frequency and blade natural frequency are set as a constraint in the optimization process.

The optimization processes result in blades with all glass material called an optimized NREL 5 MW for the 5 MW ratings and upscaled + optimized NREL 5 at the 10, 15, and 20 MW. The spanwise distribution of blade mass density is shown in Figure 4.36.

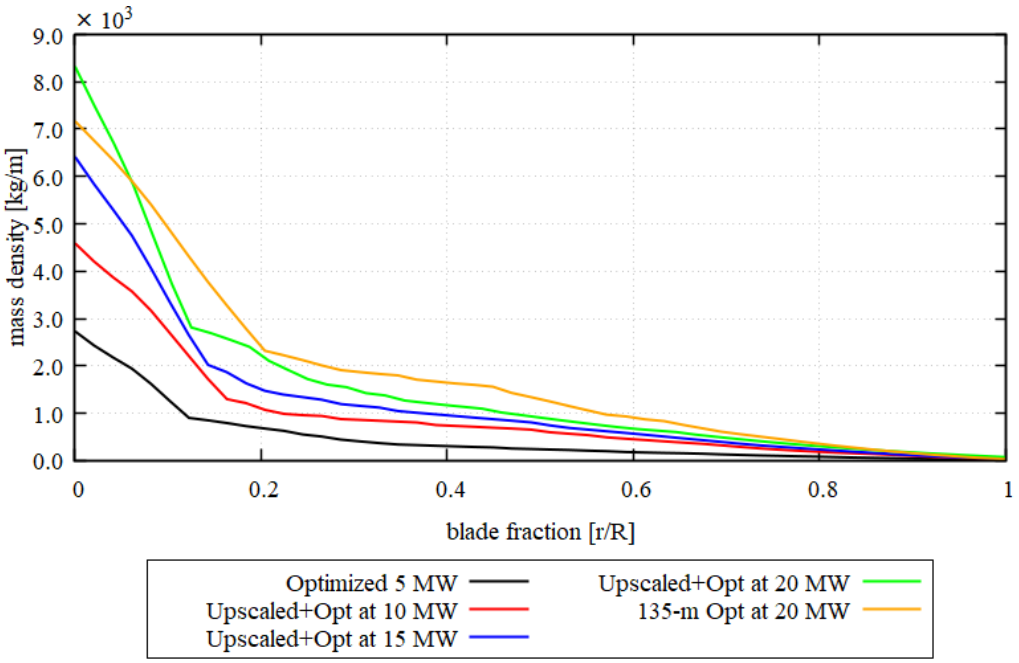

Figure 4.36. Blade mass density distribution of optimized NREL5 and upscaled + optimized NREL5 blade up to 20 MW

As shown in Figure 4.36, contrary to the baseline NREL 5 MW, all the optimized blades have a monotonic decrease in the mass density distribution. A drastic decrease in the blade mass density is observed from the root section to the end of the root

transition region. The end of the root transition region is the station with the maximum chord length, typically at the first 20% of the blade length. The root transition region is not aerodynamically critical, and most of the airfoils in this region are blunt airfoils. After the root transition region, the mass of the blade decreases more gradually until the tip of the blade.

Higher mass at the root transition region shows that the root needs to be stronger than the rest of the blade. It is related to the thickness of the lamina that is concentrated in the root transition region, later shown in Figure 4.39 to Figure 4.43. Correspondingly, at the root transition region, edgewise and flapwise stiffness distribution is also higher than the rest of the blade. Higher strength is required to maintain the blade within the structural envelope and keep a safe blade tip-to-tower clearance throughout the operation. The distributions of edgewise and flapwise stiffness are shown in Figure 4.37 and Figure 4.38. Both figures clearly show that the root transition region has a more significant edgewise and flapwise stiffness distribution than the region after that.

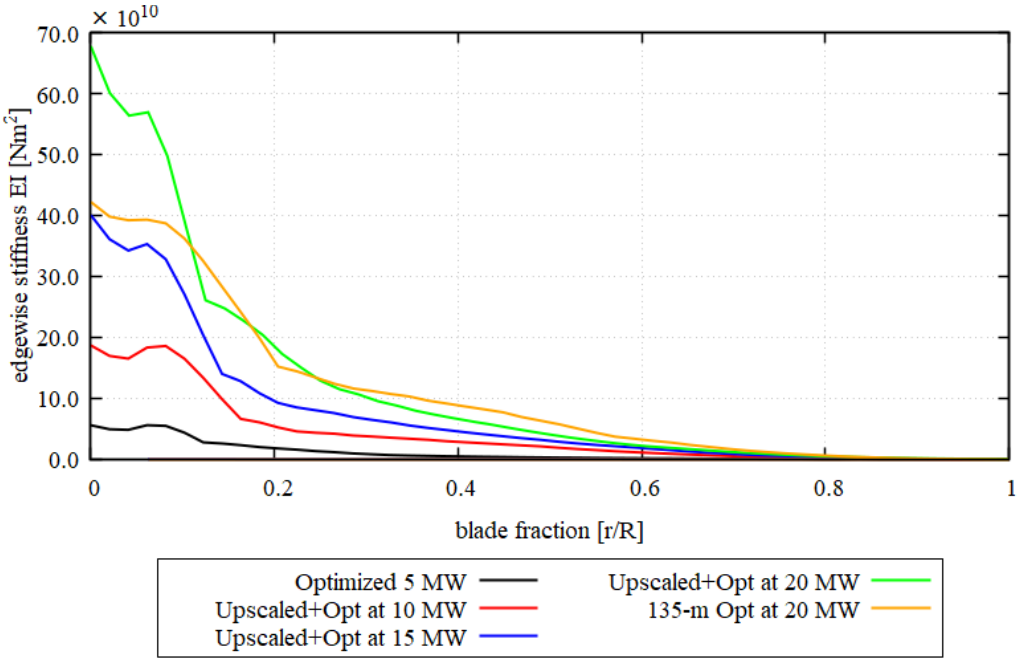

Figure 4.37. Blade edgewise stiffness distribution of optimized NREL5 and upscaled + optimized NREL5 blade up to 20 MW

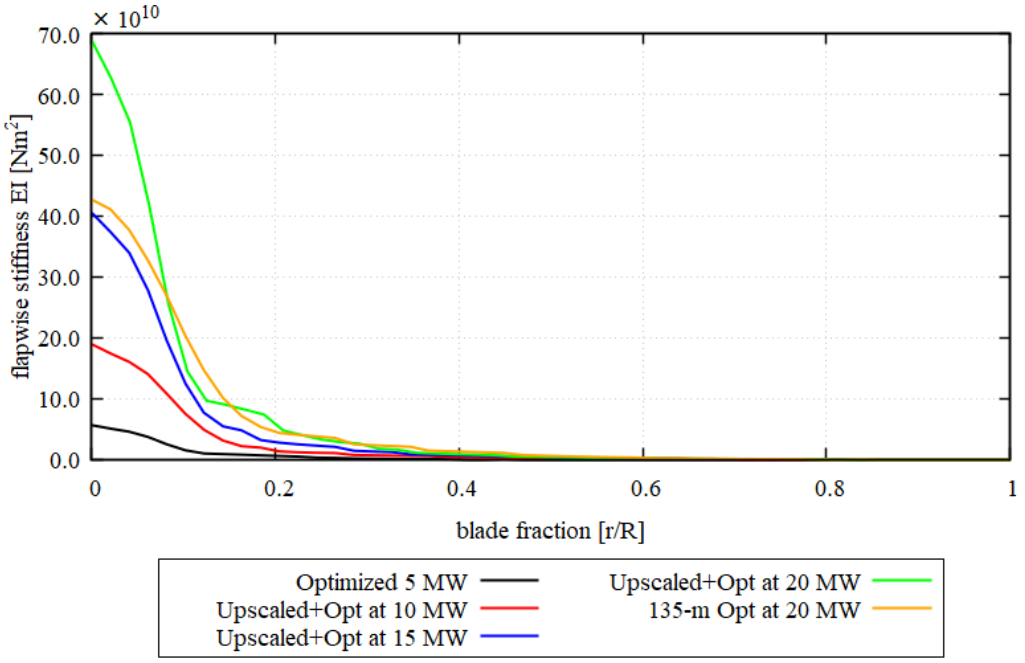

Figure 4.38. Blade flapwise stiffness distribution of optimized NREL5 and upscaled + optimized NREL5 blade up to 20 MW

Figure 4.39 to Figure 4.43 show the thickness distributions of blade shells and shear webs of all the optimized NREL 5 blades from 5 MW to 20 MW. The blade shell and shear webs are concentrated at the root section, explaining the increase in mass density, edgewise, and flapwise stiffness distribution near the root section.

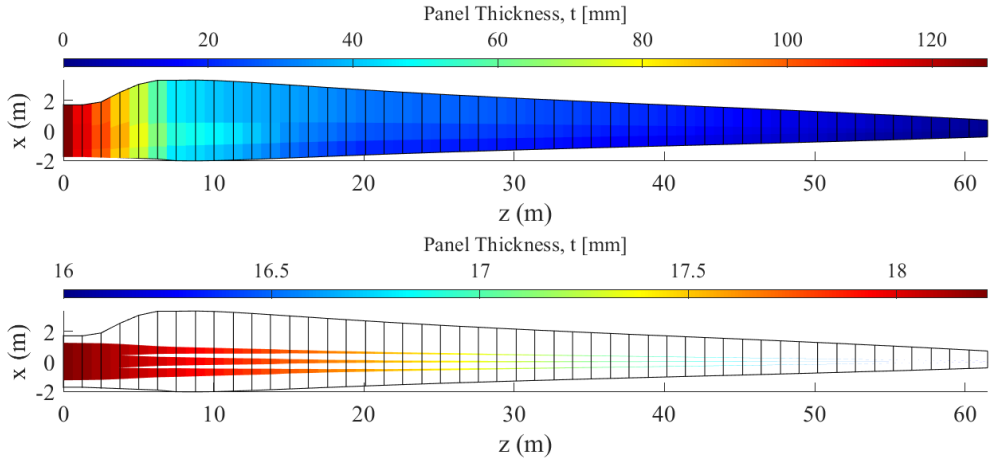

Figure 4.39. Blade shell (up) and shear web (bottom) thickness of the optimized NREL 5 at 5 MW

Figure 4.39 shows the thickness distributions of blade shells and shear webs for optimized NREL 5 MW. The blade shell in the root section is thicker than the rest of the blade. After the root transition region, the shell thickness gradually decreases from more than 120 mm at the root to nearly zero at the tip. The spar caps' location at each blade element can be observed from the shell thickness discoloration at around 0.25 to 0.50 chord length. At the spar caps, the shell thickness of the blade element is higher than the surroundings. The shear webs' thickness is also concentrated at the root section. The root section has a thicker shear web, and it gradually decreases towards the tip. However, the root and tip's shear web difference is not bigger than 3 mm.

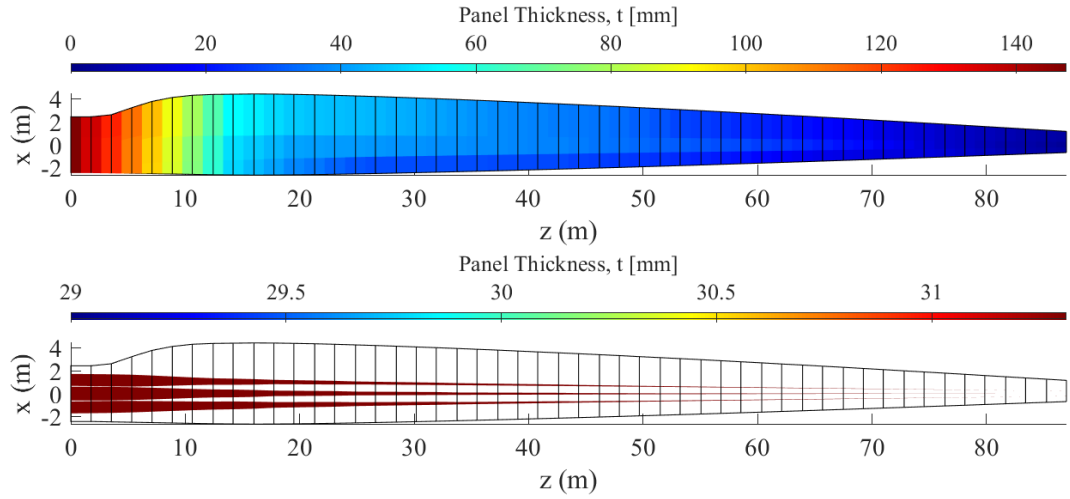

Figure 4.40. Blade shell (up) and shear web (bottom) thickness of the upscaled + optimized NREL 5 at 10 MW

Figure 4.40 shows the blade shell and shear web thickness for 10 MW upscaled + optimized NREL 5. The blade shell is concentrated and significantly thicker at the root transition region than the rest of the blade. After this region, the shell's thickness gradually decreases from more than 140 mm at the root decreases to nearly zero at the tip. At around 0.25 to 0.50 chord length in each blade element, the spar caps' location can be observed as it causes higher shell thickness than the surroundings. For the 10 MW upscaled + optimized NREL 5 blades, the shear webs' thickness is constant from the root to the tip of the blade.

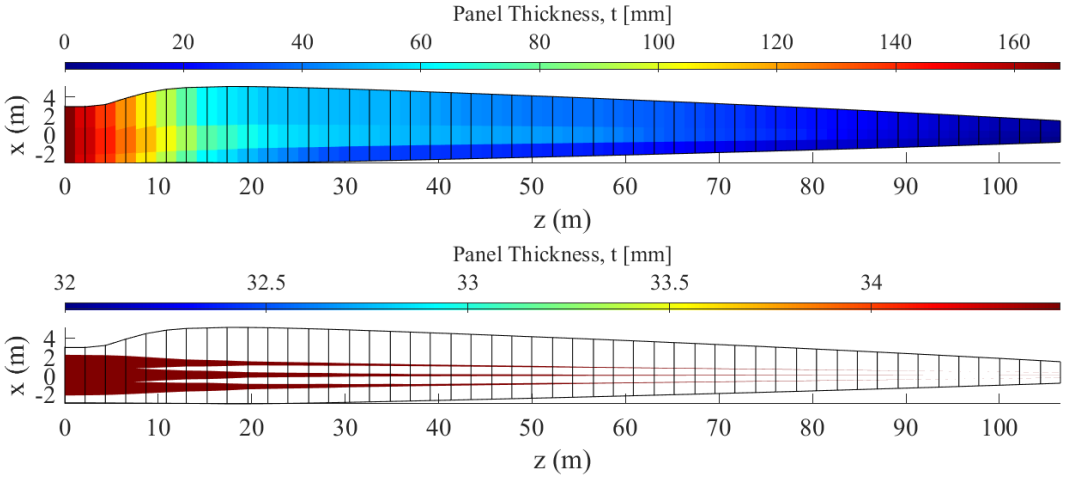

Figure 4.41. Blade shell (up) and shear web (bottom) thickness of the upscaled + optimized NREL 5 at 15 MW

Figure 4.41 shows the blade shell and shear web thickness for 15 MW upscaled + optimized NREL 5. The blade shell is significantly thicker at the root transition region than the rest of the blade. The shell's thickness gradually decreases from more than 160 mm at the root decreases to nearly zero at the tip. The spar caps' location can be observed at around 0.25 to 0.50 chord length in each blade element, causing higher shell thickness than the surroundings. For the 15 MW upscaled + optimized NREL 5 blades, the shear webs' thickness is constant from blade's root to the tip.

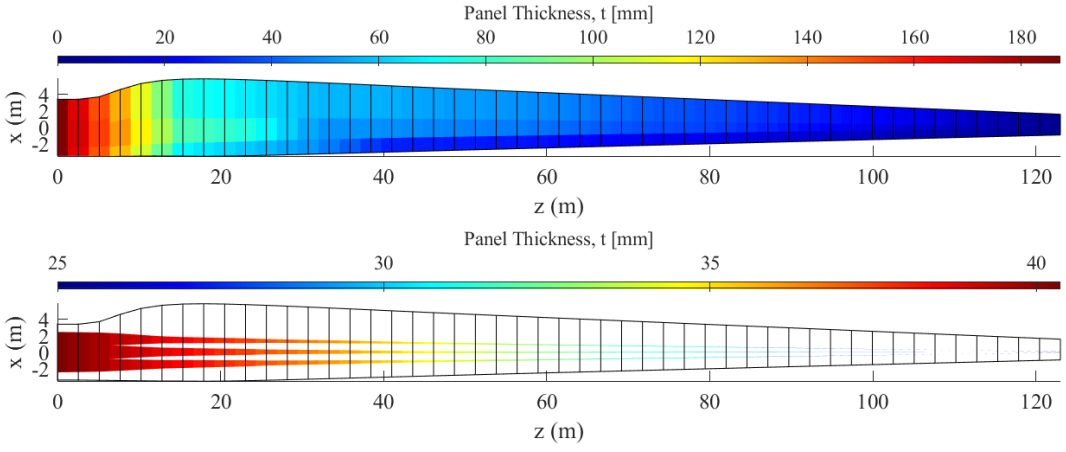

Figure 4.42. Blade shell (up) and shear web (bottom) thickness of the upscaled + optimized NREL 5 at 20 MW

Figure 4.42 shows the blade shell and shear web thickness for 20 MW upscaled + optimized NREL 5. The blade shell is concentrated and significantly thicker at the root transition region than the rest of the blade. After the root transition region, the shell's thickness gradually decreases from more than 180 mm at the root decreases to nearly zero at the tip. The spar caps' location can clearly be observed at around 0.25 to 0.50 chord length in each blade element, causing higher shell thickness than the surroundings. The shear webs' thickness is also concentrated and significantly thicker at the root section, gradually decreasing towards the tip.

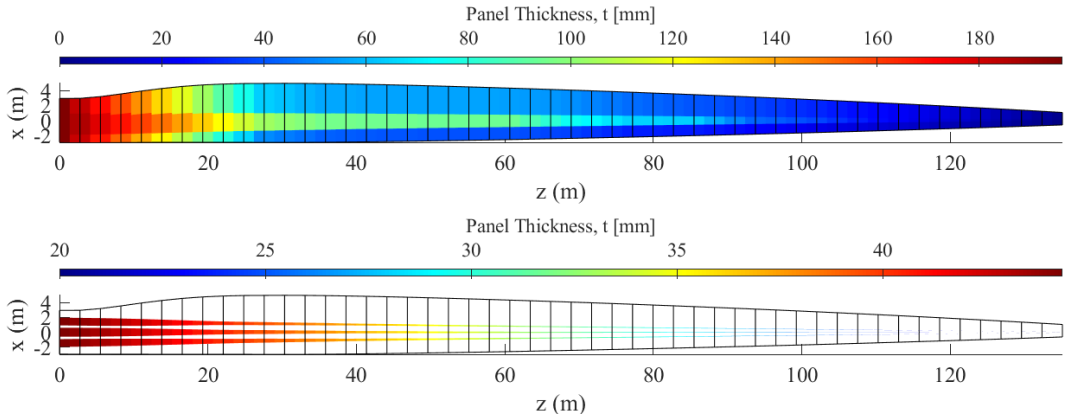

Figure 4.43. Blade shell (up) and shear web (bottom) thickness of the 135 meters optimized NREL 5 at 20 MW

Figure 4.43 shows that the blade shell and shear web thickness for the 20 MW optimized NREL 5 matched the length of the Upscaled IEA 15 at 20 MW. The blade is called the 135 meters optimized NREL 5 at 20 MW. Again, the blade shell is concentrated and significantly thicker at the root transition region than the rest of the blade. After the root transition region, the shell's thickness gradually decreases from more than 180 mm at the root decreases to nearly zero at the tip. The spar caps' location can clearly be observed at around 0.25 to 0.50 chord length in each blade element, causing higher shell thickness than the surroundings and marked by a linear region with different colors along root to tip of the blade. The shear webs' thickness of the135 meters optimized NREL 5 at 20 MW is also concentrated and significantly thicker at the root section, then it gradually decreases towards the tip.

The estimated annual energy productions (AEP) and the capacity factor of various rotor diameters ranging from 100 meters to 300 meters and for rated power of 5 MW to 20 MW are shown in Figure 4.44. The capacity factor is the ratio of the AEP to the full power capacity of the turbines, assuming the turbines produced the rated power for all 8760 hours in a year. The contours in Figure 4.44 are estimated using Weibull distribution with k = 2.00 and c = 6.8, the same shape and scale factor used in the optimization process in this study. The rotor diameter of optimized NREL 5 MW is 126 meters, and about 280 meters for the 20 MW 135-m optimized NREL 5, tabulated in detail in Table 4.6. The calculated AEP of all turbines will be discussed in Chapter 5 as part of the performance comparison.

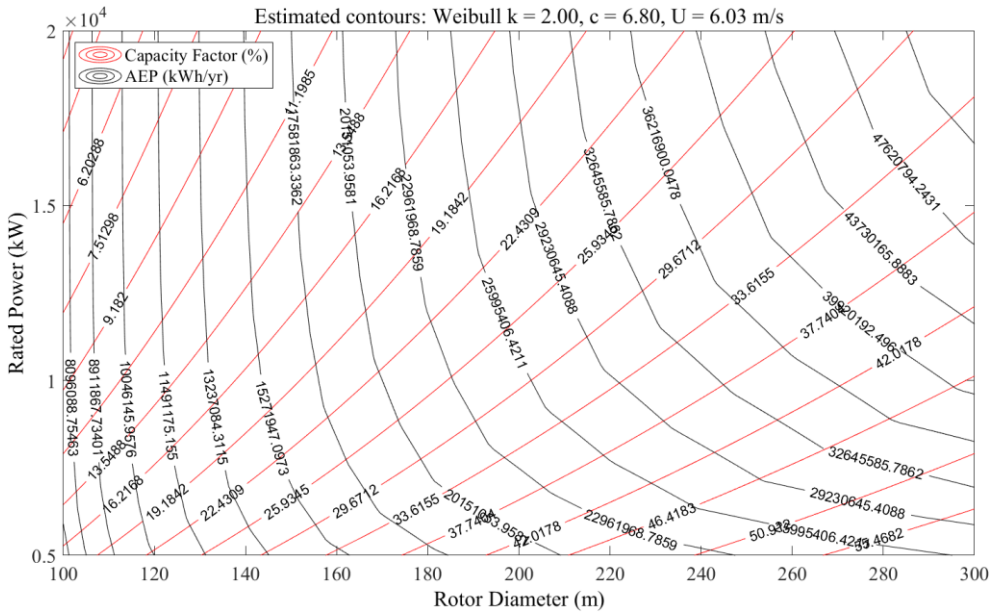

Figure 4.44. Estimated AEP and Capacity factor for various rotor sizes and rated power ranges.

Figure 4.44 demonstrates the importance of upscaling the turbine size. For a specific rated power (e.g., 5, 10, 15, and 20 MW), the larger the diameter of the rotor, the higher the AEP produced and the better the capacity factor it achieved. On the other hand, if a specific rotor diameter (e.g., 200 meters) is used and not upscaled while increasing the rated power of the turbines, the capacity factor becomes poorer. However, higher AEP can still be achieved.

The primary optimization purpose of this study is to obtain a turbine with a better aerodynamic shape, which can produce higher power but is still feasible. Optimizing the baseline NREL 5 MW is intended to observe the effect of optimization on a non-upscaled turbine. The optimization in 10, 15, and 20 MW is performed to show the effect of optimization on turbines whose blade lengths are taken from linear scaling. The optimization of 20 MW 135-m optimized NREL 5 is done to show the effect of extending blade length more than linear scaling on power production. Table 4.6 summarizes the optimized turbines' rotor size, mass, and estimated AEP in one year. The calculated AEP of all optimized NREL 5 and their improvement with respect to the baseline and upscaled NREL 5 are shown in Chapter 5.

Table 4.6 Optimized turbine's total mass and estimated AEP based on Figure 4.44

Turbine Name	**Diameter Rotor [m]**	**Total blade Mass [kg]**	**Mass increase from scaled NREL 5 [kg]**	**Estimated AEP range [KWh/year]**
5 MW optimized NREL 5	1.260E+02	2.851E+04	1.077E+04	1.005E+07 to 1.149E+07
10 MW upscaled + opt NREL 5	1.782E+02	8.047E+04	3.030E+04	2.015E+07 to 2.296E+07
15 MW upscaled + opt NREL 5	2.182E+02	1.289E+05	3.673E+04	2.923E+07 to 3.265E+07
20 MW upscaled + opt NREL 5	2.520E+02	1.879E+05	4.594E+04	3.992E+07 to 4.373E+07
20 MW 135-m opt. NREL 5	2.771E+02	2.398E+05	9.793E+04	4.762E+07 to 5.157E+07

As can be observed from Table 4.6, The mass of the 5 MW optimized NREL 5 of 28.51 tons is approximately 10.8 tons higher than the baseline NREL 5 MW with 17.74 tons. The mass of the upscaled + optimized NREL 5 at 10, 15, and 20 MW is also higher than the conventional scaling trend, s^3, performed on the mass of baseline NREL 5 MW. Higher total mass for the optimized blade than linear scaling is parallel with the findings in Sandia 13.2 MW all-glass blade. The total blade mass of the Sandia 13.2 MW turbine is 114.17 tons [23]. Linear scaling of NREL 5 MW to 13.2

MW will result in 76.09 tons of blade mass, approximately 38 tons lighter than the Sandia 13.2 MW blade. Three main reasons can explain this phenomenon. It is due to the need for additional reinforcements for structural rigidity, the addition of a third shear web, and the use of all-glass materials [23]. The distribution of mass density and flapwise stiffness on both baseline NREL 5 MW and optimized NREL 5 MW are shown in Figure 4.45.

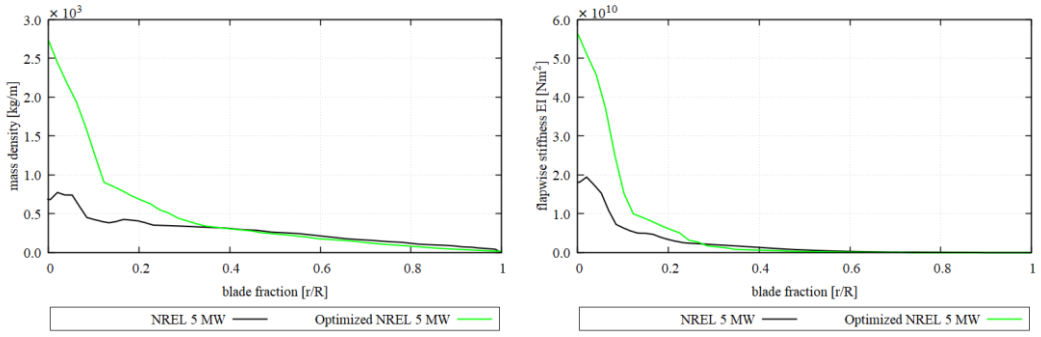

Figure 4.45. Mass density and flapwise stiffness distribution of baseline NREL 5 MW and optimized NREL 5 MW

The present study's interpretation of the mass density, edgewise stiffness, and flapwise stiffness of a 5 MW turbine is closer to the UpWind 5 MW turbine than the NREL 5 MW, mainly due to all glass material being used in the present and the UpWind study. Figure 4.46 shows the spanwise distribution of mass density and flapwise stiffness of both NREL 5 MW and Upwind 5 MW blades.

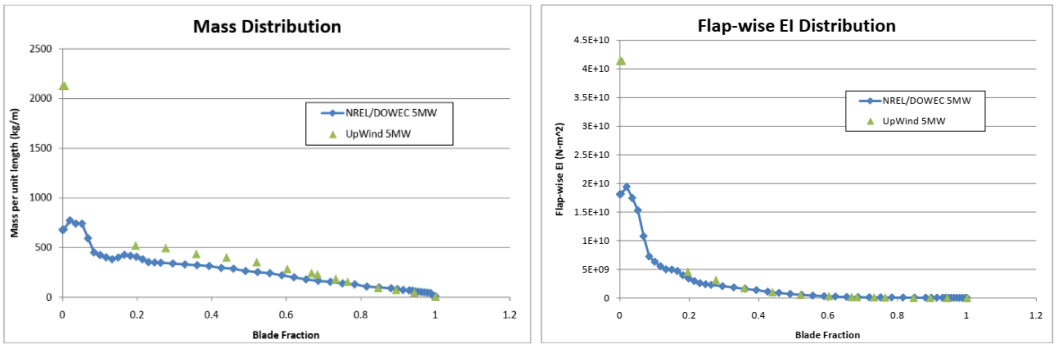

Figure 4.46. Mass density and flapwise stiffness distribution of NREL 5 MW and UpWind 5 MW (reproduced from [23])

Both NREL 5 MW and Upwind 5 MW turbines were developed using DU airfoil families used in DOWEC 6 MW's blade. The DOWEC (Dutch Offshore Wind Energy Converter) project aimed to develop a realistic 6 MW offshore wind turbine for offshore testing purposes in 2006 [44]. DOWEC turbine has a rotor radius of 64.5 meters, consisting of 62.7 meters blade and a 1.8-meter hub radius. DOWEC has been the primary reference of both NREL and UpWind 5 MW, mainly due to known blade geometry (airfoil type and location). However, the composite layup is not made available to the public. For this reason, despite having similar blade shapes, the mass and stiffness distribution of NREL 5 MW and UpWind 5 MW is different.

NREL 5 MW serves the intention of research and reference purposes, in which a large room for optimization study is intentionally left to be carried out by the wind turbine engineer. With a hub radius of 1.5 meters, the blade length of the NREL 5 MW blade was designed by truncating the 62.7 meters DOWEC blade at 61.5 meters to match the length of LM Glasfiber blades used on the actual REpower 5 MW [14]. The composite layup of NREL 5 MW was approximated by gathering as much as publicly available data of conceptual models used in the WindPACT, RECOFF, and DOWEC projects [14].

UpWind 5 MW was designed within the framework of the UpWind Project. Up until 2011, UpWind was Europe's largest wind energy research and development project, aimed to develop the design of offshore wind turbines rated 8-10 MW. DOWEC blade geometry (airfoil type and location) is used as the baseline. However, due to the unavailability of the composite layup data, UpWind researchers self-developed a composite material layup, mainly consisting of fiberglass [23].

The main difference between the present study and UpWind's mass and stiffness distribution is due to the fact that the airfoil schedule and twist angle in the present study are modified to increase power production. However, the decreasing trend of blade mass and stiffness and concentration of the mass at the root region in the present study can be understood and justified by observing the trend of the UpWind 5 MW blade.

CHAPTER 5

RESULT AND DISCUSSION

This chapter presents the results of free-decay simulation and aero-elastic coupled with the hydrodynamics performance analysis of all the references, upscaled and upscaled + optimized wind turbines atop the references, and upscaled OC4 DeepCwind semi-submersible floating platform. The performances are compared at power ratings of 5, 10, 15, and 20 MW. At the end of the chapter, several significant findings apart from the aerodynamic and hydrodynamic analysis are presented.

Due to the nature of the present study, which is based on two different engineering backgrounds, aerospace and naval (ship) engineering, the convention of the 6 degrees of freedom (DoF) are different. To help the communication purpose, mentioning the convention used for the 6 DoF are mandatory. Table 5.1 summarizes the convention of all 6 DoF in both translational and rotational motion. Figure 5.1 shows the global coordinate system, 6 degrees of freedom of the floating offshore wind turbines, and the position and heading of the floating turbine in the global coordinate axes.

Table 5.1 The 6 degrees of freedom convention in aerospace and ship engineering

Motion	Axis	Convention in aerospace eng.	Convention in ship engineering
Translation	X	Longitudinal	Surge
	Y	Lateral	Sway
	Z	Vertical	Heave
Rotation	X	Roll	Roll
	Y	Pitch	Pitch
	Z	Yaw	Yaw

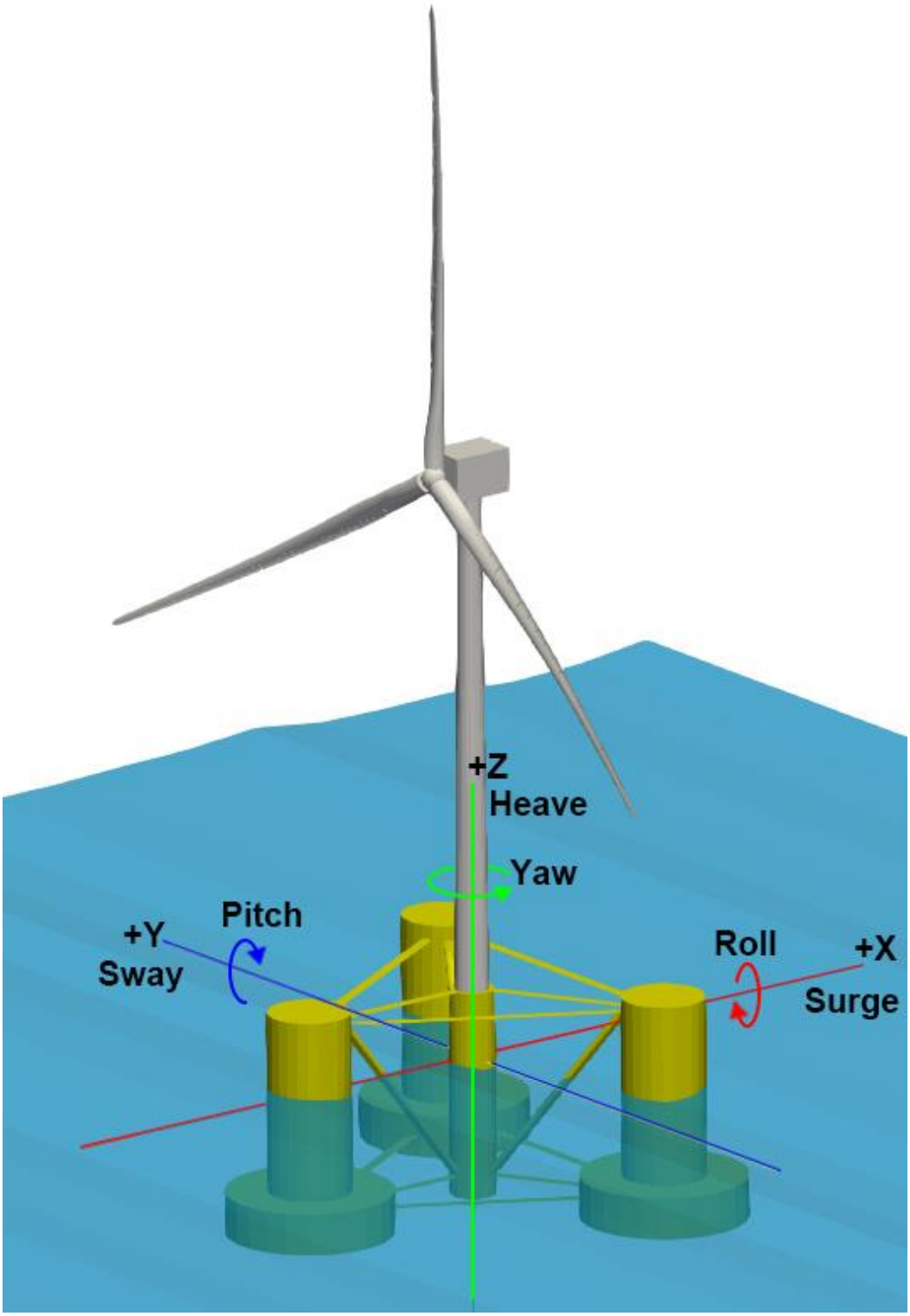

Figure 5.1. The 6 degrees of freedom for a floating offshore wind turbine

5.1 Free Decay Simulation

Natural frequency (or eigenfrequency) is the frequency at which a system tends to oscillate. The period corresponding to natural frequency is called as natural period. The natural periods of the wind turbines are calculated from sets of free-decay simulations. In the present study, the simulations are run for 8000 seconds, and the first 2000 seconds of initialization are discarded. Due to no wind condition being applied in the simulation, the AeroDyn and InflowWind module is turned off. The generator is locked, and the tower's bending mode is deactivated. Still water condition is applied in the HydroDyn module, and an initial non-zero displacement is used for the degree of freedom in interest.

Natural periods of the surge, heave, pitch, and yaw motion for all RWTs are given in Table 5.2. Theoretically, the natural periods for the wind turbine will increase by of square root of the scaling factor ($\sqrt{s}$ or $s^{1/2}$) as the rotor size increases. However, Leimeister et al. predict that the heave's natural period follows the linear scaling, while the surge and yaw are scaled with approximately $s^{3/2}$ and $s^{5/2}$, respectively [19].

Table 5.2 The natural period of the reference wind turbines

Power (MW)	Turbine	Natural Period (s) of DoF			
		Surge	Heave	Pitch	Yaw
5	NREL 5	107.12	17.54	25.64	78.93
	Optimized NREL 5	107.12	17.54	26.19	78.93
10	Upscaled NREL 5	199.97	20.83	30.15	157.87
	Up + Opt NREL 5	199.97	20.83	30.15	157.87
	IEA 10	187.47	20.83	28.70	157.87
15	Upscaled NREL 5	230.73	22.98	33.51	239.96
	Up + Opt NREL 5	230.73	22.98	33.51	239.96
	Upscaled IEA 10	230.73	22.72	32.43	239.96
	IEA 15	230.73	22.72	29.50	230.73
20	Upscaled NREL 5	299.95	24.49	36.36	299.95
	Up + Opt NREL 5	299.95	24.49	36.80	299.95
	Upscaled IEA 10	299.95	24.49	33.89	299.95
	Upscaled IEA 15	285.67	24.49	32.43	299.95

The surge, heave, pitch, and yaw natural period obtained of all turbines simulated in the present study, except for the 135-meters optimized NREL 5, is shown in Figure 5.2 to Figure 5.5. The purpose of the graph is to analyze the trend of the natural period as the rotor size increase. Due to the 20 MW 135-meters optimized NREL 5's length being intentionally designed to match the length of upscaled IEA 15, it does not directly relate to the original NREL 5 MW and is omitted in the graphs. Curve fittings are used to obtain the trend for each wind turbine from the nominal to the upscaled version. The trend line function, f(x), shows the trend for each turbine.

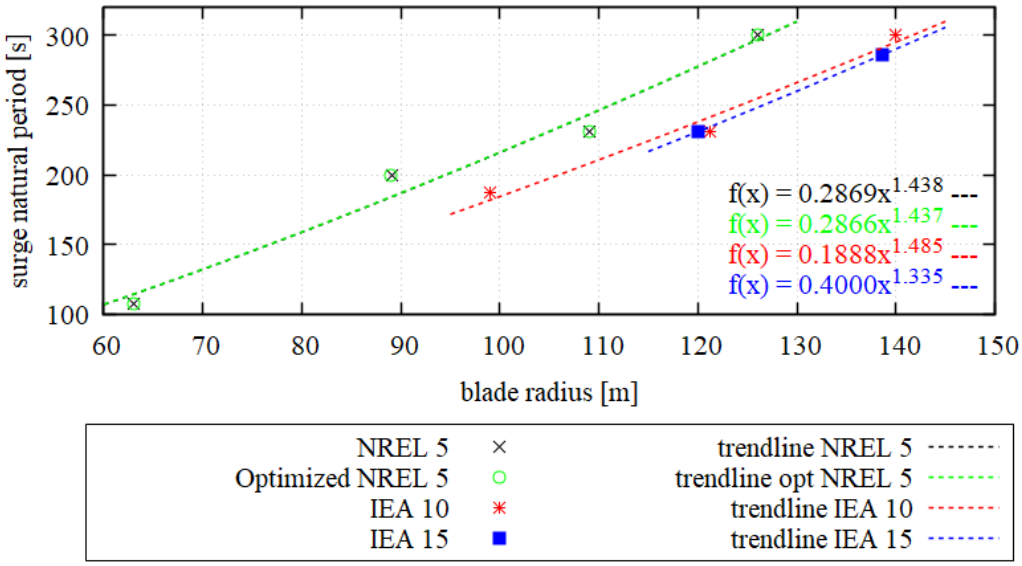

Figure 5.2. The surge natural period

From the trendline of all four turbines presented in Figure 5.2, the natural period in surge motion shows an increase with an average scaling factor of $x^{1.423}$. Conveniently, it is in good agreement with Leimeister et al., with $s^{3/2}$. The surge natural periods of the non-optimized NREL 5 at any blade length are very close to those of the optimized NREL 5. Since the blades' length of the upscaled + optimized NREL 5 are taken from linear scaling of the original NREL 5 MW, only one line is clearly visible in Figure 5.2.

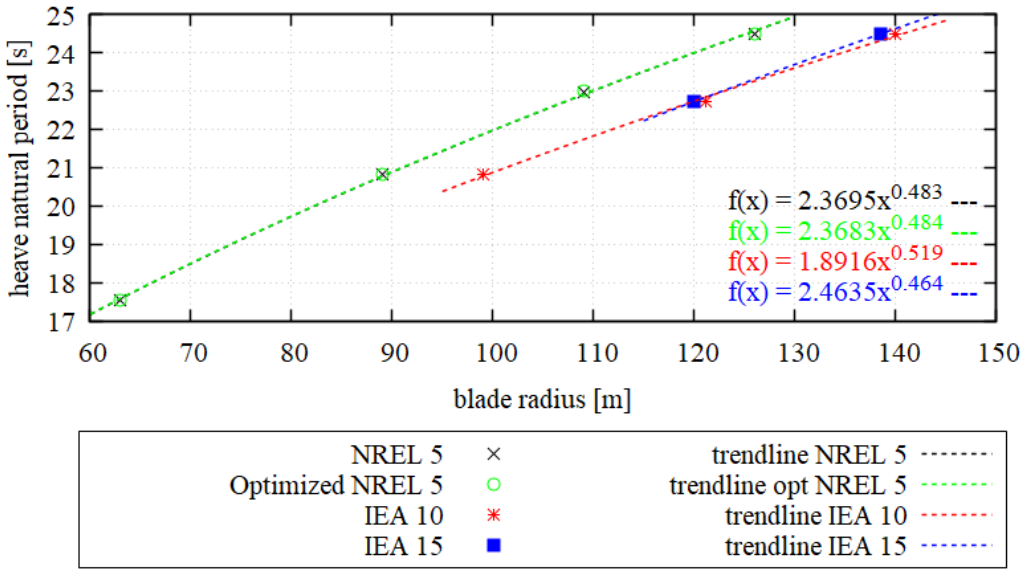

Figure 5.3. The heave natural period

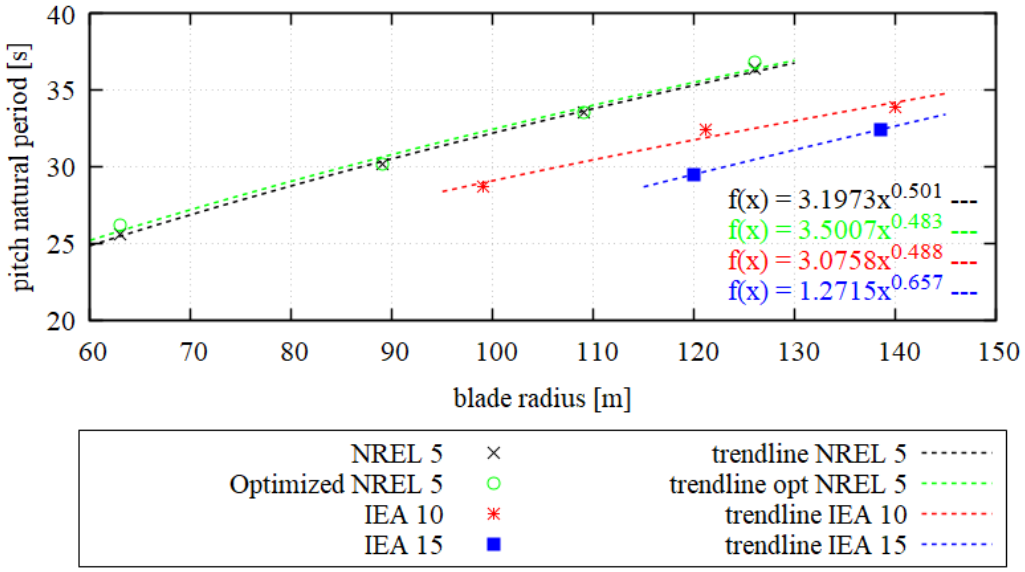

Figure 5.4. The pitch natural period

As can be seen in Figure 5.3, the heave natural period increase with an average scaling factor of $x^{0.488}$. It is in good agreement with Leimeister et al. and linear scaling, with $s^{1/2}$. Again, the heave natural period of NREL 5 at any blade length is very close to the heave natural period of the optimized NREL 5. The pitch natural

period increase with an average scaling factor of $x^{0.532}$, which can be found in Figure 5.4. The pitch natural period is in good agreement with Leimeister et al. and linear scaling, with $s^{1/2}$. For the pitching motion, a slight difference between the natural period of NREL 5 and optimized NREL 5 can be observed at any blade length.

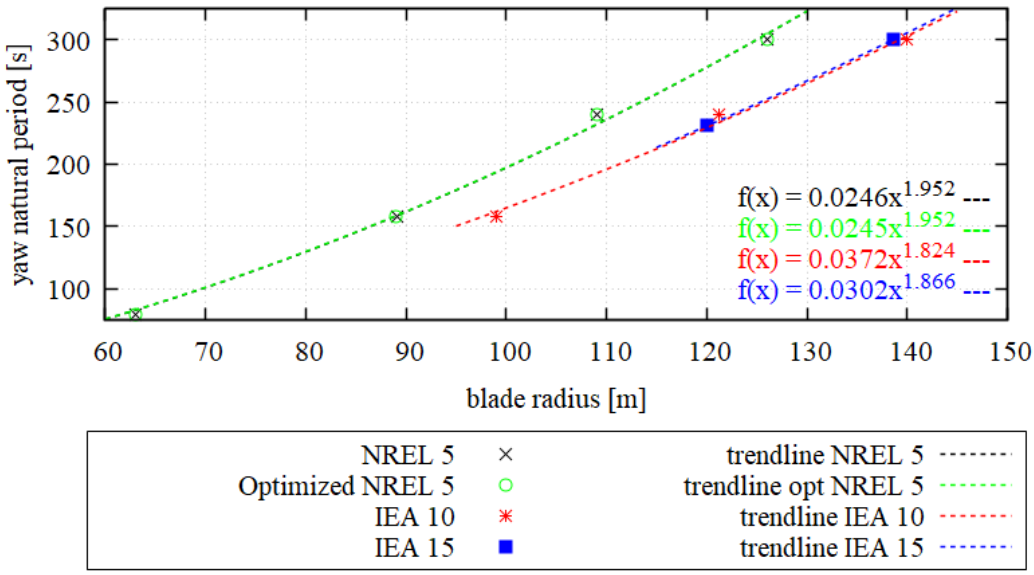

Figure 5.5. The yaw natural period

From Figure 5.5, the yaw natural period increase with an average scaling factor of $x^{1.899}$. It is closer to $s^{4/2}$, which is less when compared to Leimeister et al. with $s^{5/2}$. The yaw natural period of NREL 5 at any blade length is very close to the heave natural period of the optimized NREL 5. Thus, only one line is visible in Figure 5.5.

5.2 5 MW Turbines' performance

In the 5 MW rated power category, the performance of the original NREL 5 MW and optimized NREL 5 MW atop the original OC4 DeepCwind semi-submersibles are compared. This is performed to validate the model, design load cases, and calculation of PSD and RAO. Adding optimized NREL 5 MW to the comparison shows the optimization process's effect on the turbine's overall performance. Recall from the optimization process that the length and the root chord of the blade are kept

constant. However, the chord length, twist angle, airfoil location, shell thickness, and mass density distribution are pretty much unconstrained. The two turbines simulated in the 5 MW rated power category are shown in Figure 5.6.

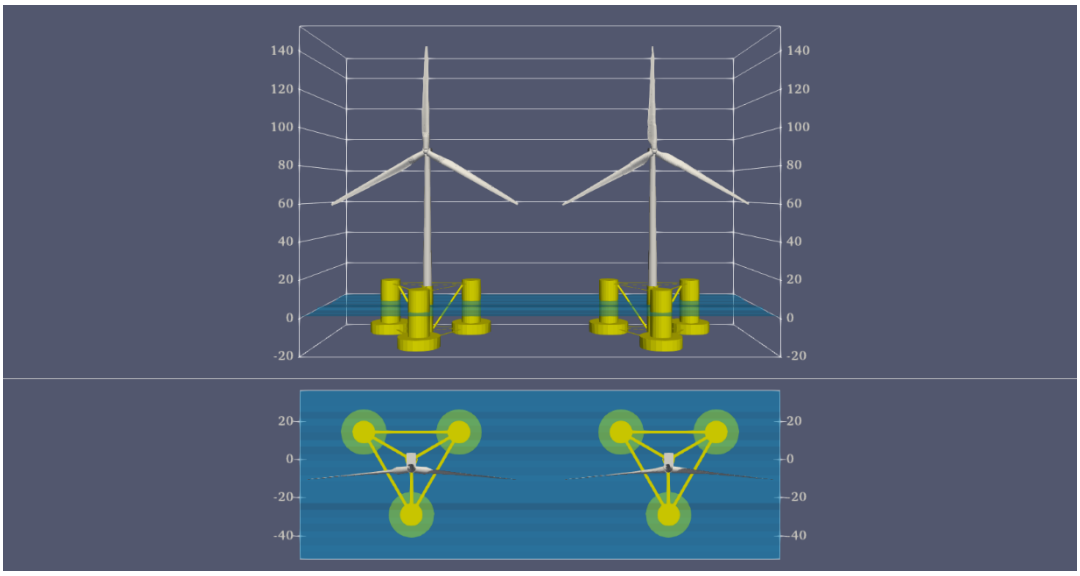

Figure 5.6. Size comparison of 5 MW rated power of NREL 5 and Optimized NREL 5 MW, respectively

A comparison of the chord, twist angle, flapwise stiffness, edgewise stiffness, and mass density of the two turbines is shown in Figure 5.7 to Figure 5.9. Given the large optimization space, the maximum chord of the optimized NREL 5 is larger, and its location is earlier than the original NREL 5 MW. To maintain its structural strength, the mass of the root transition section, where the shell and shear web thickness is concentrated (in Figure 4.39), is higher than the original NREL 5 MW. Consequently, edgewise and flapwise stiffness in this region is also higher than the original NREL 5 MW. Since the same airfoil types are used in the original and optimized NREL 5 MW, the twist angle distribution is relatively similar. Identical towers are used for both turbines. Hence, only one line can be observed in the tower mass density distribution, shown in Figure 5.9.

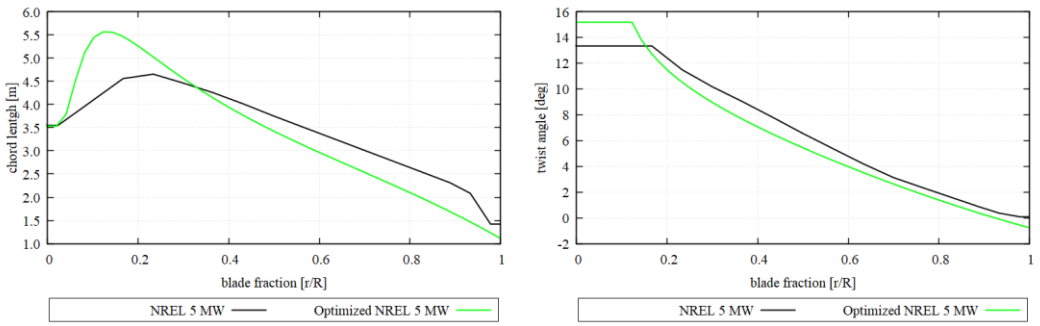

Figure 5.7. Chord length and twist angle distribution of 5 MW rated power of NREL 5 and Optimized NREL 5 MW

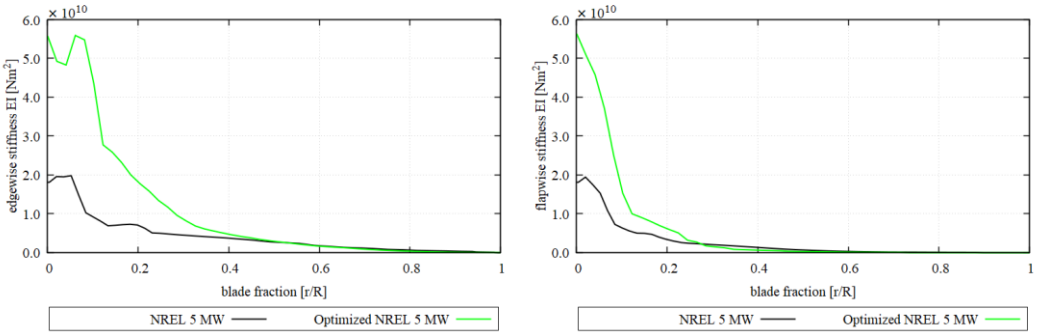

Figure 5.8. Edgewise and flapwise stiffness distribution of 5 MW rated power of NREL 5 and Optimized NREL 5 MW

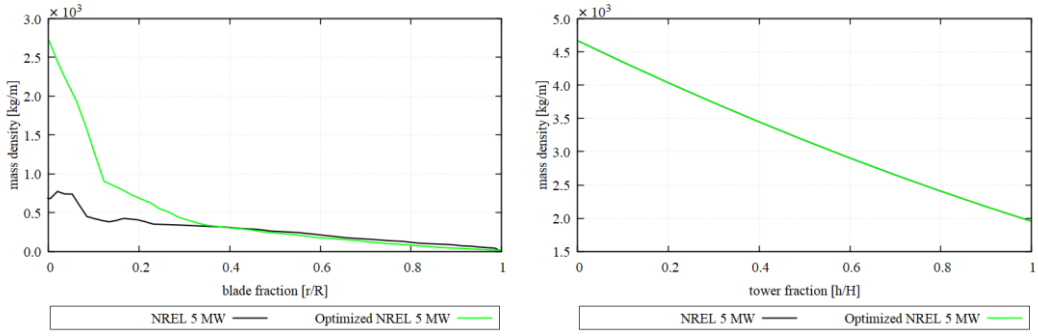

Figure 5.9. Blade and tower's mass density distribution of 5 MW rated power of NREL 5 and Optimized NREL 5 MW

5.2.1 Hydrodynamic performance

The following discussion compares the hydrodynamic performance consisting of PSDs and RAOs in the surge, heave, and pitch DoF resulting from load case 2.6 and load case 3.7. The PSD curves are shown within the frequency region of 0.0-0.5 Hz, whereas the response amplitude operator (RAO) is shown within 0.05-0.25 Hz. The RAO out of this region does not reflect any physical meaning since the PSD of the wave is very close to zero, as previously shown in Figure 3.16.

The power spectral density (PSD) of the platform is plotted using the Fast Fourier Transformation (FFT) method, and the Response Amplitude Operator (RAO) is calculated based on Equation 3.6. Overall, the PSD and RAO in the surge, heave, and pitch motion agree with OC4 [39], validating the way the simulations are conducted and the method for calculating PSD and RAO.

The two turbines' surge natural frequencies, at around 0.01 Hz, can be observed from the surge PSD curves, shown in Figure 5.10. The coupling of surge and pitch motion can be seen from the PSD curve at around 0.04 Hz. Finally, the RAOs of both turbines are shown in Figure 5.11.

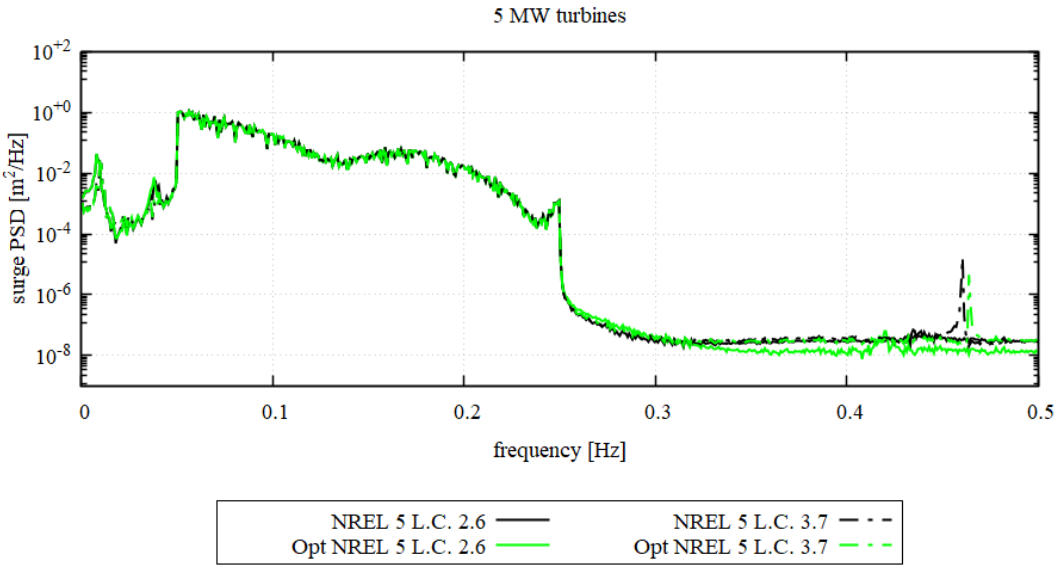

Figure 5.10. Surge PSD of NREL 5 MW and Optimized NREL 5 MW

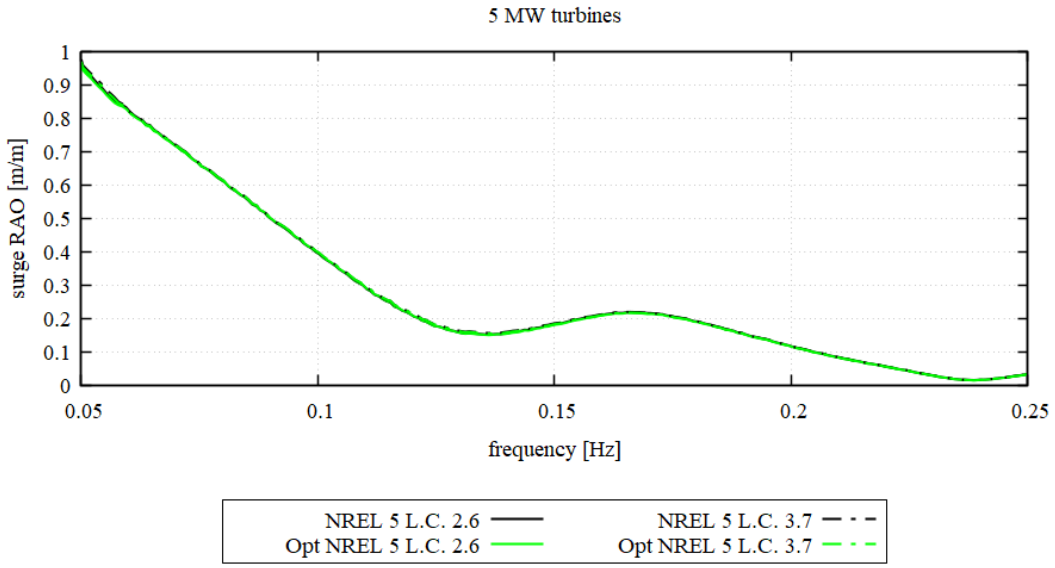

Figure 5.11. Surge RAO of NREL 5 MW and Optimized NREL 5 MW

From Figure 5.10, the surge PSD of load cases 2.6 and 3.7 are approximately similar in the wave excitation region (0.05 Hz -0.25 Hz). It indicates that the wind does not significantly affect the surge PSD in this region. Outside the wave excitation region, at a frequency higher than 0.25 Hz, there were spikes for the load case 3.7 for both turbines, indicating that the wind heavily affects the surge PSD outside the wave-excitation region.

Response amplitude operators of DLC 2.6 and 3.7 of both original and optimized NREL 5 MW are approximately similar due to the negligible effect of the wind in the wave excitation region, as shown in Figure 5.11. The surge RAOs are maximum at the low wave frequency, or in other words, at a relatively long wave. The RAO at 0.05 Hz is approximately a unit value, indicating that the turbines are surging together with the long wave.

The two turbines' heave natural frequencies, at around 0.057 Hz, can be observed from the heave PSD curves, shown in Figure 5.12, whereas the heave RAOs of both turbines are shown in Figure 5.13. The heave natural frequency lies within the wave excitation region.

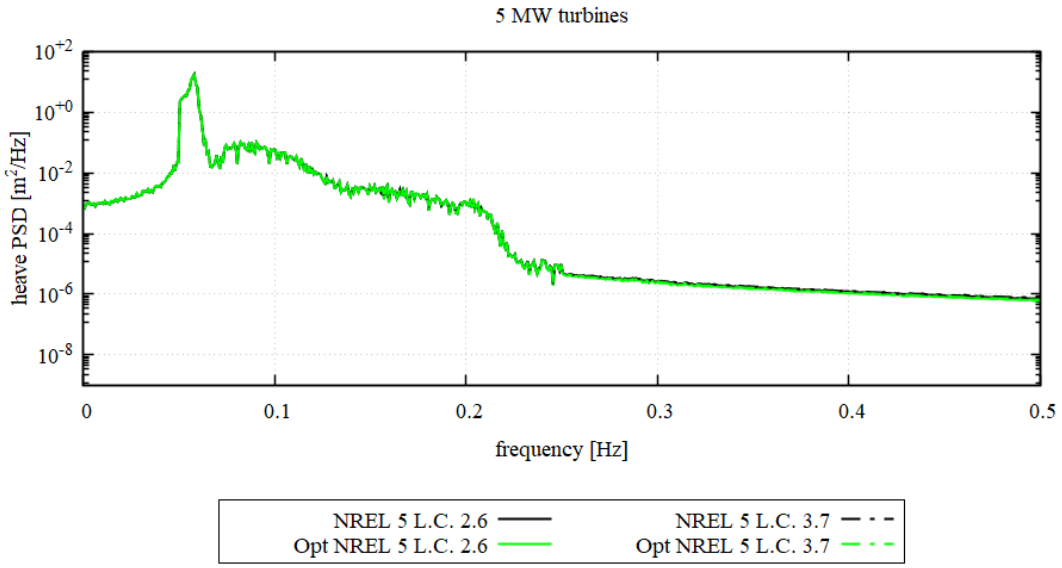

Figure 5.12. Heave PSD of NREL 5 MW and Optimized NREL 5 MW

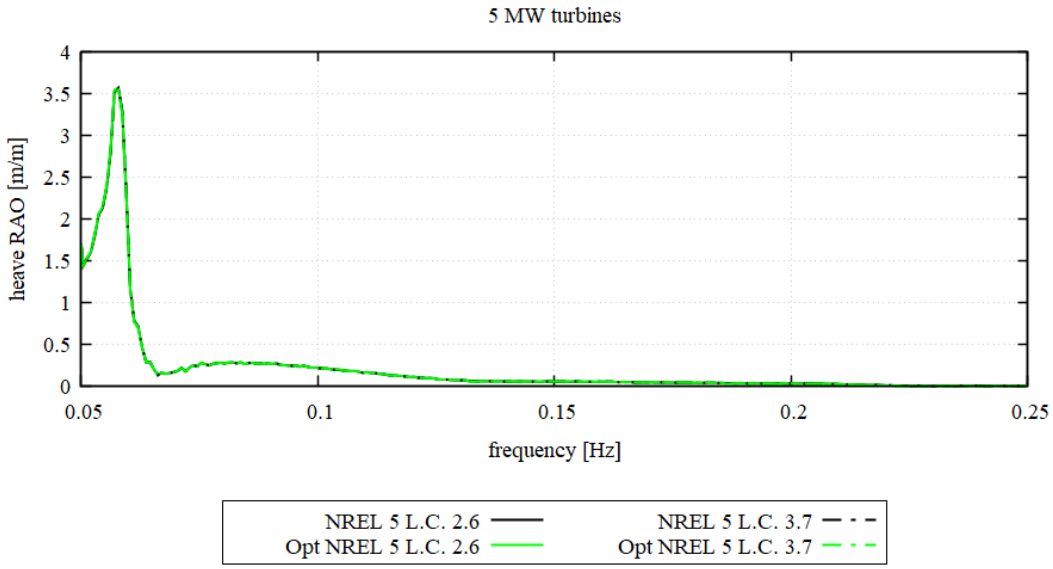

Figure 5.13. Heave RAO of NREL 5 MW and Optimized NREL 5 MW

From Figure 5.12, the heave PSD shows that heave motion is independent of the other degrees of freedom. Wind effect on the PSD is negligible in any region, inside and outside the wave excitation region. The RAO is maximum at the heave natural frequency with a value much more than 1. Certainly, the original OC4 semi-submersible is heaving under a wave with a frequency of ±0.06 Hz.

Pitch natural frequencies of the two turbines can be observed from the pitch PSD curves shown in Figure 5.14, at around 0.04 Hz, whereas the pitch RAOs of both turbines are shown in Figure 5.15. The pitch and surge motion coupling can be seen from the PSD curve at around 0.01 Hz.

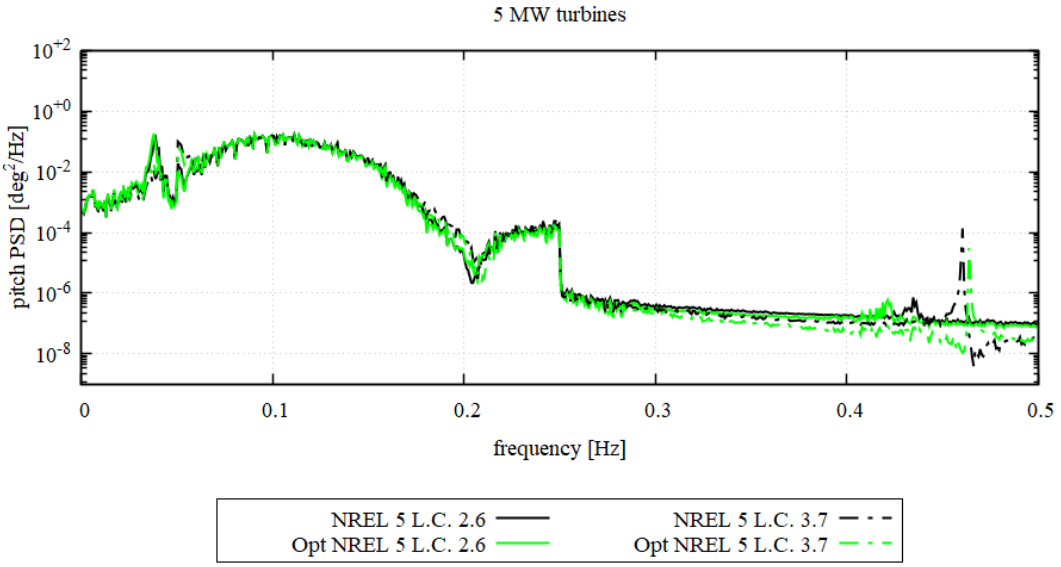

Figure 5.14. Pitch PSD of NREL 5 MW and Optimized NREL 5 MW

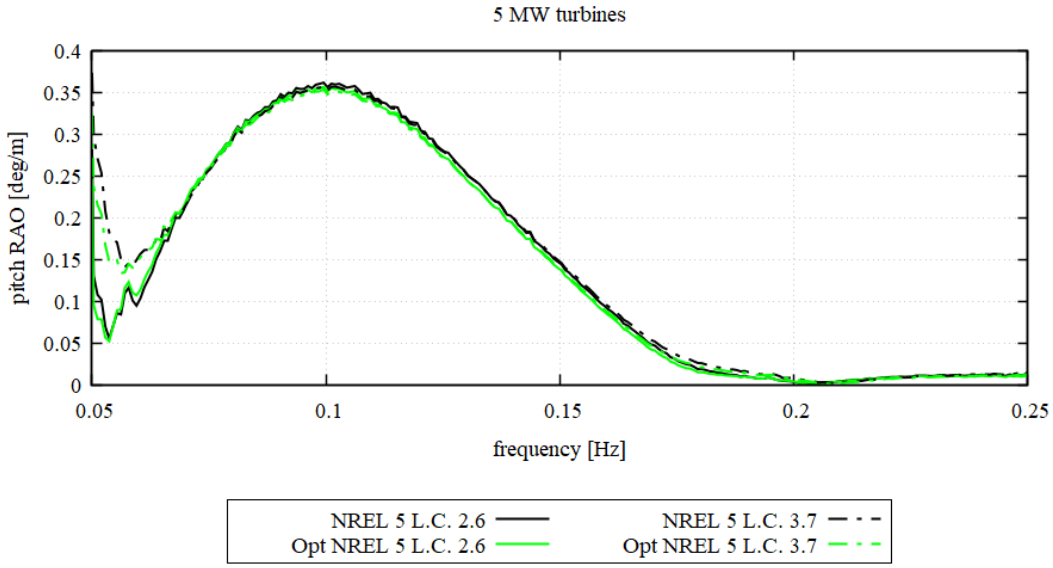

Figure 5.15. Pitch RAO of NREL 5 MW and Optimized NREL 5 MW

In the wave excitation region, as shown in Figure 5.14, the pitch PSD of load cases 2.6 and 3.7 are very similar, except in the early part of the wave excitation region, where the PSDs of DLC 3.7 is slightly above the PSD of DLC 2.6. Outside the wave excitation region, at a frequency higher than 0.25 Hz, there were spikes for the load case 3.7 for both turbines, indicating that the wind heavily affects the pitch PSD outside the wave-excitation region. Like the PSD, the response amplitude operators of DLC 2.6 and 3.7 of both original and optimized NREL 5 MW are approximately similar, except for the early part of the wave excitation region. Overall, the pitch RAO of both turbines is less than one everywhere inside the wave excitation region.

5.2.2 Aero-elastic performance

Aero-elastic performance of the original NREL 5 MW and optimized NREL 5 MW turbines are compared in the following discussion. The comparison of the two turbines will show the effect of optimization on the aero-elastic performance of the turbine. Figure 5.16 and Figure 5.17 compares the rotor aerodynamic power coefficient (CP) and rotor aerodynamic thrust coefficient (CT). Generator power and rotor thrust are compared in Figure 5.18 and Figure 5.19, respectively.

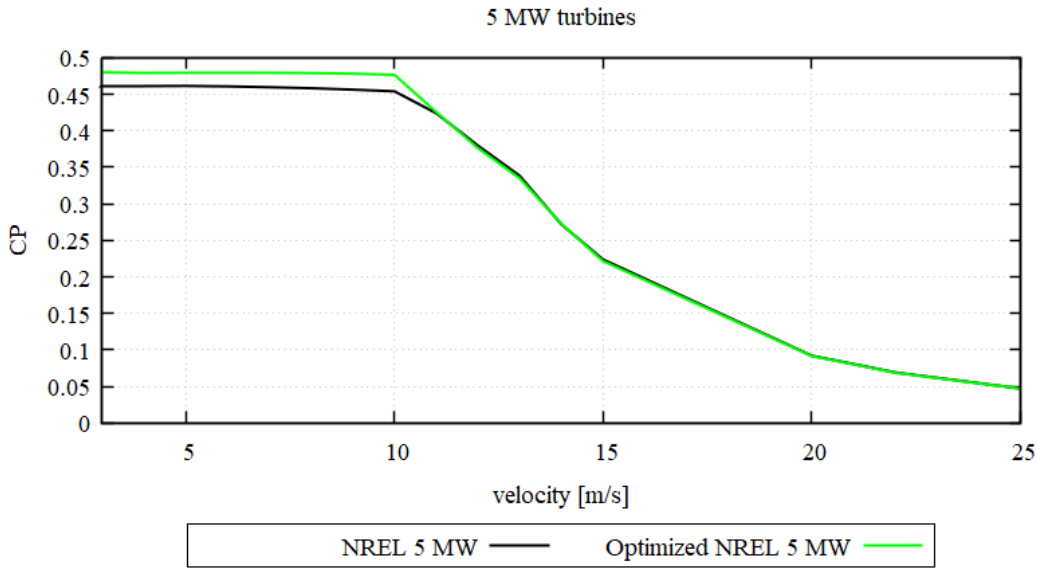

Figure 5.16. Power Coefficient of NREL 5 MW and Optimized NREL 5 MW

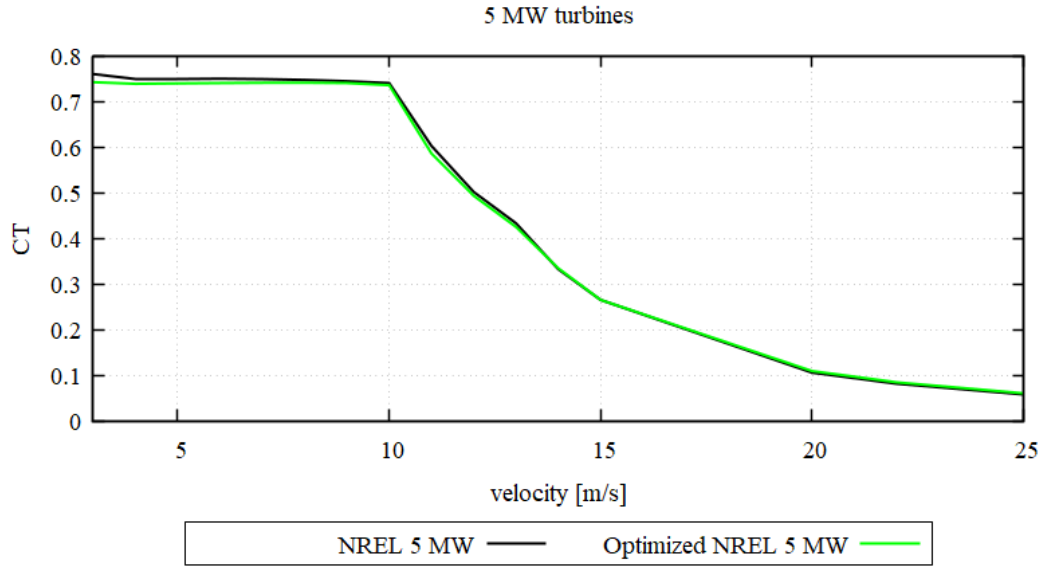

Figure 5.17. Thrust Coefficient of NREL 5 MW and Optimized NREL 5 MW

Note that an identical control strategy is applied for both original NREL 5 MW and optimized NREL 5 MW. Thus, any difference in the performance is purely due to the optimization. Recall that the only differences between the original and optimized turbines are the blade's aerodynamic shape, mass, and stiffness. The tower, hub height, generator components, platform, mooring lines, etc., are all identical to each other.

From Figure 5.16, as expected, the power coefficient of the optimized turbine is higher than the original NREL 5 MW. These differences can be observed mainly in the below-rated wind speed region, at region 2. After the rated wind speed is achieved, at region 3, the blade’s pitch control is activated and reduces the performance of both turbines, causing the CP to decline. In region 3, the performances of both turbines are relatively similar. The thrust coefficient of both turbines, CT, is relatively similar throughout the whole operating wind speed. As can be seen in Figure 5.17, ten m/s is the final velocity before the thrust coefficients of both turbines decline.

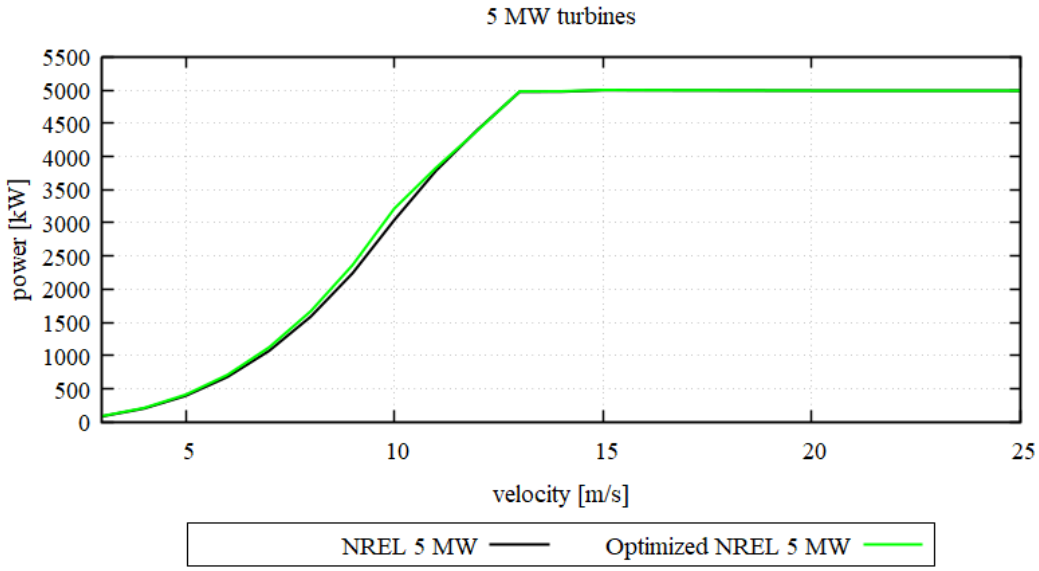

Figure 5.18. The power curve of NREL 5 MW and Optimized NREL 5 MW

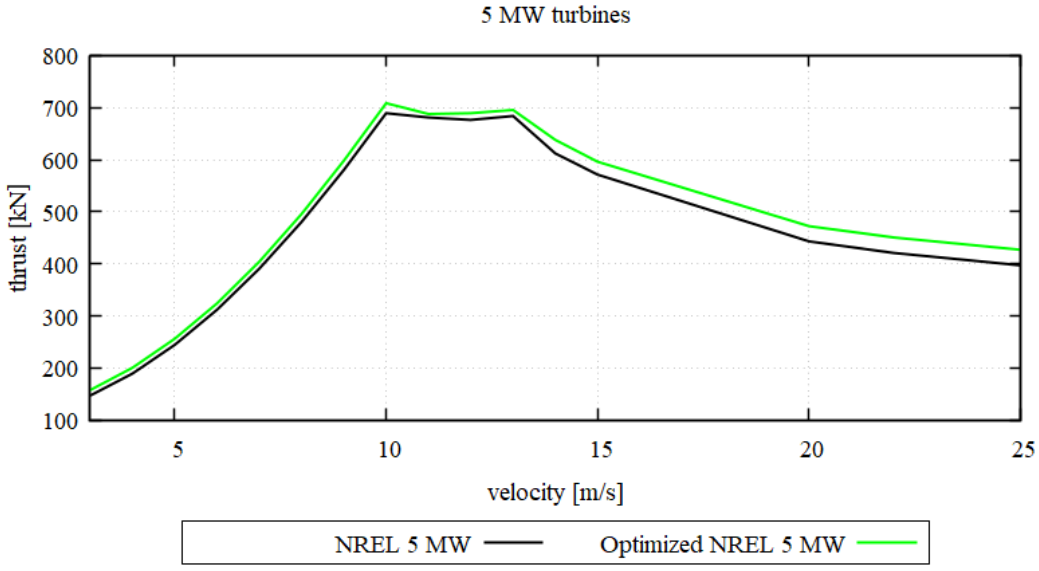

Figure 5.19. Thrust curve of NREL 5 MW and Optimized NREL 5 MW

The optimized NREL 5 MW, with higher CP, also produces higher power until the rated wind speed is achieved, as shown in Figure 5.18. However, the increase in the power curve of the optimized NREL 5 is not significant compared to the original design. This phenomenon shows that the design and performance of optimized NREL 5 MW is still conservative to the original NREL 5 MW. From Equation 3.8,

the AEP of the original NREL 5 MW is 9.760E+06 kWh/yr, while the AEP of the Optimized NREL 5 is 1.010E+07 kWh/yr, 3.4% higher than the baseline.

The rated speed for NREL 5 MW is 11.4 m/s. However, 5 MW is achieved by both turbines at a higher wind speed than 11.4 m/s. It is due to the controller's thrust peak shaving implementation, which can be observed from the thrust curve shown in Figure 5.19. The rotor thrust of the optimized turbine is always higher than the original turbine. These differences in thrust must be carefully considered when designing large wind turbines since higher thrust will result in the turbine having a lower blade-to-tower clearance.

5.3 10 MW Turbines' performance

In the 10 MW rated power category, the performance of the upscaled NREL 5, upscaled + optimized NREL 5, and the original IEA 10 MW atop the upscaled OC4 DeepCwind semi-submersibles are compared. The three turbines simulated in the 10 MW rated power category are shown in Figure 5.20.

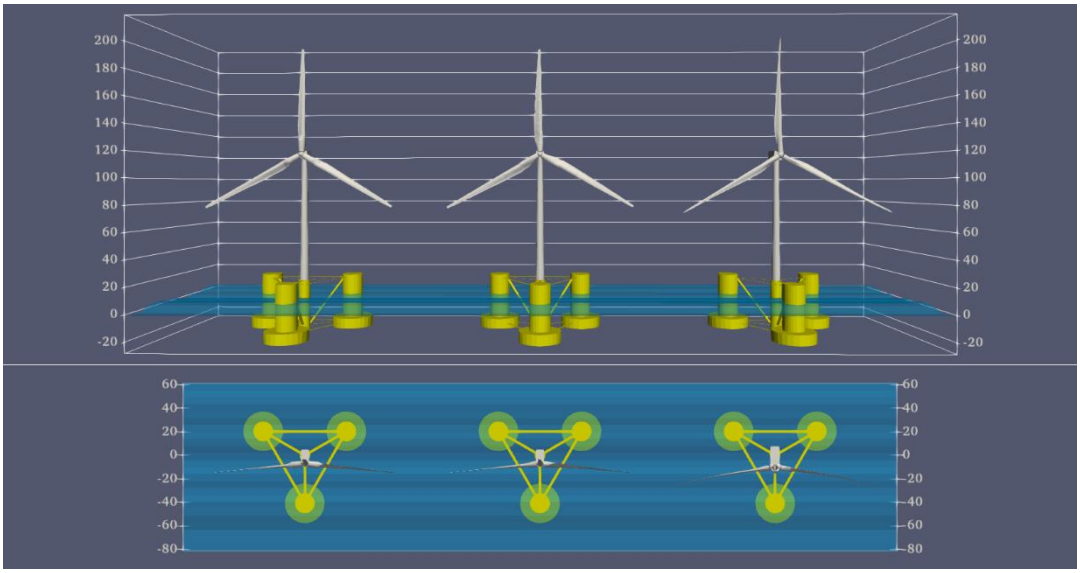

Figure 5.20. Size comparison of 10 MW rated power of upscaled NREL 5, upscaled + optimized NREL 5, and IEA 10, respectively

A comparison of the chord, twist angle, flapwise stiffness, edgewise stiffness, and mass density of the three turbines are shown in Figure 5.21 to Figure 5.23. Despite having different airfoil types, IEA 10 MW has an almost 10-meter longer blade than the upscaled NREL 5 due to its optimization process. Consequently, the required chord length to produce the intended power is shorter than the upscaled NREL 5 and upscaled + optimized NREL5. Again, the maximum chord of the upscaled + optimized NREL 5 is larger, and its location is earlier than the upscaled NREL 5. The mass, edgewise, and flapwise stiffness of the root transition section of upscaled + optimized NREL 5 are higher than the upscaled NREL 5 to maintain its structural strength. Recall from Figure 4.40 that it is where the shell and shear web thickness is concentrated. A relatively similar twist angle distribution is observed for the upscaled and upscaled + optimized NREL 5 since the same airfoil types are used.

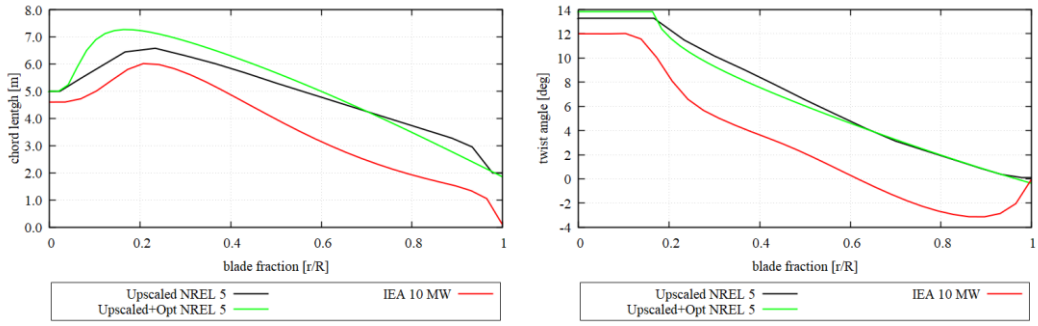

Figure 5.21. Chord length and twist angle distribution of 10 MW rated power of the upscaled NREL 5, upscaled + optimized NREL 5, and IEA 10

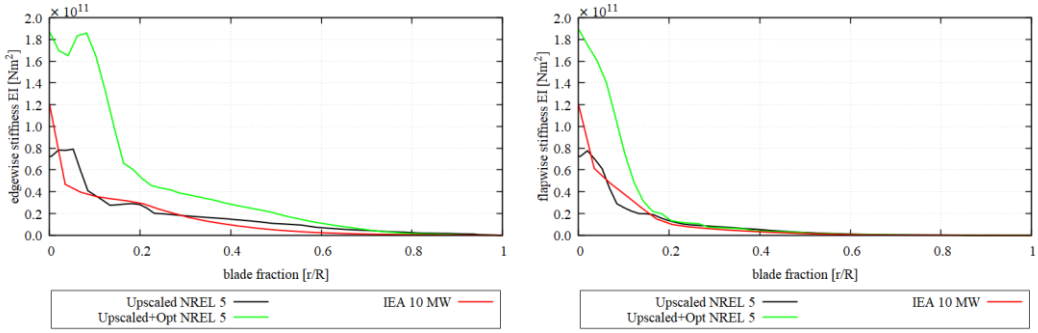

Figure 5.22. Edgewise and flapwise stiffness distribution of 10 MW rated power of upscaled NREL 5, upscaled + optimized NREL 5, and IEA 10

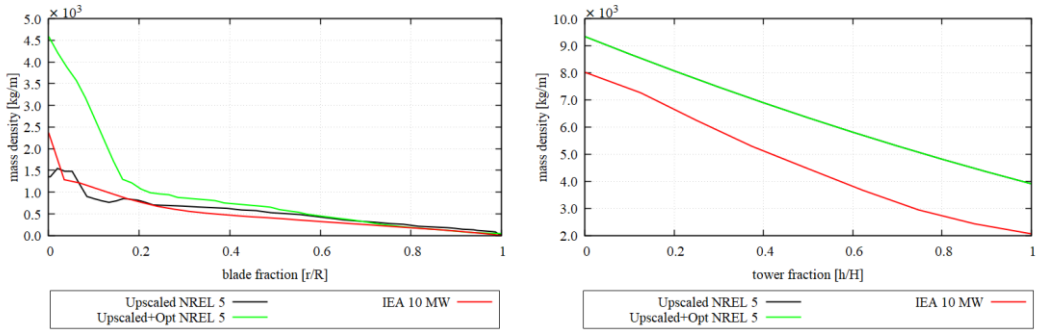

Figure 5.23. Blade and tower's mass density distribution of 10 MW rated power of upscaled NREL 5, upscaled + optimized NREL 5, and IEA 10

5.3.1 Hydrodynamic performance

Hydrodynamic performance consisting of PSDs and RAOs of 10 MW upscaled NREL 5, upscaled + optimized NREL 5, and original IEA 10 MW in the surge, heave, and pitch degrees of freedom from load case 2.6 and load case 3.7 are shown in Figure 5.24 to Figure 5.29. The PSD of the platform is plotted using the FFT method within the frequency region of 0.0-0.5 Hz, and the RAO is calculated based on Equation 3.6 and shown within the frequency region of 0.05-0.25 Hz.

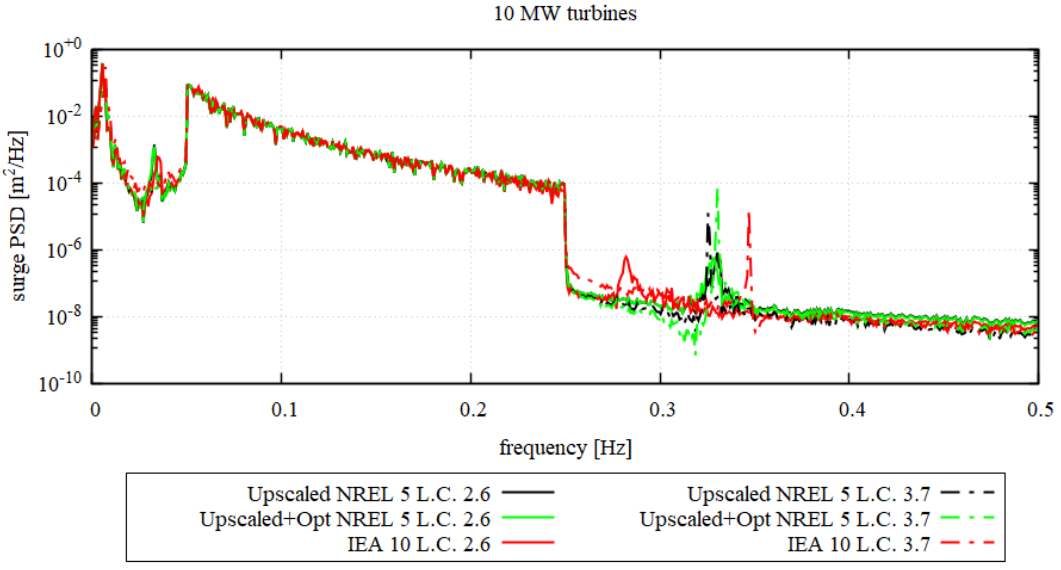

Figure 5.24. Surge PSD of 10 MW upscaled NREL 5, upscaled + optimized NREL 5, and IEA 10

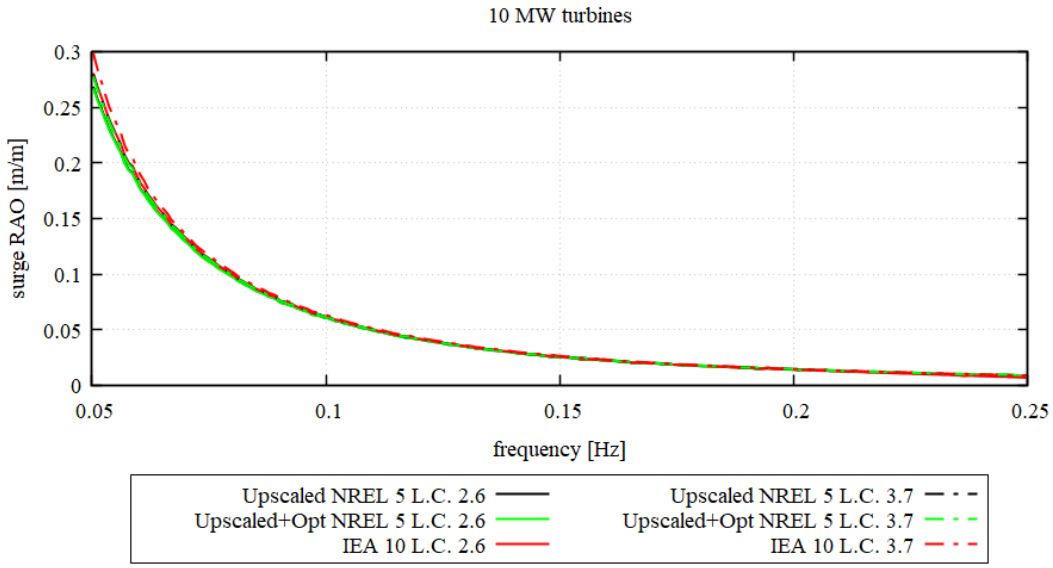

Figure 5.25. Surge RAO of 10 MW upscaled NREL 5, upscaled + optimized NREL 5, and IEA 10

The turbines' surge natural frequency can be observed from the PSD curves shown in Figure 5.24 at around 0.005 Hz. Compared to the result of 5 MW, the surge natural frequency has shifted left towards the lower frequency region. The coupling of surge and pitch motion can be seen in the PSD curve at around 0.033 Hz.

The surge PSD of load cases 2.6 and 3.7 are approximately similar in the wave excitation region (0.05 Hz -0.25 Hz), which shows that the wind does not significantly affect the surge PSD in this region. Outside the wave excitation region, at a frequency higher than 0.25 Hz, the spikes of the load case 3.7 for all turbines are more prominent than DLC 2.6, indicating the dominant effect of wind on the surge PSD outside the wave-excitation region. Like the natural frequency, these spikes also shifted left toward the wave excitation region.

The surge response amplitude operators of DLC 2.6 and 3.7 of all the three turbines are approximately similar due to the negligible effect of the wind in the wave excitation region, as shown in Figure 5.25. The surge RAOs are maximum at the low wave frequency at 0.05 Hz, or in other words, at a relatively long wave. However, the maximum RAO is less than the unit value, which shows that the turbines and

platform surge less than the 5 MW turbines under the same sea state. The platforms see the wave as a short wave, and the wave passes the platform during the entire operational condition.

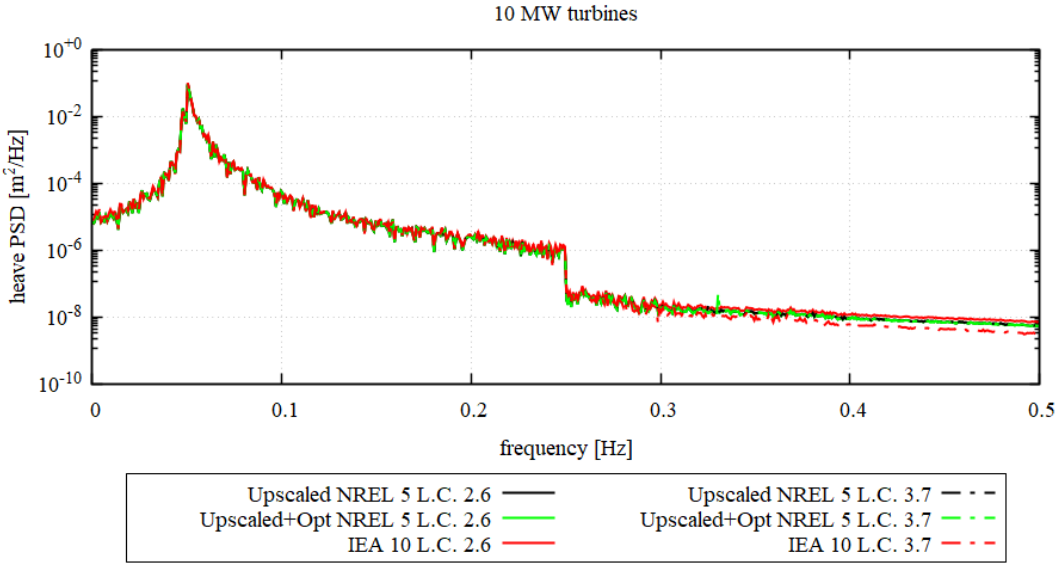

Figure 5.26. Heave PSD of 10 MW upscaled NREL 5, upscaled + optimized NREL 5, and IEA 10

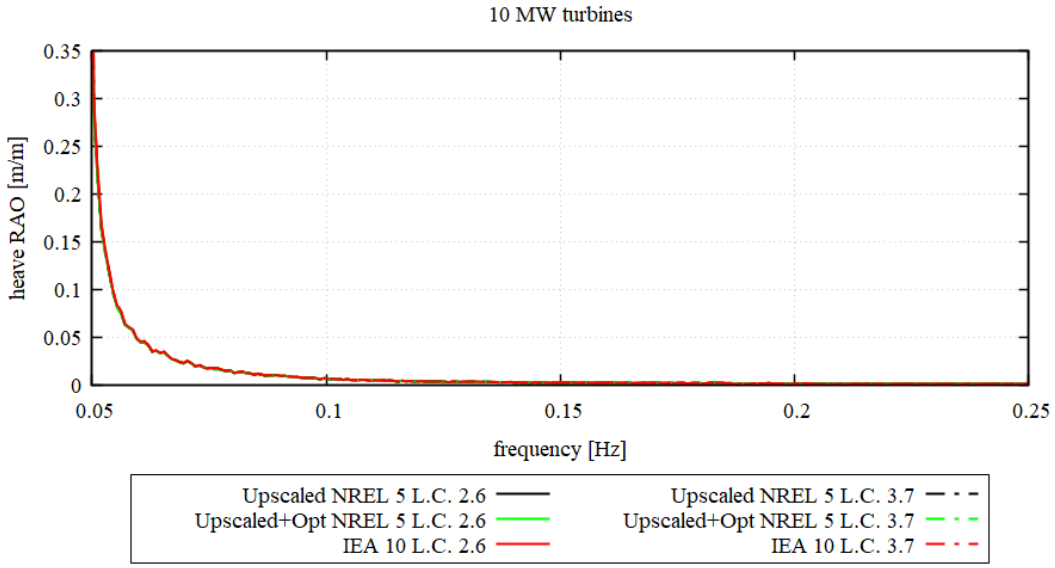

Figure 5.27. Heave RAO of 10 MW upscaled NREL 5, upscaled + optimized NREL 5, and IEA 10

The turbines' heave natural frequencies, at around 0.048 Hz, can be observed from the heave PSD curves, shown in Figure 5.26, whereas the heave RAOs are shown in Figure 5.27. The PSD curves clearly show the separation of heave natural frequency from the wave excitation region. Again, the heave PSD shows that heave motion is independent of the other degrees of freedom. Wind effect on the PSD is negligible in any region, inside and outside the wave excitation region. The insignificancy of the wind effect on the heave motion is strengthened by the heave RAO, which clearly shows no difference in the response of DLC 2.6 and DLC 3.7. Overall, the heave RAO is less than the unit value, which shows that the turbines and platform heave less under the same sea state as the original OC4 semi-submersible design.

Pitch natural frequencies of the 10 MW upscaled NREL 5, upscaled + optimized NREL 5, and the original IEA 10 can be observed from the pitch PSD curves shown in Figure 5.28, at around 0.033 Hz, whereas the pitch RAOs of the three turbines are shown in Figure 5.29. Again, the pitch natural frequency has shifted left towards the lower frequency region when compared to the result of 5 MW. The pitch and surge motion coupling can be seen from the PSD curve at around 0.005 Hz.

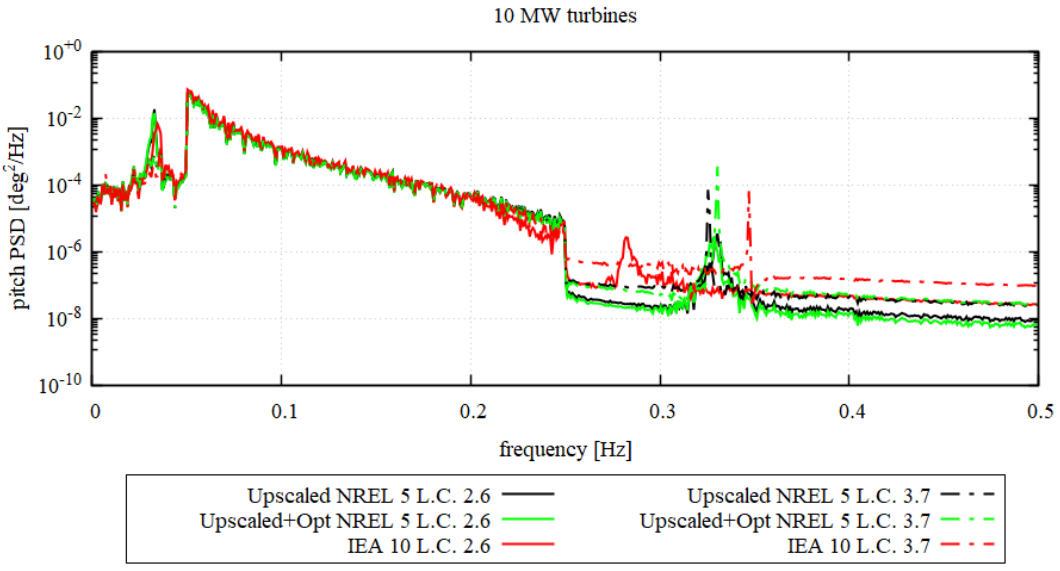

Figure 5.28. Pitch PSD of 10 MW upscaled NREL 5, upscaled + optimized NREL 5, and IEA 10

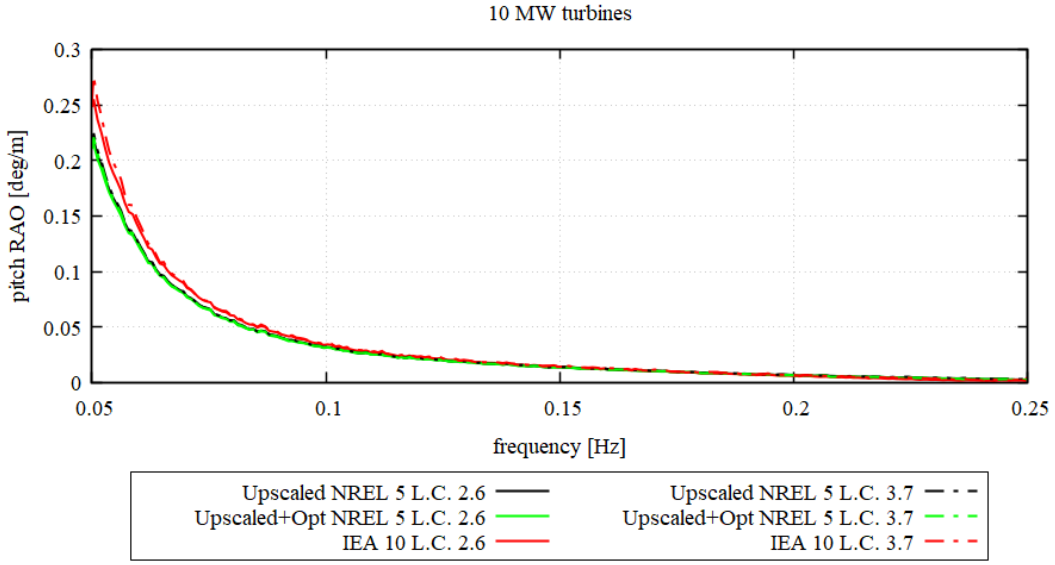

Figure 5.29. Pitch RAO of 10 MW upscaled NREL 5, upscaled + optimized NREL 5, and IEA 10

In the wave excitation region, as shown in Figure 5.28, the pitch PSD of load cases 2.6 and 3.7 are very similar. Outside the wave excitation region, at a frequency higher than 0.25 Hz, the spikes of the load case 3.7 for all turbines are more prominent that DLC 2.6, indicating the dominant effect of wind on the surge PSD outside the wave-excitation region. Like the natural frequency, these spikes also shifted left toward the wave excitation region. The pitch RAOs of all the three turbines are less than one everywhere inside the wave excitation region, as shown in Figure 5.29.

5.3.2 Aero-elastic performance

Aero-elastic performance of the 10 MW upscaled NREL 5, upscaled + optimized NREL 5, and the original IEA 10 turbines are compared in the following discussion. An identical control strategy is applied for both upscaled NREL 5 and upscaled + optimized NREL 5. Figure 5.30 and Figure 5.31 shows the rotor aerodynamic power coefficient (CP) and thrust coefficient (CT). The CP and CT of the upscaled NREL 5 are identical to the baseline NREL 5 MW due to linear scaling. Generator power and rotor thrust are compared in Figure 5.32 and Figure 5.33, respectively.

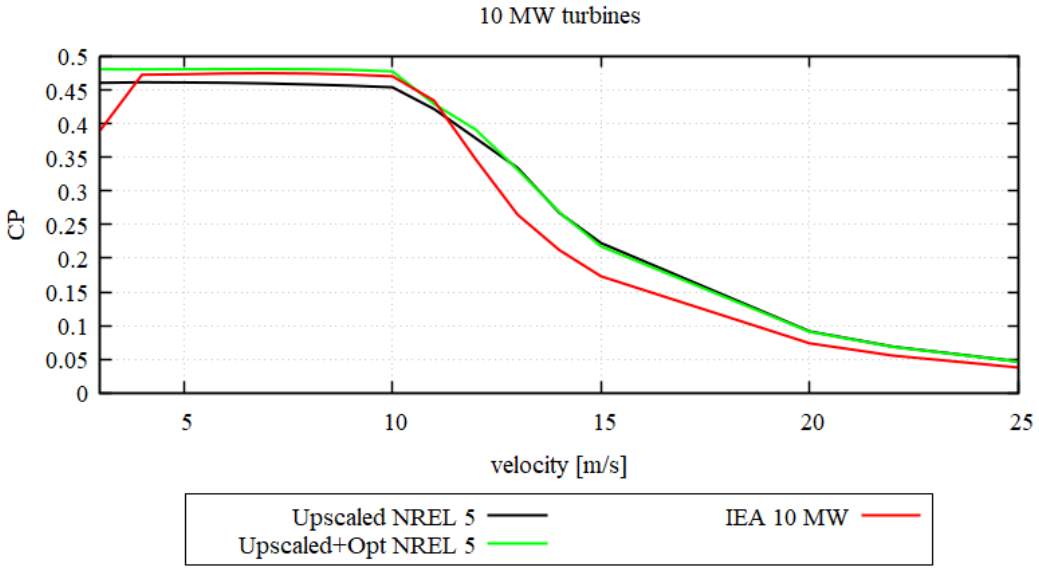

Figure 5.30. Power coefficient of 10 MW upscaled NREL 5, upscaled + optimized NREL 5, and IEA 10

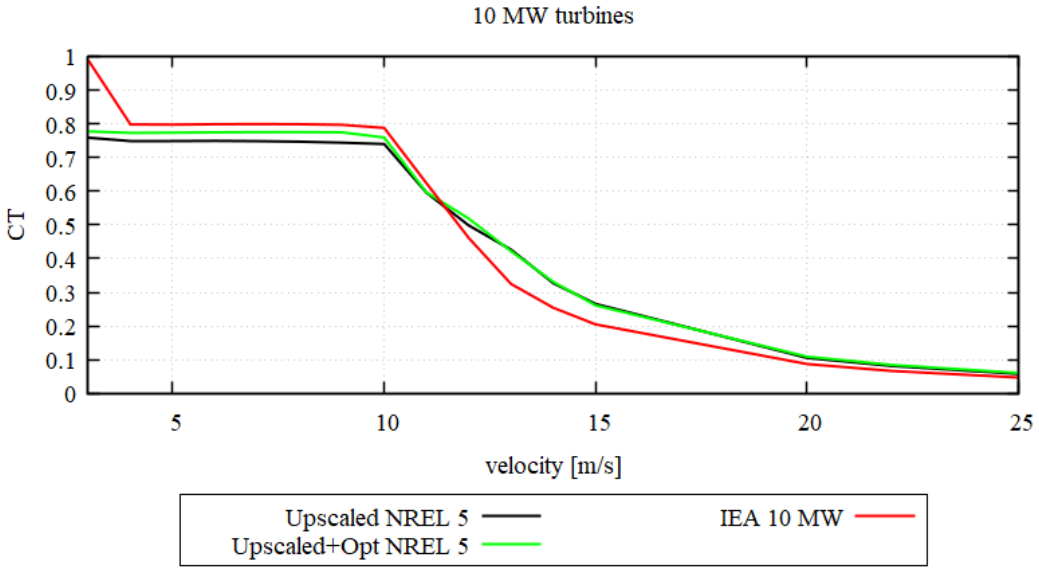

Figure 5.31. Thrust coefficient of 10 MW upscaled NREL 5, upscaled + optimized NREL 5, and IEA 10

From Figure 5.30, the power coefficients of IEA 10 are relatively different from the other two turbines due to IEA 10 having different operating points in the control, which is specially tuned for IEA 10. The power coefficient of the upscaled +

optimized NREL 5 turbine is higher than the upscaled NREL 5. These differences can be observed mainly in region 2, before the blade's pitch control is activated and reduces the performance of the turbines. After the rated wind speed is achieved, the performance of all turbines starts to decline.

Like the CP, the thrust coefficients of IEA 10 are relatively different from the other two turbines due to different operating points, as can be seen in Figure 5.31. The thrust coefficient of the upscaled + optimized NREL 5 turbine in region 2 is higher than the upscaled NREL 5. After the 10 m/s, the thrust coefficient of all the three turbines starts to decline.

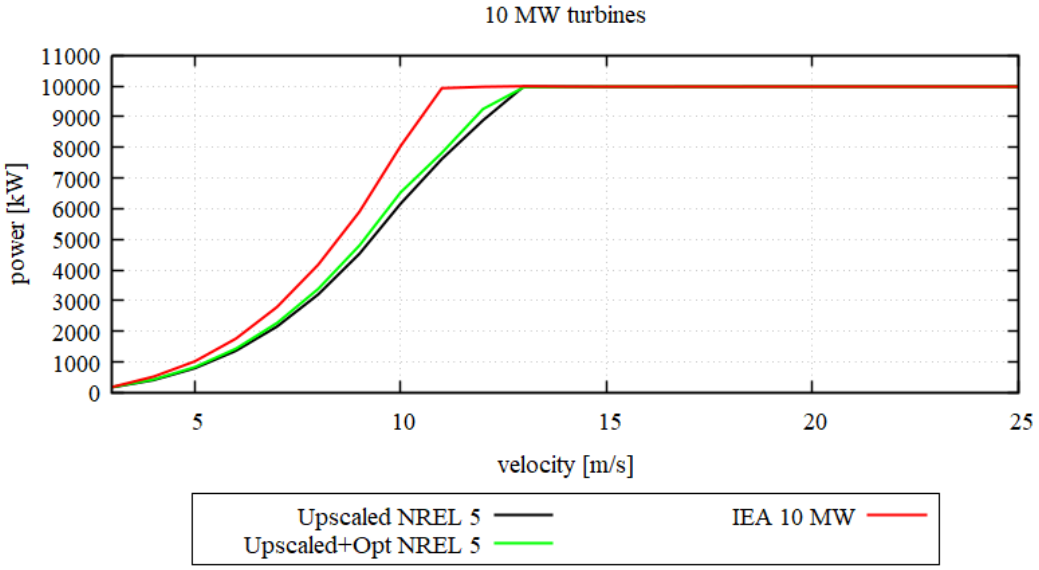

Figure 5.32. The power curve of 10 MW upscaled NREL 5, upscaled + optimized NREL 5, and IEA 10

From Figure 5.32, as expected from the CP difference, the upscaled + optimized NREL 5 produces higher power than the upscaled NREL 5 until the rated power is achieved. However, the improvement of the upscaled + optimized turbines is not significantly compared to the upscaled NREL 5, which again strengthens the conservative performance of the design. Based on Equation 3.8, the AEP of the upscaled NREL 5 is 1.965E+07 kWh/yr, while the AEP of the upscaled + optimized NREL 5 produces 4.2% higher with 2.049E+07 kWh/yr. Due to longer blades, IEA

10 produces much higher than the other two turbines with 2.433E+07 kWh/yr, 23.8% higher than upscaled NREL 5.

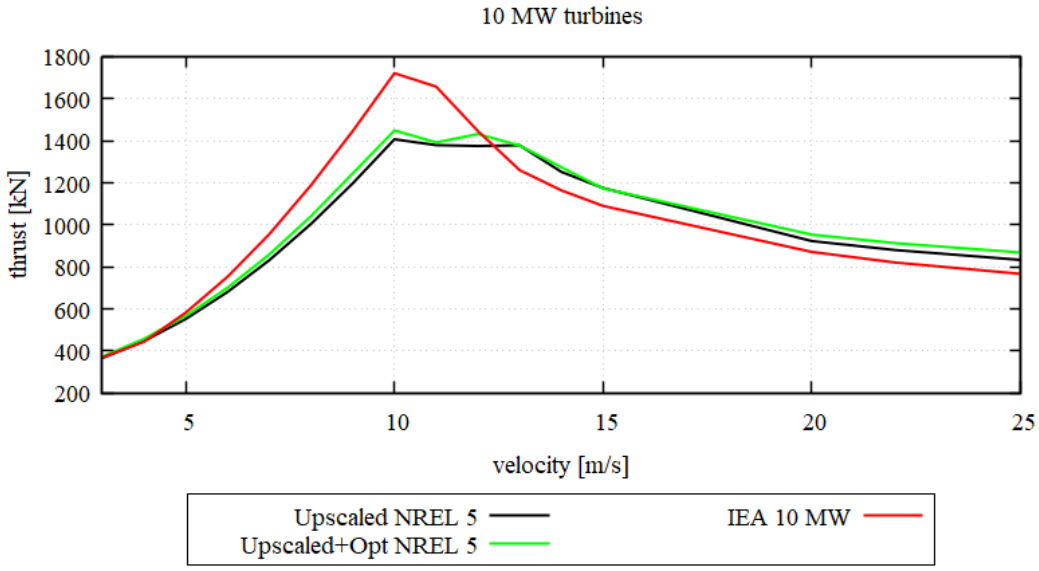

Figure 5.33. Thrust curve of 10 MW upscaled NREL 5, upscaled + optimized NREL 5, and IEA 10

The rated speed for the upscaled and upscaled + optimized NREL 5 is 11.4 m/s. However, 10 MW is achieved by both turbines at a higher wind speed than 11.4 m/s due to the controller's thrust peak shaving implementation, which can be observed from the thrust curve shown in Figure 5.33. The rotor thrust of the upscaled + optimized NREL 5 is always higher than the upscaled NREL 5. Rotor thrust is an important design parameter for large wind turbines since higher thrust will result in the turbine having a lower blade to tower clearance. The thrust of IEA 10 is significantly higher than the other two turbines until pitch control is activated. To maintain the tower clearance, IEA 10 is designed with a higher precone angle.

5.4 15 MW Turbines' performance

In the 15 MW rated power category, the performance of the upscaled NREL 5, upscaled + optimized NREL 5, upscaled IEA 10, and the original IEA 15 MW atop

the upscaled OC4 DeepCwind semi-submersibles are compared. The comparison of 15 MW turbines is important since the length, airfoil types, and twist angle of upscaled IEA 10 are close to IEA 15 MW, whereas those of upscaled + optimized NREL 5 are close to upscaled NREL 5. Thus, the comparison will demonstrate the effect of blade length on the power produced by the turbines. The four turbines simulated in the 15 MW rated power category are shown in Figure 5.34.

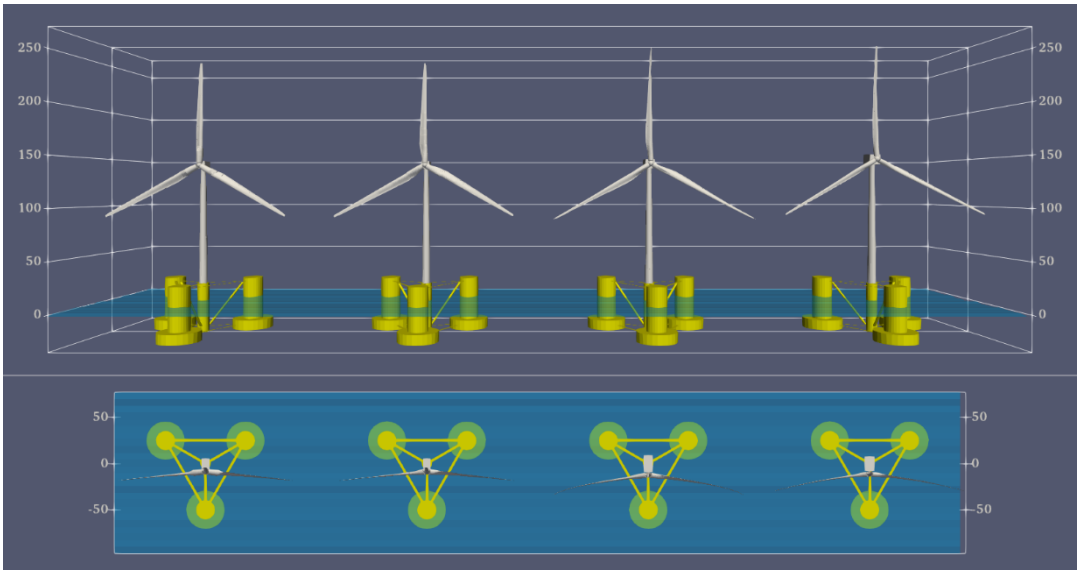

Figure 5.34. Size comparison of 15 MW rated power of upscaled NREL 5, upscaled + optimized NREL 5, upscaled IEA 10, and IEA 15, respectively

A comparison of the chord, twist angle, flapwise stiffness, edgewise stiffness, and mass density of the four turbines are shown in Figure 5.35 to Figure 5.37. Other than having different airfoil types, the upscaled IEA 10 and the IEA 15 MW have longer blades than the upscaled and upscaled + optimized NREL 5. Thus, the required chord length to produce the intended power is shorter than the two NREL 5 turbines.

The maximum chord of the upscaled + optimized NREL 5 is larger, and its location is earlier than the upscaled NREL 5. To maintain its structural strength, the mass, edgewise, and flapwise stiffness of the root transition section, where the shell and shear web thickness is concentrated (in Figure 4.41), is higher than the upscaled NREL 5. A relatively similar twist angle distribution is observed for the upscaled

and upscaled + optimized NREL 5 since the same airfoil types are used. On the other hand, the twist angle distribution of the upscaled IEA 10 and IEA 15 MW are alike since the same FFA-W3 airfoil series is used.

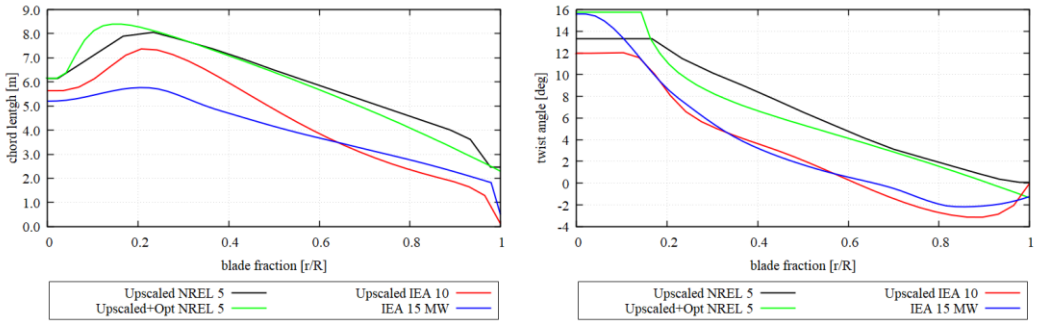

Figure 5.35. Chord length and twist angle distribution of 15 MW rated power of the upscaled NREL 5, upscaled + optimized NREL 5, upscaled IEA 10, and IEA 15

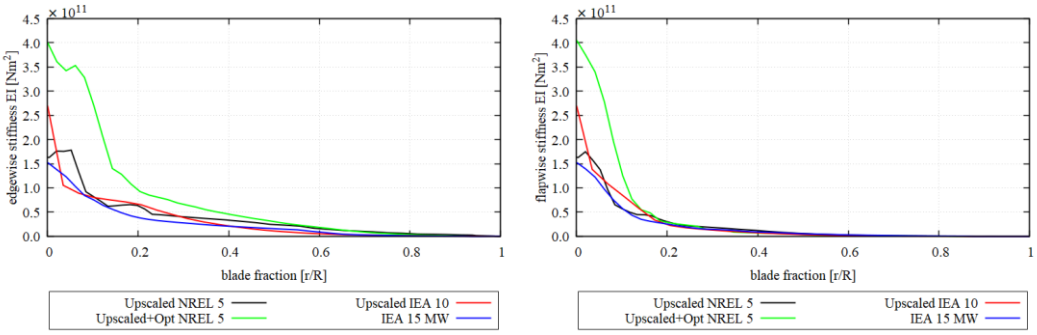

Figure 5.36. Edgewise and flapwise distribution of 15 MW rated power of the upscaled NREL 5, upscaled + optimized NREL 5, upscaled IEA 10, and IEA 15

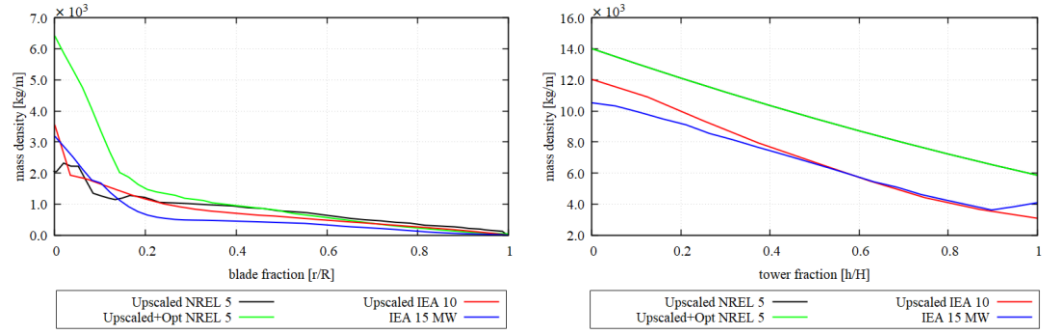

Figure 5.37. Blade and tower' mass density distribution of 15 MW rated power of the upscaled NREL 5, upscaled + optimized NREL 5, upscaled IEA 10, and IEA 15

5.4.1 Hydrodynamic performance

Hydrodynamic performance consisting of PSDs and RAOs of 15 MW upscaled NREL 5, upscaled + optimized NREL 5, upscaled IEA 10, and the original IEA 15 MW in the surge, heave, and pitch degrees of freedom from load case 2.6 and load case 3.7 are shown in Figure 5.38 to Figure 5.43. The power spectral density (PSD) of the platform is plotted using the Fast Fourier Transformation (FFT) method within the frequency region of 0.0-0.5 Hz, and the Response Amplitude Operator (RAO) is calculated based on Equation 3.6 and shown within the frequency region of 0.05-0.25 Hz.

The surge PSDs of the turbines are shown in Figure 5.38, while the surge RAOs are shown in Figure 5.39. The wave excitation region can be observed from 0.05 to 0.25 Hz in the PSD curve. The turbines' surge natural frequencies are shown in the PSD curves at around 0.004 Hz. Compared to the 5 and 10 MW results, the surge natural frequency has shifted further towards the lower frequency region. The coupling of surge and pitch motion can be seen in the PSD curve at around 0.029 Hz.

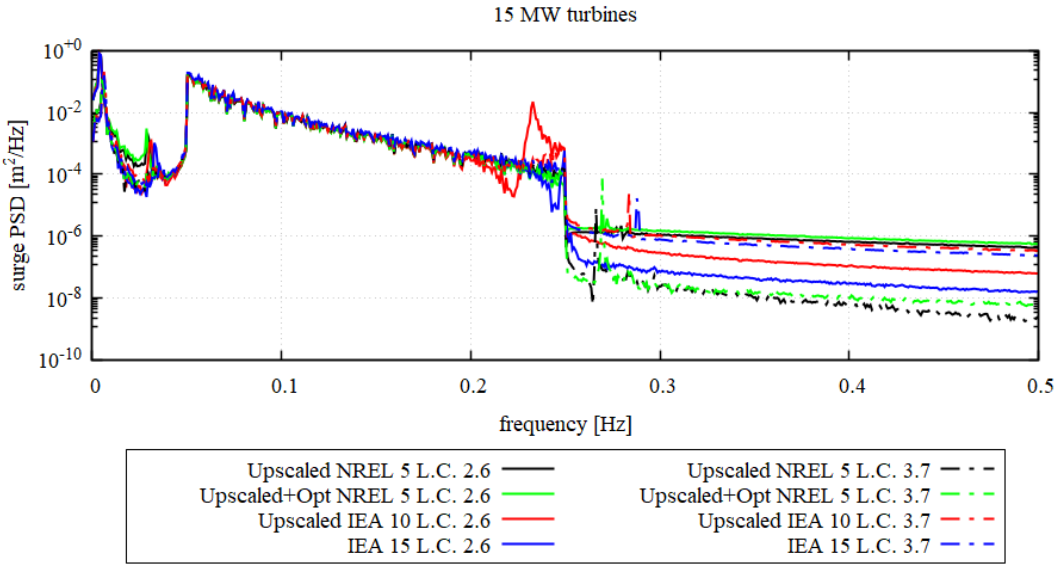

Figure 5.38. Surge PSD of 15 MW upscaled NREL 5, upscaled + optimized NREL 5, upscaled IEA 10, and IEA 15

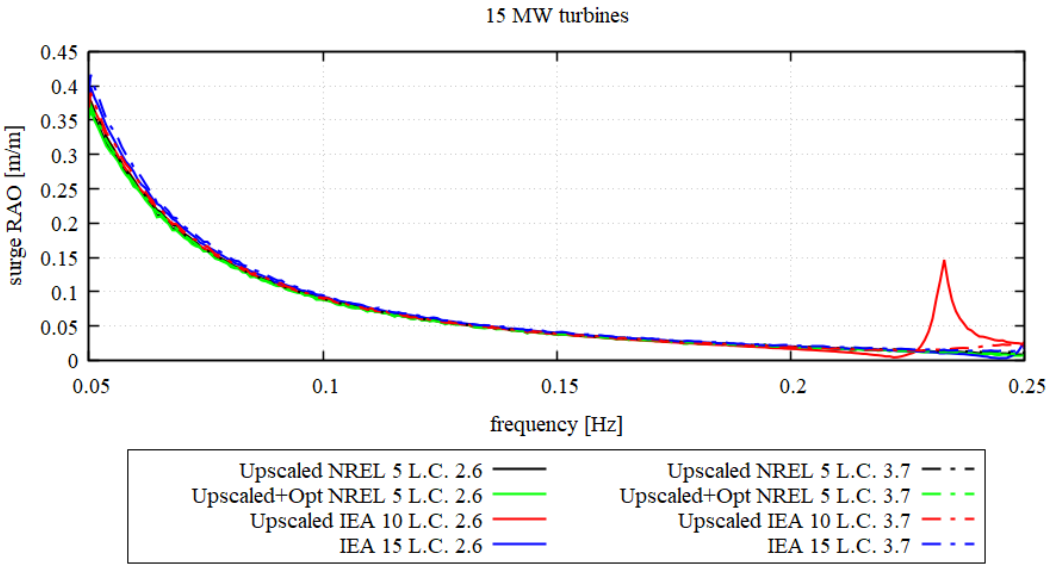

Figure 5.39. Surge RAO of 15 MW upscaled NREL 5, upscaled + optimized NREL 5, upscaled IEA 10, and IEA 15

The spikes in the surge PSD of load cases 2.6 and 3.7, initially located outside the wave excitation region, have shifted much further left. Those spikes of DLC 2.6, especially those of the upscaled IEA 10 and original IEA 15, have entered the wave excitation region and are clearly noticeable at the end of the wave region, as shown in Figure 5.38. The spikes of the DLC 3.7 remains outside the region. Inside the wave excitation region, the PSD of DLC 3.7 is less dominant than those of DLC 2.6, which shows that the wind effect on the surge PSD is less prevalent than the wave.

The overall surge response amplitude operators of DLC 2.6 and 3.7 of all the four turbines are less than the unit value, despite the RAO of DLC 2.6 (wave-only case) are disturbed at the end of the wave region. The response of DLC 3.7 are smooth everywhere in the wave excitation region. It again strengthens the previous finding that wave is more dominant than wind in driving the platform to surge.

The turbines' heave natural frequencies, at around 0.044 Hz, have fully separated from the wave excitation region, as which can be observed from the heave PSD curves shown in Figure 5.40. The heave RAOs are shown in Figure 5.41. Again, the heave PSD is independent of the other degrees of freedom. Wind effect on the PSD

is negligible in any region, inside and outside the wave excitation region. Overall, the heave RAO is less than unit value, which shows that the turbines and platform heave less under the same sea state as the original OC4 semi-submersible design.

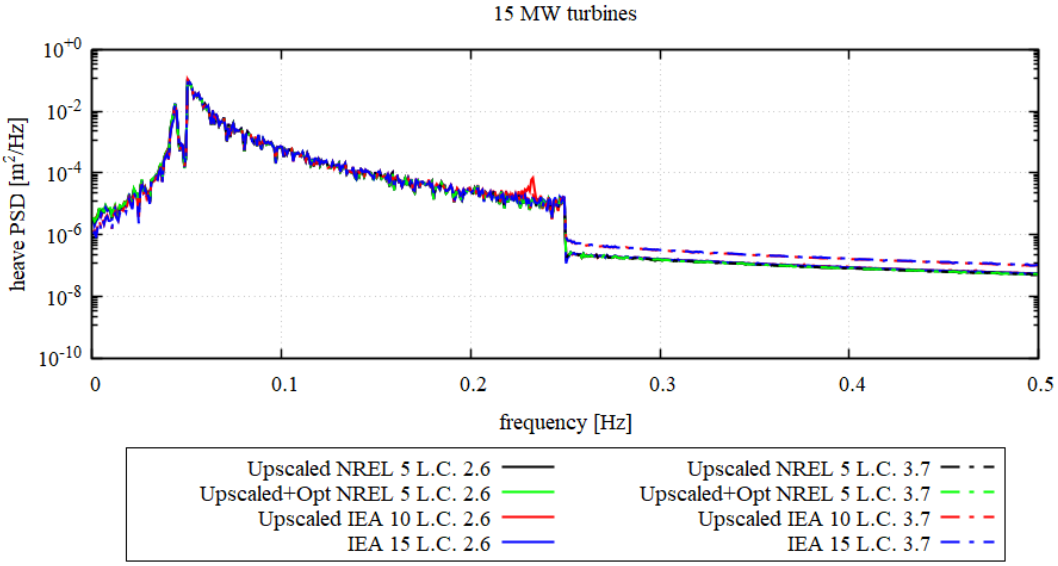

Figure 5.40. Heave PSD of 15 MW upscaled NREL 5, upscaled + optimized NREL 5, upscaled IEA 10, and IEA 15

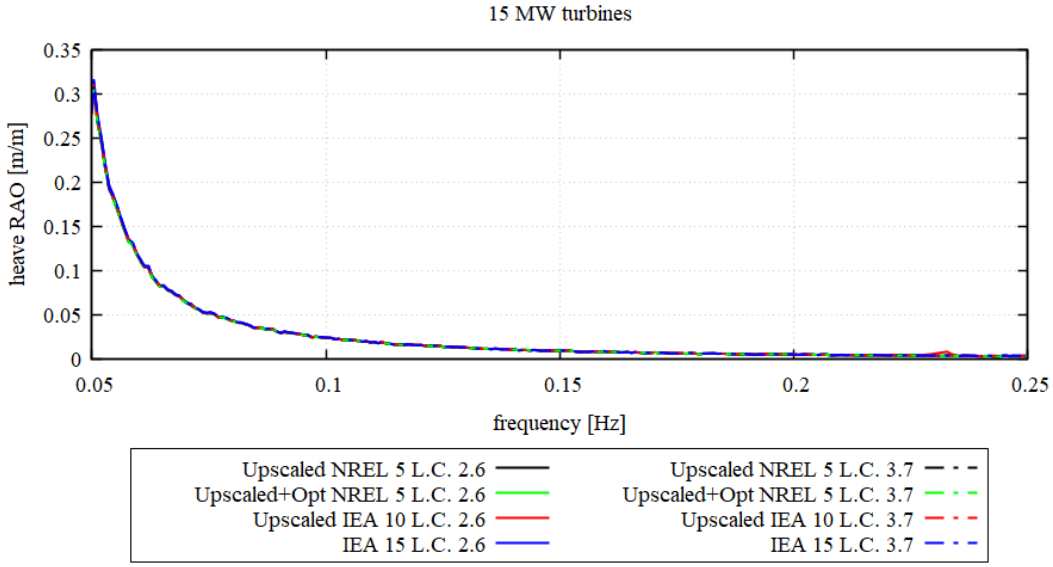

Figure 5.41. Heave RAO of 15 MW upscaled NREL 5, upscaled + optimized NREL 5, upscaled IEA 10, and IEA 15

Pitch natural frequencies of the turbines can be observed from the pitch PSD curves shown in Figure 5.42, at around 0.029 Hz, whereas the pitch RAOs of the four turbines are shown in Figure 5.43. Again, the pitch and surge motion coupling can be seen from the PSD curve at around 0.004 Hz.

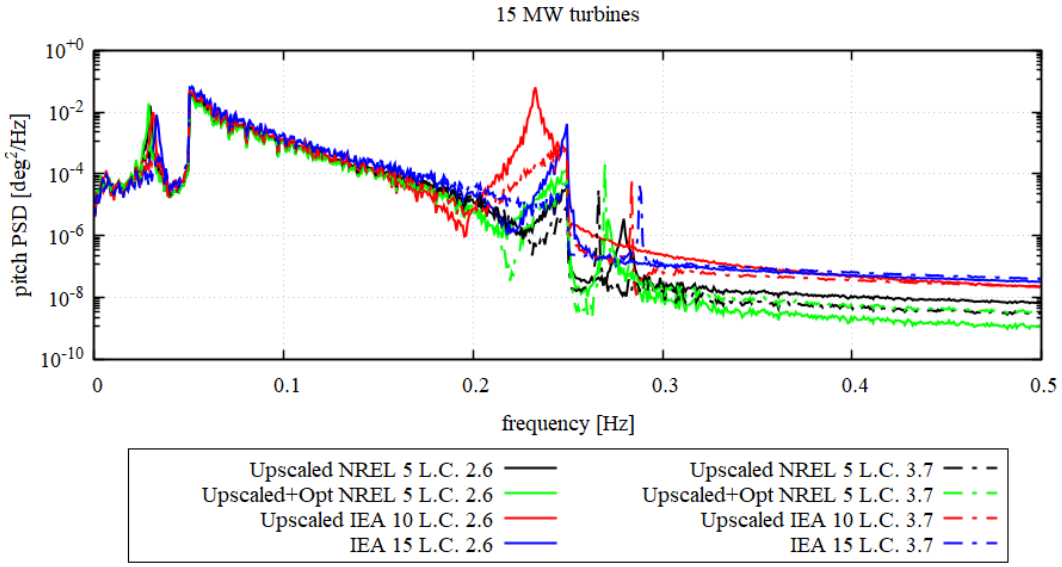

Figure 5.42. Pitch PSD of 15 MW upscaled NREL 5, upscaled + optimized NREL 5, upscaled IEA 10, and IEA 15

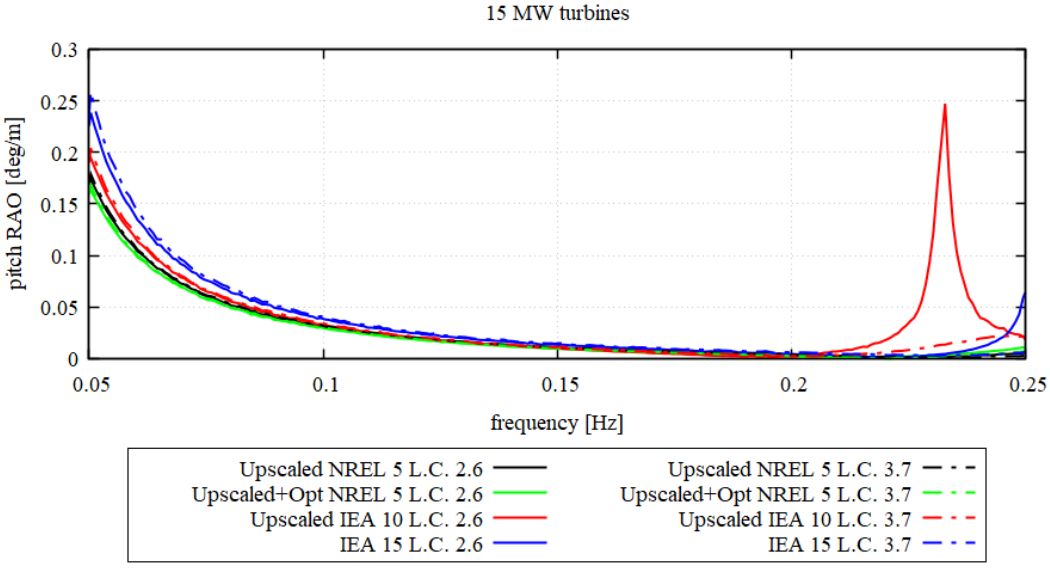

Figure 5.43. Pitch RAO of 15 MW upscaled NREL 5, upscaled + optimized NREL 5, upscaled IEA 10, and IEA 15

Like the surge motion, the spikes in the pitch PSD of load cases 2.6 and 3.7, initially located outside the wave excitation region, have shifted much further left and entered the wave excitation region. It is clearly noticeable at the end of the wave region, as shown in Figure 5.42. Inside the wave excitation region, the PSD of DLC 3.7 is less dominant than the PSD of DLC 2.6, which shows that the wind effect on the surge PSD is less prevalent than the wave inside the wave excitation region.

The overall pitch response amplitude operators of DLC 2.6 and 3.7 of all the three turbines are less than the unit value, although the RAOs of DLC 2.6 (wave-only case) are disturbed at the end of the wave region. The responses of DLC 3.7 are much smoother than the responses of DLC 2.6. It also shows that wave is more dominant than wind in driving the platform to pitch.

5.4.2 Aero-elastic performance

The following discussion compares the aero-elastic performance of the 15 MW upscaled NREL 5, upscaled + optimized NREL 5, upscaled IEA 10, and the original IEA 15 MW turbines. The comparison of 15 MW turbines is essential since the length, airfoil types, and twist angle of upscaled IEA 10 are close to IEA 15 MW, whereas those of upscaled + optimized NREL 5 are close to upscaled NREL 5.

A comparison of the rotor aerodynamic power coefficient (CP) and rotor aerodynamic thrust coefficient (CT) are shown in Figure 5.44 and Figure 5.45, respectively. The generator power and rotor thrust are compared in Figure 5.46 and Figure 5.47. The CP and CT of the upscaled NREL 5 and upscaled IEA 10 are identical to their baseline turbines, which is expected from linear scaling.

From Figure 5.44, the CP of the upscaled + optimized NREL 5 is higher than the upscaled NREL 5, especially in region 2, before the blade's pitch control is activated. CP of IEA 15 is higher than upscaled IEA 10 from a wind speed of 6 m/s up to 11 m/s. After the rated wind speed is achieved, the CP of upscaled IEA 10 starts to

decline in the same trend as the CP of original IEA 15 MW, whereas the CP of upscaled NREL 5 matches the CP of upscaled + optimized NREL 5.

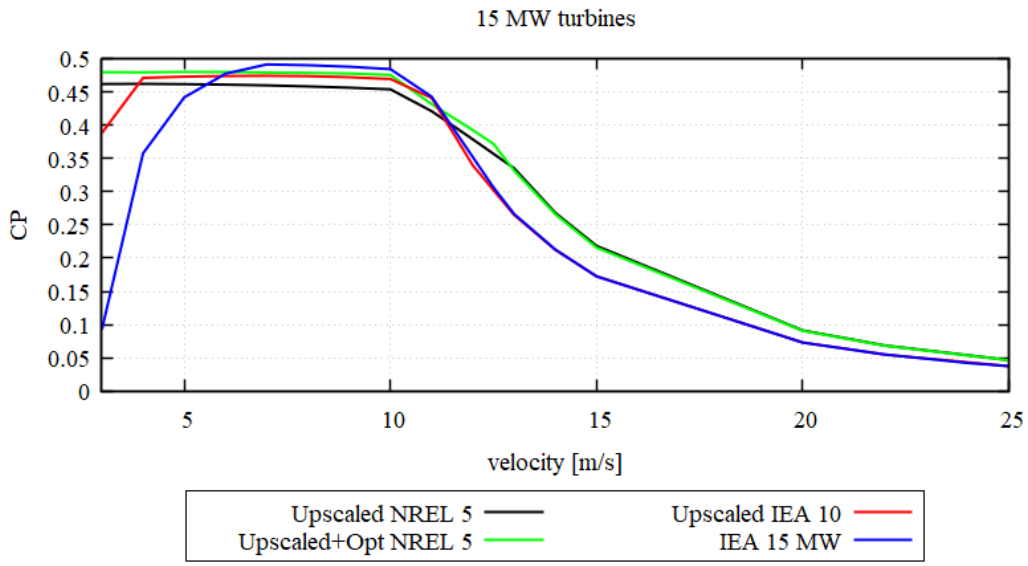

Figure 5.44. Power coefficient of 15 MW upscaled NREL 5, upscaled + optimized NREL 5, upscaled IEA 10, and IEA 15

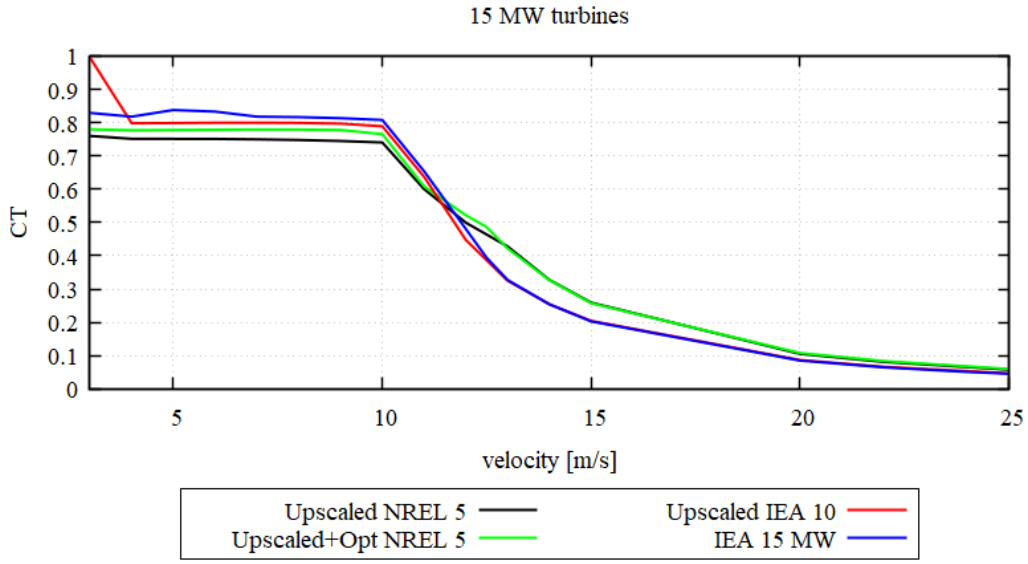

Figure 5.45. Thrust coefficient of 15 MW upscaled NREL 5, upscaled + optimized NREL 5, upscaled IEA 10, and IEA 15

The thrust coefficients of IEA 15 and upscaled IEA 10 are different from the other two turbines due to different operating points, as seen in Figure 5.45. The thrust

coefficient of the upscaled + optimized NREL 5 in region 2 is higher than the upscaled NREL 5. After 10 m/s, the thrust coefficient of all the four turbines starts to decline. The CT of upscaled IEA 10 declines in the same trend as the original IEA 15 MW, and the CT the two NREL 5-based turbines are comparable one another.

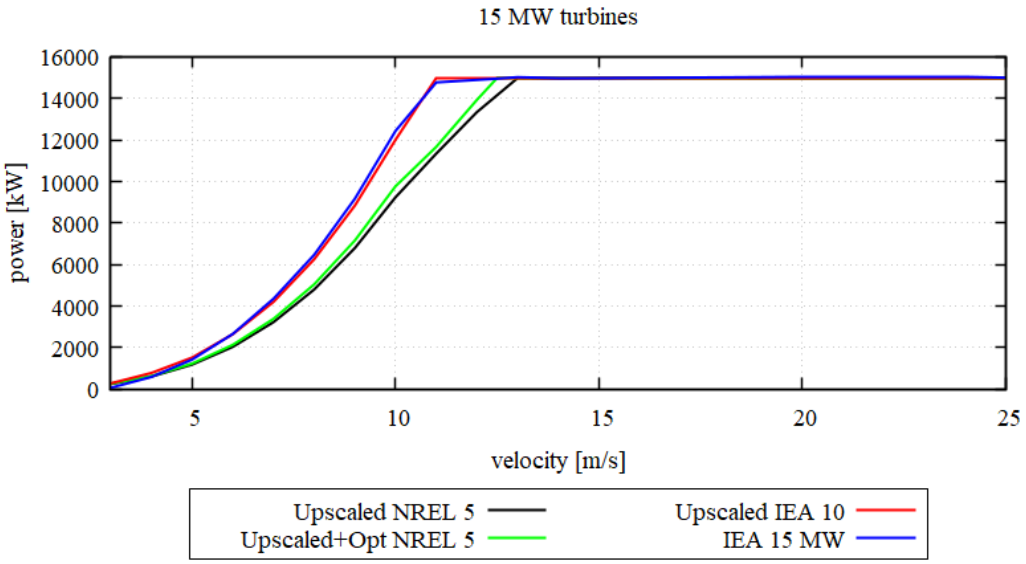

Figure 5.46. The power curve of 15 MW upscaled NREL 5, upscaled + optimized NREL 5, upscaled IEA 10, and IEA 15

From Figure 5.46, power curve of upscaled + optimized NREL 5 is still conservative compared to the upscaled NREL 5. Upscaled NREL 5 produces 2.945E+07 kWh/yr AEP, 4.0% lower than upscaled + optimized NREL 5 with 3.064E+07 kWh/yr. On the other hand, the power of the upscaled IEA 10 and original IEA 15 are much higher than the other two turbines, mainly due to the utilization of longer blades. Further observation shows that the power of the original IEA 15 is higher than the upscaled IEA 10 at the same margin where its CP is also higher. However, the power produced by the original IEA 15 is very close to the upscaled IEA 10. The AEP of the upscaled IEA 10 is 3.652E+07 kWh/yr, 0.73% lower than the original IEA 15 with 3.674E+07 kWh/yr. Recalling that their blade length, airfoil types, and twist angle are relatively similar, it is convenient to say that upscaled IEA 10 and original IEA 15 are also conservative of one another.

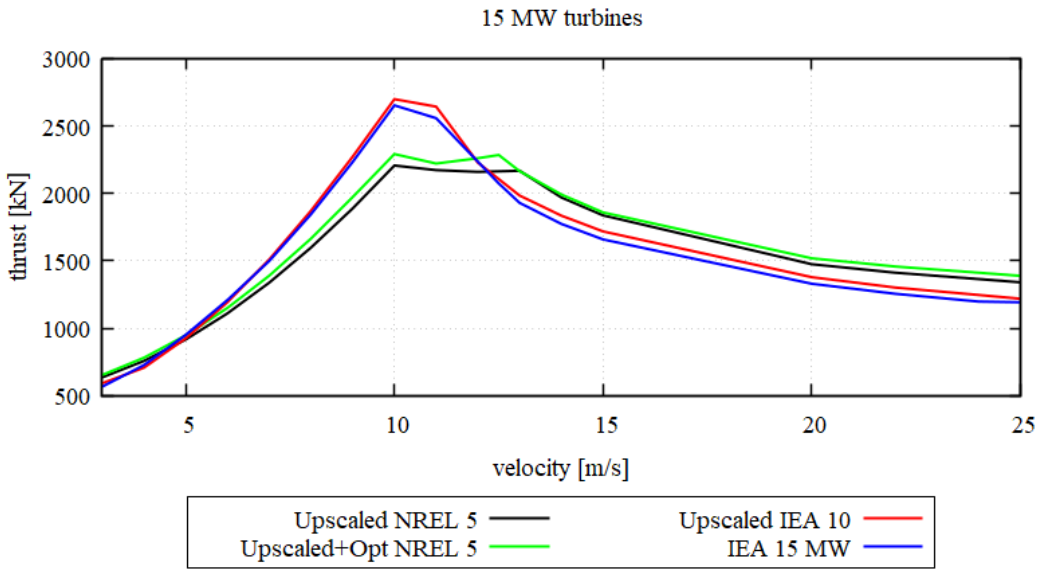

Figure 5.47. Thrust curve of 15 MW upscaled NREL 5, upscaled + optimized NREL 5, upscaled IEA 10, and IEA 15

The controller's thrust peak shaving implementation can be observed from the thrust curve shown in Figure 5.47. The rotor thrust of the upscaled + optimized NREL 5 is always higher but comparable to the upscaled NREL 5. Whereas thrust of upscaled IEA 10 is comparable to the original IEA 15, and their values are higher than the other two turbines until blade pitch control is activated. The maximum thrust occurs at 10 m/s, the final velocity before the CT declines.

5.5 20 MW Turbines' performance

In the 20 MW rated power category, the performance of the upscaled NREL 5, upscaled + optimized NREL 5, upscaled IEA 10, and upscaled IEA 15 are compared. Additionally, an optimized NREL 5 matching the length of upscaled IEA 15 (±135 meters) is added to the comparison as the fifth blade. Upscaled OC4 DeepCwind semi-submersibles are used as the floating platform. The five turbines simulated in the 20 MW rated power category are shown in Figure 5.48. Again, the length, airfoil types, and twist angle of upscaled IEA 10 are close to upscaled IEA 15, whereas those of upscaled + optimized NREL 5 are close to upscaled NREL 5. The fifth blade,

the 135-meters optimized NREL 5, has the same airfoil types and twist angle distribution similar to upscaled NREL 5, but matching the length of the upscaled IEA 15 to 20 MW. The comparison of the five turbines helps in understanding the effect of aerodynamic optimization with enlarging blade length at the initial stage.

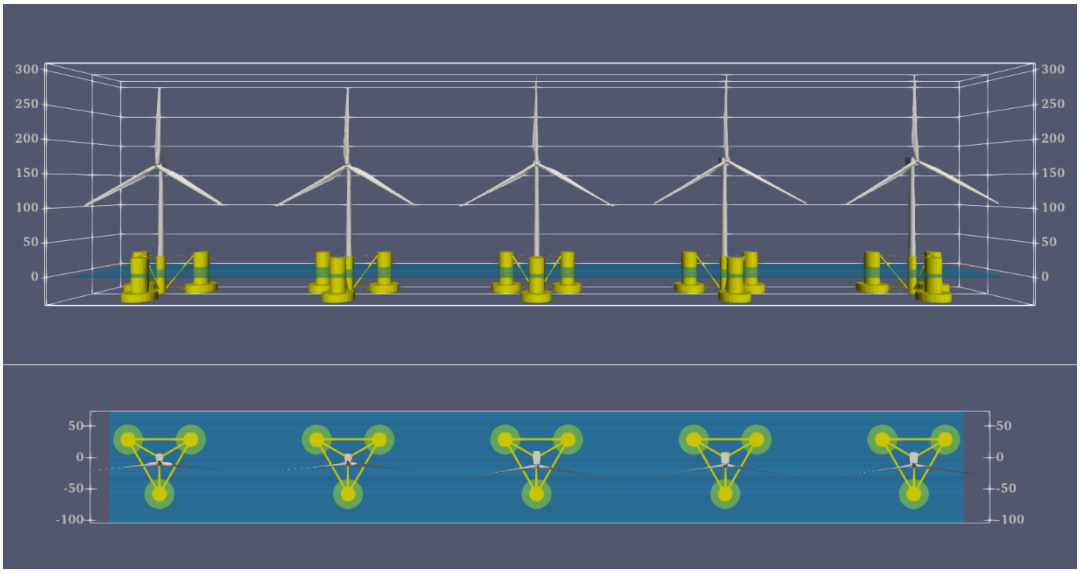

Figure 5.48. Size comparison of 20 MW rated power of Upscaled NREL 5, Upscaled + optimized NREL 5, Upscaled IEA 10, and Upscaled IEA 15, and 135 meters Optimized NREL 5, respectively

A comparison of the chord, twist angle, edgewise stiffness, flapwise stiffness, and mass density of all turbines are shown in Figure 5.49 to Figure 5.51. The upscaled IEA 10, upscaled IEA 15, and the 135m optimized NREL 5 have longer blades and shorter maximum chord length than the upscaled and upscaled + optimized NREL 5. The maximum chord of the upscaled + optimized NREL 5 is larger, and its location is earlier than the upscaled NREL 5. To maintain its structural strength, the mass, edgewise, and flapwise stiffness of the root transition section of the upscaled + optimized NREL 5 and the 135-meters optimized NREL 5 are higher than the upscaled NREL 5.

A relatively similar twist angle distribution is observed for the upscaled IEA 10 and upscaled IEA 15 since both turbines used the FFA-W3 airfoil series. On the other

hand, the twist angle of the upscaled, upscaled + optimized , and the 135 meters optimized NREL 5 MW are alike since the same airfoil types of DU-series are used.

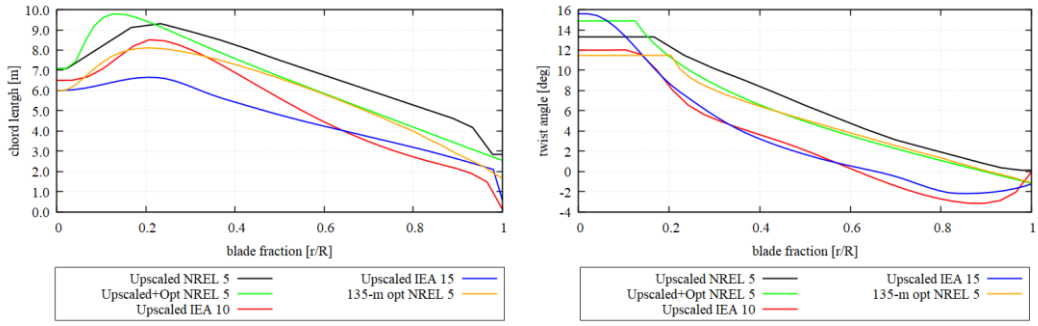

Figure 5.49. Chord length and twist angle of 20 MW upscaled NREL 5, upscaled + optimized NREL 5, upscaled IEA 10, upscaled IEA 15, 135m optimized NREL 5

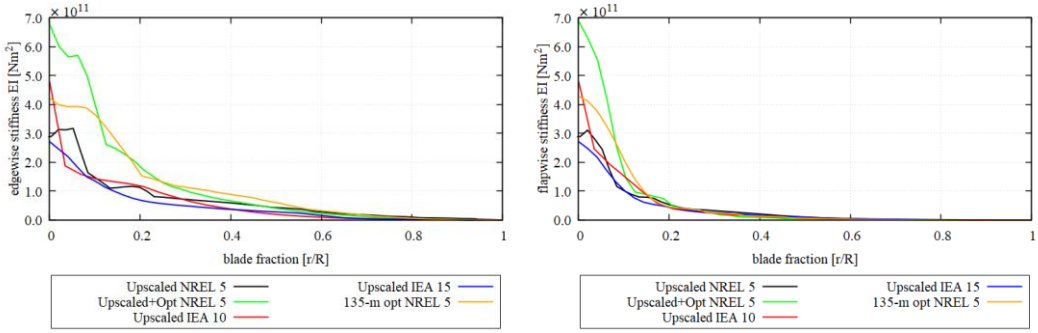

Figure 5.50. Edgewise-flapwise stiffness of 20 MW upscaled NREL 5, upscaled + optimized NREL 5, upscaled IEA 10, upscaled IEA 15, 135m optimized NREL5

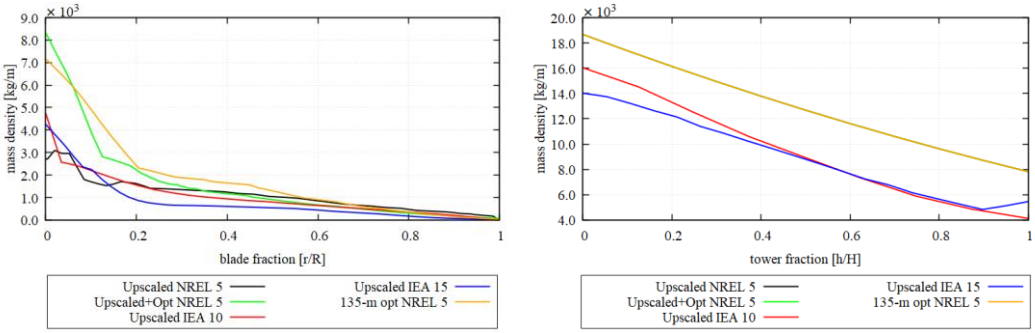

Figure 5.51. Blade & tower's mass density of 20 MW upscaled NREL 5, upscaled + optimized NREL 5, upscaled IEA10, upscaled IEA15, 135m optimized NREL5

5.5.1 Hydrodynamic performance

Hydrodynamic performance consisting of PSDs and RAOs of 20 MW upscaled NREL 5, upscaled + optimized NREL 5, upscaled IEA 10, upscaled IEA 15, and 135-meter optimized NREL 5 in the surge, heave, and pitch degrees of freedom from load case 2.6 and load case 3.5 are shown in Figure 5.52 to Figure 5.57. The power spectral density (PSD) of the platform is plotted using the Fast Fourier Transformation (FFT) method within the frequency region of 0.0-0.5 Hz, and the Response Amplitude Operator (RAO) is calculated based on Equation 3.6 and shown within the frequency region of 0.05-0.25 Hz.

The surge PSDs of the turbines are shown in Figure 5.52, while the surge RAOs are shown in Figure 5.53. The wave excitation region can be observed from 0.05 to 0.25 Hz in the PSD curve. The turbines' surge natural frequencies are shown in the PSD curves at around 0.003 Hz. Compared to the 5, 10, and 15 MW results, the surge natural frequency has shifted further towards the lower frequency region. The coupling of surge and pitch can be seen in the PSD curve at around 0.027 Hz.

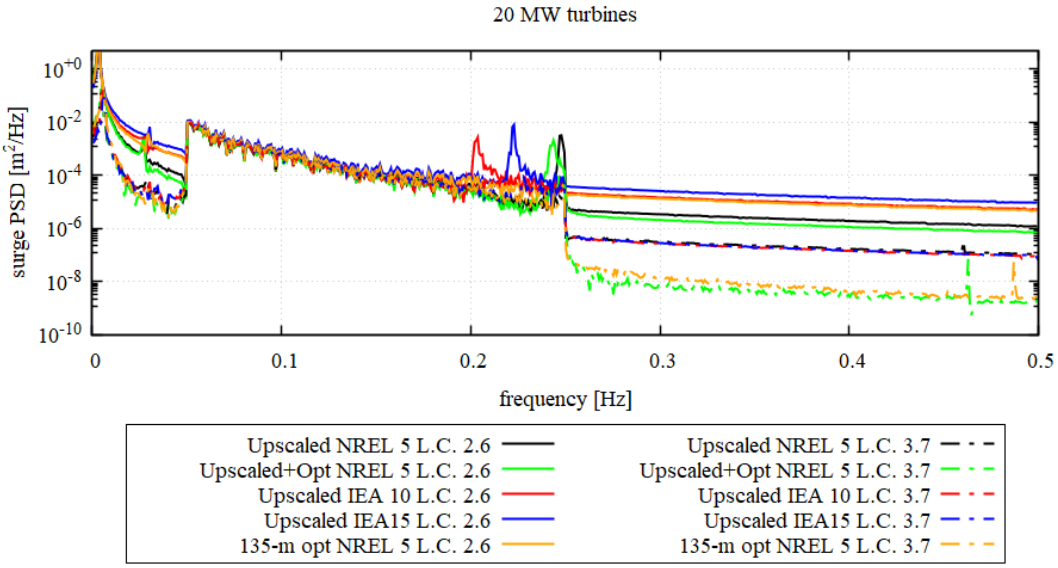

Figure 5.52. Surge PSD of 20 MW Upscaled NREL 5, upscaled + optimized NREL 5, upscaled IEA 10, upscaled IEA 15, and 135 meters optimized NREL 5

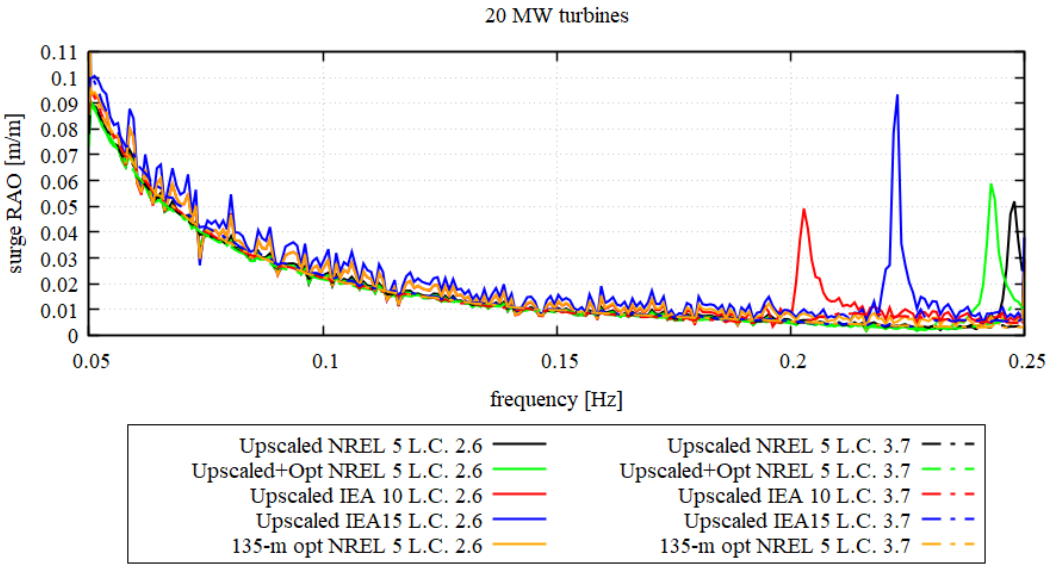

Figure 5.53. Surge RAO of 20 MW upscaled NREL 5, upscaled + optimized NREL 5, upscaled IEA 10, upscaled IEA 15, and 135 meters optimized NREL 5

From surge PSD in Figure 5.52, all the spikes of load cases 2.6 and 3.7, initially located outside the wave excitation region, have shifted much further left and entered the wave excitation region. At the end of the wave region, the spikes of DLC 2.6 of all turbines are more prominent than spikes of DLC 3.7. It again shows that inside the wave excitation region, the wind effect on the surge PSD is less dominant than the wave.

The response amplitude operator of DLC 2.6 (wave-only case) are disturbed at the end of the wave region, while the response of DLC 3.7 are smooth everywhere in the wave excitation region. It again strengthens the previous finding that wave is more dominant than wind in driving the platform to surge. The overall surge response amplitude operators of DLC 2.6 and 3.7 of all the five turbines are less than the unit value, which means that the surge of the turbines and platforms very is minimal under the same sea state as the original OC4 semi-submersible design.

The turbines' heave natural frequencies, at around 0.041 Hz, have fully separated from the wave excitation region, which is shown in the heave PSD curves in Figure 5.54. The heave RAOs are shown in Figure 5.55. Again, the heave PSD is

independent of the other degrees of freedom. Wind effect on the PSD is negligible in any region, inside and outside the wave excitation region. Overall, the heave RAO is less than the unit value.

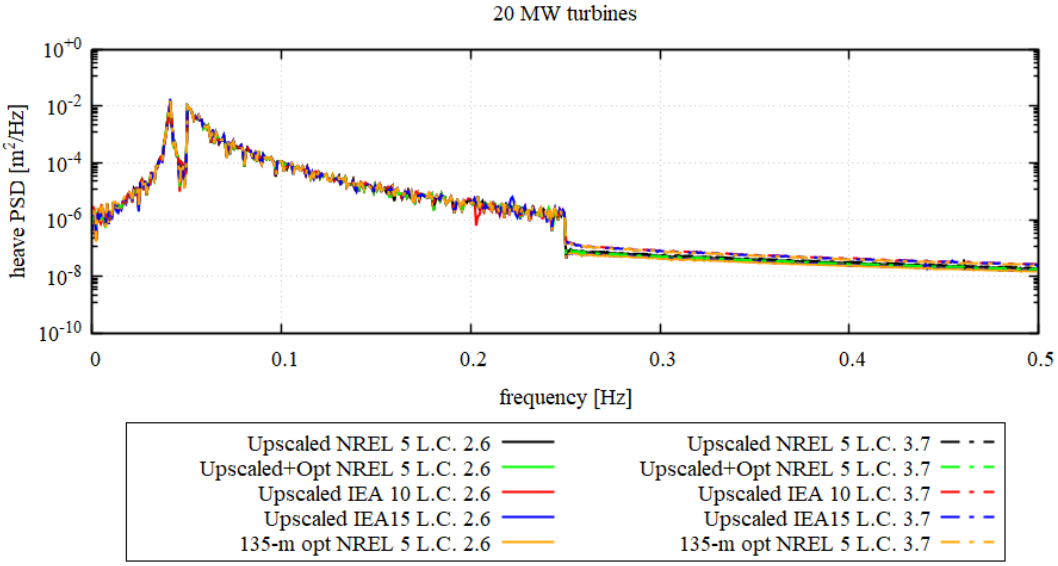

Figure 5.54. Heave PSD of 20 MW upscaled NREL 5, upscaled + optimized NREL 5, upscaled IEA 10, upscaled IEA 15, and 135 meters optimized NREL 5

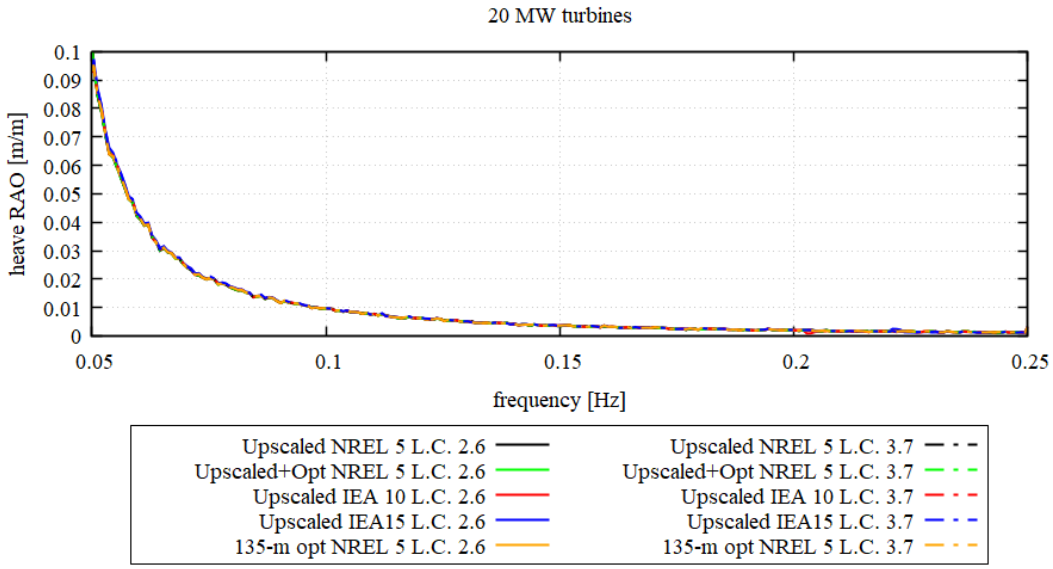

Figure 5.55. Heave RAO of 20 MW upscaled NREL 5, upscaled + optimized NREL 5, upscaled IEA 10, upscaled IEA 15, and 135 meters optimized NREL 5

Pitch natural frequencies of the turbines, at around 0.027 Hz, can be observed from the pitch PSD curves shown in Figure 5.56, whereas the pitch RAOs of all turbines are shown in Figure 5.57. Again, the pitch and surge motion coupling can be seen from the PSD curve at around 0.003 Hz.

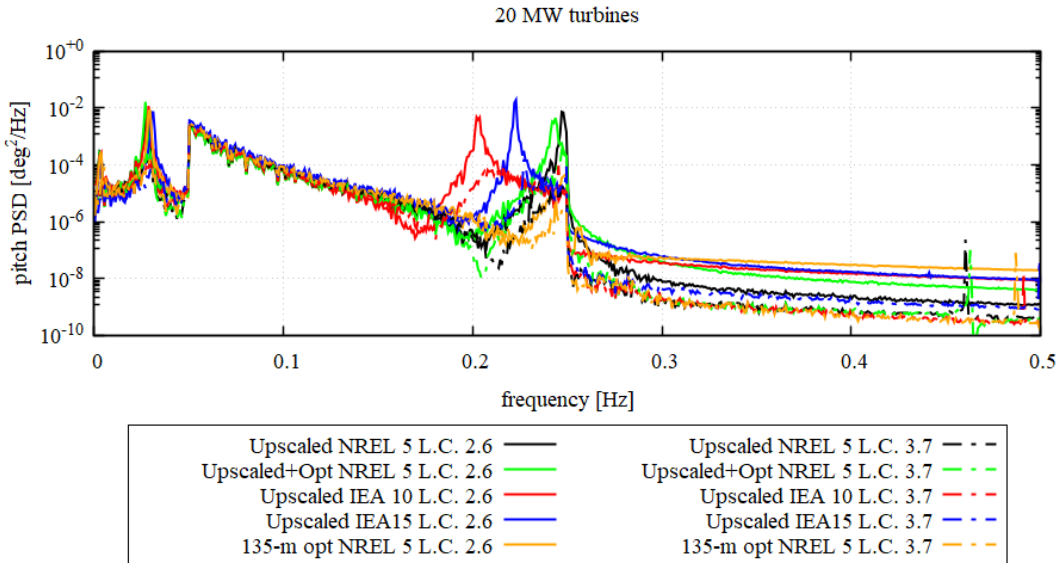

Figure 5.56. Pitch PSD of 20 MW upscaled NREL 5, upscaled + optimized NREL 5, upscaled IEA 10, upscaled IEA 15, and 135 meters optimized NREL 5

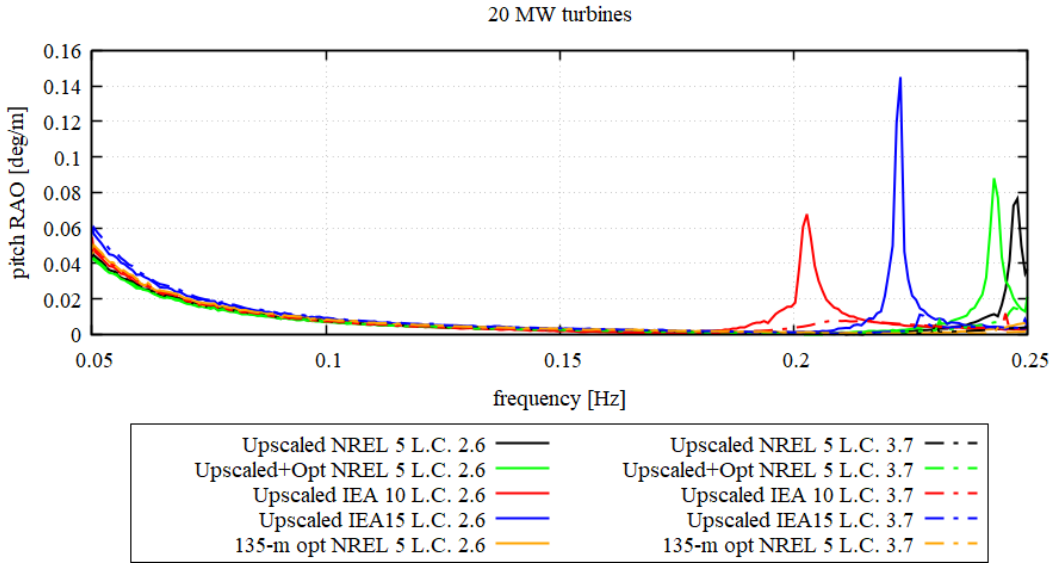

Figure 5.57. Pitch RAO of 20 MW upscaled NREL 5, upscaled + optimized NREL 5, upscaled IEA 10, upscaled IEA 15, and 135 meters optimized NREL 5

Like the surge motion, the spikes in the pitch PSD of load cases 2.6 and 3.7, initially located outside the wave excitation region, have all shifted much further left and entered the wave excitation region. It is clearly noticeable at the end of the wave region, as shown in Figure 5.56. Inside the wave excitation region, the PSD of DLC 3.7 is less dominant than the PSD of DLC 2.6, which shows that the wind effect on the surge PSD is less prevalent than the wave inside the wave excitation region.

The overall pitch response amplitude operators of DLC 2.6 and 3.7 of all the five turbines are less than the unit value, although the RAOs of DLC 2.6 (wave-only case) are disturbed at the end of the wave region. Despite the fact that the spikes of DLC 3.7 have also entered the wave excitation region, the responses of DLC 3.7 are much smoother than the responses of DLC 2.6. It also shows that wave is more dominant than wind in driving the platform to pitch.

5.5.2 Aero-elastic performance

The following discussion compares the aero-elastic performance of the 15 MW upscaled NREL 5, upscaled + optimized NREL 5, upscaled IEA 10, upscaled IEA 15, and the 135-meter optimized NREL 5 turbines. Comparing 20 MW turbines is important since the length, airfoil types, and twist angle of upscaled IEA 10 are close to upscaled IEA 15, and those of upscaled + optimized NREL 5 are close to upscaled NREL 5. Additionally, a blade based on NREL 5 with the same control tunning and length of 135.1 meters as upscaled IEA 15 has also been included to show the effect of extending blade length to the power produced.

Figure 5.58 and Figure 5.59 compares the rotor aerodynamic power coefficient (CP) and rotor aerodynamic thrust coefficient (CT). Generator power and rotor thrust are compared in Figure 5.60 and Figure 5.61, respectively. The CP and CT of the upscaled NREL 5, upscaled IEA 10, and upscaled IEA 15 are identical to their baseline turbines, which is expected from linear scaling.

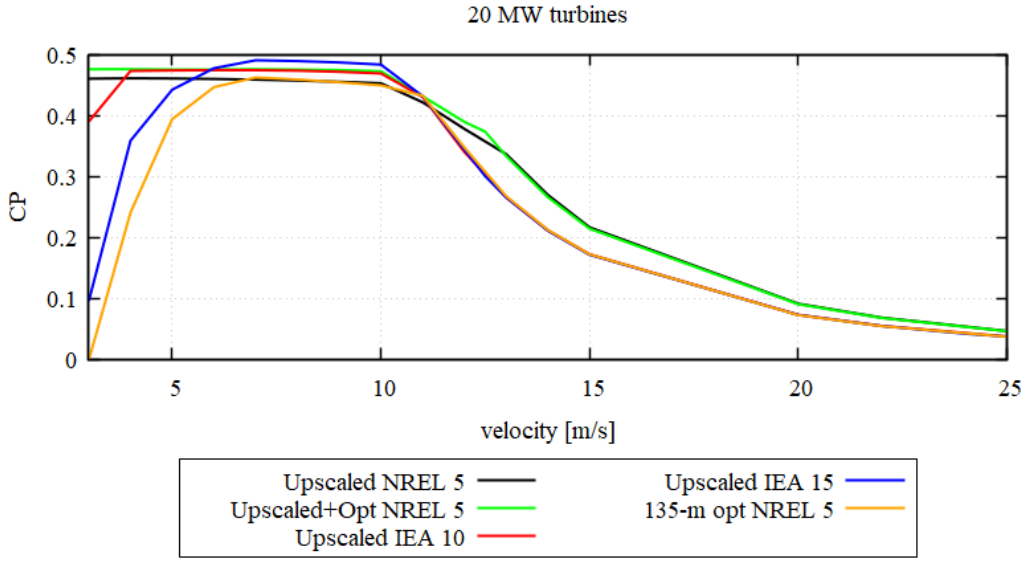

Figure 5.58. Power coefficient of 20 MW upscaled NREL 5, upscaled + optimized NREL 5, upscaled IEA 10, upscaled IEA 15, and 135 meters optimized NREL 5

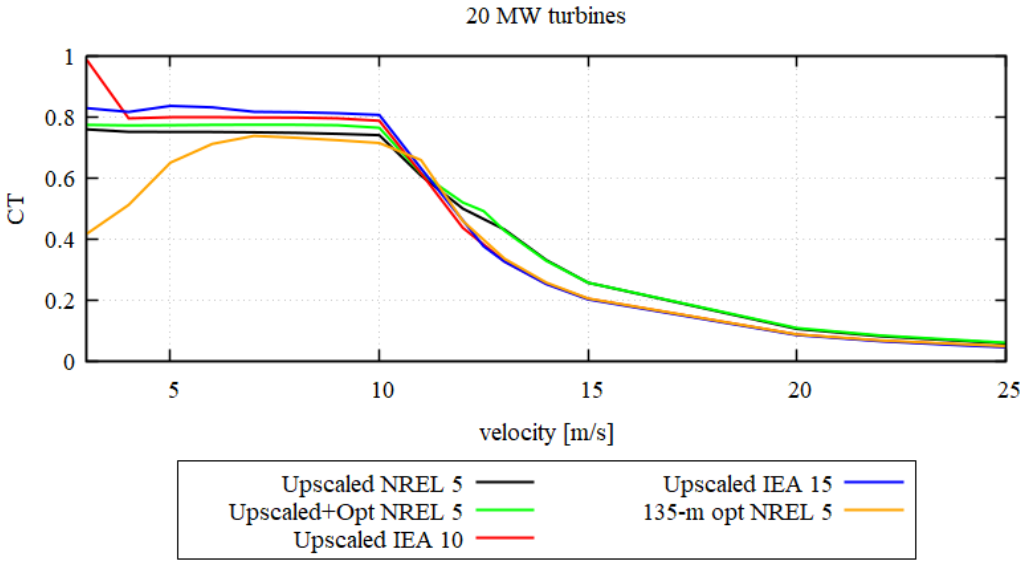

Figure 5.59. Thrust coefficient of 20 MW upscaled NREL 5, upscaled + optimized NREL 5, upscaled IEA 10, upscaled IEA 15, and 135 meters optimized NREL 5

From Figure 5.58, the CP of the upscaled + optimized NREL 5 is higher than the upscaled NREL 5, especially before the blade's pitch control is activated. CP of upscaled IEA 15 is higher than upscaled IEA 10 from a wind speed of 6 m/s up to almost 11 m/s. Borrowing the control of IEA 15, CP of the 135-meter opmitimized

NREL 5 follows the trend of upscaled IEA 15, but with lower magnitude until the rated speed is achieved. After the blade pitch control is activated, the CP of upscaled NREL 5 starts to decline in the same trend as upscaled + optimized NREL 5. On the other hand, the CP of upscaled the 135 meters optimized NREL 5 matches the CP of upscaled IEA 10 and upscaled IEA 15.

The thrust coefficients of upscaled IEA 15 and upscaled IEA 10 are different from the upscaled and upscaled + optimized NREL 5 turbines due to different operating points, as seen in Figure 5.59. The thrust coefficient of the upscaled + optimized NREL 5 in region 2 is slightly higher than the upscaled NREL 5. Borrowing the control of upscaled IEA 15, CT of the 135-m optimized NREL 5 is lower than the upscaled IEA 15, especially at low wind speed. After 10 m/s, the thrust coefficient of all the five turbines starts to decline. The CT of the 135-m optimized NREL 5 declines in the same trend as the upscaled IEA 10 and upscaled IEA 15 MW, whereas the CT of upscaled NREL 5 matches the CT of upscaled + optimized NREL 5.

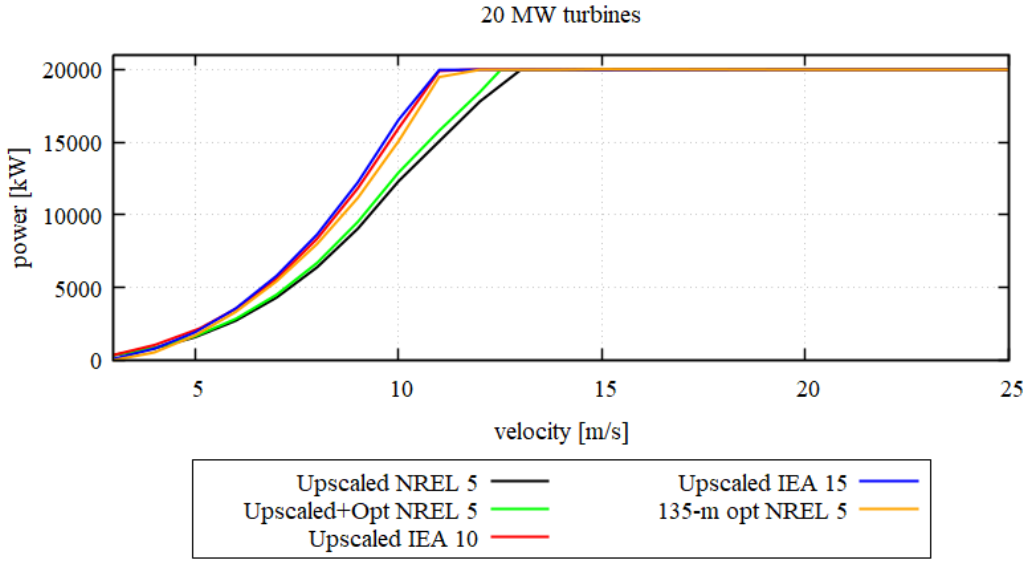

Figure 5.60. The power curve of 20 MW upscaled NREL 5, upscaled + optimized NREL 5, upscaled IEA 10, upscaled IEA 15, and 135 meters optimized NREL 5

As shown in Figure 5.60, the upscaled + optimized NREL 5 produces higher power than upscaled NREL 5 until the rated power is achieved, although not significantly

improved. From Equation 3.8, the AEP of the upscaled + optimized NREL 5 is 4.051E+07 kWh/yr, 3.3% higher than upscaled NREL 5 with 3.921E+07 kWh/yr. More significant power is produced by upscaled IEA 10, upscaled IEA 15, and the 135 meters optimized NREL 5 due to having longer blade. Although the power curve of the 135-meter optimized NREL 5 blade is still lower than the upscaled IEA turbines, it has improved significantly from the upscaled NREL 5 and being comparable to the upscaled IEA 10 and upscaled IEA 15. The 135-meter optimized NREL 5 produced 4.602E+07 kWh/yr, 17.4% increased from the upscaled NREL 5. Upscaled IEA 10 produces 4.879E+07 kWh/yr, and 4.908E+07 kWh/yr for the upscaled IEA 15.

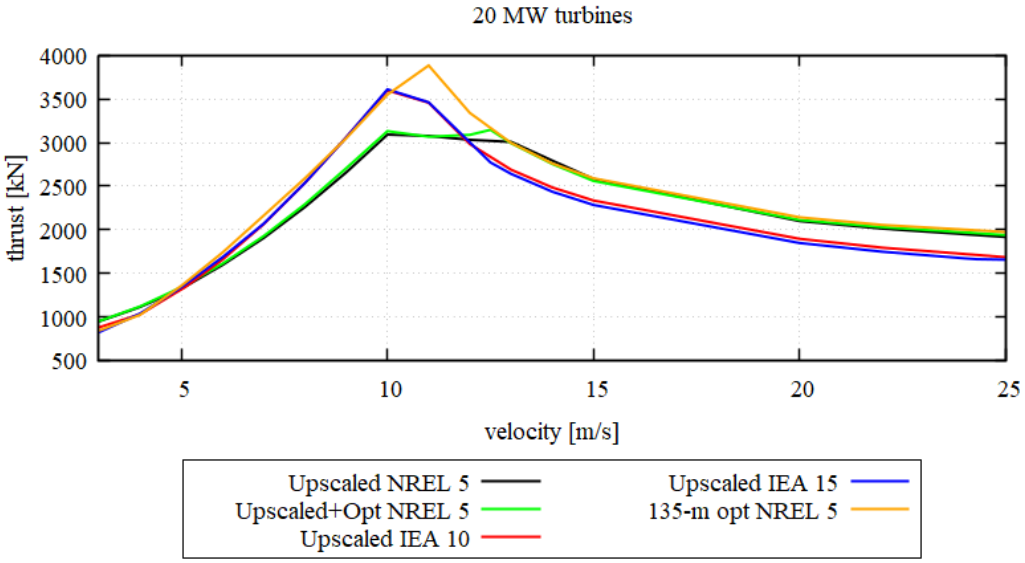

Figure 5.61. Thrust curve of 20 MW upscaled NREL 5, upscaled + optimized NREL 5, upscaled IEA 10, upscaled IEA 15, and 135 meters optimized NREL 5

From Figure 5.61. The thrust of the 135-meter optimized NREL 5 in region 2 is similar to the upscaled IEA 15. However, the matching blade is not experiencing identical thrust peak shaving and ends up having a higher thrust than the upscaled IEA 15. These thrust curves are essential to give us an idea of critical velocity and how the blade will bend under the effect of various wind speeds. The higher the thrust, the further the rotor bend.

5.6 Discussion

Hydrodynamic and aero-elastic performance of all the 5, 10, 15, and 20 MW turbines shows that upscaling the floating offshore wind turbine is possible and advantageous. Hydrodynamically, upscaling the floating platform lowers the natural frequencies, or in other words, increases the natural period of the floating offshore wind turbines in all degrees of freedom. Upscaling also decreases RAOs and makes the FOWT less influenced by the wave when operating under the same sea state as the baseline turbines, which greatly benefits power production. It is mainly due to an increase in the inertia of the FOWT as the turbine is upscaled.

In this study, the mooring lines are rearranged but not upscaled. Thus, the unstretched length and the diameter of the mooring lines remain the same as the original OC4 DeepCwind semi-submersible. Consequently, the masses of the mooring lines are the same regardless of the size of the platform. The tower lengths are also scaled by a value of less than s^1 to maintain a similar air gap between the blade's tip and the tower's base. However, the platform's volume is scaled by s^3. Due to this, an increase in heave motion is expected as the turbine and platform size grow. The rise in heave for all turbines in the first 1000 seconds in 10 m/s wind speed simulations is shown in Figure 5.62.

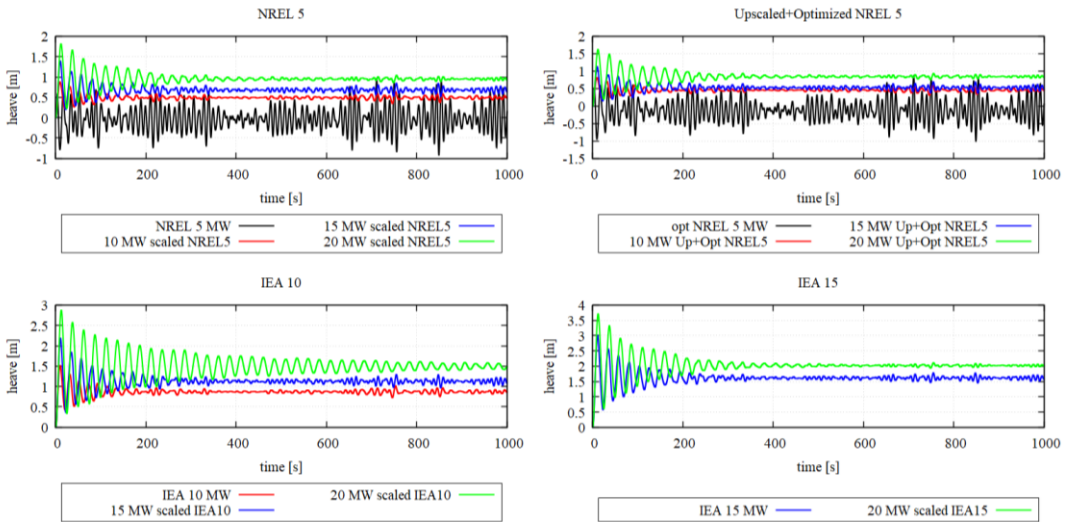

Figure 5.62. Heave of all turbines at a wind speed of 10 m/s

Like the heave, the platform's surge increases as the turbine's size grows. However, the increase in the surge is more predictable than the heave motion. Figure 5.63 shows the rise in the surge of all turbines in the first 1000 seconds of 10 m/s wind speed simulations. As can be observed from Figure 5.63, the surge motion follows an approximately s^1 relation as the turbines' power increases. Upscaled NREL 5 and upscaled + optimized NREL 5 surge approximately 7 meters at 5 MW and increase to almost 15 meters for 20 MW. Despite its predictive value, the surge motion must be carefully considered, especially when designing a wind farm with many FOWTs.

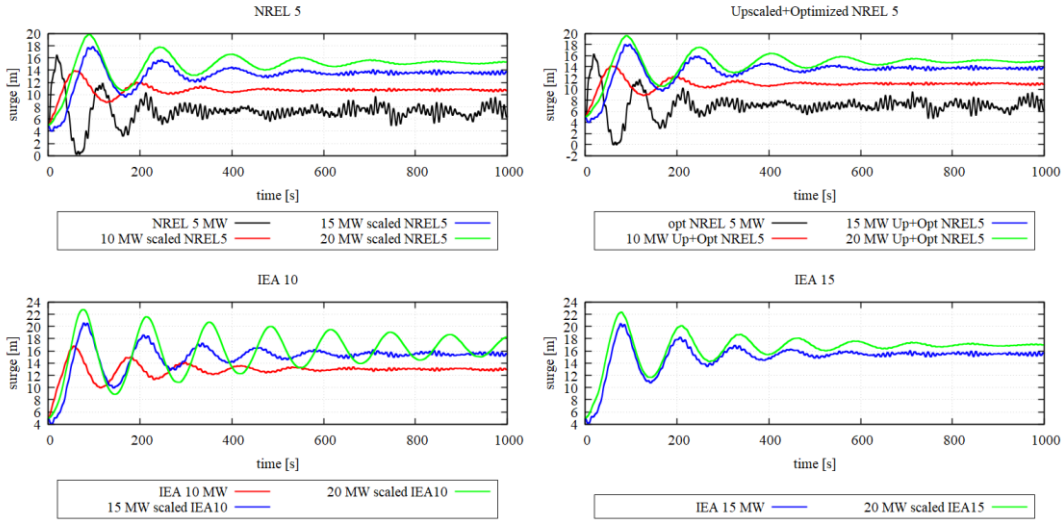

Figure 5.63. The surge of all turbines at a wind speed of 10 m/s

Since the mooring size remains constant, the tension force in the mooring lines becomes a critical design consideration as the platform size increases. The mooring lines survived all the given wind-wave conditions for all simulated turbines in the present study. No "line break" error notification was issued by the MAP++, considering MAP++ can detect such an issue. Mooring line number 2 experiences the highest tension compared to the other lines since it is located parallel to the x-axis in the global coordinate system. The x-axis is the wind and wave flows axis in all simulations performed in this study. It is also the direction of the platforms' surge. The increase in tension of the fairing lead and anchor of mooring line 2 is shown in Figure 5.64 and Figure 5.65, respectively.

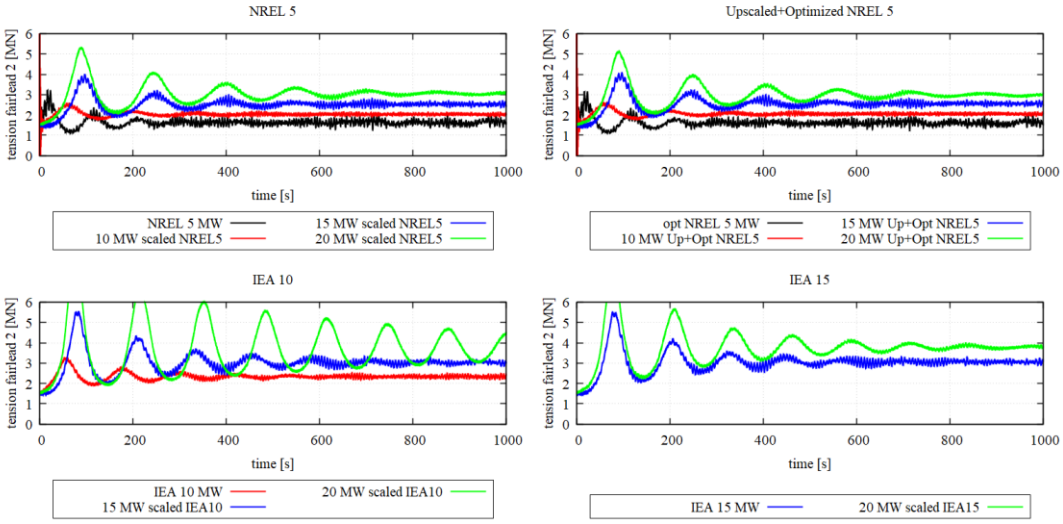

Figure 5.64. Tension at fairlead 2 of all turbines at a wind speed of 10 m/s

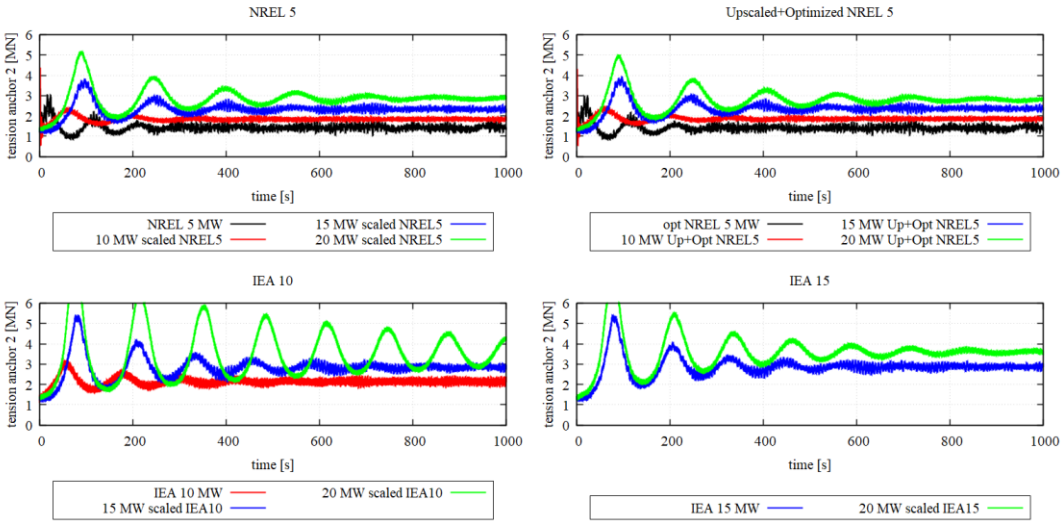

Figure 5.65. Tension at anchor 2 of all turbines at a wind speed of 10 m/s

Aerodynamically, the upscaling process increases the power produced by the rotor. If linear scaling is used, the upscaled turbines' power coefficient and thrust coefficient remain the same as the baseline wind turbines. A higher power coefficient can be gained by optimizing the aerodynamic shape of the blade. However, the performance is relatively conservative, and significant improvements in the power produced are not observed. A more substantial increase in the power can be achieved by increasing the blade's length more than linear scaling before optimizing the

aerodynamic shape of the blade. Thus, optimizing the blade length in the initial stage of optimization is recommended, as performed in the IEA10 MW.

Optimizing the blade's internal structure is as important as the external shape. It helps maintain structural strength and keeps the tower clearance safe in all operating conditions. From IEA 10, IEA 15, and Upscaled + optimized NREL 5, the blade needed a more robust structural strength at the root section, causing high blade mass concentrated at the root section. Optimizing NREL 5 causes the overall blade's mass increases more than linear scaling, although all glass-fiber composite blades have been developed.

Recall that the rotor thrust of upscaled + optimized NREL 5 is always higher than the original or upscaled NREL 5 in all power ratings. It is mainly due to the utilization of thinner airfoils in the optimized blade. Higher thrust causes the tip-to-tower clearance of the upscaled + optimized NREL 5 to be consistently lower than the baseline or upscaled NREL 5. Blade tip to the tower clearance is an important design consideration since failing to maintain a safe clearance can easily cause catastrophic failure during the operation. The difference in blade tip to tower clearance of all turbines at a wind speed of 10 m/s is shown in Figure 5.66. Ten m/s is the thrust curve's peak, and the final velocity before the CP and CT drops.

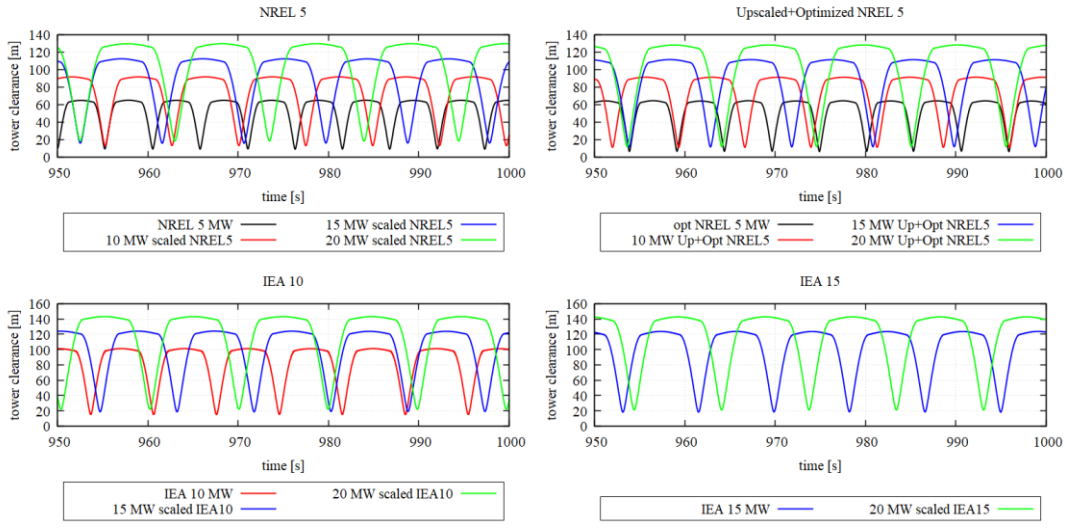

Figure 5.66. Tower clearance of all turbines at a wind speed of 10 m/s

As previously mentioned in Section 2.3, upscaling also causes an increase in blade mass, aerodynamic forces, and moment. Consequently, the bending moment in blade root and tower base also increases. Blade roots' flapwise and edgewise bending moment at the first 1000 seconds of 10 m/s wind speed simulations are shown in Figure 5.67 and Figure 5.68, respectively.

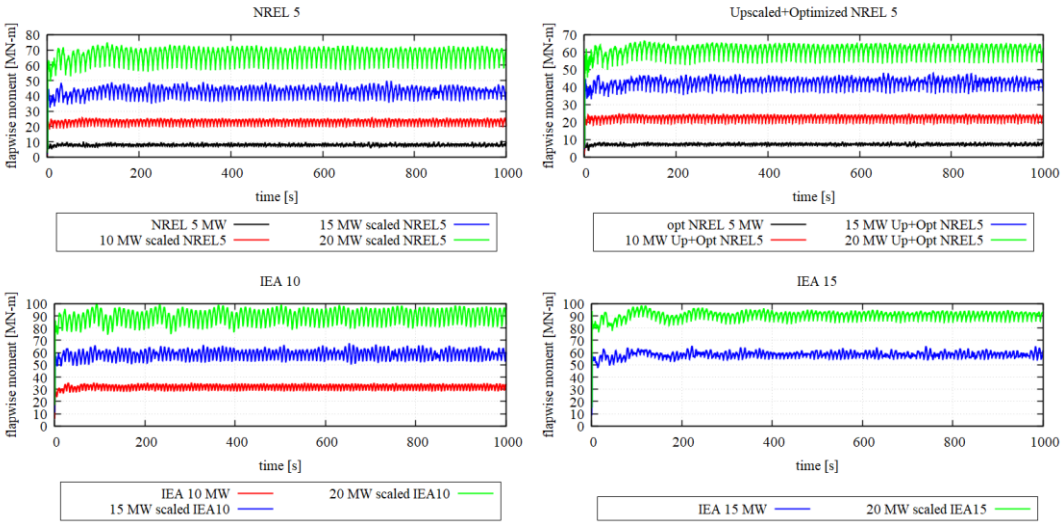

Figure 5.67. Flapwise bending moment at blade root of all turbines at a wind speed of 10 m/s

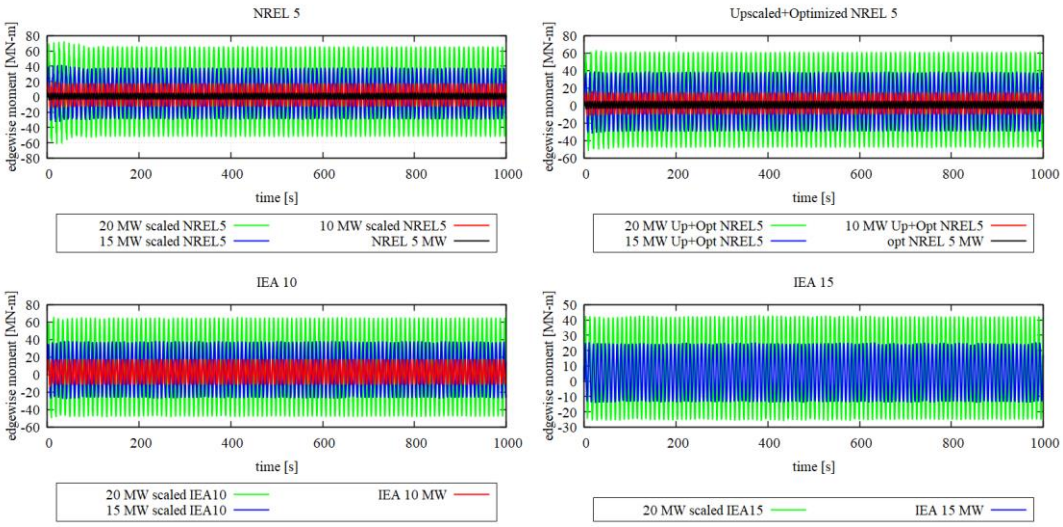

Figure 5.68. Edgewise bending moment at blade root of all turbines at a wind speed of 10 m/s

The root bending moments shown in Figure 5.67 and Figure 5.68 are important parameters in the design of the blade. Theoretically, the rise of this moment will follow the s^3 relation. The time-domain analysis of all turbines with ten m/s wind velocity shows a good agreement with the theoretical relation.

Tower bending moments are as important as blade root's bending moment. Due to the increasing mass, aerodynamic force, and moments on the RNA, the tower experience higher bending moment. The first 1000 seconds of 10 m/s wind speed simulations for the tower's base fore to aft bending for all turbine moments are shown in Figure 5.69. Theoretically, the rise of this moment will follow the s^3 relation. However, since the tower's length is not exactly scaled with s^1, the time-domain analysis of all turbines at ten m/s wind velocity shows that the fore to aft bending moment increases with an approximately $s^{2.8}$ relation. It is in good agreement, although a little lower than the theoretical relation.

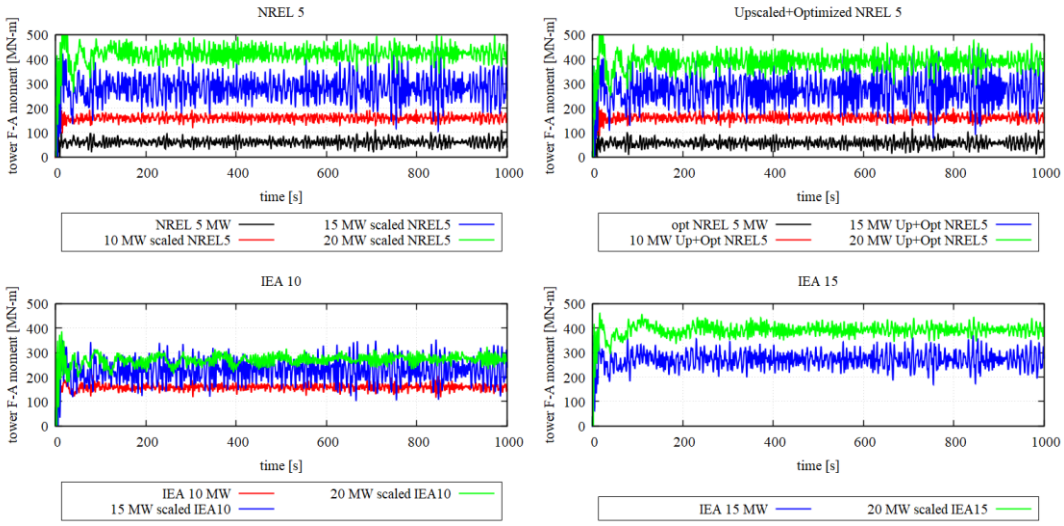

Figure 5.69. The fore-aft bending moment at the tower base of all turbines at a wind speed of 10 m/s

CHAPTER 6

CONCLUSION

6.1 Concluding Remark

This study is performed to develop the preliminary designs of multi-megawatt floating offshore wind turbines based on the linear scaling process and to analyze the aerodynamics coupled with the hydrodynamics effect resulting from the upscaling process on the performance of the FOWT.

In this thesis study, the NREL 5 MW, IEA 10 MW, and IEA 15 MW reference wind turbines are upscaled in the range of 5 MW up to 20 MW. A scaling factor, determined by the square root of the turbine's power rating ratio, is used to upscale turbines, except for the air gap between the tower's base and the blade's tip. OC4 DeepCwind semi-submersible, initially designed for NREL 5 MW, is used as the baseline floating platform and upscaled to support the RWTs in each power rating. However, the mooring lines are not upscaled, but the positions of the anchors are rearranged. The hydrodynamic modeling of the upscaled semi-submersibles is carried out using the open-source potential flow solver, HAMS.

In each power rating, FOWT's performances are compared, and upscaling effects on the aerodynamic and hydrodynamic of the FOWTs are analyzed. Additionally, on 5 MW, a turbine whose blade length is similar to the baseline but with an all-fiberglass material and optimized aerodynamic shape is compared to the baseline NREL 5 MW. It is performed to study the effect of optimization for the non-upscaled turbine. Three turbines with upscaled + optimized NREL 5 blades are added to the comparison at 10, 15, and 20 MW to enrich the analysis for the upscaling process performed in this study. The length of the upscaled + optimized NREL 5 blades is taken by linearly scaling the baseline NREL 5 MW length.

The aerodynamic shape of the blade (airfoil location, chord length, and twist angle) is optimized based on the BEM theory and GA using HARP_Opt. After obtaining the optimum aerodynamic (outer shape) of the blade, the internal structure of the optimized blades is modeled, and mass is minimized using the CLT with an Euler-Bernoulli and shear flow theory in Co-Blade. However, due to the composite layup of the DOWEC blade is not made available to the public, so all fiber-glass material of the Sandia 13.2 MW turbine is used. The whole optimization process results in all-glass wind turbine blades.

Despite the optimization objective in Co-Blade to minimize blade mass, the total mass of the optimized blades is always heavier than the linearly upscaled blade, mainly due to additional reinforcements, the need for a third shear web, and the use of all-glass materials. This finding parallels the other all-glass blade like the UpWind 5 MW and Sandia 13.2 MW. The concentration of blade mass is located at the root section, where the thicknesses of the blade shell and shear web are concentrated. Higher stiffness at the root section is essential to maintain the structural rigidity of the blade and a safe tip-to-tower clearance in the entire operational conditions.

All the turbines' aerodynamic and hydrodynamic performance shows that upscaling is possible and advantageous. Hydrodynamically, upscaling the floating platform lowers the natural frequencies, or in other words, increases the natural period of the floating offshore wind turbines in all degrees of freedom. Upscaling also decreases RAOs and makes the FOWT less influenced by the wave when operating under the same sea state as the baseline turbines, which greatly benefits power production. Inside the wave excitation region, the effect of the wave is more dominant than wind.

Aerodynamically, the upscaling process helps to increase the power produced by the rotor. When linear scaling is used, the upscaled turbines' power and thrust coefficients remain the same as the baseline wind turbines. A higher power coefficient can be gained by optimizing the aerodynamic shape of the blade. However, the performance is relatively conservative to the linearly scaled blade, and

improvements in the power produced are insignificant. These findings again strengthen the UpWind 20 MW pre-design result in [22].

A more substantial increase in the power can be achieved by increasing the blade's length more than linear scaling before optimizing the aerodynamic shape of the blade. Extending the blade length of the 20 MW upscaled and optimized NREL 5 to match the span of 20 MW upscaled IEA 15 significantly increases the produced power and eliminates the conservative behavior of the design. Thus, optimizing the blade length in the initial stage of the optimization procedure is recommended.

The present study contributes to the state of the art by strengthening the knowledge of the application of linear scaling on floating offshore wind turbines, especially for the latest IEA 10 MW and IEA 15 MW. These two RWTs are relatively new, and currently, there are still few upscaling studies performed to upscale IEA 10 MW and IEA 15 MW.

The author presents the study's originality in applying coupled GA - BEM, followed by CLT with an Euler-Bernoulli and shear flow theory in optimizing the linearly upscaled NREL 5 blade’s aerodynamic and internal structure. However, HARP_Opt and Co-Blade are not coupled, which is one limitation of this study. The optimized blade is presented at 5, 10, 15, and 20 MW. Additionally, for 20 MW, another blade based on NREL 5 but matches the length of Upscaled IEA 15 at 20 MW is added and analyzed. Another originality is repositioning the anchor location of the three mooring lines of the linearly upscaled OC4 DeepCwind semisubmersibles. The mooring is rearranged to maintain similar total tension as the baseline semisubmersible in still water conditions.

6.2 Future Recommendation

The purpose of the present study was to predict the effect of aerodynamic and hydrodynamic effects of upscaling FOWT. This study can be used as an initial guide

in developing FOWT. There are many possible ways the present study can be developed, and some future recommendations are summarized as follows:

- To compare the results of the present study with CFD results.
- To validate the results of the present study with the experimental result.
- To couple HARP_Opt and Co-Blade for a more sophisticated aero-elastic optimization
- To use carbon fiber for the spar caps and shear web since carbon fiber is much stiffer and lighter than glass fiber.
- To add blade length as a free variable in the optimization study.
- To carry out analysis for 50-year return period storm (parked turbine), especially for the mooring lines, since the mooring lines are not scaled in the present study.
- In order to have a more sophisticated platform response, the mass ratio between the upscaled and baseline's tower and RNA can be used for upscaling the platform rather than the ratio rotor's size.
- To retune each turbine (in ROSCO) after upscaling since the control strategy is not discussed in detail in the present study.
- To use met ocean data (real-time measurement) such as Turkey's wind and sea state conditions to analyze for deployability of the turbines.

REFERENCES

[1] Elias SA. Climate Change and Energy. Elsevier Inc.; 2018. https://doi.org/10.1016/B978-0-12-809665-9.10515-4.

[2] Fraile D, Mbistrova A. Wind in power 2017. 2018.

[3] International Energy Agency. Market Report Series Renewables 2018. 2018.

[4] Lee J, Zhao F. Global Wind Report | GWEC. 2021.

[5] Hlevca D, Degeratu M. Atmospheric boundary layer modeling in a short wind tunnel. Eur J Mech B/Fluids 2020;79:367–75. https://doi.org/10.1016/j.euromechflu.2019.10.003.

[6] Shields M, Beiter P, Nunemaker J, Cooperman A, Duffy P. Impacts of turbine and plant upsizing on the levelized cost of energy for offshore wind. Appl Energy 2021;298:117189. https://doi.org/10.1016/j.apenergy.2021.117189.

[7] IRENA. Wind power - technology Brief. Energy 2016:1–24.

[8] NREL. The Leading Edge: April 2020 Wind Energy Newsletter 2020.

[9] Sun X, Huang D, Wu G. The current state of offshore wind energy technology development. Energy 2012;41:298–312. https://doi.org/10.1016/j.energy.2012.02.054.

[10] DTU. Global Wind Atlas 3.0 n.d. https://globalwindatlas.info/area/Turkey (accessed June 5, 2022).

[11] Wang X, Zeng X, Li J, Yang X, Wang H. A review on recent advancements of substructures for offshore wind turbines. Energy Convers Manag 2018;158:103–19. https://doi.org/10.1016/j.enconman.2017.12.061.

[12] Uzunoglu E, Oguz E, Soares CG. An Overview of Platform Types Used in

Floating Wind Energy. 2nd Int Congr Sh Mar Technol 2021.

[13] Otter A, Murphy J, Pakrashi V, Robertson A, Desmond C. A review of modelling techniques for floating offshore wind turbines. Wind Energy 2021:1–27. https://doi.org/10.1002/we.2701.

[14] Jonkman J, Butterfield S, Musial W, Scott G. Definition of a 5-MW reference wind turbine for offshore system development. Contract 2009:1–75.

[15] Bortolotti P, Canet Tarrés H, Dykes K, Merz K, Sethuraman L, Verelst D, et al. Systems Engineering in Wind Energy - WP2.1 Reference Wind Turbines. IEA Wind TCP Task 37 2019.

[16] Gaertner E, Rinker J, Sethuraman L, Anderson B, Zahle F, Barter G. IEA Wind TCP Task 37: Definition of the IEA 15 MW Offshore Reference Wind Turbine 2020.

[17] Robertson A, Jonkman J, Masciola M, Song H, Goupee A, Coulling A. Definition of the Semisubmersible Floating System for Phase II of OC4. 2014.

[18] NREL. OpenFAST Documentation Release v2.5.0 2021.

[19] Leimeister M, Bachynski EE, Muskulus M, Thomas P. Rational Upscaling of a Semi-submersible Floating Platform Supporting a Wind Turbine. Energy Procedia 2016;94:434–42. https://doi.org/10.1016/j.egypro.2016.09.212.

[20] Malcolm DJ, Hansen AC. WindPACT Turbine Rotor Design Study: June 2000--June 2002 (Revised) 2006.

[21] Rinker J, Dykes K. WindPACT Reference Wind Turbines. Nrel/Tp-5000-67667 2018.

[22] Peeringa J, Brood R, Ceyhan O, Engels W, de Winkel G, Winkel G De.

Upwind 20MW Wind Turbine Pre-Design: Blade design and control. ECN-E--11-017 December 2011:1–53.

[23] Griffith DT, Ashwill TD. The Sandia 100-meter All-glass Baseline Wind Turbine Blade : SNL100-00. 2011.

[24] Ashuri T, Zaaijer MB. Size effect on wind turbine blade's design drivers. Eur Wind Energy Conf Exhib 2008 2008;6:3371–6.

[25] Capponi PC, Ashuri T, Van Bussel GJW, Kallesoe B. A non-linear upscaling approach for wind turbines blades based on stresses. Eur Wind Energy Conf Exhib 2011, EWEC 2011 2011:115–8.

[26] Caduff M, Huijbregts MAJ, Althaus HJ, Koehler A, Hellweg S. Wind power electricity: The bigger the turbine, the greener the electricity? Environ Sci Technol 2012;46:4725–33. https://doi.org/10.1021/es204108n.

[27] Sieros G, Chaviaropoulos P, Sørensen JD, Bulder BH, Jamieson P. Upscaling wind turbines: theoretical and practical aspects and their impact on the cost of energy. Wind Energy 2012;15:3–17. https://doi.org/10.1002/we.527.

[28] Ashuri T. Beyond Classical Upscaling : Integrated Aeroservoelastic Design and Optimization of Large Offshore Wind Turbines. 2012. https://doi.org/10.4233/uuid:d10726c1-693c-408e-8505-dfca1810a59a.

[29] Kazacoks R, Jamieson P. Influence of scaling effects on hub loads of a horizontal wind turbine. IET Conf Publ 2014;2014:1–6. https://doi.org/10.1049/cp.2014.0915.

[30] Liu J, Thomas E, Manuel L, Griffith T, Ruehl KM, Barone M. Integrated system design for a large wind turbine supported on a moored semi-submersible platform. J Mar Sci Eng 2018;6. https://doi.org/10.3390/jmse6010009.

[31] Sağol E. Site Specific Design Optimization of a Horizontal Axis Wind

Turbine Based on Minimum Cost of Energy. 2010.

[32] Yi J-H, Sale D. Blade Shape Optimization of Wind Turbines Using Genetic Algorithms and Pattern Search Method. J Korean Soc Civ Eng 2012;32:369–78. https://doi.org/10.12652/ksce.2012.32.6a.369.

[33] Sale D, Li Y. Structural Optimization of Composite Blades for Wind and Hydrokinetic Turbines. 1 St Mar Energy Technol Conf 2013.

[34] Bekele A, Ababa A. Site Specific Design Optimization Of Horizontal Axis Wind Turbine Based On Minimum Cost Of Energy For Adama I Wind Farm 2013;2:862–70.

[35] Kesikbas O. Investigations of Upscaling Effects for Aerodynamic Design of Large Wind Turbine Rotors by Using BEM Theory and Optimization. 2019.

[36] Oğuz K. Aerodynamic Optimization of Horizontal Axis Wind Turbine Blades by Using CST Method, BEM Theory and Genetic Algorithm. 2019.

[37] Ram KR, Lal SP, Ahmed MR. Design and optimization of airfoils and a 20 kW wind turbine using multi-objective genetic algorithm and HARP_Opt code. Renew Energy 2019;144:56–67. https://doi.org/10.1016/j.renene.2018.08.040.

[38] Khlaifat N, Altaee A, Zhou J, Huang Y, Braytee A. Optimization of a small wind turbine for a rural area: A case study of Deniliquin, New South Wales, Australia. Energies 2020;13. https://doi.org/10.3390/en13092292.

[39] Robertson A, Jonkman J, Vorpahl F, Popko W, Qvist J, Frøyd L, et al. Offshore code comparison collaboration continuation within IEA wind task 30: Phase II results regarding a floating semisubmersible wind system. Proc Int Conf Offshore Mech Arct Eng - OMAE 2014;9B. https://doi.org/10.1115/OMAE2014-24040.

[40] Jamieson P. Innovation in Wind Turbine Design: Second Edition. John Wiley & Sons Ltd; 2018.

[41] Ashuri T, Zaaijer MB, Martins JRRA, Zhang J. Multidisciplinary design optimization of large wind turbines - Technical, economic, and design challenges. Energy Convers Manag 2016;123:56–70. https://doi.org/10.1016/j.enconman.2016.06.004.

[42] Wu J, Kim M. Generic Upscaling Methodology of a Floating Offshore Wind Turbine 2021:1–14.

[43] Abbas NJ, Wright AD, Pao LY. An Update to the NREL Baseline Wind Turbine Controller. NAWEA/WindTech 2019:17.

[44] Lindenburg C, Winkelaar D, Hooft EL Van Der. DOWEC 6 MW PRE-DESIGN Aero-elastic modelling of the DOWEC 6 MW pre-design in PHATAS. 2003.

[45] Lindenburg C. Aeroelastic Analysis of the LMH64-5 Blade Concept 2003:1–51.

[46] Heijdra JJ, Hendriks HB. DOWEC CONCEPT STUDY Task 11 : Selection of feasible concepts. n.d.

[47] Bak C, Zahle F, Bitsche R, Kim T, Yde A, Henriksen LC, et al. The DTU 10-MW Reference Wind Turbine 2013.

[48] Kim B sung, Jin J won, Bitkina O, Kang K weon. Ultimate load characteristics of NREL 5-MW offshore wind turbines with different substructures. Int J Energy Res 2016;40:639–50. https://doi.org/10.1002/er.3430.

[49] Bredmose H, Rinker J, Skrzypinski W, Zahle F, Meng F, Dykes K, et al. Definition of the 15 MW Reference Wind Turbine 2020:1–40.

[50] Uçar M, Uzunoglu E, Oguz E. Comparison and Evaluation of Open-Source Panel Method Codes against Commercial Codes. 2nd Int. Congr. Sh. Mar. Technol. (GMO-SHIPMAR 2021), 2021.

[51] Liu Y. HAMS: A frequency-domain preprocessor for wave-structure interactions-Theory, development, and application. J Mar Sci Eng 2019;7:1–19. https://doi.org/10.3390/jmse7030081.

[52] Liu Y. Introduction of the Open-Source Boundary Element Method Solver HAMS to the Ocean Renewable Energy Community 2021:1–6.

[53] Liu Y, Iwashita H, Hu C. A calculation method for finite depth Free-Surface green function. Int J Nav Archit Ocean Eng 2015;7:375–89. https://doi.org/10.1515/ijnaoe-2015-0026.

[54] Liu Y, Hu C, Sueyoshi M, Iwashita H, Kashiwagi M. Motion response prediction by hybrid panel-stick models for a semi-submersible with bracings. J Mar Sci Technol 2016;21:742–57. https://doi.org/10.1007/s00773-016-0390-1.

[55] Liu Y, Yoshida S, Hu C, Sueyoshi M, Sun L, Gao J, et al. A reliable open-source package for performance evaluation of floating renewable energy systems in coastal and offshore regions. Energy Convers Manag 2018;174:516–36. https://doi.org/10.1016/j.enconman.2018.08.012.

[56] Sale DC. HARP_Opt User's Guide. NWTC Des Codes, Available Http//Wind Nrel Gov/Designcodes/Simulators/HARP_Opt/Last Modif 2010.

[57] Platt AD, Buhl ML. WT_Perf User Guide for Version 3.05.00. Natl Renew Energy Lab 2012.

[58] Lugo Reyes SO. Artificial intelligence in precision health: Systems in practice. Artif Intell Precis Heal 2020:499–519. https://doi.org/10.1016/b978-0-12-817133-2.00021-5.

[59] Hansen MOL. Aerodynamics of Wind Turbines. second. London: Earthscan; 2008.

[60] Sale DC. co-blade: Software for Analysis and Design of Composite Blades. See Also URL Https//Code Google Com/p/Co-Blade 2015.

[61] Bagherpoor T, Xuemin L. Structural Optimization Design of 2MW Composite Wind Turbine Blade. Energy Procedia 2017;105:1226–33. https://doi.org/10.1016/j.egypro.2017.03.420.

[62] Chehouri A, Younes R, Ilinca A, Perron J, Lakiss H. Optimal design for a composite wind turbine blade with fatigue and failure constraints. Trans Can Soc Mech Eng 2015;39:171–86. https://doi.org/10.1139/tcsme-2015-0013.

[63] Chehouri A. Optimisation of wind turbine blade structures using a genetic algorithm 2018.

[64] Jonkman BJ, Jonkman JM. FAST v8.16.00a-bjj User's Guide. Nrel 2016:58.

[65] Larsen TJ, Hansen AM. How 2 HAWC2, the user's manual. vol. 1597. 2014.

[66] Driscoll F, Jonkman J, Robertson A, Sirnivas S, Skaare B, Nielsen FG. Validation of a FAST Model of the Statoil-hywind Demo Floating Wind Turbine. Energy Procedia 2016;94:3–19. https://doi.org/10.1016/j.egypro.2016.09.181.

[67] Andersen MT, Wendt FF, Robertson AN, Jonkman JM, Hall M. Verification and validation of multisegmented mooring capabilities in FAST v8. Proc Int Offshore Polar Eng Conf 2016;2016-Janua:371–8.

[68] Jonkman, Jason. Demonstration of NREL Modeling Capability to Design the Next Generation of Floating Offshore Wind Turbines with Stiesdal and Magellan Wind: Cooperative Research and Development Final Report, CRADA Number CRD-19-00787 2022.

[69] Jonkman JM, Hayman GJ, Jonkman BJ, Damiani RR. AeroDyn v15 User's Guide and Theory Manual. Renew Energy 2015:46.

[70] Cruz J, Atcheson M. Floating Offshore Wind Energy. vol. 10. 2016.

APPENDICES

A. Example input for OpenFAST

```
------- OpenFAST EXAMPLE INPUT FILE -------------------------------------------
Optimized+ NREL5 at 20 MW offshore baseline blade input properties.
---------------------- SIMULATION CONTROL --------------------------------------
False          Echo            - Echo input data to <RootName>.ech (flag)
"FATAL"       AbortLevel      - Error level when simulation should abort (string)
  {"WARNING", "SEVERE", "FATAL"}
       8000  TMax            - Total run time (s)
     0.0125   DT              - Recommended module time step (s)
          2   InterpOrder     - Interpolation order for input/output time history (-)
  {1=linear, 2=quadratic}
          0   NumCrctn        - Number of correction iterations (-) {0=explicit
  calculation, i.e., no corrections}
      99999   DT_UJac         - Time between calls to get Jacobians (s)
      1E+06   UJacSclFact     - Scaling factor used in Jacobians (-)
---------------------- FEATURE SWITCHES AND FLAGS ------------------------------
          1   CompElast       - Compute structural dynamics (switch) {1=ElastoDyn;
  2=ElastoDyn + BeamDyn for blades}
          1   CompInflow      - Compute inflow wind velocities (switch) {0=still air;
  1=InflowWind; 2=external from OpenFOAM}
          2   CompAero        - Compute aerodynamic loads (switch) {0=None; 1=AeroDyn
  v14; 2=AeroDyn v15}
          1   CompServo       - Compute control and electrical-drive dynamics (switch)
  {0=None; 1=ServoDyn}
          1   CompHydro       - Compute hydrodynamic loads (switch) {0=None;
  1=HydroDyn}
          0   CompSub         - Compute sub-structural dynamics (switch) {0=None;
  1=SubDyn; 2=External Platform MCKF}
          1   CompMooring     - Compute mooring system (switch) {0=None; 1=MAP++;
  2=FEAMooring; 3=MoorDyn; 4=OrcaFlex}
          0   CompIce         - Compute ice loads (switch) {0=None; 1=IceFloe;
  2=IceDyn}
---------------------- INPUT FILES ---------------------------------------------
"NRELOffshrBsline5MW_OC4DeepCwindSemi_ElastoDyn.dat"    EDFile          - Name of file
  containing ElastoDyn input parameters (quoted string)
"NRELOffshrBsline5MW_BeamDyn.dat"    BDBldFile(1)    - Name of file containing BeamDyn
  input parameters for blade 1 (quoted string)
"NRELOffshrBsline5MW_BeamDyn.dat"    BDBldFile(2)    - Name of file containing BeamDyn
  input parameters for blade 2 (quoted string)
"NRELOffshrBsline5MW_BeamDyn.dat"    BDBldFile(3)    - Name of file containing BeamDyn
  input parameters for blade 3 (quoted string)
"NRELOffshrBsline5MW_InflowWind_12mps.dat"    InflowFile      - Name of file
  containing inflow wind input parameters (quoted string)
"NRELOffshrBsline5MW_OC3Hywind_AeroDyn15.dat"    AeroFile        - Name of file
  containing aerodynamic input parameters (quoted string)
"NRELOffshrBsline5MW_OC4DeepCwindSemi_ServoDyn.dat"    ServoFile       - Name of file
  containing control and electrical-drive input parameters (quoted string)
"NRELOffshrBsline5MW_OC4DeepCwindSemi_HydroDyn.dat"    HydroFile       - Name of file
  containing hydrodynamic input parameters (quoted string)
"unused"      SubFile         - Name of file containing sub-structural input
  parameters (quoted string)
"NRELOffshrBsline5MW_OC4DeepCwindSemi_MAP.dat"    MooringFile     - Name of file
  containing mooring system input parameters (quoted string)
"unused"      IceFile         - Name of file containing ice input parameters (quoted
  string)
---------------------- OUTPUT --------------------------------------------------
False         SumPrint        - Print summary data to "<RootName>.sum" (flag)
         10   SttsTime        - Amount of time between screen status messages (s)
       9000   ChkptTime       - Amount of time between creating checkpoint files for
  potential restart (s)
```

```
37  "default"   DT_Out          - Time step for tabular output (s) (or "default")
38       2001   TStart          - Time to begin tabular output (s)
39          1   OutFileFmt      - Format for tabular (time-marching) output file
  (switch) {0: uncompressed binary [<RootName>.outb], 1: text file [<RootName>.out], 2:
  binary file [<RootName>.outb], 3: both 1 and 2}
40 True          TabDelim        - Use tab delimiters in text tabular output file? (flag)
  {uses spaces if false}
41 "ES15.7E2"    OutFmt          - Format used for text tabular output, excluding the
  time channel.  Resulting field should be 10 characters. (quoted string)
42 ---------------------- LINEARIZATION -----------------------------------------
43 False          Linearize       - Linearization analysis (flag)
44 False         CalcSteady      - Calculate a steady-state periodic operating point
  before linearization? [unused if Linearize=False] (flag)
45          3   TrimCase        - Controller parameter to be trimmed {1:yaw; 2:torque;
  3:pitch} [used only if CalcSteady=True] (-)
46      0.001   TrimTol         - Tolerance for the rotational speed convergence [used
  only if CalcSteady=True] (-)
47       0.01   TrimGain        - Proportional gain for the rotational speed error (>0)
  [used only if CalcSteady=True] (rad/(rad/s) for yaw or pitch; Nm/(rad/s) for torque)
48          0   Twr_Kdmp        - Damping factor for the tower [used only if
  CalcSteady=True] (N/(m/s))
49          0   Bld_Kdmp        - Damping factor for the blades [used only if
  CalcSteady=True] (N/(m/s))
50          1   NLinTimes       - Number of times to linearize (-) [>=1] [unused if
  Linearize=False]
51          0   LinTimes        - List of times at which to linearize (s) [1 to
  NLinTimes] [used only when Linearize=True and CalcSteady=False]
52          1   LinInputs       - Inputs included in linearization (switch) {0=none;
  1=standard; 2=all module inputs (debug)} [unused if Linearize=False]
53          1   LinOutputs      - Outputs included in linearization (switch) {0=none;
  1=from OutList(s); 2=all module outputs (debug)} [unused if Linearize=False]
54 False         LinOutJac       - Include full Jacobians in linearization output (for
  debug) (flag) [unused if Linearize=False; used only if LinInputs=LinOutputs=2]
55 False         LinOutMod       - Write module-level linearization output files in
  addition to output for full system? (flag) [unused if Linearize=False]
56 ---------------------- VISUALIZATION -----------------------------------------
57          0   WrVTK           - VTK visualization data output: (switch) {0=none;
  1=initialization data only; 2=animation; 3=mode shapes}
58          1   VTK_type        - Type of VTK visualization data: (switch) {1=surfaces;
  2=basic meshes (lines/points); 3=all meshes (debug)} [unused if WrVTK=0]
59 false         VTK_fields      - Write mesh fields to VTK data files? (flag)
  {true/false} [unused if WrVTK=0]
60         10   VTK_fps         - Frame rate for VTK output (frames per second){will use
  closest integer multiple of DT} [used only if WrVTK=2 or WrVTK=3]
```

Figure A.1. Example input for OpenFAST v2.5

B. Example input for ElastoDyn

```
------- ELASTODYN for OpenFAST INPUT FILE -------------------------------------------
Optimized+ NREL5 at 20 MW offshore baseline blade input properties.
---------------------- SIMULATION CONTROL --------------------------------------
False         Echo        - Echo input data to "<RootName>.ech" (flag)
          3   Method      - Integration method: {1: RK4, 2: AB4, or 3: ABM4} (-)
"DEFAULT"     DT          - Integration time step (s)
---------------------- ENVIRONMENTAL CONDITION ---------------------------------
    9.80665   Gravity     - Gravitational acceleration (m/s^2)
---------------------- DEGREES OF FREEDOM --------------------------------------
True          FlapDOF1    - First flapwise blade mode DOF (flag)
True          FlapDOF2    - Second flapwise blade mode DOF (flag)
True          EdgeDOF     - First edgewise blade mode DOF (flag)
False         TeetDOF     - Rotor-teeter DOF (flag) [unused for 3 blades]
True          DrTrDOF     - Drivetrain rotational-flexibility DOF (flag)
True          GenDOF      - Generator DOF (flag)
True          YawDOF      - Yaw DOF (flag)
True          TwFADOF1    - First fore-aft tower bending-mode DOF (flag)
True          TwFADOF2    - Second fore-aft tower bending-mode DOF (flag)
True          TwSSDOF1    - First side-to-side tower bending-mode DOF (flag)
True          TwSSDOF2    - Second side-to-side tower bending-mode DOF (flag)
True          PtfmSgDOF   - Platform horizontal surge translation DOF (flag)
True          PtfmSwDOF   - Platform horizontal sway translation DOF (flag)
True          PtfmHvDOF   - Platform vertical heave translation DOF (flag)
True          PtfmRDOF    - Platform roll tilt rotation DOF (flag)
True          PtfmPDOF    - Platform pitch tilt rotation DOF (flag)
True          PtfmYDOF    - Platform yaw rotation DOF (flag)
---------------------- INITIAL CONDITIONS --------------------------------------
          0   OoPDefl     - Initial out-of-plane blade-tip displacement (meters)
          0   IPDefl      - Initial in-plane blade-tip deflection (meters)
          0   BlPitch(1)  - Blade 1 initial pitch (degrees)
          0   BlPitch(2)  - Blade 2 initial pitch (degrees)
          0   BlPitch(3)  - Blade 3 initial pitch (degrees) [unused for 2 blades]
          0   TeetDefl    - Initial or fixed teeter angle (degrees) [unused for 3
  blades]
          0   Azimuth     - Initial azimuth angle for blade 1 (degrees)
      4.500 RotSpeed    - Initial or fixed rotor speed (rpm)
          0   NacYaw      - Initial or fixed nacelle-yaw angle (degrees)
          0   TTDspFA     - Initial fore-aft tower-top displacement (meters)
          0   TTDspSS     - Initial side-to-side tower-top displacement (meters)
          5   PtfmSurge   - Initial or fixed horizontal surge translational
  displacement of platform (meters)
          0   PtfmSway    - Initial or fixed horizontal sway translational
  displacement of platform (meters)
          0   PtfmHeave   - Initial or fixed vertical heave translational
  displacement of platform (meters)
          0   PtfmRoll    - Initial or fixed roll tilt rotational displacement of
  platform (degrees)
          0   PtfmPitch   - Initial or fixed pitch tilt rotational displacement of
  platform (degrees)
          0   PtfmYaw     - Initial or fixed yaw rotational displacement of platform
  (degrees)
---------------------- TURBINE CONFIGURATION -----------------------------------
        3.0   NumBl       - Number of blades (-)
126.000000 TipRad      - The distance from the rotor apex to the blade tip (meters)
  3.000000 HubRad      - The distance from the rotor apex to the blade root (meters)
       -2.5   PreCone(1)  - Blade 1 cone angle (degrees)
       -2.5   PreCone(2)  - Blade 2 cone angle (degrees)
       -2.5   PreCone(3)  - Blade 3 cone angle (degrees) [unused for 2 blades]
  0.000000 HubCM       - Distance from rotor apex to hub mass [positive downwind]
  (meters)
        0.0   UndSling    - Undersling length [distance from teeter pin to the rotor
  apex] (meters) [unused for 3 blades]
        0.0  Delta3      - Delta-3 angle for teetering rotors (degrees) [unused for 3
```

```
55         0.0   AzimB1Up    - Azimuth value to use for I/O when blade 1 points up
  (degrees)
56 -10.038200 OverHang    - Distance from yaw axis to rotor apex [3 blades] or teeter
  pin [2 blades] (meters)
57   3.824000 ShftGagL    - Distance from rotor apex [3 blades] or teeter pin [2 blades]
  to shaft strain gages [positive for upwind rotors] (meters)
58          -5   ShftTilt    - Rotor shaft tilt angle (degrees)
59   3.800000 NacCMxn     - Downwind distance from the tower-top to the nacelle CM
  (meters)
60   0.000000 NacCMyn     - Lateral  distance from the tower-top to the nacelle CM
  (meters)
61   3.500000 NacCMzn     - Vertical distance from the tower-top to the nacelle CM
  (meters)
62  -6.190560 NcIMUxn     - Downwind distance from the tower-top to the nacelle IMU
  (meters)
63   0.000000 NcIMUyn     - Lateral  distance from the tower-top to the nacelle IMU
  (meters)
64   4.466720 NcIMUzn     - Vertical distance from the tower-top to the nacelle IMU
  (meters)
65   3.925120 Twr2Shft    - Vertical distance from the tower-top to the rotor shaft
  (meters)
66 158.653333 TowerHt     - Height of tower above ground level [onshore] or MSL
  [offshore] (meters)
67  20.000000  TowerBsHt   - Height of tower base above ground level [onshore] or MSL
  [offshore] (meters)
68         0.0   PtfmCMxt    - Downwind distance from the ground level [onshore] or MSL
  [offshore] to the platform CM (meters)
69         0.0   PtfmCMyt    - Lateral distance from the ground level [onshore] or MSL
  [offshore] to the platform CM (meters)
70 -17.317600 PtfmCMzt    - Vertical distance from the ground level [onshore] or MSL
  [offshore] to the platform CM (meters)
71         0.0   PtfmRefzt   - Vertical distance from the ground level [onshore] or MSL
  [offshore] to the platform reference point (meters)
72 ---------------------- MASS AND INERTIA ----------------------------------------
73 0                  TipMass(1)  - Tip-brake mass, blade 1 (kg)
74 0                  TipMass(2)  - Tip-brake mass, blade 2 (kg)
75 0                  TipMass(3)  - Tip-brake mass, blade 3 (kg) [unused for 2 blades]
76    454240.00      HubMass     - Hub mass (kg)
77   0.37096E+07      HubIner     - Hub inertia about rotor axis [3 blades] or teeter
  axis [2 blades] (kg m^2)
78   0.17092E+05      GenIner     - Generator inertia about HSS (kg m^2)
79   0.19200E+07      NacMass     - Nacelle mass (kg)
80   0.83452E+08      NacYIner    - Nacelle inertia about yaw axis (kg m^2)
81   0.00000E+00 YawBrMass   - Yaw bearing mass (kg)
82      30817440.000   PtfmMass    - Platform mass (kg)
83   81981760000.000   PtfmRIner   - Platform inertia for roll tilt rotation about the
  platform CM (kg m^2)
84   81981760000.000   PtfmPIner   - Platform inertia for pitch tilt rotation about the
  platform CM (kg m^2)
85  135764800000.000   PtfmYIner   - Platform inertia for yaw rotation about the
  platform CM (kg m^2)
86 ---------------------- BLADE ---------------------------------------------------
87          49   BldNodes    - Number of blade nodes (per blade) used for analysis (-)
88 "NRELOffshrBsline5MW_blade.dat"    BldFile(1)  - Name of file containing properties
  for blade 1 (quoted string)
89 "NRELOffshrBsline5MW_blade.dat"    BldFile(2)  - Name of file containing properties
  for blade 2 (quoted string)
90 "NRELOffshrBsline5MW_blade.dat"    BldFile(3)  - Name of file containing properties
  for blade 3 (quoted string) [unused for 2 blades]
91 ---------------------- ROTOR-TEETER --------------------------------------------
92           0   TeetMod     - Rotor-teeter spring/damper model {0: none, 1: standard,
  2: user-defined from routine UserTeet} (switch) [unused for 3 blades]
93           0   TeetDmpP    - Rotor-teeter damper position (degrees) [used only for 2
  blades and when TeetMod=1]
94           0   TeetDmp     - Rotor-teeter damping constant (N-m/(rad/s)) [used only
  for 2 blades and when TeetMod=1]
95           0   TeetCDmp    - Rotor-teeter rate-independent Coulomb-damping moment (N-
  m) [used only for 2 blades and when TeetMod=1]
```

```
 96           0   TeetSStP    - Rotor-teeter soft-stop position (degrees) [used only for
   2 blades and when TeetMod=1]
 97           0   TeetHStP    - Rotor-teeter hard-stop position (degrees) [used only for
   2 blades and when TeetMod=1]
 98           0   TeetSSSp    - Rotor-teeter soft-stop linear-spring constant (N-m/rad)
   [used only for 2 blades and when TeetMod=1]
 99           0   TeetHSSp    - Rotor-teeter hard-stop linear-spring constant (N-m/rad)
   [used only for 2 blades and when TeetMod=1]
100 ---------------------- DRIVETRAIN --------------------------------------------------
101       100.0   GBoxEff     - Gearbox efficiency (%)
102        97.0   GBRatio     - Gearbox ratio (-)
103   0.69411E+10 DTTorSpr    - Drivetrain torsional spring (N-m/rad)
104   0.99440E+08 DTTorDmp    - Drivetrain torsional damper (N-m/(rad/s))
105 ---------------------- FURLING -----------------------------------------------------
106 False         Furling     - Read in additional model properties for furling turbine
   (flag) [must currently be FALSE)
107 "unused"      FurlFile    - Name of file containing furling properties (quoted
   string) [unused when Furling=False]
108 ---------------------- TOWER -------------------------------------------------------
109          20   TwrNodes    - Number of tower nodes used for analysis (-)
110 "NRELOffshrBsline5MW_OC4DeepCwindSemi_ElastoDyn_Tower.dat"    TwrFile     - Name of
   file containing tower properties (quoted string)
111 ---------------------- OUTPUT ------------------------------------------------------
112 False          SumPrint    - Print summary data to "<RootName>.sum" (flag)
113           2   OutFile     - Switch to determine where output will be placed: {1: in
   module output file only; 2: in glue code output file only; 3: both} (currently
   unused)
114 True          TabDelim    - Use tab delimiters in text tabular output file? (flag)
   (currently unused)
115 "ES10.3E2"    OutFmt      - Format used for text tabular output (except time).
   Resulting field should be 10 characters. (quoted string) (currently unused)
116           0   TStart      - Time to begin tabular output (s) (currently unused)
117           1   DecFact     - Decimation factor for tabular output {1: output every
   time step} (-) (currently unused)
118           1   NTwGages    - Number of tower nodes that have strain gages for output
   [0 to 9] (-)
119          10   TwrGagNd    - List of tower nodes that have strain gages [1 to
   TwrNodes] (-) [unused if NTwGages=0]
120           1   NBlGages    - Number of blade nodes that have strain gages for output
   [0 to 9] (-)
121           9   BldGagNd    - List of blade nodes that have strain gages [1 to
   BldNodes] (-) [unused if NBlGages=0]
122               OutList     - The next line(s) contains a list of output parameters.
   See OutListParameters.xlsx for a listing of available output channels, (-)
123 "BldPitch1"               - Pitch angles for blades 1, 2, and 3
124 "BldPitch2"               - Pitch angles for blades 1, 2, and 3
125 "BldPitch3"               - Pitch angles for blades 1, 2, and 3
126 "Azimuth"                 - Blade 1 azimuth angle
127 "RotSpeed"                - Low-speed shaft and high-speed shaft speeds
128 "GenSpeed"                - Low-speed shaft and high-speed shaft speeds
129 "NacYaw"                  - Nacelle yaw angle and nacelle yaw error estimate
130 "OoPDefl1"                - Blade 1 out-of-plane and in-plane deflections and tip
   twist
131 "IPDefl1"                 - Blade 1 out-of-plane and in-plane deflections and tip
   twist
132 "TwstDefl1"               - Blade 1 out-of-plane and in-plane deflections and tip
   twist
133 "OoPDefl2"                - Blade 2 out-of-plane and in-plane deflections and tip
   twist
134 "IPDefl2"                 - Blade 2 out-of-plane and in-plane deflections and tip
   twist
135 "TwstDefl2"               - Blade 2 out-of-plane and in-plane deflections and tip
   twist
136 "OoPDefl3"                - Blade 3 out-of-plane and in-plane deflections and tip
   twist
137 "IPDefl3"                 - Blade 3 out-of-plane and in-plane deflections and tip
   twist
```

```
138 "TwstDefl3"              - Blade 3 out-of-plane and in-plane deflections and tip
    twist
139 "TwrClrnc1"              - Tip-to-tower clearance estimate for blades 1, 2, and 3
140 "TwrClrnc2"              - Tip-to-tower clearance estimate for blades 1, 2, and 3
141 "TwrClrnc3"              - Tip-to-tower clearance estimate for blades 1, 2, and 3
142 "NcIMUTAxs"              - Nacelle IMU translational accelerations (absolute) in the
    nonrotating, shaft coordinate system
143 "NcIMUTAys"              - Nacelle IMU translational accelerations (absolute) in the
    nonrotating, shaft coordinate system
144 "NcIMUTAzs"              - Nacelle IMU translational accelerations (absolute) in the
    nonrotating, shaft coordinate system
145 "TTDspFA"                - Tower fore-aft and side-to-side displacements and top
    twist
146 "TTDspSS"                - Tower fore-aft and side-to-side displacements and top
    twist
147 "TTDspTwst"              - Tower fore-aft and side-to-side displacements and top
    twist
148 "PtfmSurge"              - Platform translational surge, sway, and heave
    displacements
149 "PtfmSway"               - Platform translational surge, sway, and heave
    displacements
150 "PtfmHeave"              - Platform translational surge, sway, and heave
    displacements
151 "PtfmRoll"               - Platform rotational roll, pitch and yaw displacements
152 "PtfmPitch"              - Platform rotational roll, pitch and yaw displacements
153 "PtfmYaw"                - Platform rotational roll, pitch and yaw displacements
154 "PtfmTAxt"               - Platform translation accelerations (absolute) in the
    tower-base coordinate system
155 "PtfmTAyt"               - Platform translation accelerations (absolute) in the
    tower-base coordinate system
156 "PtfmTAzt"               - Platform translation accelerations (absolute) in the
    tower-base coordinate system
157 "RootFxc1"               - Out-of-plane shear, in-plane shear, and axial forces at
    the root of blade 1
158 "RootFyc1"               - Out-of-plane shear, in-plane shear, and axial forces at
    the root of blade 1
159 "RootFzc1"               - Out-of-plane shear, in-plane shear, and axial forces at
    the root of blade 1
160 "RootMxc1"               - In-plane bending, out-of-plane bending, and pitching
    moments at the root of blade 1
161 "RootMyc1"               - In-plane bending, out-of-plane bending, and pitching
    moments at the root of blade 1
162 "RootMxb1"               - Blade 1 edgewise moment (i.e., the moment caused by
    edgewise forces) at the blade root
163 "RootMyb1"               - Blade 1 flapwise moment (i.e., the moment caused by
    flapwise forces) at the blade root
164 "RootMzc1"               - In-plane bending, out-of-plane bending, and pitching
    moments at the root of blade 1
165 "RootFzc2"               - Out-of-plane shear, in-plane shear, and axial forces at
    the root of blade 2
166 "RootMxc2"               - In-plane bending, out-of-plane bending, and pitching
    moments at the root of blade 2
167 "RootMyc2"               - In-plane bending, out-of-plane bending, and pitching
    moments at the root of blade 2
168 "RootMzc2"               - In-plane bending, out-of-plane bending, and pitching
    moments at the root of blade 2
169 "RootFxc3"               - Out-of-plane shear, in-plane shear, and axial forces at
    the root of blade 3
170 "RootFyc3"               - Out-of-plane shear, in-plane shear, and axial forces at
    the root of blade 3
171 "RootFzc3"               - Out-of-plane shear, in-plane shear, and axial forces at
    the root of blade 3
172 "RootMxc3"               - In-plane bending, out-of-plane bending, and pitching
    moments at the root of blade 3
173 "RootMyc3"               - In-plane bending, out-of-plane bending, and pitching
    moments at the root of blade 3
```

```
174 "RootMzc3"               - In-plane bending, out-of-plane bending, and pitching
    moments at the root of blade 3
175 "Spn1MLxb1"              - Blade 1 local edgewise bending, flapwise bending, and
    pitching moments at span station 1 (approx. 50% span)
176 "Spn1MLyb1"              - Blade 1 local edgewise bending, flapwise bending, and
    pitching moments at span station 1 (approx. 50% span)
177 "Spn1MLzb1"              - Blade 1 local edgewise bending, flapwise bending, and
    pitching moments at span station 1 (approx. 50% span)
178 "Spn1MLxb2"              - Blade 2 local edgewise bending, flapwise bending, and
    pitching moments at span station 1 (approx. 50% span)
179 "Spn1MLyb2"              - Blade 2 local edgewise bending, flapwise bending, and
    pitching moments at span station 1 (approx. 50% span)
180 "Spn1MLzb2"              - Blade 2 local edgewise bending, flapwise bending, and
    pitching moments at span station 1 (approx. 50% span)
181 "Spn1MLxb3"              - Blade 3 local edgewise bending, flapwise bending, and
    pitching moments at span station 1 (approx. 50% span)
182 "Spn1MLyb3"              - Blade 3 local edgewise bending, flapwise bending, and
    pitching moments at span station 1 (approx. 50% span)
183 "Spn1MLzb3"              - Blade 3 local edgewise bending, flapwise bending, and
    pitching moments at span station 1 (approx. 50% span)
184 "RotThrust"              - Rotor thrust and low-speed shaft 0- and 90-rotating shear
    forces at the main bearing
185 "LSSGagFya"              - Rotor thrust and low-speed shaft 0- and 90-rotating shear
    forces at the main bearing
186 "LSSGagFza"              - Rotor thrust and low-speed shaft 0- and 90-rotating shear
    forces at the main bearing
187 "RotTorq"                - Rotor torque and low-speed shaft 0- and 90-rotating
    bending moments at the main bearing
188 "LSSGagMya"              - Rotor torque and low-speed shaft 0- and 90-rotating
    bending moments at the main bearing
189 "LSSGagMza"              - Rotor torque and low-speed shaft 0- and 90-rotating
    bending moments at the main bearing
190 "YawBrFxp"               - Fore-aft shear, side-to-side shear, and vertical forces
    at the top of the tower (not rotating with nacelle yaw)
191 "YawBrFyp"               - Fore-aft shear, side-to-side shear, and vertical forces
    at the top of the tower (not rotating with nacelle yaw)
192 "YawBrFzp"               - Fore-aft shear, side-to-side shear, and vertical forces
    at the top of the tower (not rotating with nacelle yaw)
193 "YawBrMxp"               - Side-to-side bending, fore-aft bending, and yaw moments
    at the top of the tower (not rotating with nacelle yaw)
194 "YawBrMyp"               - Side-to-side bending, fore-aft bending, and yaw moments
    at the top of the tower (not rotating with nacelle yaw)
195 "YawBrMzp"               - Side-to-side bending, fore-aft bending, and yaw moments
    at the top of the tower (not rotating with nacelle yaw)
196 "TwrBsFxt"               - Fore-aft shear, side-to-side shear, and vertical forces
    at the base of the tower (platform)
197 "TwrBsFyt"               - Fore-aft shear, side-to-side shear, and vertical forces
    at the base of the tower (platform)
198 "TwrBsFzt"               - Fore-aft shear, side-to-side shear, and vertical forces
    at the base of the tower (platform)
199 "TwrBsMxt"               - Side-to-side bending, fore-aft bending, and yaw moments
    at the base of the tower (platform)
200 "TwrBsMyt"               - Side-to-side bending, fore-aft bending, and yaw moments
    at the base of the tower (platform)
201 "TwrBsMzt"               - Side-to-side bending, fore-aft bending, and yaw moments
    at the base of the tower (platform)
202 "TwHt1MLxt"              - Local side-to-side bending, fore-aft bending, and yaw
    moments at tower gage 1 (approx. 50% elevation)
203 "TwHt1MLyt"              - Local side-to-side bending, fore-aft bending, and yaw
    moments at tower gage 1 (approx. 50% elevation)
204 "TwHt1MLzt"              - Local side-to-side bending, fore-aft bending, and yaw
    moments at tower gage 1 (approx. 50% elevation)
205 END of input file (the word "END" must appear in the first 3 columns of this last
    OutList line)
```

Figure B.2. Example input for ElastoDyn's module

```
------- ELASTODYN V1.00.* TOWER INPUT FILE -------------------------------------
Optimized+ NREL5 at 20 MW offshore baseline blade input properties.
---------------------- TOWER PARAMETERS ------------------------------------------
   11         NTwInpSt    - Number of input stations to specify tower geometry
          1   TwrFADmp(1) - Tower 1st fore-aft mode structural damping ratio (%)
          1   TwrFADmp(2) - Tower 2nd fore-aft mode structural damping ratio (%)
          1   TwrSSDmp(1) - Tower 1st side-to-side mode structural damping ratio (%)
          1   TwrSSDmp(2) - Tower 2nd side-to-side mode structural damping ratio (%)
---------------------- TOWER ADJUSTMUNT FACTORS ----------------------------------
          1   FAStTunr(1) - Tower fore-aft modal stiffness tuner, 1st mode (-)
          1   FAStTunr(2) - Tower fore-aft modal stiffness tuner, 2nd mode (-)
          1   SSStTunr(1) - Tower side-to-side stiffness tuner, 1st mode (-)
          1   SSStTunr(2) - Tower side-to-side stiffness tuner, 2nd mode (-)
          1   AdjTwMa     - Factor to adjust tower mass density (-)
          1   AdjFASt     - Factor to adjust tower fore-aft stiffness (-)
          1   AdjSSSt     - Factor to adjust tower side-to-side stiffness (-)
---------------------- DISTRIBUTED TOWER PROPERTIES ------------------------------
  HtFract       TMassDen         TwFAStif       TwSSStif
   (-)           (kg/m)           (Nm^2)         (Nm^2)
   0.00000E+00   0.18668E+05   0.96624E+13   0.96624E+13
   0.10000E+00   0.17381E+05   0.82823E+13   0.82823E+13
   0.20000E+00   0.16139E+05   0.70548E+13   0.70548E+13
   0.30000E+00   0.14942E+05   0.59684E+13   0.59684E+13
   0.40000E+00   0.13789E+05   0.50118E+13   0.50118E+13
   0.50000E+00   0.12682E+05   0.41744E+13   0.41744E+13
   0.60000E+00   0.11619E+05   0.34458E+13   0.34458E+13
   0.70000E+00   0.10601E+05   0.28164E+13   0.28164E+13
   0.80000E+00   0.96275E+04   0.22768E+13   0.22768E+13
   0.90000E+00   0.86991E+04   0.18181E+13   0.18181E+13
   0.10000E+01   0.78155E+04   0.14318E+13   0.14318E+13
---------------------- TOWER FORE-AFT MODE SHAPES --------------------------------
     1.1533   TwFAM1Sh(2) - Mode 1, coefficient of x^2 term
    -0.8622   TwFAM1Sh(3) -       , coefficient of x^3 term
     1.8042   TwFAM1Sh(4) -       , coefficient of x^4 term
    -1.5035   TwFAM1Sh(5) -       , coefficient of x^5 term
     0.4082   TwFAM1Sh(6) -       , coefficient of x^6 term
    19.1169   TwFAM2Sh(2) - Mode 2, coefficient of x^2 term
    -6.8956   TwFAM2Sh(3) -       , coefficient of x^3 term
     -8.185   TwFAM2Sh(4) -       , coefficient of x^4 term
    -5.1085   TwFAM2Sh(5) -       , coefficient of x^5 term
     2.0722   TwFAM2Sh(6) -       , coefficient of x^6 term
---------------------- TOWER SIDE-TO-SIDE MODE SHAPES -----------------------------
     1.1438   TwSSM1Sh(2) - Mode 1, coefficient of x^2 term
     -0.874   TwSSM1Sh(3) -       , coefficient of x^3 term
     1.8388   TwSSM1Sh(4) -       , coefficient of x^4 term
    -1.5306   TwSSM1Sh(5) -       , coefficient of x^5 term
      0.422   TwSSM1Sh(6) -       , coefficient of x^6 term
    11.2222   TwSSM2Sh(2) - Mode 2, coefficient of x^2 term
    -3.2615   TwSSM2Sh(3) -       , coefficient of x^3 term
    -5.1208   TwSSM2Sh(4) -       , coefficient of x^4 term
      -0.86   TwSSM2Sh(5) -       , coefficient of x^5 term
    -0.9798   TwSSM2Sh(6) -       , coefficient of x^6 term
```

Figure B.3. Example input for ElastoDyn's tower

```
------- ELASTODYN V1.00.* INDIVIDUAL BLADE INPUT FILE -------------------------
Optimized+ NREL5 at 20 MW offshore baseline blade input properties.
---------------------- BLADE PARAMETERS --------------------------------------
   49                  NBlInpSt    - Number of blade input stations (-)
0.477465               BldFlDmp(1) - Blade flap mode #1 structural damping in percent
 of critical (%)
0.477465               BldFlDmp(2) - Blade flap mode #2 structural damping in percent
 of critical (%)
0.477465               BldEdDmp(1) - Blade edge mode #1 structural damping in percent
 of critical (%)
---------------------- BLADE ADJUSTMENT FACTORS -------------------------------
1              FlStTunr(1) - Blade flapwise modal stiffness tuner, 1st mode (-)
1              FlStTunr(2) - Blade flapwise modal stiffness tuner, 2nd mode (-)
1.04536                AdjBlMs     - Factor to adjust blade mass density (-)
1                      AdjFlSt     - Factor to adjust blade flap stiffness (-)
1                      AdjEdSt     - Factor to adjust blade edge stiffness (-)
---------------------- DISTRIBUTED BLADE PROPERTIES ---------------------------
  BlFract   PitchAxis    StrcTwst    BMassDen    FlpStff     EdgStff
    (-)         (-)        (deg)       (kg/m)      (Nm^2)      (Nm^2)
0.0000E+00     5.0000E-01     1.4910E+01     8.3252E+03     6.8816E+11     6.7746E+11
2.0833E-02     5.0000E-01     1.4910E+01     7.4948E+03     6.2709E+11     6.0039E+11
4.1667E-02     4.8090E-01     1.4910E+01     6.7037E+03     5.5375E+11     5.6360E+11
6.2500E-02     4.2950E-01     1.4910E+01     5.8296E+03     4.1787E+11     5.6914E+11
8.3333E-02     3.9560E-01     1.4910E+01     4.7730E+03     2.5644E+11     4.9756E+11
1.0417E-01     3.8090E-01     1.4910E+01     3.7255E+03     1.4471E+11     3.7882E+11
1.2500E-01     3.7500E-01     1.4910E+01     2.8121E+03     9.6635E+10     2.6078E+11
1.4583E-01     3.7500E-01     1.3640E+01     2.6932E+03     9.0023E+10     2.4742E+11
1.6667E-01     3.7500E-01     1.2650E+01     2.5523E+03     8.2112E+10     2.2684E+11
1.8750E-01     3.7500E-01     1.1830E+01     2.4027E+03     7.3988E+10     2.0357E+11
2.0833E-01     3.7500E-01     1.1100E+01     2.1066E+03     4.7965E+10     1.7281E+11
2.2917E-01     3.7500E-01     1.0460E+01     1.9106E+03     4.0120E+10     1.5015E+11
2.5000E-01     3.7500E-01     9.8640E+00     1.7205E+03     3.3059E+10     1.2894E+11
2.7083E-01     3.7500E-01     9.3200E+00     1.6055E+03     2.8680E+10     1.1495E+11
2.9167E-01     3.7500E-01     8.8110E+00     1.5511E+03     2.6244E+10     1.0636E+11
3.1250E-01     3.7500E-01     8.3370E+00     1.4253E+03     1.7870E+10     9.5377E+10
3.3333E-01     3.7500E-01     7.8880E+00     1.3752E+03     1.6244E+10     8.7977E+10
3.5417E-01     3.7500E-01     7.4610E+00     1.2688E+03     1.1076E+10     7.9470E+10
3.7500E-01     3.7500E-01     7.0570E+00     1.2222E+03     9.9735E+09     7.3118E+10
3.9583E-01     3.7500E-01     6.6710E+00     1.1770E+03     8.9801E+09     6.7165E+10
4.1667E-01     3.7500E-01     6.3010E+00     1.1361E+03     8.1133E+09     6.1653E+10
4.3750E-01     3.7500E-01     5.9460E+00     1.0961E+03     7.3268E+09     5.6516E+10
4.5833E-01     3.7500E-01     5.6040E+00     1.0146E+03     5.0863E+09     5.0931E+10
4.7917E-01     3.7500E-01     5.2730E+00     9.6129E+02     4.4927E+09     4.5562E+10
5.0000E-01     3.7500E-01     4.9540E+00     9.0704E+02     3.9527E+09     4.0517E+10
5.2083E-01     3.7500E-01     4.6440E+00     8.5448E+02     3.4699E+09     3.5907E+10
5.4167E-01     3.7500E-01     4.3430E+00     8.0345E+02     3.0382E+09     3.1700E+10
5.6250E-01     3.7500E-01     4.0500E+00     7.5423E+02     2.6536E+09     2.7883E+10
5.8333E-01     3.7500E-01     3.7640E+00     7.0667E+02     2.3109E+09     2.4424E+10
6.0417E-01     3.7500E-01     3.4850E+00     6.6566E+02     2.0193E+09     2.1547E+10
6.2500E-01     3.7500E-01     3.2120E+00     6.3402E+02     1.7806E+09     1.9324E+10
6.4583E-01     3.7500E-01     2.9440E+00     6.0311E+02     1.5651E+09     1.7274E+10
6.6667E-01     3.7500E-01     2.6820E+00     5.4835E+02     1.0823E+09     1.5166E+10
6.8750E-01     3.7500E-01     2.4240E+00     5.0435E+02     9.0674E+08     1.2995E+10
7.0833E-01     3.7500E-01     2.1710E+00     4.6235E+02     7.5418E+08     1.1062E+10
7.2917E-01     3.7500E-01     1.9200E+00     4.2222E+02     6.2200E+08     9.3455E+09
7.5000E-01     3.7500E-01     1.6730E+00     3.8512E+02     5.1198E+08     7.8321E+09
7.7083E-01     3.7500E-01     1.4290E+00     3.5003E+02     4.1819E+08     6.5105E+09
7.9167E-01     3.7500E-01     1.1870E+00     3.1668E+02     3.3811E+08     5.3571E+09
8.1250E-01     3.7500E-01     9.4720E-01     2.8526E+02     2.7055E+08     4.3613E+09
8.3333E-01     3.7500E-01     7.0920E-01     2.5561E+02     2.1385E+08     3.5065E+09
8.5417E-01     3.7500E-01     4.7260E-01     2.2771E+02     1.6668E+08     2.7776E+09
```

```
8.7500E-01     3.7500E-01     2.3700E-01     2.0168E+02     1.2907E+08     2.1639E+09
8.9583E-01     3.7500E-01     2.5000E-03     1.7730E+02     9.9365E+07     1.6530E+09
9.1667E-01     3.7500E-01     -2.3160E-01    1.5447E+02     7.5138E+07     1.2314E+09
9.3750E-01     3.7500E-01     -4.6550E-01    1.3292E+02     5.5542E+07     8.8098E+08
9.5833E-01     3.7500E-01     -6.9930E-01    1.1134E+02     3.9032E+07     5.7092E+08
9.7917E-01     3.7500E-01     -9.3340E-01    9.1609E+01     2.6299E+07     3.3409E+08
1.0000E+00     3.7500E-01     -1.1680E+00    7.3722E+01     1.6673E+07     1.5874E+08
---------------------- BLADE MODE SHAPES -------------------------------------
     0.0622   BldFl1Sh(2) - Flap mode 1, coeff of x^2
     1.7254   BldFl1Sh(3) -            , coeff of x^3
    -3.2452   BldFl1Sh(4) -            , coeff of x^4
     4.7131   BldFl1Sh(5) -            , coeff of x^5
    -2.2555   BldFl1Sh(6) -            , coeff of x^6
    -0.5809   BldFl2Sh(2) - Flap mode 2, coeff of x^2
     1.2067   BldFl2Sh(3) -            , coeff of x^3
   -15.5349   BldFl2Sh(4) -            , coeff of x^4
    29.7347   BldFl2Sh(5) -            , coeff of x^5
   -13.8255   BldFl2Sh(6) -            , coeff of x^6
     0.3627   BldEdgSh(2) - Edge mode 1, coeff of x^2
     2.5337   BldEdgSh(3) -            , coeff of x^3
    -3.5772   BldEdgSh(4) -            , coeff of x^4
      2.376   BldEdgSh(5) -            , coeff of x^5
    -0.6952   BldEdgSh(6) -            , coeff of x^6
```

Figure B.4. Example input for ElastoDyn's Blade

C. Example input for InflowWind

```
------- InflowWind v3.01.* INPUT FILE ------------------------------------------
Optimized+ NREL5 at 20 MW offshore baseline blade input properties.
---------------------------------------------------------------------------------
False         Echo           - Echo input data to <RootName>.ech (flag)
          1   WindType       - switch for wind file type (1=steady; 2=uniform;
3=binary TurbSim FF; 4=binary Bladed-style FF; 5=HAWC format; 6=User defined)
          0   PropagationDir - Direction of wind propagation (meteoroligical rotation
from aligned with X (positive rotates towards -Y) -- degrees)
               0.0       VFlowAng    - Upflow angle (degrees) (not used for native
Bladed format WindType=7)
          1   NWindVel       - Number of points to output the wind velocity (0 to 9)
          0   WindVxiList    - List of coordinates in the inertial X direction (m)
          0   WindVyiList    - List of coordinates in the inertial Y direction (m)
163.000000     WindVziList   - List of coordinates in the inertial Z direction (m)
======== Parameters for Steady Wind Conditions [used only for WindType = 1] =========
8          HWindSpeed     - Horizontal windspeed                            (m/s)
163.000000     RefHt          - Reference height for horizontal wind speed      (m)
        0.2    PLexp          - Power law exponent                              (-)
======== Parameters for Uniform wind file   [used only for WindType = 2] ============
"Wind/90m_12mps_twr.bts"    Filename_Uni        - Filename of time series data for
uniform wind field.      (-)
     90       RefHt_Uni           - Reference height for horizontal wind speed (m)
     125.88   RefLength      - Reference length for linear horizontal and vertical
sheer (-)
==== Parameters for Binary TurbSim Full-Field files   [used only for WindType = 3] ===
"Wind/input.bts"    Filename_BTS       - Name of the Full field wind file to use
(.bts)
===== Parameters for Binary Bladed-style Full-Field [used only for WindType = 4] ====
"Wind/90m_12mps_twr"    FilenameRoot   - Rootname of the full-field wind file to use
(.wnd, .sum)
False         TowerFile      - Have tower file (.twr) (flag)
====== Parameters for HAWC-format binary files  [Only used with WindType = 5] =======
"wasp\Output\basic_5u.bin"    FileName_u     - name of the file containing the u-
component fluctuating wind (.bin)
"wasp\Output\basic_5v.bin"    FileName_v     - name of the file containing the v-
component fluctuating wind (.bin)
"wasp\Output\basic_5w.bin"    FileName_w     - name of the file containing the w-
component fluctuating wind (.bin)
         64   nx             - number of grids in the x direction (in the 3 files
above) (-)
         32   ny             - number of grids in the y direction (in the 3 files
above) (-)
         32   nz             - number of grids in the z direction (in the 3 files
above) (-)
         16   dx       - distance (in meters) between points in the x direction    (m)
          3   dy       - distance (in meters) between points in the y direction    (m)
          3   dz       - distance (in meters) between points in the z direction    (m)
         90   RefHt_Hawc          - reference height; the height (in meters) of the
vertical center of the grid (m)
  ----------   Scaling parameters for turbulence   ---------------------------
          1   ScaleMethod    - Turbulence scaling method   [0 = none, 1 = direct
scaling, 2 = calculate scaling factor based on a desired standard deviation]
          1   SFx            - Turbulence scaling factor for the x direction (-)
[ScaleMethod=1]
          1   SFy            - Turbulence scaling factor for the y direction (-)
[ScaleMethod=1]
          1   SFz            - Turbulence scaling factor for the z direction (-)
[ScaleMethod=1]
         12   SigmaFx        - Turbulence standard deviation to calculate scaling from
in x direction (m/s)    [ScaleMethod=2]
```

```
          8   SigmaFy        - Turbulence standard deviation to calculate scaling from
  in y direction (m/s)    [ScaleMethod=2]
          2   SigmaFz        - Turbulence standard deviation to calculate scaling from
  in z direction (m/s)    [ScaleMethod=2]
   --------   Mean wind profile parameters (added to HAWC-format files)   -------------
          5   URef           - Mean u-component wind speed at the reference height
  (m/s)
          2   WindProfile    - Wind profile type (0=constant;1=logarithmic,2=power
  law)
        0.2   PLExp_Hawc     - Power law exp (-) (used for PL wind profile type only)
        0.03   Z0             - Surface roughness length (m) (used for LG wind profile
  type only)
                 0       XOffset     - Initial offset in +x direction (shift of wind
  box) (-)
====================== OUTPUT ==================================================
False         SumPrint     - Print summary data to <RootName>.IfW.sum (flag)
              OutList      - The next line(s) contains a list of output parameters.
  See OutListParameters.xlsx for a listing of available output channels, (-)
"Wind1VelX"               X-direction wind velocity at point WindList(1)
"Wind1VelY"               Y-direction wind velocity at point WindList(1)
"Wind1VelZ"               Z-direction wind velocity at point WindList(1)
END of input file (the word "END" must appear in the first 3 columns of this last
  OutList line)
```

Figure C.5. Example input for InflowWind's module

D. Example input for AeroDyn

```
1 ------- AERODYN v15 for OpenFAST INPUT FILE ------------------------------------
2 Optimized+ NREL5 at 20 MW offshore baseline blade input properties.
3 ======  General Options  ============================================================
4 False         Echo               - Echo the input to "<rootname>.AD.ech"?  (flag)
5 "default"     DTAero             - Time interval for aerodynamic calculations {or
  "default"} (s)
6           1   WakeMod            - Type of wake/induction model (switch) {0=none,
  1=BEMT, 2=DBEMT, 3=OLAF} [WakeMod cannot be 2 or 3 when linearizing]
7           2   AFAeroMod          - Type of blade airfoil aerodynamics model (switch)
  {1=steady model, 2=Beddoes-Leishman unsteady model} [AFAeroMod must be 1 when
  linearizing]
8           1   TwrPotent          - Type tower influence on wind based on potential
  flow around the tower (switch) {0=none, 1=baseline potential flow, 2=potential flow
  with Bak correction}
9 True         TwrShadow          - Calculate tower influence on wind based on
  downstream tower shadow (switch) {0=none, 1=Powles model, 2=Eames model}
10 True          TwrAero            - Calculate tower aerodynamic loads? (flag)
11 False         FrozenWake         - Assume frozen wake during linearization? (flag)
  [used only when WakeMod=1 and when linearizing]
12 False         CavitCheck         - Perform cavitation check? (flag) [AFAeroMod must
  be 1 when CavitCheck=true]
13 False         CompAA             - Flag to compute AeroAcoustics calculation [used
  only when WakeMod = 1 or 2]
14 "unused"      AA_InputFile       - AeroAcoustics input file [used only when
  CompAA=true]
15 ======  Environmental Conditions  ===========================================
16      1.225   AirDens            - Air density (kg/m^3)
17  1.464E-05   KinVisc            - Kinematic air viscosity (m^2/s)
18        335   SpdSound           - Speed of sound (m/s)
19     103500   Patm               - Atmospheric pressure (Pa) [used only when
  CavitCheck=True]
20       1700   Pvap               - Vapour pressure of fluid (Pa) [used only when
  CavitCheck=True]
21        0.5   FluidDepth         - Water depth above mid-hub height (m) [used only
  when CavitCheck=True]
22 ======  Blade-Element/Momentum Theory Options  ========= [unused when WakeMod=0 or 3]
23          2   SkewMod            - Type of skewed-wake correction model (switch)
  {1=uncoupled, 2=Pitt/Peters, 3=coupled} [unused when WakeMod=0 or 3]
24 "default"     SkewModFactor      - Constant used in Pitt/Peters skewed wake model {or
  "default" is 15/32*pi} (-) [used only when SkewMod=2; unused when WakeMod=0 or 3]
25 True          TipLoss            - Use the Prandtl tip-loss model? (flag) [unused
  when WakeMod=0 or 3]
26 True          HubLoss            - Use the Prandtl hub-loss model? (flag) [unused
  when WakeMod=0 or 3]
27 True          TanInd             - Include tangential induction in BEMT calculations?
  (flag) [unused when WakeMod=0 or 3]
28 False         AIDrag             - Include the drag term in the axial-induction
  calculation? (flag) [unused when WakeMod=0 or 3]
29 False         TIDrag             - Include the drag term in the tangential-induction
  calculation? (flag) [unused when WakeMod=0,3 or TanInd=FALSE]
30 "Default"     IndToler           - Convergence tolerance for BEMT nonlinear solve
  residual equation {or "default"} (-) [unused when WakeMod=0 or 3]
31        100   MaxIter            - Maximum number of iteration steps (-) [unused when
  WakeMod=0]
32 ====== Dynamic Blade-Element/Momentum Theory Options ===== [used only when WakeMod=2]
33          2   DBEMT_Mod          - Type of dynamic BEMT (DBEMT) model {1=constant
  tau1, 2=time-dependent tau1} (-) [used only when WakeMod=2]
34          4   tau1_const         - Time constant for DBEMT (s) [used only when
  WakeMod=2 and DBEMT_Mod=1]
35 ======  OLAF -- cOnvecting LAgrangian Filaments Options  ==================
36 "unused"      OLAFInputFileName  - Input file for OLAF [used only when WakeMod=3]
37 ======  Beddoes-Leishman Options  ==================[used only when AFAeroMod=2]
```

```
          3   UAMod              - Unsteady Aero Model Switch (switch) {1=Baseline
  model (Original), 2=Gonzalez's variant (changes in Cn,Cc,Cm), 3=Minnema/Pierce
  variant (changes in Cc and Cm)} [used only when AFAeroMod=2]
True          FLookup            - Flag to indicate whether a lookup for f' will be
  calculated (TRUE) or whether best-fit exponential equations will be used (FALSE); if
  FALSE S1-S4 must be provided in airfoil input files (flag) [used only when
  AFAeroMod=2]
======  Airfoil Information ===========================================================
          1   AFTabMod           - Interpolation method for multiple airfoil tables
  {1=1D interpolation on AoA (first table only); 2=2D interpolation on AoA and Re; 3=2D
  interpolation on AoA and UserProp} (-)
          1   InCol_Alfa         - The column in the airfoil tables that contains the
  angle of attack (-)
          2   InCol_Cl           - The column in the airfoil tables that contains the
  lift coefficient (-)
          3   InCol_Cd           - The column in the airfoil tables that contains the
  drag coefficient (-)
          4   InCol_Cm           - The column in the airfoil tables that contains the
  pitching-moment coefficient; use zero if there is no Cm column (-)
          0   InCol_Cpmin        - The column in the airfoil tables that contains the
  Cpmin coefficient; use zero if there is no Cpmin column (-)
49                NumAFfiles  - Number of airfoil files used (-)
"Airfoil_Data\NREL5_1000.dat"  AFNames
"Airfoil_Data\NREL5_1000.dat"
"Airfoil_Data\NREL5_0929.dat"
"Airfoil_Data\NREL5_0733.dat"
"Airfoil_Data\NREL5_0561.dat"
"Airfoil_Data\NREL5_0446.dat"
"Airfoil_Data\NREL5_0400.dat"
"Airfoil_Data\NREL5_0400.dat"
"Airfoil_Data\NREL5_0400.dat"
"Airfoil_Data\NREL5_0400.dat"
"Airfoil_Data\NREL5_0350.dat"
"Airfoil_Data\NREL5_0350.dat"
"Airfoil_Data\NREL5_0350.dat"
"Airfoil_Data\NREL5_0350.dat"
"Airfoil_Data\NREL5_0350.dat"
"Airfoil_Data\NREL5_0300.dat"
"Airfoil_Data\NREL5_0300.dat"
"Airfoil_Data\NREL5_0250.dat"
"Airfoil_Data\NREL5_0250.dat"
"Airfoil_Data\NREL5_0250.dat"
"Airfoil_Data\NREL5_0250.dat"
"Airfoil_Data\NREL5_0250.dat"
"Airfoil_Data\NREL5_0210.dat"
"Airfoil_Data\NREL5_0210.dat"
"Airfoil_Data\NREL5_0210.dat"
"Airfoil_Data\NREL5_0210.dat"
"Airfoil_Data\NREL5_0210.dat"
"Airfoil_Data\NREL5_0210.dat"
"Airfoil_Data\NREL5_0210.dat"
"Airfoil_Data\NREL5_0210.dat"
"Airfoil_Data\NREL5_0210.dat"
"Airfoil_Data\NREL5_0180.dat"
"Airfoil_Data\NREL5_0180.dat"
"Airfoil_Data\NREL5_0180.dat"
"Airfoil_Data\NREL5_0180.dat"
"Airfoil_Data\NREL5_0180.dat"
"Airfoil_Data\NREL5_0180.dat"
"Airfoil_Data\NREL5_0180.dat"
"Airfoil_Data\NREL5_0180.dat"
"Airfoil_Data\NREL5_0180.dat"
"Airfoil_Data\NREL5_0180.dat"
```

```
 93 "Airfoil_Data\NREL5_0180.dat"
 94 "Airfoil_Data\NREL5_0180.dat"
 95 "Airfoil_Data\NREL5_0180.dat"
 96 "Airfoil_Data\NREL5_0180.dat"
 97 ======  Rotor/Blade Properties  ===================================================
 98 True          UseBlCm            - Include aerodynamic pitching moment in
    calculations?  (flag)
 99 "NRELOffshrBsline5MW_AeroDyn_blade.dat"    ADBlFile(1)        - Name of file
    containing distributed aerodynamic properties for Blade #1 (-)
100 "NRELOffshrBsline5MW_AeroDyn_blade.dat"    ADBlFile(2)        - Name of file
    containing distributed aerodynamic properties for Blade #2 (-) [unused if NumBl <
    2]
101 "NRELOffshrBsline5MW_AeroDyn_blade.dat"    ADBlFile(3)        - Name of file
    containing distributed aerodynamic properties for Blade #3 (-) [unused if NumBl <
    3]
102 ======  Tower Influence and Aerodynamics ========================================
103 11         NumTwrNds          - Number of tower nodes used in the analysis  (-)
104 TwrElev        TwrDiam        TwrCd          TwrTI (used only with TwrShadow=2)
105 (m)              (m)           (-)             (-)
106    0.20000E+02   0.13000E+02   0.10000E+01   0.10000E+00
107    0.32165E+02   0.12480E+02   0.10000E+01   0.10000E+00
108    0.46220E+02   0.11940E+02   0.10000E+01   0.10000E+00
109    0.60274E+02   0.11420E+02   0.10000E+01   0.10000E+00
110    0.74328E+02   0.10900E+02   0.10000E+01   0.10000E+00
111    0.88382E+02   0.10360E+02   0.10000E+01   0.10000E+00
112    0.10244E+03   0.98400E+01   0.10000E+01   0.10000E+00
113    0.11649E+03   0.93200E+01   0.10000E+01   0.10000E+00
114    0.13054E+03   0.88000E+01   0.10000E+01   0.10000E+00
115    0.14460E+03   0.82600E+01   0.10000E+01   0.10000E+00
116    0.15865E+03   0.77400E+01   0.10000E+01   0.10000E+00
117 ======  Outputs  ==========================================================
118 False          SumPrint            - Generate a summary file listing input options
    and interpolated properties to "<rootname>.AD.sum"?  (flag)
119 3                             NBlOuts             - Number of blade node outputs [0
    - 9] (-)
120 1,          9,         19    BlOutNd             - Blade nodes whose values will be
    output  (-)
121 0                       NTwOuts             - Number of tower node outputs [0 - 9]
    (-)
122 1,          2,          6    TwOutNd             - Tower nodes whose values will be
    output  (-)
123                    OutList             - The next line(s) contains a list of output
    parameters.  See OutListParameters.xlsx for a listing of available output channels,
    (-)
124 "RtAeroCp"
125 "RtAeroCq"
126 "RtAeroCt"
127 "RtAeroPwr"
128 "RtSpeed"
129 "RtTSR"
130 END of input file (the word "END" must appear in the first 3 columns of this last
    OutList line)
```

Figure D.6. Example input for AeroDyn's module

```
------- AERODYN v15.00.* BLADE DEFINITION INPUT FILE ----------------------------
Optimized+ NREL5 at 20 MW offshore baseline blade input properties.
====== Blade Properties ========================================================
49       NumBlNds    - Number of blade nodes used in the analysis (-)
  BlSpn        BlCrvAC      BlSwpAC     BlCrvAng      BlTwist      BlChord      BlAFID
    (m)          (m)          (m)         (deg)         (deg)        (m)          (-)
0.0000E+00  0.0000E+00  0.0000E+00  0.0000E+00  1.4910E+01  7.0840E+00  1.0000E+00
2.5625E+00  0.0000E+00  0.0000E+00  0.0000E+00  1.4910E+01  7.0840E+00  2.0000E+00
5.1250E+00  0.0000E+00  0.0000E+00  0.0000E+00  1.4910E+01  7.4270E+00  3.0000E+00
7.6875E+00  0.0000E+00  0.0000E+00  0.0000E+00  1.4910E+01  8.3870E+00  4.0000E+00
1.0250E+01  0.0000E+00  0.0000E+00  0.0000E+00  1.4910E+01  9.1810E+00  5.0000E+00
1.2813E+01  0.0000E+00  0.0000E+00  0.0000E+00  1.4910E+01  9.6140E+00  6.0000E+00
1.5375E+01  0.0000E+00  0.0000E+00  0.0000E+00  1.4910E+01  9.7790E+00  7.0000E+00
1.7938E+01  0.0000E+00  0.0000E+00  0.0000E+00  1.3640E+01  9.7770E+00  8.0000E+00
2.0500E+01  0.0000E+00  0.0000E+00  0.0000E+00  1.2650E+01  9.6830E+00  9.0000E+00
2.3063E+01  0.0000E+00  0.0000E+00  0.0000E+00  1.1830E+01  9.5380E+00  1.0000E+01
2.5625E+01  0.0000E+00  0.0000E+00  0.0000E+00  1.1100E+01  9.3660E+00  1.1000E+01
2.8188E+01  0.0000E+00  0.0000E+00  0.0000E+00  1.0460E+01  9.1790E+00  1.2000E+01
3.0750E+01  0.0000E+00  0.0000E+00  0.0000E+00  9.8640E+00  8.9830E+00  1.3000E+01
3.3313E+01  0.0000E+00  0.0000E+00  0.0000E+00  9.3200E+00  8.7850E+00  1.4000E+01
3.5875E+01  0.0000E+00  0.0000E+00  0.0000E+00  8.8110E+00  8.5850E+00  1.5000E+01
3.8438E+01  0.0000E+00  0.0000E+00  0.0000E+00  8.3370E+00  8.3870E+00  1.6000E+01
4.1000E+01  0.0000E+00  0.0000E+00  0.0000E+00  7.8880E+00  8.1900E+00  1.7000E+01
4.3563E+01  0.0000E+00  0.0000E+00  0.0000E+00  7.4610E+00  7.9960E+00  1.8000E+01
4.6125E+01  0.0000E+00  0.0000E+00  0.0000E+00  7.0570E+00  7.8050E+00  1.9000E+01
4.8688E+01  0.0000E+00  0.0000E+00  0.0000E+00  6.6710E+00  7.6150E+00  2.0000E+01
5.1250E+01  0.0000E+00  0.0000E+00  0.0000E+00  6.3010E+00  7.4280E+00  2.1000E+01
5.3813E+01  0.0000E+00  0.0000E+00  0.0000E+00  5.9460E+00  7.2430E+00  2.2000E+01
5.6375E+01  0.0000E+00  0.0000E+00  0.0000E+00  5.6040E+00  7.0610E+00  2.3000E+01
5.8938E+01  0.0000E+00  0.0000E+00  0.0000E+00  5.2730E+00  6.8790E+00  2.4000E+01
6.1500E+01  0.0000E+00  0.0000E+00  0.0000E+00  4.9540E+00  6.7000E+00  2.5000E+01
6.4063E+01  0.0000E+00  0.0000E+00  0.0000E+00  4.6440E+00  6.5220E+00  2.6000E+01
6.6625E+01  0.0000E+00  0.0000E+00  0.0000E+00  4.3430E+00  6.3450E+00  2.7000E+01
6.9188E+01  0.0000E+00  0.0000E+00  0.0000E+00  4.0500E+00  6.1690E+00  2.8000E+01
7.1750E+01  0.0000E+00  0.0000E+00  0.0000E+00  3.7640E+00  5.9940E+00  2.9000E+01
7.4313E+01  0.0000E+00  0.0000E+00  0.0000E+00  3.4850E+00  5.8190E+00  3.0000E+01
7.6875E+01  0.0000E+00  0.0000E+00  0.0000E+00  3.2120E+00  5.6450E+00  3.1000E+01
7.9438E+01  0.0000E+00  0.0000E+00  0.0000E+00  2.9440E+00  5.4710E+00  3.2000E+01
8.2000E+01  0.0000E+00  0.0000E+00  0.0000E+00  2.6820E+00  5.2970E+00  3.3000E+01
8.4563E+01  0.0000E+00  0.0000E+00  0.0000E+00  2.4240E+00  5.1240E+00  3.4000E+01
8.7125E+01  0.0000E+00  0.0000E+00  0.0000E+00  2.1710E+00  4.9510E+00  3.5000E+01
8.9688E+01  0.0000E+00  0.0000E+00  0.0000E+00  1.9200E+00  4.7780E+00  3.6000E+01
9.2250E+01  0.0000E+00  0.0000E+00  0.0000E+00  1.6730E+00  4.6040E+00  3.7000E+01
9.4813E+01  0.0000E+00  0.0000E+00  0.0000E+00  1.4290E+00  4.4310E+00  3.8000E+01
9.7375E+01  0.0000E+00  0.0000E+00  0.0000E+00  1.1870E+00  4.2580E+00  3.9000E+01
9.9938E+01  0.0000E+00  0.0000E+00  0.0000E+00  9.4720E-01  4.0850E+00  4.0000E+01
1.0250E+02  0.0000E+00  0.0000E+00  0.0000E+00  7.0920E-01  3.9120E+00  4.1000E+01
1.0506E+02  0.0000E+00  0.0000E+00  0.0000E+00  4.7260E-01  3.7390E+00  4.2000E+01
1.0763E+02  0.0000E+00  0.0000E+00  0.0000E+00  2.3700E-01  3.5660E+00  4.3000E+01
1.1019E+02  0.0000E+00  0.0000E+00  0.0000E+00  2.5000E-03  3.3940E+00  4.4000E+01
1.1275E+02  0.0000E+00  0.0000E+00  0.0000E+00 -2.3160E-01  3.2220E+00  4.5000E+01
1.1531E+02  0.0000E+00  0.0000E+00  0.0000E+00 -4.6550E-01  3.0520E+00  4.6000E+01
1.1788E+02  0.0000E+00  0.0000E+00  0.0000E+00 -6.9930E-01  2.8810E+00  4.7000E+01
1.2044E+02  0.0000E+00  0.0000E+00  0.0000E+00 -9.3340E-01  2.7130E+00  4.8000E+01
1.2300E+02  0.0000E+00  0.0000E+00  0.0000E+00 -1.1680E+00  2.5450E+00  4.9000E+01
```

Figure D.7. Example input for AeroDyn's blade

E. Example input for ServoDyn

```
1 ------- SERVODYN v1.05.* INPUT FILE ------------------------------------------
2 Optimized+ NREL5 at 20 MW offshore baseline blade input properties.
3 ---------------------- SIMULATION CONTROL --------------------------------------
4 false         Echo         - Echo input data to <RootName>.ech (flag)
5 "default"     DT           - Communication interval for controllers (s) (or "default")
6 ---------------------- PITCH CONTROL -------------------------------------------
7           5   PCMode       - Pitch control mode {0: none, 3: user-defined from routine
  PitchCntrl, 4: user-defined from Simulink/Labview, 5: user-defined from Bladed-style
  DLL} (switch)
8           0   TPCOn        - Time to enable active pitch control (s) [unused when
  PCMode=0]
9      9999.9   TPitManS(1)  - Time to start override pitch maneuver for blade 1 and end
  standard pitch control (s)
10     9999.9   TPitManS(2)  - Time to start override pitch maneuver for blade 2 and end
  standard pitch control (s)
11     9999.9   TPitManS(3)  - Time to start override pitch maneuver for blade 3 and end
  standard pitch control (s) [unused for 2 blades]
12          1   PitManRat(1) - Pitch rate at which override pitch maneuver heads toward
  final pitch angle for blade 1 (deg/s)
13          1   PitManRat(2) - Pitch rate at which override pitch maneuver heads toward
  final pitch angle for blade 2 (deg/s)
14          1   PitManRat(3) - Pitch rate at which override pitch maneuver heads toward
  final pitch angle for blade 3 (deg/s) [unused for 2 blades]
15          0   BlPitchF(1)  - Blade 1 final pitch for pitch maneuvers (degrees)
16          0   BlPitchF(2)  - Blade 2 final pitch for pitch maneuvers (degrees)
17          0   BlPitchF(3)  - Blade 3 final pitch for pitch maneuvers (degrees) [unused
  for 2 blades]
18 ---------------------- GENERATOR AND TORQUE CONTROL ----------------------------
19          5   VSContrl     - Variable-speed control mode {0: none, 1: simple VS, 3:
  user-defined from routine UserVSCont, 4: user-defined from Simulink/Labview, 5: user-
  defined from Bladed-style DLL} (switch)
20          2   GenModel     - Generator model {1: simple, 2: Thevenin, 3: user-defined
  from routine UserGen} (switch) [used only when VSContrl=0]
21       94.4   GenEff       - Generator efficiency [ignored by the Thevenin and user-
  defined generator models] (%)
22 True         GenTiStr     - Method to start the generator {T: timed using TimGenOn,
  F: generator speed using SpdGenOn} (flag)
23 True         GenTiStp     - Method to stop the generator {T: timed using TimGenOf, F:
  when generator power = 0} (flag)
24     9999.9   SpdGenOn     - Generator speed to turn on the generator for a startup
  (HSS speed) (rpm) [used only when GenTiStr=False]
25          0   TimGenOn     - Time to turn on the generator for a startup (s) [used
  only when GenTiStr=True]
26     9999.9   TimGenOf     - Time to turn off the generator (s) [used only when
  GenTiStp=True]
27 ---------------------- SIMPLE VARIABLE-SPEED TORQUE CONTROL --------------------
28     9999.9   VS_RtGnSp    - Rated generator speed for simple variable-speed generator
  control (HSS side) (rpm) [used only when VSContrl=1]
29     9999.9   VS_RtTq      - Rated generator torque/constant generator torque in
  Region 3 for simple variable-speed generator control (HSS side) (N-m) [used only when
  VSContrl=1]
30     9999.9   VS_Rgn2K     - Generator torque constant in Region 2 for simple
  variable-speed generator control (HSS side) (N-m/rpm^2) [used only when VSContrl=1]
31     9999.9   VS_SlPc      - Rated generator slip percentage in Region 2 1/2 for
  simple variable-speed generator control (%) [used only when VSContrl=1]
32 ---------------------- SIMPLE INDUCTION GENERATOR ------------------------------
33     9999.9   SIG_SlPc     - Rated generator slip percentage (%) [used only when
  VSContrl=0 and GenModel=1]
34     9999.9   SIG_SySp     - Synchronous (zero-torque) generator speed (rpm) [used
  only when VSContrl=0 and GenModel=1]
35     9999.9   SIG_RtTq     - Rated torque (N-m) [used only when VSContrl=0 and
  GenModel=1]
36     9999.9   SIG_PORt     - Pull-out ratio (Tpullout/Trated) (-) [used only when
  VSContrl=0 and GenModel=1]
```

```
36      9999.9   SIG_PORt     - Pull-out ratio (Tpullout/Trated) (-) [used only when
  VSContrl=0 and GenModel=1]
37 ---------------------- THEVENIN-EQUIVALENT INDUCTION GENERATOR -----------------
38      9999.9   TEC_Freq     - Line frequency [50 or 60] (Hz) [used only when VSContrl=0
  and GenModel=2]
39       9998    TEC_NPol     - Number of poles [even integer > 0] (-) [used only when
  VSContrl=0 and GenModel=2]
40      9999.9   TEC_SRes     - Stator resistance (ohms) [used only when VSContrl=0 and
  GenModel=2]
41      9999.9   TEC_RRes     - Rotor resistance (ohms) [used only when VSContrl=0 and
  GenModel=2]
42      9999.9   TEC_VLL      - Line-to-line RMS voltage (volts) [used only when
  VSContrl=0 and GenModel=2]
43      9999.9   TEC_SLR      - Stator leakage reactance (ohms) [used only when
  VSContrl=0 and GenModel=2]
44      9999.9   TEC_RLR      - Rotor leakage reactance (ohms) [used only when VSContrl=0
  and GenModel=2]
45      9999.9   TEC_MR       - Magnetizing reactance (ohms) [used only when VSContrl=0
  and GenModel=2]
46 ---------------------- HIGH-SPEED SHAFT BRAKE ---------------------------------
47          0    HSSBrMode    - HSS brake model {0: none, 1: simple, 3: user-defined from
  routine UserHSSBr, 4: user-defined from Simulink/Labview, 5: user-defined from Bladed-
  style DLL} (switch)
48      9999.9   THSSBrDp     - Time to initiate deployment of the HSS brake (s)
49        0.6    HSSBrDT      - Time for HSS-brake to reach full deployment once
  initiated (sec) [used only when HSSBrMode=1]
50     28116.2   HSSBrTqF     - Fully deployed HSS-brake torque (N-m)
51 ---------------------- NACELLE-YAW CONTROL ------------------------------------
52          0    YCMode       - Yaw control mode {0: none, 3: user-defined from routine
  UserYawCont, 4: user-defined from Simulink/Labview, 5: user-defined from Bladed-style
  DLL} (switch)
53      9999.9   TYCOn        - Time to enable active yaw control (s) [unused when
  YCMode=0]
54          0    YawNeut      - Neutral yaw position--yaw spring force is zero at this
  yaw (degrees)
55 9.02832E+09   YawSpr       - Nacelle-yaw spring constant (N-m/rad)
56  1.916E+07    YawDamp      - Nacelle-yaw damping constant (N-m/(rad/s))
57      9999.9   TYawManS     - Time to start override yaw maneuver and end standard yaw
  control (s)
58          2    YawManRat    - Yaw maneuver rate (in absolute value) (deg/s)
59          0    NacYawF      - Final yaw angle for override yaw maneuvers (degrees)
60 ---------------------- TUNED MASS DAMPER --------------------------------------
61 False         CompNTMD     - Compute nacelle tuned mass damper {true/false} (flag)
62 "unused"      NTMDfile     - Name of the file for nacelle tuned mass damper (quoted
  string) [unused when CompNTMD is false]
63 False         CompTTMD     - Compute tower tuned mass damper {true/false} (flag)
64 "unused"      TTMDfile     - Name of the file for tower tuned mass damper (quoted
  string) [unused when CompTTMD is false]
65 ------------------ BLADED INTERFACE --------------- [used only with Bladed Interface]
66 "libdiscon.dll"    DLL_FileName - Name/location of the dynamic library {.dll [Windows]
  or .so [Linux]} in the Bladed-DLL format (-) [used only with Bladed Interface]
67 "DISCON.IN"    DLL_InFile   - Name of input file sent to the DLL (-) [used only with
  Bladed Interface]
68 "DISCON"      DLL_ProcName - Name of procedure in DLL to be called (-) [case
  sensitive; used only with DLL Interface]
69 "default"     DLL_DT       - Communication interval for dynamic library (s) (or
  "default") [used only with Bladed Interface]
70 false         DLL_Ramp     - Whether a linear ramp should be used between DLL_DT time
  steps [introduces time shift when true] (flag) [used only with Bladed Interface]
71      9999.9   BPCutoff     - Cuttoff frequency for low-pass filter on blade pitch from
  DLL (Hz) [used only with Bladed Interface]
72          0    NacYaw_North - Reference yaw angle of the nacelle when the upwind end
  points due North (deg) [used only with Bladed Interface]
73          0    Ptch_Cntrl   - Record 28: Use individual pitch control {0: collective
  pitch; 1: individual pitch control} (switch) [used only with Bladed Interface]
74          0    Ptch_SetPnt  - Record  5: Below-rated pitch angle set-point (deg) [used
  only with Bladed Interface]
```

```
75           0   Ptch_Min     - Record  6: Minimum pitch angle (deg) [used only with
  Bladed Interface]
76           0   Ptch_Max     - Record  7: Maximum pitch angle (deg) [used only with
  Bladed Interface]
77           0   PtchRate_Min - Record  8: Minimum pitch rate (most negative value
  allowed) (deg/s) [used only with Bladed Interface]
78           0   PtchRate_Max - Record  9: Maximum pitch rate  (deg/s) [used only with
  Bladed Interface]
79           0   Gain_OM      - Record 16: Optimal mode gain (Nm/(rad/s)^2) [used only
  with Bladed Interface]
80           0   GenSpd_MinOM - Record 17: Minimum generator speed (rpm) [used only with
  Bladed Interface]
81           0   GenSpd_MaxOM - Record 18: Optimal mode maximum speed (rpm) [used only
  with Bladed Interface]
82           0   GenSpd_Dem   - Record 19: Demanded generator speed above rated (rpm)
  [used only with Bladed Interface]
83           0   GenTrq_Dem   - Record 22: Demanded generator torque above rated (Nm)
  [used only with Bladed Interface]
84           0   GenPwr_Dem   - Record 13: Demanded power (W) [used only with Bladed
  Interface]
85 ---------------------- BLADED INTERFACE TORQUE-SPEED LOOK-UP TABLE -------------
86           0   DLL_NumTrq   - Record 26: No. of points in torque-speed look-up table {0
  = none and use the optimal mode parameters; nonzero = ignore the optimal mode
  PARAMETERs by setting Record 16 to 0.0} (-) [used only with Bladed Interface]
87  GenSpd_TLU   GenTrq_TLU
88   (rpm)          (Nm)
89 ---------------------- OUTPUT --------------------------------------------------
90 False          SumPrint     - Print summary data to <RootName>.sum (flag) (currently
  unused)
91           1   OutFile      - Switch to determine where output will be placed: {1: in
  module output file only; 2: in glue code output file only; 3: both} (currently unused)
92 True           TabDelim     - Use tab delimiters in text tabular output file? (flag)
  (currently unused)
93 "ES10.3E2"    OutFmt       - Format used for text tabular output (except time).
  Resulting field should be 10 characters. (quoted string) (currently unused)
94          30   TStart       - Time to begin tabular output (s) (currently unused)
95               OutList      - The next line(s) contains a list of output parameters.
  See OutListParameters.xlsx for a listing of available output channels, (-)
96 "GenPwr"                  - Electrical generator power and torque
97 "GenTq"                   - Electrical generator power and torque
98 END of input file (the word "END" must appear in the first 3 columns of this last
  OutList line)
99 ---------------------------------------------------------------------------------
```

Figure E.8. Example input for ServoDyn’s module

F. Example input for HydroDyn

```
1 ------- HydroDyn Input File ----------------------------------------------------
2 Optimized+ NREL5 at 20 MW offshore baseline blade input properties.
3 False            Echo           - Echo the input file data (flag)
4 ---------------------- ENVIRONMENTAL CONDITIONS --------------------------------
5           1025   WtrDens        - Water density (kg/m^3)
6            200   WtrDpth        - Water depth (meters)
7              0   MSL2SWL        - Offset between still-water level and mean sea level
  (meters) [positive upward; unused when WaveMod = 6; must be zero if PotMod=1 or 2]
8 ---------------------- WAVES ---------------------------------------------------
9              2   WaveMod        - Incident wave kinematics model {0: none=still
  water, 1: regular (periodic), 1P#: regular with user-specified phase, 2:
  JONSWAP/Pierson-Moskowitz spectrum (irregular), 3: White noise spectrum (irregular),
  4: user-defined spectrum from routine UserWaveSpctrm (irregular), 5: Externally
  generated wave-elevation time series, 6: Externally generated full wave-kinematics
  time series [option 6 is invalid for PotMod/=0]} (switch)
10             0   WaveStMod      - Model for stretching incident wave kinematics to
  instantaneous free surface {0: none=no stretching, 1: vertical stretching, 2:
  extrapolation stretching, 3: Wheeler stretching} (switch) [unused when WaveMod=0 or
  when PotMod/=0]
11          3630   WaveTMax       - Analysis time for incident wave calculations (sec)
  [unused when WaveMod=0; determines WaveDOmega=2Pi/WaveTMax in the IFFT]
12          0.20   WaveDT         - Time step for incident wave calculations     (sec)
  [unused when WaveMod=0; 0.1<=WaveDT<=1.0 recommended; determines
  WaveOmegaMax=Pi/WaveDT in the IFFT]
13             6   WaveHs         - Significant wave height of incident waves (meters)
  [used only when WaveMod=1, 2, or 3]
14            10   WaveTp         - Peak-spectral period of incident waves       (sec)
  [used only when WaveMod=1 or 2]
15 "DEFAULT"       WavePkShp      - Peak-shape parameter of incident wave spectrum (-)
  or DEFAULT (string) [used only when WaveMod=2; use 1.0 for Pierson-Moskowitz]
16             0   WvLowCOff      - Low  cut-off frequency or lower frequency limit of
  the wave spectrum beyond which the wave spectrum is zeroed (rad/s) [unused when
  WaveMod=0, 1, or 6]
17           500   WvHiCOff       - High cut-off frequency or upper frequency limit of
  the wave spectrum beyond which the wave spectrum is zeroed (rad/s) [unused when
  WaveMod=0, 1, or 6]
18             0   WaveDir        - Incident wave propagation heading direction
  (degrees) [unused when WaveMod=0 or 6]
19             0   WaveDirMod     - Directional spreading function {0: none, 1: COS2S}
  (-)       [only used when WaveMod=2,3, or 4]
20             1   WaveDirSpread  - Wave direction spreading coefficient ( > 0 )
  (-)       [only used when WaveMod=2,3, or 4 and WaveDirMod=1]
21             1   WaveNDir       - Number of wave directions
  (-)       [only used when WaveMod=2,3, or 4 and WaveDirMod=1; odd number only]
22             0   WaveDirRange   - Range of wave directions (full range: WaveDir +/-
  1/2*WaveDirRange) (degrees) [only used when WaveMod=2,3,or 4 and WaveDirMod=1]
23     123456789   WaveSeed(1)    - First  random seed of incident waves [-2147483648
  to 2147483647]    (-)       [unused when WaveMod=0, 5, or 6]
24         RANLUX   WaveSeed(2)    - Second random seed of incident waves [-2147483648
  to 2147483647] for intrinsic pRNG, or an alternative pRNG: "RanLux"    (-)
  [unused when WaveMod=0, 5, or 6]
25 FALSE           WaveNDAmp      - Flag for normally distributed amplitudes
  (flag)    [only used when WaveMod=2, 3, or 4]
26 ""              WvKinFile      - Root name of externally generated wave data file(s)
  (quoted string)    [used only when WaveMod=5 or 6]
27             1   NWaveElev      - Number of points where the incident wave elevations
  can be computed (-)       [maximum of 9 output locations]
28             0   WaveElevxi     - List of xi-coordinates for points where the
  incident wave elevations can be output (meters) [NWaveElev points, separated by
  commas or white space; usused if NWaveElev = 0]
29             0   WaveElevyi     - List of yi-coordinates for points where the
  incident wave elevations can be output (meters) [NWaveElev points, separated by
  commas or white space; usused if NWaveElev = 0]
```

```
30 -------------------- 2ND-ORDER WAVES ------------------- [unused with WaveMod=0 or 6]
31 False            WvDiffQTF      - Full difference-frequency 2nd-order wave kinematics
   (flag)
32 False            WvSumQTF       - Full summation-frequency  2nd-order wave kinematics
   (flag)
33             0   WvLowCOffD     - Low  frequency cutoff used in the difference-
   frequencies (rad/s) [Only used with a difference-frequency method]
34           3.5   WvHiCOffD      - High frequency cutoff used in the difference-
   frequencies (rad/s) [Only used with a difference-frequency method]
35           0.1   WvLowCOffS     - Low  frequency cutoff used in the summation-
   frequencies  (rad/s) [Only used with a summation-frequency  method]
36           3.5   WvHiCOffS      - High frequency cutoff used in the summation-
   frequencies  (rad/s) [Only used with a summation-frequency  method]
37 -------------------- CURRENT ------------------------------ [unused with WaveMod=6]
38             0   CurrMod        - Current profile model {0: none=no current, 1:
   standard, 2: user-defined from routine UserCurrent} (switch)
39             0   CurrSSV0       - Sub-surface current velocity at still water level
   (m/s) [used only when CurrMod=1]
40 "DEFAULT"        CurrSSDir      - Sub-surface current heading direction (degrees) or
   DEFAULT (string) [used only when CurrMod=1]
41            20   CurrNSRef      - Near-surface current reference depth
   (meters) [used only when CurrMod=1]
42             0   CurrNSV0       - Near-surface current velocity at still water level
   (m/s) [used only when CurrMod=1]
43             0   CurrNSDir      - Near-surface current heading direction
   (degrees) [used only when CurrMod=1]
44             0   CurrDIV        - Depth-independent current velocity
   (m/s) [used only when CurrMod=1]
45             0   CurrDIDir      - Depth-independent current heading direction
   (degrees) [used only when CurrMod=1]
46 --------------------- FLOATING PLATFORM -------------------- [unused with WaveMod=6]
47             1   PotMod         - Potential-flow model {0: none=no potential flow, 1:
   frequency-to-time-domain transforms based on WAMIT output, 2: fluid-impulse theory
   (FIT)} (switch)
48 "../../HydroData/Buoy20"    PotFile        - Root name of potential-flow model data;
   WAMIT output files containing the linear, nondimensionalized, hydrostatic restoring
   matrix (.hst), frequency-dependent hydrodynamic added mass matrix and damping matrix
   (.1), and frequency- and direction-dependent wave excitation force vector per unit
   wave amplitude (.3) (quoted string) [MAKE SURE THE FREQUENCIES INHERENT IN THESE
   WAMIT FILES SPAN THE PHYSICALLY-SIGNIFICANT RANGE OF FREQUENCIES FOR THE GIVEN
   PLATFORM; THEY MUST CONTAIN THE ZERO- AND INFINITE-FREQUENCY LIMITS!]
49             1   WAMITULEN      - Characteristic body length scale used to
   redimensionalize WAMIT output (meters) [only used when PotMod=1]
50    0.111336E+06 PtfmVol0       - Displaced volume of water when the platform is in
   its undisplaced position (m^3) [only used when PotMod=1; USE THE SAME VALUE COMPUTED
   BY WAMIT AS OUTPUT IN THE .OUT FILE!]
51             0   PtfmCOBxt      - The xt offset of the center of buoyancy (COB) from
   the platform reference point (meters)  [only used when PotMod=1]
52             0   PtfmCOByt      - The yt offset of the center of buoyancy (COB) from
   the platform reference point (meters)  [only used when PotMod=1]
53            1   ExctnMod       - Wave-excitation model {0: no wave-excitation
   calculation, 1: DFT, 2: state-space} (switch) [only used when PotMod=1; STATE-SPACE
   REQUIRES *.ssexctn INPUT FILE]
54             1   RdtnMod        - Radiation memory-effect model {0: no memory-effect
   calculation, 1: convolution, 2: state-space} (switch) [only used when PotMod=1;
   STATE-SPACE REQUIRES *.ss INPUT FILE]
55            60   RdtnTMax       - Analysis time for wave radiation kernel
   calculations (sec) [only used when PotMod=1; determines RdtnDOmega=Pi/RdtnTMax in the
   cosine transform; MAKE SURE THIS IS LONG ENOUGH FOR THE RADIATION IMPULSE RESPONSE
   FUNCTIONS TO DECAY TO NEAR-ZERO FOR THE GIVEN PLATFORM!]
56 "DEFAULT"        RdtnDT         - Time step for wave radiation kernel calculations
   (sec) [only used when PotMod=1; DT<=RdtnDT<=0.1 recommended; determines
   RdtnOmegaMax=Pi/RdtnDT in the cosine transform]
57 ---------------------- 2ND-ORDER FLOATING PLATFORM FORCES ----------------------
58             0   MnDrift        - Mean-drift 2nd-order forces computed
   {0: None; [7, 8, 9, 10, 11, or 12]: WAMIT file to use} [Only one of MnDrift,
   NewmanApp, or DiffQTF can be non-zero]
```

```
59             0   NewmanApp      - Mean- and slow-drift 2nd-order forces computed with
  Newman's approximation {0: None; [7, 8, 9, 10, 11, or 12]: WAMIT file to use} [Only
  one of MnDrift, NewmanApp, or DiffQTF can be non-zero. Used only when WaveDirMod=0]
60             0   DiffQTF        - Full difference-frequency 2nd-order forces computed
  with full QTF          {0: None; [10, 11, or 12]: WAMIT file to use}          [Only
  one of MnDrift, NewmanApp, or DiffQTF can be non-zero]
61             0   SumQTF         - Full summation -frequency 2nd-order forces computed
  with full QTF          {0: None; [10, 11, or 12]: WAMIT file to use}
62 ------------ FLOATING PLATFORM FORCE FLAGS  ---------------- [unused with WaveMod=6]
63 True             PtfmSgF        - Platform horizontal surge translation force (flag)
  or DEFAULT
64 True             PtfmSwF        - Platform horizontal sway translation force (flag)
  or DEFAULT
65 True             PtfmHvF        - Platform vertical heave translation force (flag) or
  DEFAULT
66 True             PtfmRF         - Platform roll tilt rotation force (flag) or DEFAULT
67 True             PtfmPF         - Platform pitch tilt rotation force (flag) or
  DEFAULT
68 True             PtfmYF         - Platform yaw rotation force (flag) or DEFAULT
69 ---------------------- PLATFORM ADDITIONAL STIFFNESS AND DAMPING  --------------
70             0             0             0             0             0             0
  AddF0    - Additional preload (N, N-m)
71             0             0             0             0             0             0
  AddCLin  - Additional linear stiffness (N/m, N/rad, N-m/m, N-m/rad)
72             0             0             0             0             0             0
73             0             0             0             0             0             0
74   0.00000E+00   0.00000E+00   0.00000E+00   2.32208E+10   0.00000E+00   0.00000E+00
75   0.00000E+00   0.00000E+00   0.00000E+00   0.00000E+00   2.32208E+10   0.00000E+00
76             0             0             0             0             0             0
77             0             0             0             0             0             0
  AddBLin  - Additional linear damping(N/(m/s), N/(rad/s), N-m/(m/s), N-m/(rad/s))
78             0             0             0             0             0             0
79             0             0             0             0             0             0
80             0             0             0             0             0             0
81             0             0             0             0             0             0
82             0             0             0             0             0             0
83             0             0             0             0             0             0
  AddBQuad - Additional quadratic drag(N/(m/s)^2, N/(rad/s)^2, N-m(m/s)^2, N-
  m/(rad/s)^2)
84             0             0             0             0             0             0
85             0             0             0             0             0             0
86             0             0             0             0             0             0
87             0             0             0             0             0             0
88             0             0             0             0             0             0
89 ---------------------- AXIAL COEFFICIENTS -------------------------------------
90             2   NAxCoef        - Number of axial coefficients (-)
91 AxCoefID  AxCd     AxCa     AxCp
92    (-)    (-)      (-)      (-)
93     1     0.00     0.00     1.00
94     2     9.60     0.00     1.00
95 ---------------------- MEMBER JOINTS ------------------------------------------
96 44   NJoints  - Number of joints (-)   [must be exactly 0 or at least 2]
97 JointID   Jointxi Jointyi Jointzi  JointAxID   JointOvrlp   [JointOvrlp= 0: do
  nothing at joint, 1: eliminate overlaps by calculating super member]
98    (-) (m)  (m)  (m)  (-)  (switch)
99    0.10000E+01   0.00000E+00   0.00000E+00  -0.40000E+02   0.10000E+01   0.00000E+00
100   0.20000E+01   0.00000E+00   0.00000E+00   0.20000E+02   0.10000E+01   0.00000E+00
101   0.30000E+01   0.28839E+02   0.50000E+02  -0.28000E+02   0.10000E+01   0.00000E+00
102   0.40000E+01   0.28839E+02   0.50000E+02   0.24000E+02   0.10000E+01   0.00000E+00
103   0.50000E+01  -0.57721E+02  -0.00000E+00  -0.28000E+02   0.10000E+01   0.00000E+00
104   0.60000E+01  -0.57721E+02  -0.00000E+00   0.24000E+02   0.10000E+01   0.00000E+00
105   0.70000E+01   0.28839E+02  -0.50000E+02  -0.28000E+02   0.10000E+01   0.00000E+00
106   0.80000E+01   0.28839E+02  -0.50000E+02   0.24000E+02   0.10000E+01   0.00000E+00
107   0.90000E+01   0.28839E+02   0.50000E+02  -0.40000E+02   0.20000E+01   0.00000E+00
108   0.10000E+02  -0.57721E+02  -0.00000E+00  -0.40000E+02   0.20000E+01   0.00000E+00
109   0.11000E+02   0.28839E+02  -0.50000E+02  -0.40000E+02   0.20000E+01   0.00000E+00
110   0.12000E+02   0.18448E+02   0.43998E+02   0.20000E+02   0.10000E+01   0.00000E+00
```

```
111    0.13000E+02  -0.47330E+02   0.59292E+01   0.20000E+02   0.10000E+01   0.00000E+00
112    0.14000E+02  -0.47330E+02  -0.60752E+01   0.20000E+02   0.10000E+01   0.00000E+00
113    0.15000E+02   0.18448E+02  -0.43998E+02   0.20000E+02   0.10000E+01   0.00000E+00
114    0.16000E+02   0.28847E+02  -0.38000E+02   0.20000E+02   0.10000E+01   0.00000E+00
115    0.17000E+02   0.28847E+02   0.38000E+02   0.20000E+02   0.10000E+01   0.00000E+00
116    0.18000E+02   0.80573E+01   0.37996E+02  -0.34000E+02   0.10000E+01   0.00000E+00
117    0.19000E+02  -0.36939E+02   0.11931E+02  -0.34000E+02   0.10000E+01   0.00000E+00
118    0.20000E+02  -0.36939E+02  -0.12077E+02  -0.34000E+02   0.10000E+01   0.00000E+00
119    0.21000E+02   0.80573E+01  -0.37996E+02  -0.34000E+02   0.10000E+01   0.00000E+00
120    0.22000E+02   0.28855E+02  -0.26000E+02  -0.34000E+02   0.10000E+01   0.00000E+00
121    0.23000E+02   0.28855E+02   0.26000E+02  -0.34000E+02   0.10000E+01   0.00000E+00
122    0.24000E+02   0.32476E+01   0.56305E+01   0.20000E+02   0.10000E+01   0.00000E+00
123    0.25000E+02   0.22844E+02   0.39605E+02   0.20000E+02   0.10000E+01   0.00000E+00
124    0.26000E+02  -0.65000E+01  -0.00000E+00   0.20000E+02   0.10000E+01   0.00000E+00
125    0.27000E+02  -0.45721E+02  -0.00000E+00   0.20000E+02   0.10000E+01   0.00000E+00
126    0.28000E+02   0.32476E+01  -0.56305E+01   0.20000E+02   0.10000E+01   0.00000E+00
127    0.29000E+02   0.22844E+02  -0.39605E+02   0.20000E+02   0.10000E+01   0.00000E+00
128    0.30000E+02   0.32476E+01   0.56305E+01  -0.34000E+02   0.10000E+01   0.00000E+00
129    0.31000E+02   0.16848E+02   0.29210E+02  -0.34000E+02   0.10000E+01   0.00000E+00
130    0.32000E+02  -0.65000E+01  -0.00000E+00  -0.34000E+02   0.10000E+01   0.00000E+00
131    0.33000E+02  -0.33721E+02  -0.00000E+00  -0.34000E+02   0.10000E+01   0.00000E+00
132    0.34000E+02   0.32476E+01  -0.56305E+01  -0.34000E+02   0.10000E+01   0.00000E+00
133    0.35000E+02   0.16848E+02  -0.29210E+02  -0.34000E+02   0.10000E+01   0.00000E+00
134    0.36000E+02   0.32476E+01   0.56305E+01  -0.32400E+02   0.10000E+01   0.00000E+00
135    0.37000E+02   0.22844E+02   0.39605E+02   0.18260E+02   0.10000E+01   0.00000E+00
136    0.38000E+02  -0.65000E+01  -0.00000E+00  -0.32400E+02   0.10000E+01   0.00000E+00
137    0.39000E+02  -0.45721E+02  -0.00000E+00   0.18260E+02   0.10000E+01   0.00000E+00
138    0.40000E+02   0.32476E+01  -0.56305E+01  -0.32400E+02   0.10000E+01   0.00000E+00
139    0.41000E+02   0.22844E+02  -0.39605E+02   0.18260E+02   0.10000E+01   0.00000E+00
140    0.42000E+02   0.28839E+02   0.50000E+02  -0.39880E+02   0.10000E+01   0.00000E+00
141    0.43000E+02  -0.57721E+02  -0.00000E+00  -0.39880E+02   0.10000E+01   0.00000E+00
142    0.44000E+02   0.28839E+02  -0.50000E+02  -0.39880E+02   0.10000E+01   0.00000E+00
143 ---------------------- MEMBER CROSS-SECTION PROPERTIES -------------------------
144  4   NPropSets  - Number of member property sets (-)
145 PropSetID   PropD  PropThck
146    (-)        (m)    (m)
147  1.0   0.130E+02   0.600E-01   !
148  2.0   0.240E+02   0.120E+00   !
149  3.0   0.480E+02   0.120E+00   !
150  4.0   0.320E+01   0.350E-01   !
151 ---------------------- SIMPLE HYDRODYNAMIC COEFFICIENTS (model 1) --------------
152 SimplCd   SimplCdMG   SimplCa   SimplCaMG   SimplCp   SimplCpMG   SimplAxCd
    SimplAxCdMG   SimplAxCa   SimplAxCaMG   SimplAxCp   SimplAxCpMG
153 (-)   (-)   (-)   (-)   (-)   (-)   (-)   (-)   (-)   (-)   (-)   (-)
154 0.00  0.00  0.00  0.00  1.00  1.00  0.00  0.00  0.00  0.00  1.00  1.00
155 ---------------------- DEPTH-BASED HYDRODYNAMIC COEFFICIENTS (model 2) ---------
156  0   NCoefDpth  - Number of depth-dependent coefficients (-)
157 Dpth  DpthCd   DpthCdMG   DpthCa   DpthCaMG  DpthCp   DpthCpMG   DpthAxCd
    DpthAxCdMG   DpthAxCa   DpthAxCaMG   DpthAxCp   DpthAxCpMG
158 (m)   (-)    (-)    (-)    (-)    (-)    (-)    (-)    (-)    (-)    (-)    (-)
159 ---------------------- MEMBER-BASED HYDRODYNAMIC COEFFICIENTS (model 3) --------
160 25   NCoefMembers  - Number of member-based coefficients (-)
161 MemberIDMemberCd1 MemberCd2MemberCdMG1   MemberCdMG2MemberCa1 MemberCa2MemberCaMG1
    MemberCaMG2MemberCp1 MemberCp2MemberCpMG1   MemberCpMG2   MemberAxCd1   MemberAxCd2
    MemberAxCdMG1 MemberAxCdMG2  MemberAxCa1   MemberAxCa2  MemberAxCaMG1 MemberAxCaMG2
    MemberAxCp1  MemberAxCp2   MemberAxCpMG1   MemberAxCpMG2
162 (-)    (-)    (-)    (-)    (-)    (-)  (-)    (-)    (-)    (-)    (-)    (-)    (-)    (-)
    (-)    (-)    (-)    (-)    (-)    (-)    (-)    (-)    (-)    (-)    (-)
163 1  0.56  0.56  0.00  0.00  0.00  0.00  0.00  0.00  0.00  0.00  0.00  0.00  0.00  0.00
    0.00  0.00  0.00  0.00  0.00  0.00  0.00  0.00  0.00  0.00  ! Main Column
164 2  0.61  0.61  0.00  0.00  0.00  0.00  0.00  0.00  0.00  0.00  0.00  0.00  0.00  0.00
    0.00  0.00  0.00  0.00  0.00  0.00  0.00  0.00  0.00  0.00  ! Upper Column 1
165 3  0.61  0.61  0.00  0.00  0.00  0.00  0.00  0.00  0.00  0.00  0.00  0.00  0.00  0.00
    0.00  0.00  0.00  0.00  0.00  0.00  0.00  0.00  0.00  0.00  ! Upper Column 2
166 4  0.61  0.61  0.00  0.00  0.00  0.00  0.00  0.00  0.00  0.00  0.00  0.00  0.00  0.00
    0.00  0.00  0.00  0.00  0.00  0.00  0.00  0.00  0.00  0.00  ! Upper Column 3
```

```
5  0.68  0.68  0.00  0.00  0.00  0.00  0.00  0.00  0.00  0.00  0.00  0.00  0.00  0.00
   0.00  0.00  0.00  0.00  0.00  0.00  0.00  0.00  0.00  0.00  ! Base Column 1
6  0.68  0.68  0.00  0.00  0.00  0.00  0.00  0.00  0.00  0.00  0.00  0.00  0.00  0.00
   0.00  0.00  0.00  0.00  0.00  0.00  0.00  0.00  0.00  0.00  ! Base Column 2
7  0.68  0.68  0.00  0.00  0.00  0.00  0.00  0.00  0.00  0.00  0.00  0.00  0.00  0.00
   0.00  0.00  0.00  0.00  0.00  0.00  0.00  0.00  0.00  0.00  ! Base Column 3
23  0.68  0.68  0.00  0.00  0.00  0.00  0.00  0.00  0.00  0.00  0.00  0.00  0.00  0.00
   0.00  0.00  0.00  0.00  0.00  0.00  0.00  0.00  0.00  0.00  0.00  ! Base column cap 1
24  0.68  0.68  0.00  0.00  0.00  0.00  0.00  0.00  0.00  0.00  0.00  0.00  0.00  0.00
   0.00  0.00  0.00  0.00  0.00  0.00  0.00  0.00  0.00  0.00  0.00  ! Base column cap 2
25  0.68  0.68  0.00  0.00  0.00  0.00  0.00  0.00  0.00  0.00  0.00  0.00  0.00  0.00
   0.00  0.00  0.00  0.00  0.00  0.00  0.00  0.00  0.00  0.00  0.00  ! Base column cap 3
8  0.63  0.63  0.00  0.00  0.00  0.00  0.00  0.00  0.00  0.00  0.00  0.00  0.00  0.00
   0.00  0.00  0.00  0.00  0.00  0.00  0.00  0.00  0.00  0.00  ! Delta Pontoon, Upper 1
9  0.63  0.63  0.00  0.00  0.00  0.00  0.00  0.00  0.00  0.00  0.00  0.00  0.00  0.00
   0.00  0.00  0.00  0.00  0.00  0.00  0.00  0.00  0.00  0.00  ! Delta Pontoon, Upper 2
10  0.63  0.63  0.00  0.00  0.00  0.00  0.00  0.00  0.00  0.00  0.00  0.00  0.00
   0.00  0.00  0.00  0.00  0.00  0.00  0.00  0.00  0.00  0.00  0.00  ! Delta Pontoon,
   Upper 3
11  0.63  0.63  0.00  0.00  0.00  0.00  0.00  0.00  0.00  0.00  0.00  0.00  0.00
   0.00  0.00  0.00  0.00  0.00  0.00  0.00  0.00  0.00  0.00  0.00  ! Delta Pontoon,
   Lower 1
12  0.63  0.63  0.00  0.00  0.00  0.00  0.00  0.00  0.00  0.00  0.00  0.00  0.00
   0.00  0.00  0.00  0.00  0.00  0.00  0.00  0.00  0.00  0.00  0.00  ! Delta Pontoon,
   Lower 2
13  0.63  0.63  0.00  0.00  0.00  0.00  0.00  0.00  0.00  0.00  0.00  0.00  0.00
   0.00  0.00  0.00  0.00  0.00  0.00  0.00  0.00  0.00  0.00  0.00  ! Delta Pontoon,
   Lower 3
14  0.63  0.63  0.00  0.00  0.00  0.00  0.00  0.00  0.00  0.00  0.00  0.00  0.00  0.00
   0.00  0.00  0.00  0.00  0.00  0.00  0.00  0.00  0.00  0.00  0.00 ! Y Pontoon, Upper 1
15  0.63  0.63  0.00  0.00  0.00  0.00  0.00  0.00  0.00  0.00  0.00  0.00  0.00  0.00
   0.00  0.00  0.00  0.00  0.00  0.00  0.00  0.00  0.00  0.00  0.00 ! Y Pontoon, Upper 2
16  0.63  0.63  0.00  0.00  0.00  0.00  0.00  0.00  0.00  0.00  .00  0.00  0.00  0.00
   0.00  0.00  0.00  0.00  0.00  0.00  0.00  0.00  0.00  0.00  ! Y Pontoon, Upper 3
17  0.63  0.63  0.00  0.00  0.00  0.00  0.00  0.00  0.00  0.00  0.00  0.00  0.00  0.00
   0.00  0.00  0.00  0.00  0.00  0.00  0.00  0.00  0.00  0.00  0.00 ! Y Pontoon, Lower 1
18  0.63  0.63  0.00  0.00  0.00  0.00  0.00  0.00  0.00  0.00  0.00  0.00  0.00  0.00
   0.00  0.00  0.00  0.00  0.00  0.00  0.00  0.00  0.00  0.00  0.00 ! Y Pontoon, Lower 2
19  0.63  0.63  0.00  0.00  0.00  0.00  0.00  0.00  0.00  0.00  0.00  0.00  0.00  0.00
   0.00  0.00  0.00  0.00  0.00  0.00  0.00  0.00  0.00  0.00  0.00 ! Y Pontoon, Lower 3
20  0.63  0.63  0.00  0.00  0.00  0.00  0.00  0.00  0.00  0.00  0.00  0.00  0.00  0.00
   0.00  0.00  0.00  0.00  0.00  0.00  0.00  0.00  0.00  0.00  0.00  ! Cross Brace 1
21  0.63  0.63  0.00  0.00  0.00  0.00  0.00  0.00  0.00  0.00  0.00  0.00  0.00  0.00
   0.00  0.00  0.00  0.00  0.00  0.00  0.00  0.00  0.00  0.00  0.00  ! Cross Brace 2
22  0.63  0.63  0.00  0.00  0.00  0.00  0.00  0.00  0.00  0.00  0.00  0.00  0.00  0.00
   0.00  0.00  0.00  0.00  0.00  0.00  0.00  0.00  0.00  0.00  0.00  ! Cross Brace 3
---------------------- MEMBERS -----------------------------------------------------
     25   NMembers  - Number of members (-)
MemberID  MJointID1  MJointID2  MPropSetID1  MPropSetID2  MDivSize   MCoefMod
   PropPot   [MCoefMod=1: use simple coeff table, 2: use depth-based coeff table, 3: use
   member-based coeff table] [ PropPot/=0 if member is modeled with potential-flow
   theory]
  (-)  (-)  (-)  (-)  (-)  (m)  (switch)   (flag)
    1   1   2    11  1.0000  3  TRUE   ! Main Column
    2   3   4    22  1.0000  3  TRUE   ! Upper Column 1
    3   5   6    22  1.0000  3  TRUE   ! Upper Column 2
    4   7   8    22  1.0000  3  TRUE   ! Upper Column 3
    5   42  3    33  1.0000  3  TRUE   ! Base Column 1
    6   43  5    33  1.0000  3  TRUE   ! Base Column 2
    7   44  7    33  1.0000  3  TRUE   ! Base Column 3
    23  9   42   33  1.0000  3  TRUE   ! Base column cap 1
    24  10  43   33  1.0000  3  TRUE   ! Base column cap 2
    25  11  44   33  1.0000  3  TRUE   ! Base column cap 3
    8   12  13   44  1.0000  3  TRUE   ! Delta Pontoon, Upper 1
    9   14  15   44  1.0000  3  TRUE   ! Delta Pontoon, Upper 2
    10  16  17   44  1.0000  3  TRUE   ! Delta Pontoon, Upper 3
    11  18  19   44  1.0000  3  TRUE   ! Delta Pontoon, Lower 1
```

```
206    12  20  21   44  1.0000  3  TRUE   ! Delta Pontoon, Lower 2
207    13  22  23   44  1.0000  3  TRUE   ! Delta Pontoon, Lower 3
208    14  24  25   44  1.0000  3  TRUE   ! Y Pontoon, Upper 1
209    15  26  27   44  1.0000  3  TRUE   ! Y Pontoon, Upper 2
210    16  28  29   44  1.0000  3  TRUE   ! Y Pontoon, Upper 3
211    17  30  31   44  1.0000  3  TRUE   ! Y Pontoon, Lower 1
212    18  32  33   44  1.0000  3  TRUE   ! Y Pontoon, Lower 2
213    19  34  35   44  1.0000  3  TRUE   ! Y Pontoon, Lower 3
214    20  36  37   44  1.0000  3  TRUE   ! Cross Brace 1
215    21  38  39   44  1.0000  3  TRUE   ! Cross Brace 2
216    22  40  41   44  1.0000  3  TRUE   ! Cross Brace 3
217 ---------------------- FILLED MEMBERS --------------------------------------
218    2   NFillGroups - Number of filled member groups (-) [If FillDens = DEFAULT, then
    FillDens = WtrDens; FillFSLoc is related to MSL2SWL]
219 FillNumM FillMList FillFSLoc FillDens
220 (-)   (-)(m)    (kg/m^3)
221  3.0 2.0 3.0 4.0  -0.12340E+02   0.10250E+04
222  3.0 5.0 6.0 7.0  -0.29780E+02   0.10250E+04
223 ---------------------- MARINE GROWTH ---------------------------------------
224  0   NMGDepths  - Number of marine-growth depths specified (-)
225 MGDpth MGThck  MGDens
226 (m)   (m)   (kg/m^3)
227 ---------------------- MEMBER OUTPUT LIST ----------------------------------
228  0   NMOutputs  - Number of member outputs (-) [must be < 10]
229 MemberID   NOutLocNodeLocs [NOutLoc < 10; node locations are normalized distance from
    the start of the member, and must be >=0 and <= 1] [unused if NMOutputs=0]
230   (-)   (-)   (-)
231 ---------------------- JOINT OUTPUT LIST -----------------------------------
232  0   NJOutputs  - Number of joint outputs [Must be < 10]
233  0   JOutLst  - List of JointIDs which are to be output (-)[unused if NJOutputs=0]
234 ---------------------- OUTPUT ----------------------------------------------
235 False HDSum  - Output a summary file [flag]
236 False        OutAll  - Output all user-specified member and joint loads (only at each
    member end, not interior locations) [flag]
237     2        OutSwtch  - Output requested channels to: [1=Hydrodyn.out,
    2=GlueCode.out, 3=both files]
238 "E15.7e2"    OutFmt  - Output format for numerical results (quoted string) [not
    checked for validity!]
239 "A11"OutSFmt  - Output format for header strings (quoted string) [not checked for
    validity!]
240 ---------------------- OUTPUT CHANNELS -------------------------------------
241 "Wave1Elev"  - Wave elevation at the platform reference point (0,  0)
242 END of output channels and end of file. (the word "END" must appear in the first 3
    columns of this line)
```

Figure F.9. Example input for HydroDyn's module

G. Example input for MAP++

```
1 ---------------------- LINE DICTIONARY ---------------------------------------
2 LineType     Diam     MassDenInAir    EA         CB   CIntDamp  Ca   Cdn  Cdt
3 (-)          (m)      (kg/m)          (N)        (-)    (Pa-s)    (-)  (-)  (-)
4 Material     0.0766    113.35      7.536E8       1.0    0          0    0    0
5 ---------------------- NODE PROPERTIES ---------------------------------------
6 Node Type       X        Y        Z     M     B     FX    FY    FZ
7 (-)  (-)       (m)      (m)      (m)   (kg)  (m^3)  (N)   (N)   (N)
8 1    fix    441.193    764.913   depth   0     0     #     #     #
9 2    Vessel  40.8605  70.7725    -28.0   0     0     #     #     #
10 ---------------------- LINE PROPERTIES ---------------------------------------
11 Line   LineType  UnstrLen    NodeAnch  NodeFair  Flags
12 (-)      (-)       (m)         (-)       (-)       (-)
13 1       Material   835.3500     1       2       tension_fair tension_anch
14 ---------------------- SOLVER OPTIONS-----------------------------------------
15 Option
16 (-)
17 repeat 240 120
18 ref_position 0 0 0
```

Figure G.10. Example input for MAP++ module

H. Example input for HAMS

```
9.807
1025
.\20_Symmetric.gdf
0       0       -26.92
0       0       0

The format is as below:
gravity acceleration
sea water density
mesh file name (gdf format)
Centre of gravity
Centre of rotation
```

Figure H.11. Example input HAMS' WAMIT_MeshTran

```
 Center of Gravity:
  0.000000000000000E+000  0.000000000000000E+000  0.000000000000000E+000
 Body Mass Matrix:
   0.11309E+09   0.00000E+00   0.00000E+00   0.00000E+00  -0.30445E+10   0.00000E+00
   0.00000E+00   0.11309E+09   0.00000E+00   0.30445E+10   0.00000E+00   0.00000E+00
   0.00000E+00   0.00000E+00   0.11309E+09   0.00000E+00   0.00000E+00   0.00000E+00
   0.00000E+00   0.30445E+10   0.00000E+00   0.27355E+12  -0.69344E+08   0.15074E+09
  -0.30445E+10   0.00000E+00   0.00000E+00  -0.69344E+08   0.27353E+12  -0.19117E+08
   0.00000E+00   0.00000E+00   0.00000E+00   0.15074E+09  -0.19117E+08   0.34245E+12
 External Linear Damping Matrix:
   0.00000E+00   0.00000E+00   0.00000E+00   0.00000E+00   0.00000E+00   0.00000E+00
   0.00000E+00   0.00000E+00   0.00000E+00   0.00000E+00   0.00000E+00   0.00000E+00
   0.00000E+00   0.00000E+00   0.00000E+00   0.00000E+00   0.00000E+00   0.00000E+00
   0.00000E+00   0.00000E+00   0.00000E+00   0.00000E+00   0.00000E+00   0.00000E+00
   0.00000E+00   0.00000E+00   0.00000E+00   0.00000E+00   0.00000E+00   0.00000E+00
   0.00000E+00   0.00000E+00   0.00000E+00   0.00000E+00   0.00000E+00   0.00000E+00
 External Quadratic Damping Matrix:
   3.95000E+05   0.00000E+00   0.00000E+00   0.00000E+00   0.00000E+00   0.00000E+00
   0.00000E+00   3.95000E+05   0.00000E+00   0.00000E+00   0.00000E+00   0.00000E+00
   0.00000E+00   0.00000E+00   3.88000E+06   0.00000E+00   0.00000E+00   0.00000E+00
   0.00000E+00   0.00000E+00   0.00000E+00   3.70000E+10   0.00000E+00   0.00000E+00
   0.00000E+00   0.00000E+00   0.00000E+00   0.00000E+00   3.70000E+10   0.00000E+00
   0.00000E+00   0.00000E+00   0.00000E+00   0.00000E+00   0.00000E+00   4.08000E+09
 Hydrostatic Restoring Matrix:
   0.00000E+00   0.00000E+00   0.00000E+00   0.00000E+00   0.00000E+00   0.00000E+00
   0.00000E+00   0.00000E+00   0.00000E+00   0.00000E+00   0.00000E+00   0.00000E+00
   0.00000E+00   0.00000E+00   1.53440E+07   0.00000E+00   0.00000E+00   0.00000E+00
   0.00000E+00   0.00000E+00   0.00000E+00  -6.04160E+09   0.00000E+00   0.00000E+00
   0.00000E+00   0.00000E+00   0.00000E+00   0.00000E+00  -6.04160E+09   0.00000E+00
   0.00000E+00   0.00000E+00   0.00000E+00   0.00000E+00   0.00000E+00   0.00000E+00
 External Restoring Matrix:
   8.00e+04      5.99e-02      4.02e-02      8.91e+02     -3.23e+05     -3.19e-01
   5.45e-01      8.00e+04     -4.29e-02      3.23e+05      8.86e+02     -2.30e+00
   4.42e-02      4.59e-01      1.98e+04      1.42e+00     -5.53e-01     -1.78e+03
   8.89e+02      3.27e+05     -2.15e-01      1.86e+08      5.26e+04      1.06e+01
  -3.27e+05      8.87e+02     -8.17e-01     -5.28e+04      1.86e+08      1.00e+02
  -3.47e-01     -2.30e+00     -1.78e+03     -9.20e+01      4.31e+01      2.50e+08
```

Figure H.12. Example input HAMS' Hydrostatic

```
1    --------------HAMS Control file---------------
2
3    Waterdepth  -200.D0
4
5    #Start Definition of Wave Frequencies
6     0_inf_frequency_limits      1       # 0: not to include; 1: to include
7     Input_frequency_type        2
8     Output_frequency_type       2
9     Number_of_frequencies      -3
10    Minimum_frequency_Wmin    0.5D0
11    Frequency_step            0.5D0
12   #End Definition of Wave Frequencies
13
14   #Start Definition of Wave Headings
15    Number_of_headings         -19
16    Minimum_heading           0.D0
17    Heading_step             10.D0
18   #End Definition of Wave Headings
19
20    Reference_body_center   0.000   0.000   0.000
21    Reference_body_length   1.D0
22    Wave_diffrac_solution    2
23    If_remove_irr_freq       1
24    Number of threads       16
25
26   #Start Definition of Pressure and/or Elevation (PE)
27    Number_of_field_points     6       # number of field points where to calculate PE
28    150.000   150.000  0.000    Global_coords_point_1
29    175.000   175.000  0.000    Global_coords_point_2
30    200.000   200.000  0.000     Global_coords_point_3
31    150.000  -150.000  0.000    Global_coords_point_4
32    175.000  -175.000  0.000    Global_coords_point_5
33    200.000  -200.000  0.000     Global_coords_point_6
34   #End Definition of Pressure and/or Elevation
35
36   ----------End HAMS Control file---------------
37
38
39   Input_frequency_type options:
40   1--deepwater wave number; 2--finite-depth wave number; 3--wave frequency; 4--wave
  period; 5--wave length
41   Output_frequency_type options: same as Input_frequency_type options
```

Figure H.13. Example input HAMS' ControlFile

I. Example input for Co-Blade

```
 1 -----  Input File  ------------------------------------------------------------
 2 Optimized+ NREL5 at 20 MW offshore baseline blade input properties.
 3 This line is for user comments.
 4 ----   Development Settings  ---------------------------------------------------
 5 0               DEBUG_LVL       Controls the level of output from Co-Blade (0 for no
   debug messages, 1 and greater for more debugging messages and figures)
 6 100              RAND_SEED       A positive integer that seeds all random number
   generators.
 7 -----  Analysis Options  -------------------------------------------------------
 8 true            SELF_WEIGHT:    Include self-weight as a body force? (choose true or
   false)
 9 false           BUOYANCY:       Include buoyancy as a body force? (choose true or
   false)
10 true            CENTRIF:        Include centrifugal force as a body force? (choose
   true or false)
11 true            DISP_CF:        Apply correction factors to the beam displacements?
   (choose true or false)
12 0               N_MODES:        Number of modes to be computed
13 100             N_ELEMS:        Number of blade finite elements to be used in the
   modal analysis
14 false           VARY_MAT_PROPS: Perform Monte Carlo analysis with uncertain material
   properties?
15 100             SAMPLE_SIZE:    Sample size for Monte Carlo analysis
16 0.10            MAT_COV:        Coefficient of variation (cov = std/mean) for
   uncertain material properties
17 -----  Optimization  -----------------------------------------------------------
18 true            OPTIMIZE:       Perform optimization of composite layup?
19 PS              OPT_METHOD:     Optimization algorithm for the optimization of
   composite layup (choose 'PS', 'GS', 'GA', or 'PSO')
20 true          OPT_PITAXIS:    Optimize the pitch axis?
21 0.375           PITAXIS_VAL:    Pitch axis value outboard of max chord (ignored if
   OPT_PITAXIS = false)
22 1               INB_STN:        Inboard station where the leading and trailing edge
   panels, spar caps, and shear webs begin
23 7               TRAN_STN:       Station where the root transition ends
24 49              OUB_STN:        Outboard station where the leading and trailing edge
   panels, spar caps, and shear webs end
25 14               NUM_CP:         Number of control points between INB_STN and OUB_STN
26 false           READ_INITX:     Read the initial values for the design variables from
   INITX_FILE?
27 none            INITX_FILE:     Input file for the intitial values of the design
   variables.
28 false           WRITE_STR:      Write structural input files at each function
   evaluation? (recommended to set = false, unless for debugging purposes)
29 false           WRITE_F_ALL:    Write the fitness value and penalty factors at each
   function evaluation? (recommended to set = false, unless for debugging purposes)
30 false           WRITE_X_ALL:    Write the design variables at each function
   evaluation? (recommended to set = false, unless for debugging purposes)
31 false           WRITE_X_ITER:   Write the design variables at each iteration?
   (recommended to set = false, unless for debugging purposes)
32 -----  Constraints  ------------------------------------------------------------
33 10.0            MAX_TIP_D:      Maximum allowable tip deflection (m) (deflection in
   the x-direction of global coord. system)
34 1             MIN_FREQ_SEP:   Minimum allowable difference between the blade
   rotation frequency and blade natural frequencies (Hz)
35 -----  Environmental Data  -----------------------------------------------------
36 1.225           FLUID_DEN:      Fluid density (kg/m^3)
37 9.81            GRAV:           Gravitational acceleration (m/s^2)
38 -----  Blade Data  -------------------------------------------------------------
39 49              NUM_SEC:        Number of blade cross sections
40 123             BLD_LENGTH:     Blade length (m)
41 3.0             HUB_RAD:        Hub radius (m)
42 5.0             SHAFT_TILT:     Shaft tilt angle (deg)
```

```
43 -2.5            PRE_CONE:       Pre-cone angle (deg)
44 270              AZIM:           Azimuth angle (deg)
45 2.282E+01             BLD_PITCH:      Blade pitch angle (deg)
46 0.6050E+01             ROT_SPD:        Rotor rotational speed (rpm)
47 equal          INTERP_AF:      Interpolate airfoil coordinates? (choose "none",
   "cosine", or "equal" with no quotation marks)
48 60              N_AF:           Number of points in interpolated airfoil coordinates
   (ignored if INTERP_AF = none)
49 mats-Wind.inp   MATS_FILE:      Input file for material properties
50 0               FILLER_DENS:    (CURRENTLY IGNORED) Density of blade filler material
   (kg/m^3) (enter 0 if no filler material exists)
51 zFrac     aeroTwst        chord      pitAxis         px_a         py_a         qz_a
   af_shape_file    int_str_file
52 (-)       (deg)       (m)       (-)       (N/m)       (N/m)       (N)       (-)       (-)
53 0.000E+00       1.491E+01       7.084E+00       5.000E-01       1.965E+03       5.235E+02
          0.000E+00       NREL5_1000.prof
54 2.083E-02       1.491E+01       7.084E+00       5.000E-01       1.974E+03       5.256E+02
          0.000E+00       NREL5_1000.prof
55 4.167E-02       1.491E+01       7.427E+00       4.950E-01       1.725E+03       1.314E+03
          -3.564E+02      NREL5_0929.prof
56 6.250E-02       1.491E+01       8.387E+00       4.460E-01       8.085E+02       3.920E+03
          -1.745E+03      NREL5_0733.prof
57 8.333E-02       1.491E+01       9.181E+00       3.900E-01       -2.549E+02      6.789E+03
          -3.536E+03      NREL5_0561.prof
58 1.042E-01       1.491E+01       9.614E+00       3.750E-01       -1.121E+03      9.086E+03
          -5.067E+03      NREL5_0446.prof
59 1.250E-01       1.491E+01       9.779E+00       3.750E-01       -1.547E+03      1.036E+04
          -5.915E+03      NREL5_0400.prof
60 1.458E-01       1.364E+01       9.777E+00       3.750E-01       -1.587E+03      1.038E+04
          -5.895E+03      NREL5_0400.prof
61 1.667E-01       1.265E+01       9.683E+00       3.750E-01       -1.617E+03      1.049E+04
          -5.961E+03      NREL5_0400.prof
62 1.875E-01       1.183E+01       9.538E+00       3.750E-01       -1.650E+03      1.065E+04
          -6.114E+03      NREL5_0400.prof
63 2.083E-01       1.110E+01       9.366E+00       3.750E-01       -2.174E+03      1.187E+04
          -7.431E+03      NREL5_0350.prof
64 2.292E-01       1.046E+01       9.179E+00       3.750E-01       -2.060E+03      1.191E+04
          -7.788E+03      NREL5_0350.prof
65 2.500E-01       9.864E+00       8.983E+00       3.750E-01       -1.950E+03      1.195E+04
          -8.117E+03      NREL5_0350.prof
66 2.708E-01       9.320E+00       8.785E+00       3.750E-01       -1.844E+03      1.198E+04
          -8.381E+03      NREL5_0350.prof
67 2.917E-01       8.811E+00       8.585E+00       3.750E-01       -1.745E+03      1.202E+04
          -8.670E+03      NREL5_0350.prof
68 3.125E-01       8.337E+00       8.387E+00       3.750E-01       -1.689E+03      1.240E+04
          -9.831E+03      NREL5_0300.prof
69 3.333E-01       7.888E+00       8.190E+00       3.750E-01       -1.619E+03      1.255E+04
          -1.021E+04      NREL5_0300.prof
70 3.542E-01       7.461E+00       7.996E+00       3.750E-01       -1.572E+03      1.312E+04
          -1.111E+04      NREL5_0250.prof
71 3.750E-01       7.057E+00       7.805E+00       3.750E-01       -1.500E+03      1.327E+04
          -1.142E+04      NREL5_0250.prof
72 3.958E-01       6.671E+00       7.615E+00       3.750E-01       -1.434E+03      1.342E+04
          -1.172E+04      NREL5_0250.prof
73 4.167E-01       6.301E+00       7.428E+00       3.750E-01       -1.371E+03      1.356E+04
          -1.200E+04      NREL5_0250.prof
74 4.375E-01       5.946E+00       7.243E+00       3.750E-01       -1.308E+03      1.368E+04
          -1.224E+04      NREL5_0250.prof
75 4.583E-01       5.604E+00       7.061E+00       3.750E-01       -1.261E+03      1.418E+04
          -1.189E+04      NREL5_0210.prof
76 4.792E-01       5.273E+00       6.879E+00       3.750E-01       -1.193E+03      1.428E+04
          -1.206E+04      NREL5_0210.prof
77 5.000E-01       4.954E+00       6.700E+00       3.750E-01       -1.125E+03      1.434E+04
          -1.219E+04      NREL5_0210.prof
78 5.208E-01       4.644E+00       6.522E+00       3.750E-01       -1.057E+03      1.440E+04
          -1.231E+04      NREL5_0210.prof
```

```
 79 5.417E-01       4.343E+00       6.345E+00       3.750E-01       -9.876E+02      1.442E+04
           -1.239E+04      NREL5_0210.prof
 80 5.625E-01       4.050E+00       6.169E+00       3.750E-01       -9.170E+02      1.442E+04
           -1.244E+04      NREL5_0210.prof
 81 5.833E-01       3.764E+00       5.994E+00       3.750E-01       -8.456E+02      1.440E+04
           -1.245E+04      NREL5_0210.prof
 82 6.042E-01       3.485E+00       5.819E+00       3.750E-01       -7.739E+02      1.435E+04
           -1.243E+04      NREL5_0210.prof
 83 6.250E-01       3.212E+00       5.645E+00       3.750E-01       -6.959E+02      1.418E+04
           -1.232E+04      NREL5_0210.prof
 84 6.458E-01       2.944E+00       5.471E+00       3.750E-01       -6.191E+02      1.398E+04
           -1.218E+04      NREL5_0210.prof
 85 6.667E-01       2.682E+00       5.297E+00       3.750E-01       -4.805E+02      1.209E+04
           -9.831E+03      NREL5_0180.prof
 86 6.875E-01       2.424E+00       5.124E+00       3.750E-01       -4.130E+02      1.181E+04
           -9.605E+03      NREL5_0180.prof
 87 7.083E-01       2.171E+00       4.951E+00       3.750E-01       -3.477E+02      1.151E+04
           -9.354E+03      NREL5_0180.prof
 88 7.292E-01       1.920E+00       4.778E+00       3.750E-01       -2.852E+02      1.118E+04
           -9.068E+03      NREL5_0180.prof
 89 7.500E-01       1.673E+00       4.604E+00       3.750E-01       -2.258E+02      1.081E+04
           -8.733E+03      NREL5_0180.prof
 90 7.708E-01       1.429E+00       4.431E+00       3.750E-01       -1.695E+02      1.042E+04
           -8.381E+03      NREL5_0180.prof
 91 7.917E-01       1.187E+00       4.258E+00       3.750E-01       -1.168E+02      1.001E+04
           -8.010E+03      NREL5_0180.prof
 92 8.125E-01       9.472E-01       4.085E+00       3.750E-01       -6.768E+01      9.564E+03
           -7.620E+03      NREL5_0180.prof
 93 8.333E-01       7.092E-01       3.912E+00       3.750E-01       -2.214E+01      9.099E+03
           -7.202E+03      NREL5_0180.prof
 94 8.542E-01       4.726E-01       3.739E+00       3.750E-01       1.928E+01       8.612E+03
           -6.774E+03      NREL5_0180.prof
 95 8.750E-01       2.370E-01       3.566E+00       3.750E-01       5.633E+01       8.106E+03
           -6.341E+03      NREL5_0180.prof
 96 8.958E-01       2.458E-03       3.394E+00       3.750E-01       8.883E+01       7.584E+03
           -5.903E+03      NREL5_0180.prof
 97 9.167E-01       -2.316E-01      3.222E+00       3.750E-01       1.167E+02       7.047E+03
           -5.487E+03      NREL5_0180.prof
 98 9.375E-01       -4.655E-01      3.052E+00       3.750E-01       1.397E+02       6.501E+03
           -5.072E+03      NREL5_0180.prof
 99 9.583E-01       -6.993E-01      2.881E+00       3.750E-01       1.580E+02       5.946E+03
           -4.655E+03      NREL5_0180.prof
100 9.792E-01       -9.334E-01      2.713E+00       3.750E-01       1.715E+02       5.391E+03
           -4.245E+03      NREL5_0180.prof
101 1.000E+00       -1.168E+00      2.545E+00       3.750E-01       1.805E+02       4.832E+03
           -3.854E+03      NREL5_0180.prof
102 -----  Shear Web Data  ------------------------------------------------------------
103 3               NUM_WEBS:       number of webs
104 20              WEB_NODES:      number of nodes in each web (ignored if NUM_WEBS = 0)
105 webNum    inbStn    oubStn     inbChLoc     oubChLoc (This table of values is ignored
    if OPTIMIZE = true)
106    (-)       (-)       (-)          (-)          (-)
107     1         4         49       0.3695       0.1095
108     2         4         49       0.6300       0.6405
109     3        10         41       0.7800       0.6800
110 -----  Output Options  ------------------------------------------------------------
111 true            TAB_DEL:        Tab delimited text output files?
112 true            PROPS_FILE:     Write structural properties text output file?
113 true            LOAD_DSP_FILE:  Write loads and displacement text output file?
114 true            PANEL_FILE:     Write panel data text output file?
115 true            LAMINA_FILE:    Write lamina data text output file?
116 true            DATA_GUI:       Open graphical user interface (GUI) to visualize
    geometry, panel, and layer data?
117 true            SAVE_PLOTS:     Save plots to a file? (only saves plots which are
    actually created)
118 -fig,-png           SAVE_FIG_FMT:   Image file format. Enter -fig to save as MATLAB
    .fig, otherwise enter a comma delimited (no spaces) list of format options (ex: -
    png,-r300,-a2)
```

```
119 true            PLOT_OPT_ITER:  Plot information on design variables and convergence
    criteria during optimization iterations? (ignored if OPTIMIZE = false)
120 true           PLOT_F_BLD:     Plot applied forces on the blade geometry?
121 false           PLOT_DISP_BLD:  Plot displaced blade geometry?
122 true            PLOT_GBL_SYS:   Plot the applied forces & displaced blade geometry in
    the global coordinate system? (ignored if PLOT_F_BLD and PLOT_DISP_BLD are false)
123 false           PLOT_YMOD:      Plot panel effective Young's modulus?
124 false           PLOT_GMOD:      Plot panel effective shear modulus?
125 true            PLOT_MASS_DEN:  Plot mass distribution?
126 false           PLOT_PRIN_ANG:  Plot angle of principal axes?
127 false           PLOT_AT_STFF:   Plot axial and torsional stiffness?
128 true            PLOT_BSTFF:     Plot bending stiffness?
129 false           PLOT_INER:      Plot mass moments of inertia?
130 false           PLOT_CENTERS:   Plot locations of mass center, tension center, and
    shear center?
131 false           PLOT_NORMS:     Plot panel normal stress?
132 false           PLOT_SHEARS:    Plot panel shear stress?
133 false           PLOT_BCRIT:     Plot panel buckling criteria?
134 false           PLOT_E11:       Plot lamina 1st principal strain?
135 false           PLOT_E22:       Plot lamina 2nd principal strain?
136 false           PLOT_E12:       Plot lamina principal shear strain?
137 false           PLOT_S11:       Plot lamina 1st principal stress?
138 false           PLOT_S22:       Plot lamina 2nd principal stress?
139 false           PLOT_S12:       Plot lamina principal shear stress?
140 false           PLOT_S11_FC:    Plot lamina 1st principal stress failure criteria?
141 false           PLOT_S22_FC:    Plot lamina 2nd principal stress failure criteria?
142 false           PLOT_S12_FC:    Plot lamina principal shear stress failure criteria?
143 false           PLOT_MODE_D:    Plot modal displacements?
144 false           PLOT_MODE_S:    Plot modal slopes?
145 false           PLOT_APPLOADS:  Plot applied loads?
146 false           PLOT_RESLOADS:  Plot resultant loads?
147 false           PLOT_DEFLECT:   Plot blade centroidal deflections?
```

Figure I.14. Example input Co-Blade